Geological Survey of Finland, Bulletin 362

THE CALEDONIAN HALTI-RIDNITSOHKKA IGNEOUS COMPLEX IN LAPLAND

by

PEKKA SIPILÄ

with 40 figures, 7 tables in
the text and 13 appendices

GEOLOGIAN TUTKIMUSKESKUS
ESPOO 1992

Sipilä, P. 1992. The Caledonian Halti-Ridnitsohkka igneous complex in Lapland. *Geological Survey of Finland, Bulletin 362,* 75 pages, 40 figures, 7 tables, and 13 appendices.

The Halti-Ridnitsohkka mafic-ultramafic complex is located in northwest of Finnish Lapland, straddling the Norwegian border, and forms an allochthonous thrust sheet at the highest topographical and structural level within the Finnish Caledonides. The complex consists of the Ridnitsohkka gabbro sill unit in its eastern part and the Halti dunite-troctolite-olivine gabbro sequence in the west. These are cogenetic and both belong structurally to the same nappe. The contact between the cumulate sequence and the underlying gneissic basement is clearly tectonic and discordant with respect to cumulate lithological layering. The precise nature of the contact between the gabbro sill unit and the basement gneisses in the east is less certain, although a contact metamorphic aureole is preserved.

The oblique convergence of Fennoscandia and Laurentia plates during closure of the Iapetus ocean may have initiated extensional zones of weakness into which the Ridnitsohkka gabbroic sills and the picritic parent magmas to the Halti cumulates were emplaced. The regional magmatic evolution is interpreted as regressive. The earliest intrusions were the Ridnitsohkka Al-rich tholeiitic gabbro sills, which crystallized at pressures of 7—8 kbar and caused local partial melting of intervening gneiss remnants, as well as a more widespread thermal aureole. The chemistry of the sills became progressively more primitive, culminating in a picritic phase which, during subsequent fractionation, gave rise to the Halti cumulates. Picritic magmas were intruded in several pulses and the Mg-content of olivine remained high (Fo_{90-92}) throughout the entire duration of dunite crystallization. Successive high temperature pulses of picritic magma caused the replacement of earlier crystallized plagioclase-bearing lithologies by secondary dunite. Coarse-grained gabbroic pegmatite dykes crystallized from the last remaining residual magmas, and cut across earlier units. This same magma caused the metasomatic replacement of troctolite by coarse-grained olivine gabbro in the contact zone between the sill unit and the cumulate sequence. The regional pressure maximum, around 10 kbar, was attained after the main phase of magmatism, resulting in the formation of corona textures between olivine and plagioclase, and because of the overall high activity of water, plagioclase-bearing cumulates were altered either partially or totally to kyanite bearing amphibole rocks. Country-rock gneiss interlayers between the Ridnitsohkka sills were similarly subjected to intense hydrothermal metamorphism at high pressures.

The Halti-Ridnitsohkka complex is situated tectonostratigraphically within the controversial boundary zone between the Kalak Nappe Complex in the Middle Allochthon, formed during the Finnmarkian phase of the Caledonian Orogeny, and the Reisa Nappe Complex in the Upper Allochthon, associated with the Scandian phase of the Orogeny. However, recently obtained U-Pb ages of 445—425 Ma for badelleyite and zircon from both the Ridnitsohkka gabbroic sills and the anatectic granite in the contact metamorphic aureole indicate that the Halti-Ridnitsohkka complex is of Scandian age and thus belongs to the Upper Allochthon.

Key words (GeoRef Thesaurus): gabbros, sills, cumulates, petrography, geochemistry, metamorphism, evolution, Caledonides, Paleozoic, Halti, Enontekiö, Lapland, Finland, Norway.

Pekka Sipilä
University of Turku
Department of Geology
SF-20500 Turku
Finland

Present address:
Geological Survey of Finland
Betonimiehenkuja 4
SF-02150 Espoo
Finland

ISBN 951-690-459-9
ISSN 0367-522X

Vammalan Kirjapaino Oy 1992

CONTENTS

FOREWORD

The Scandinavian Caledonides are represented in Finland by a small area in the northwestern part of the Enontekiö district in the extreme north of the country, adjacent to the Norwegian and Swedish borders. On account of its remote location, the geology of the region had not been examined in detail until the early 1980's, when the University of Turku, in conjunction with the Geological Survey of Finland, initiated a bedrock mapping program. Earlier reconnaissance studies (Hausen, 1941, 1942a; Bøe, 1976) had however, referred to the existence of mafic and ultramafic rocks in the Halti and Ridnitsohkka area. The purpose of this investigation therefore was to determine the nature and origin of the Halti-Ridnitsohkka magmatic complex and its position within the Caledonian Orogeny. Fundamental questions include whether the complex is related to initial rifting of the Iapetus ocean or represents a segment of ocean floor obducted onto the Fennoscandian shield during subsequent closure, or even whether it is perhaps a synorogenic intrusion. The project was also of inherent interest because it deals with the Caledonian allochthons, which are not represented elsewhere in Finland.

INTRODUCTION

The bulk of the Caledonian fold belt formed during the Late Silurian Scandian phase of the Orogeny, when the convergence of Laurentia and Fennoscandia led to the closure of the Iapetus ocean. In northern Scandinavia however, a distinctly older, late Cambrian event, known as the Finnmarkian orogenic phase, has also been recognized. As a result of continual erosion and vertical block movements since Mid-Devonian time, the whole history of development and destruction of Iapetus is exposed within the Caledonides.

During the late Precambrian rift phase, extensional sedimentary basins formed as a result of thinning of continental crust. This rifting culminated in the opening of Iapetus and separation of the Laurentian and Fennoscandian plates, with sedimentation continuing on both passive margins. Subduction of oceanic crust throughout the Ordovician (510—440 Ma) (Cowie and Basett, 1989) and Early Silurian (440—420 Ma) resulted in the formation of volcanic arcs and associated obduction of ophiolites. Continuing convergence during the Late Silurian led to collision of the Laurentian and Fennoscandian plates, with the latter being partly thrust under the former, causing widespread high pressure metamorphism. This was associated with telescoping of the Fennoscandian margin and an increase in crustal thickness and strength, accompanied by the emplacement of far travelled allochthonous thrust nappes and the formation of sedimentary basins within the foreland (Roberts and Gee, 1985; Piper, 1985; Gayer, 1989).

Mafic rocks associated with the above events are very well preserved and exposed in the

Caledonides. Dolerites and amphibolites related during the rift-phase comprise a major part of the Särv Nappe of the Middle Allochthon and the Seve Nappe of the Upper Allochthon. In northern Norway, mafic dykes belonging to this early magmatism are most abundant within the upper part of the Kalak Nappe Complex, which belongs to the Middle Allochthon. The Köli and Skibotn Nappes of the Upper Allochthon (Gayer et al., 1985) contain volcanic and subvolcanic associations formed in an oceanic setting, including ophiolites, while synorogenic mafic and ultramafic intrusions occur within the Middle (in Seiland), Upper and Uppermost Allochthons (Stephens et al., 1985).

The Finnish Caledonides consist predominantly of autochthonous and allochthonous latest Precambrian and Cambrian sediments deposited during the initial stages of Iapetus extension, as well as during the subsequent passive margin stage (Lehtovaara, 1984, 1988). During thrusting however, these units were tectonically intercalated with crystalline basement. The mafic and ultramafic lithologies exposed in the Halti-Ridnitsohkka area represent the only such Caledonian magmatic units preserved in Finland. They occur at the highest tectonostratigraphical level in the allochthon, at the controversial boundary zone between the Scandian and Finnmarkian phase nappes.

PREVIOUS INVESTIGATIONS

The Finnish Caledonides have not been studied in great detail. The earliest references to the region are those of Pettersen (1870, 1876a, 1876b), who visited Halti during his general survey of northern Norway. Stjernvall (1892) published an account of the geology between Könkämäeno and the Norwegian border and Tanner (1914) published a reconnaissance bedrock geology map in conjunction with his surficial deposit investigations. Hausen (1942b) published the results of regional surveys carried out during the 1930's, as well as more specific studies dealing with the Halti massif (Hausen, 1936, 1941, 1942a). However, until recently the main source of information of the regional geology has been the 1:400 000 scale geological map published by Matisto (1959, 1969). Tynni (1980) found fossils of Caledonian age in lower Cambrian sediments in the Porojärvi area. Lehtovaara (1984, 1986a, 1989) has subsequently published structural interpretations of the Finnish Caledonides based on comparisons and correlations with the tectonostratigraphic scheme developed in adjacent parts of northern Norway. Further publications include those concerned with the sub-Caledonian erosional surface (Lehtovaara, 1985), alum-shale deposits (Lehtovaara, 1986b), mafic dykes at Ridnitsohkka (Lehtovaara, 1987) and the paleosedimentology of the autochthonous sequence (Lehtovaara, 1988). Magmatism and tectonostratigraphy in the area have also been briefly reviewed by Lehtovaara and Sipilä (1987), while Sipilä (1987) studied the olivine-plagioclase corona textures of the troctolites and olivine gabbros. Sipilä (1989, 1990, 1991) further described the mafic and ultramafic magmatism of the Halti-Ridnitsohkka complex. Vaasjoki et al. (in prep.) present new radiometric age determinations for the Ridnitsohkka gabbro sills and for the anatectic granite occurring on the contact metamorphic aureole of the sill area. An abstract by Mattson and Lindqvist (1990) briefly discusses regional metamorphism and Sm-Nd isotopic data. Mertanen et al. (1990) have presented preliminary paleomagnetic data for the Ridnitsohkka gabbro sills.

Relevant Norwegian work includes that of Padget (1955) who described Caledonian geology

in the northern part of the Birtavarre region. Bøe (1976) first described the entire Halti cumulate sequence and the Ridnitsohkka mafic dykes. The Cier'te 1:50 000 bedrock map, along with accompanying explanatory notes, covering contiguous areas in Norway is also available (Fareth et al., 1977), as is the 1:250 000 Nordreisa mapsheet (Zwaan, 1988). Binns and Gayer (1980) established the regional tectonostratigraphical relationships on the basis of an Ordovician fauna from the nearby Guolasjavri carbonate sequence. Zwaan and Roermund (1990) correlated the Halti sequence with the mafic dyke swarm in the northern Corrovarre Nappe, while Roberts (1990) discussed the geochemistry of these dykes.

SAMPLE MATERIAL AND ANALYTICAL TECHNIQUES

Sample material

For the purposes of this investigation, a total of 404 samples were collected from throughout the study area, although particular emphasis was placed upon sampling from three traverses made perpendicular to magmatic layering. Where there was no obvious variation in lithology, as on the western slopes of Haltitunturi and within the Ridnitsohkka gabbro sills, an attempt was made to take samples at regular intervals of 150—200 m. On the eastern slopes of Haltitunturi, rhythmic magmatic layering forms distinct units up to several meters in thickness which can, after the classification scheme of Irvine (1982), be described as macrorhythmic units. Each of these macrorhythmic units were sampled along two separate traverses. The majority of the chemical analyses and thin sections were made from samples collected from the Finnish part of the profiles (Profile X—XX, Appendix 13).

A total of 198 thin sections, including 141 polished sections were made, as well as an additional 9 polished chips, all having been prepared at the Geology and Mineralogy Department of the University of Turku.

Whole-rock analytical techniques

The majority of whole-rock analyses (80) were performed at the laboratories of the University of Turku Geology and Mineralogy Department, where the major element oxides SiO_2, TiO_2, Al_2O_3, FeO, CaO and K_2O were determined by X-ray fluorescence and MnO, MgO and Na_2O by atomic absorption spectrophotometry. Trace as well as major element compositions for 15 samples were determined by XRF at the Outokumpu Geoanalytical Laboratories, while trace element compositions of a further 48 samples were analyzed at the Reactor Laboratory at the Finnish National Technical Research Center at Otaniemi. REE analyses were made for five samples at the same laboratory using Instrumental Neutron Activation Analysis (INAA). Platinum group elements, Au, Se, Ru, Co, Ni, Cu and S were also determined for two massive chrome spinel samples at the X-ray Assay Laboratories in Canada.

Mineral data

Most determinations of mineral compositions were made using a LINK AN 1000 EDS system connected with a CAMBRIDGE S 200 electron microscope in the Material Sciences Laboratory at the University of Turku Physics Department. The compositions of 40 olivine grains were determined with the WDS technique using a JEOL JCXA 733 microprobe at the Institute of Electron Optics at the University of Oulu. A total of 349 individual mineral samples were analyzed, along with 14 analyses made on 3 samples of fine-grained intergrowths from gneiss interlayers within the Ridnitsohkka sills. In addition microprobe traverses were undertaken to ascertain the degree of zonation in a total of 11 plagioclase, olivine, clinopyroxene and chrome spinel samples.

For the quantitative determinations made at Turku, an accelerating potential of 20 kV was used with a corresponding sample current of 1 Na. Pyroxenes were analyzed using a dispersed (10 µm) electron beam, but otherwise a focused (1 µm) beam was used. Each sample was measured for 100 s. Standards employed were both metallic (Mg, Al, Ti, Mn and Fe) and minerals (quartz (Si), calcite (Ca), albite (Na) and orthoclase (K)). The ZAF—4/FLS correction program was used and relative errors for elements exceeding 10 wt% was around 5 %, with somewhat higher values for elements present at smaller concentrations. Detection limits varied according to mineral and sample variations but was on average between 0.2—0.4 wt%. Each mineral was analyzed 3—4 times, including measurements at both rim and core and the mean of these values was taken as the result. A greater number of measurements and closer spacing between analyses were required for determinations of compositional zonation.

An acceleration potential of 15 kV was used for the Oulu University analyses, with a sample current of 33 Na and the ZAF on-line correction program was used. Detection limits for Al, Ca, Mn and Ni, which are present in trace amounts in olivine, were 0.04 wt% at the 95 % confidence level. The diameter of the electron beam used was 10 µm and only a single determination was made for each sample. The procedure is described in greater detail by Alapieti and Sivonen (1983).

The equipment at Turku was also used in qualitative determination of sulfide phases and a number of minerals were in addition identified on the basis of X-ray diffractometry at the University of Turku Geology Department.

REGIONAL GEOLOGICAL SETTING

General summary of the Caledonian tectonostratigraphy of northern Scandinavia

The mountainous terrain of the study area, including the peaks of Halti and Ridnitsohkka, form part of the Scandinavian Caledonian mountain chain which, in Finland, is restricted to a relatively small area in the Enontekiö district, in the extreme northwest of the country (Figs. 1, 2).

Caledonian structures in the region are characterized by extensive allochthonous thrust nappes that dip gently towards the northwest and which were thrust southeastwards over the Precambrian Fennoscandian Shield during the Caledonian Orogeny. The uppermost of these allochthonous units have evidently travelled hundreds of kilometers (Roberts and Gee, 1985). In Finnmark, in northernmost Norway, two major groups of nappes have been recognized — the lower, Finnmarkian nappes and the upper, Scandian nappes. This subdivision is based upon the recognition

of two major phases of Caledonian deformation, the Finnmarkian phase being dated as Late Cambrian (540—520 Ma) (Sturt et al., 1975, 1978; Pedersen et al., 1989), while the Scandian phase took place during the Middle and Late Silurian (ca. 420 Ma), perhaps even continuing until the earliest Devonian (Ramsay and Sturt, 1977). Krill and Zwaan (1987) have recently contended that the Finnmarkian phase was not a distinct event, although this proposal has not received unqualified support (Sturt and Ramsay, 1988; Roberts, 1988).

The Scandian and Finnmarkian phases have also been recognized as distinct events further southwest in the Tromsö area, adjacent to the Finnish Caledonides, although the distinction is not quite so clear as in Finnmark (Andresen et al., 1985). The precise location of the boundary between units belonging to the two phases has been the subject of debate, and the Finnish Caledonides are situated broadly within this controversial zone. The entire allochthonous sequence in Finland is usually assigned to the Finnmarkian phase and correlated with the Kalak Nappe Complex (Zwaan and Roberts, 1978). Fig. 1 presents the main tectonostratigraphic elements in the Nordreisa district, which is contiguous with the Finnish Caledonides, mainly following the classification of Zwaan (1988). According to this interpretation, the Kalak Nappe Complex in Finland consists essentially of two units, namely the Nalganas and Nabar Nappes. However, on the basis of new isotopic age data (Vaasjoki et al., in prep.), the Halti-Ridnitsohkka area is considered to belong to the Reisa Nappe Complex instead and in this respect, Fig. 1 departs from earlier interpretations. According to Zwaan (1988), the Reisa Nappe Complex does not extend into Finland, although its lowermost unit, the Vaddas Nappe can be traced to within a few kilometers of the national border, at Guolasjavri. After the discovery of Silurian and Late Ordovician fossils within the Vaddas Nappe (Binns and Gayer, 1980), the boundary between the Finnmarkian and Scandian orogenic phases has been placed within its lower part (Ramsay et al., 1981). Lehtovaara (1984) considered the possibility that the rocks of the Halti area belong to the lower part of the Vaddas Nappe and are therefore the only representatives of the Scandian phase in Finland. According to Zwaan et al. (1990) however, the Halti and Ridnitsohkka units belong to the upper part of the Kalak Nappe Complex and may be correlated with the ultramafic and gabbroic lithologies in the northern Corrovarri Nappe. Tholeiitic dykes within the Corrovarri Nappe have yielded an Sm-Nd age of 580 ± 30 Ma, which has led their interpretation as intrusions in belonging to the early stages of Iapetus ocean crust formation (Zwaan and Roermund, 1989, 1990). New concordant U-Pb isotopic results for badelleyite and zircon from the Ridnitsohkka gabbro sills (434 ± 4 Ma and ca. 445 Ma respectively) and for zircon from an anatectic granite in the Ridnitsohkka contact aureole (ca. 425 Ma, cf Pb-Pb age of 450 Ma) demonstrate however that Scandian phase allochthons are indeed present in Finland (Vaasjoki et al., in press). The preliminary whole rock Sm-Nd age of 650 ± 150 Ma (initial ε_{Nd} $+4.4 \pm 0.2$) for the Halti cumulates reported by Mattson and Lindqvist (1990) is not precise and requires further refinement (Mattson, 1991, pers. comm.)

Tectonostratigraphic units in the Finnish Caledonides

Within the general Caledonian tectonostratigraphic scheme devised originally by Kulling (1964), consisting of the Autochthon/Parautochthon, and the Lower, Middle, Upper and Uppermost Allochthons, the Finnish Caledonides belong for the most part to the Middle Allochthon.

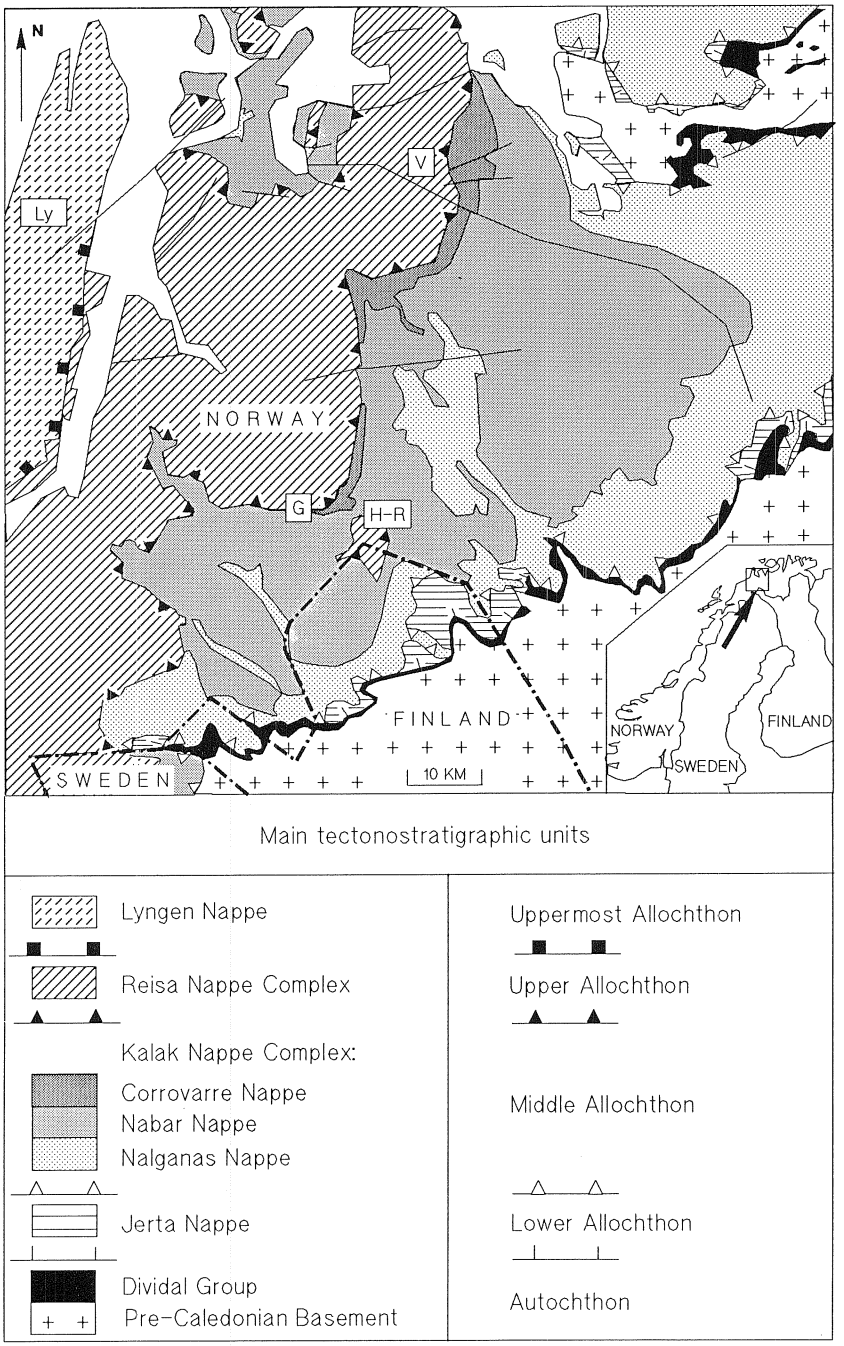

Fig. 1. Tectonostratigraphic map of the Nordreisa area, northern Norway (after Zwaan 1988, Zwaan & Roermund 1990) and of northwestern Finland (after Lehtovaara 1989). The stratigraphic interpretation of the Halti-Ridnitsohkka area is based on the present study. H-R = Halti-Ridnitsohkka, G = Guolasjavri, Ly = Lyngen, V = Vaddas.

Based on the subdivisions recognized in northern Norway, in which the Jerta Nappe belongs to the Lower Allochthon and the Kalak Nappe Complex to the Middle Allochthon (Zwaan and Roberts, 1978; Zwaan, 1988), Lehtovaara (1984, 1986a, 1989) has presented a schematic interpretation of the structure and tectonostratigraphic sequence of the Finnish Caledonides (Fig. 1).

The new age determinations for the Ridnitsohkka gabbro sills indicate however that the highest structural units within the Finnish Caledonides belong to the Upper Allochthon. Because however, the contact between the gabbro sills and the underlying Nabar Nappe is intrusive, the boundary between the Middle and Upper Allochthons in Finland has not been precisely located.

Autochton

Pre-Caledonian Basement

The basement to the southeast of the Caledonian front consists of Archean gneisses and granitoids. This is demonstrated by U-Pb age determinations of zircons from the Palovaara granite (2735 ± 51 Ma, Idman and Eilu, 1988) and the Ropinsalmi granodiorite (2800 Ma, Matisto, 1969). Similar late Archean ages have also been reported from contiguous areas in northern Sweden (Welin et al., 1971; Skiöld, 1979).

Dividal Group

Essentially unmetamorphosed sediments of the autochthonous Dividal Group attain a maximum thickness of 150 m and consist of conglomerates, orthoquartzites, siltstones and shales (Hausen, 1942b). They form a laterally persistent unit which can be traced hundreds of kilometers along the margin of the fold belt. Dividal Group sediments were deposited unconformably on the basement during latest Precambrian and Middle Cambrian time (Føyn, 1967; Roberts, 1974)

Allochthon

Lower Allochthon

The Dividal Group is overlain by the autochthonous-parautochthonous Jerta Nappe, which is considered part of the Lower Allochthon (Roberts and Gee, 1985; Lehtovaara, 1989). It consists of imbricated and weakly metamorphosed Dividal Group sediments (Ramsay et al., 1985) and slightly older Late Precambrian (Vendian) deposits (Zwaan, 1988). The Jerta Nappe varies in thickness such that in some places in Finland it is several hundred meters thick, due to tectonic imbrication, while elsewhere it may be completely absent (Lehtovaara, 1986a).

Middle and Upper Allochthons

The far-travelled nappes of the Finnmarkian phase were thrust over the Jerta Nappe and their representatives in Finland have all been assigned to a single major unit, namely the Kalak Nappe Complex (Lehtovaara, 1984). The Kalak Nappe Complex is considered to be part of the Middle Allochthon and has been subdivided, in both Norway and Finland (cf. Lehtovaara, 1989), into a lower unit consisting of homogeneous felsic mylonitic schists, known as the Nalganas Nappe and a more heterogeneous upper unit, known as the Nabar Nappe. The lower part of the Nabar Nappe consists dominantly of amphibolites but the proportion of felsic material increases upwards, with the uppermost unit being a garnet-bearing banded gray gneiss. Sedimentary units within the Kalak Nappe Complex are evidently latest Precambrian and Cambrian in age (Zwaan and Roberts, 1978), while volcanic units are almost entirely absent (Gayer et al., 1985). Amphibolites and felsic gneisses in the lower part of the Nabar Nappe are interpreted as sheets of Precambrian basement (Lehtovaara, 1987). New age determinations from the Ridnitsohkka gabbro sills intruding the Nabar gneisses (Vaasjoki et al., in prep.) indicate that they were intruded during the Scandian phase and should not be cor-

related with similar lithologies occurring in the upper part of the Corrovarri Nappe, within the Kalak Nappe Complex. Moreover, since the contact between the sills and the Nabar Nappe is demonstrably intrusive, the uppermost part of the Nabar Nappe at least must belong to the Upper Allochthon, emplaced during the Scandian phase.

In central and northern Sweden, the lower part of the Upper Allochthon is known as the Seve Nappe Complex (Kulling, 1964; Lindström et al., 1985; Kathol, 1987). Although this unit is not considered to continue further northwards or into Finland, Zachrisson (1986) and Lehtovaara (1989) suggested that the Nabar Nappe may in fact belong to the Seve Nappe Complex. However, the amphibolites of the Seve complex are considered to be comagmatic with the Ottfjället dolerite dykes in the Särv Nappe of the Middle Allochthon (Solyom et al., 1979a, 1979b; Stephens et al., 1985). The Ottfjället dykes were intruded during early stages of opening of Iapetus (Gee, 1975; Solyom et al., 1979b), around 625 Ma (Andreasson, 1987), and are thus distinctly older than the Ridnitsohkka sills. Correlation of the Nabar Nappe with the Seve Nappe Complex is therefore untenable.

Neighboring Caledonian mafic complexes

The nearest major Caledonian mafic complexes are the Vaddas gabbro some 50 km to the north of Halti and the Lyngen gabbro, which lies at a similar distance to the west. Amphibolites, gabbros (including the Bäggegähaldi gabbro about 30 km northeast of Halti) and mafic dykes occur within the Corrovarri Nappe, and are exposed in a zone trending from immediately north of Halti to the east of the Vaddas gabbro. The Seiland Igneous Province is situated about 100 km north of Halti. Pillow lavas have also been recognized in greenstones about 5 km to the northwest (Padget, 1955).

According to the description by Stevens (1982), the Vaddas gabbro resembles the Halti complex lithologically, inspite of the absence of ultramafic units. The Vaddas gabbro is a part of Vaddas Nappe forming the lower part of the Reisa Nappe Complex, which itself belongs to the Upper Allochthon (Zwaan, 1988).

The Lyngen gabbro (Munday, 1974; Minsaas and Sturt, 1985) occurs at a distinctly higher tectonostratigraphical level than any of the units exposed in the Finnish Caledonides, forming part of the Lyngsfjell Nappe in the Uppermost Allochthon, which in turn lies above the Reisa Nappe Complex (Zwaan and Roermund, 1990). The Lyngen gabbro is generally regarded as an ophiolite and is pre-Ordovician in age (Zwaan, 1988).

The Corrovarri Nappe has been dated by the Sm-Nd method at 580 ± 30 Ma (Zwaan and Roermund, 1990) and forms the highest structural unit within the Kalak Nappe Complex, and hence the Middle Allochthon, in the Nordreisa area (Fig. 1). Zwaan (1989) and Zwaan and Roermund (1990) consider the tholeiitic dykes in the Corrovarri Nappe to be correlatives of those in the Seve and Särv Nappe Complexes in Sweden and thus represent rifting associated with the opening of Iapetus. According to this interpretation the Särv mafic dykes were intruded at the beginning of rifting whereas the Corrovarri Nappe dykes record the final stages of opening. This is consistent with conclusions based on the geochemistry of the dykes (Roberts, 1990).

The Seiland Igneous Province consists of gabbros, calc-alkaline intrusions, ultramafic complexes, alkali rocks, carbonatites and mafic dyke swarms (Robins and Gardener, 1975). The province belongs tectonostratigraphically to the upper part of the Kalak Nappe Complex and is of

Lower to Middle Cambrian (540—520 Ma) age (Pedersen et al., 1989).

The Honningvåg intrusive suite in northernmost Norway intruded the Mageröy Nappe under Barrovian-type metamorphic conditions during the Scandian deformational phase (Robins et al., 1987). The suite forms a lopolith consisting of the following separate cumulate assemblages: olivine + chrome spinel, plagioclase + olivine ± chrome spinel, plagioclase + Ca-pyroxene + olivine, plagioclase + Ca-pyroxene + Ca-poor pyroxene.

PRINCIPAL UNITS WITHIN THE HALTI-RIDNITSOHKKA COMPLEX

The Halti dunite-troctolite-olivine gabbro cumulate sequence in the western part of the study area, together with the Ridnitsohkka gabbro sill unit to the east, constitute the Halti-Ridnitsohkka complex. The complex occurs as a subhorizontal allochthonous thrust sheet at the summits of the two highest peaks in the area, namely Halti and Ridnitsohkka (Figs. 1, 2) and has a maximum preserved thickness of 400 m. The rocks overlying the sheet have been removed by erosion. In the west, the contact between the Halti cumulates and gneisses of the underlying Nabar Nappe is clearly tectonic, whereas in the east, the Ridnitsohkka gabbro sills are separated from the Nabar gneisses by a contact metamorphic aureole some 500 m in thickness; in the latter area however, the nature of the lower contact against the gneisses of the Nabar Nappe is less clear.

The Halti cumulate sequence outcrops over an area of about 14 km^2 around the summit of Halti; of this only about 2.5 km^2 is in Finland, the remainder being on the Norwegian side of the border (Fig. 2). Three smaller areas of cumulates, representing erosional outliers that were formerly contiguous with the Halti sequence, have been identified further west but only one of these extends across the border into Finland. On the basis of the attitude of primary magmatic layering, it is evident that the cumulate sequence forms a syncline with a horizontal axis trending northwards in the southern part of the area and towards the northwest in the northern part. Layering is subvertical or steeply west-dipping in the central and eastern parts of the sequence, while in the western and northern parts layering dips more gently inwards. The tectonic basal contact is clearly discordant to this layering.

A relatively extensive area characterized by mafic sills occurs to the east and north of the Halti cumulate sequence. It forms a zone 2 km wide on the Finnish side of the border and can be traced further to the northwest, parallel to the margin of the Halti cumulates, at least as far as Guolasjavri (Fig. 2).

Halti cumulate sequence

Dunites

In the eastern part of the cumulate sequence, a coherent northwards-tapering horizon of dunite is present, containing narrow discontinuous layers of troctolite, anorthosite and massive chrome spinel accumulations. Dunite also occurs as sporadic lenses several meters thick within the overlying troctolite unit and is generally massive in appearance, or else weakly oriented (Fig. 3). Along its overthrust southern contact the dunite

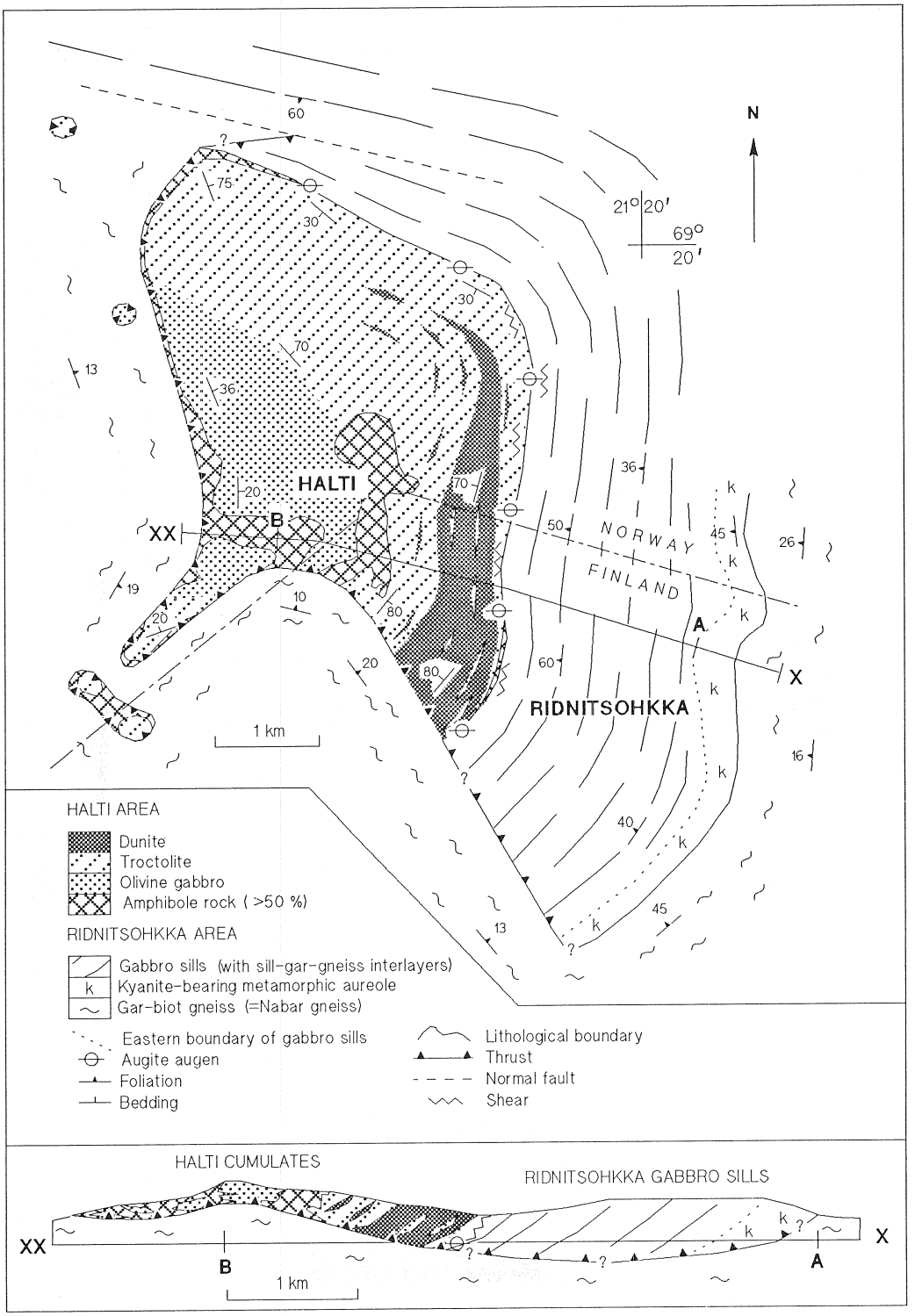

Fig. 2. Geological map of the Halti-Ridnitsohkka area. Halti cumulates and Ridnitsohkka gabbro sills together comprise the Halti-Ridnitsohkka igneous complex.

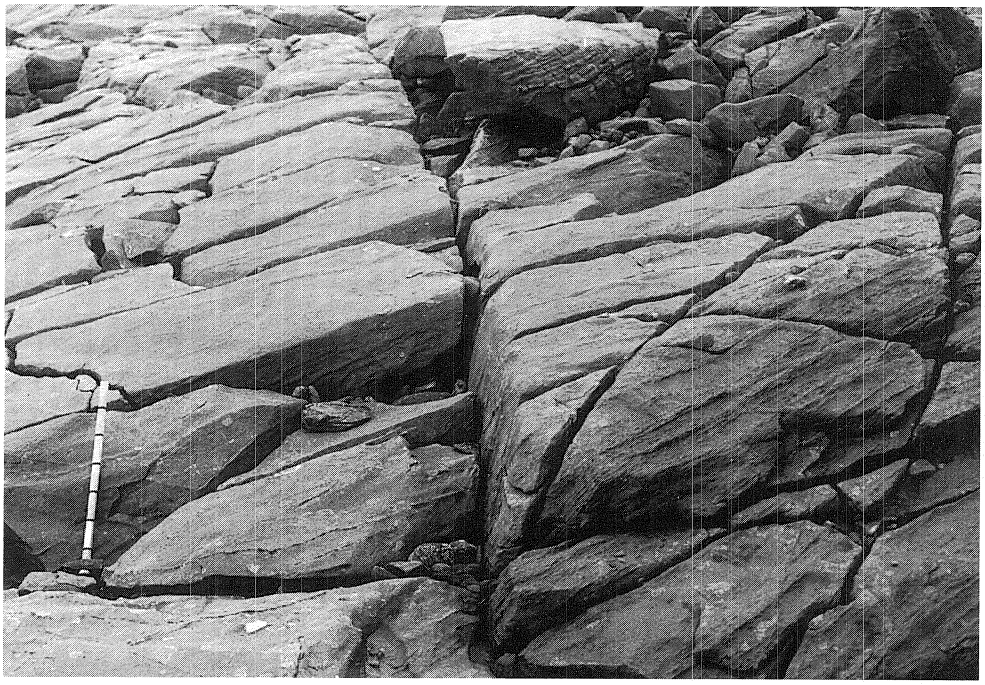

Fig. 3. Weakly sheared but still predominantly massive homogeneous dunite. Locality 374, Halti.

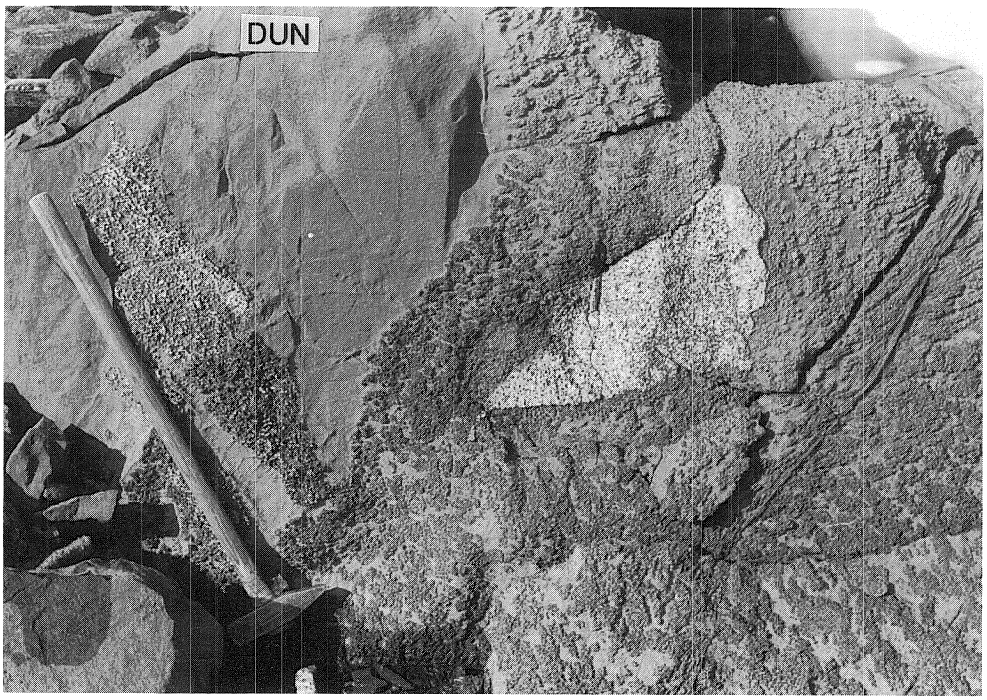

Fig. 4. Magmatic breccia in which dunite both brecciates and partly replaces troctolite. DUN = dunite. Locality 386, Halti.

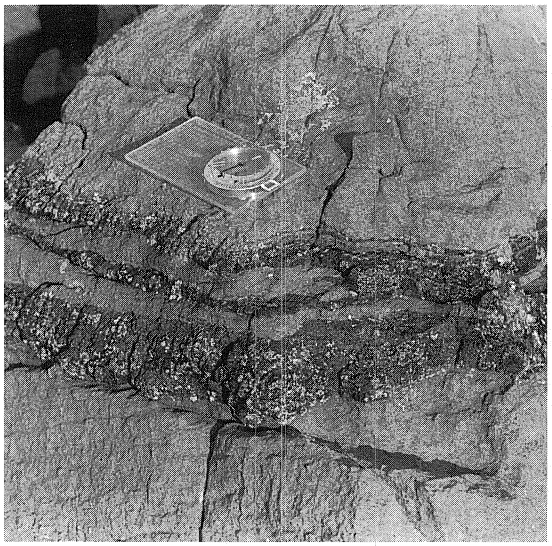

Fig. 5. Massive chrome spinel layers in dunite. Locality 380, Halti.

is highly schistose and serpentinized and talc-chlorite shear zones containing pods of magnetite are also present.

There has been a tendency for secondary dunite to form at the expense of troctolite, particularly near the western transition zone between the two rock types and in the most southerly of the three small outliers (Fig. 4).

Stratiform chrome spinel layers

The dunites contain sporadic stratiform horizons, nowhere exceeding 2 m in thickness, which are characterized by bands of massive chrome spinel (Fig. 5). These bands may be up to 20 cm thick, but are typically only 2 cm or so. They are strongly deformed and laterally impersistent in directions parallel to layering, having being traced over distances of several tens of meters.

Troctolites

Layered troctolite is the most abundant lithology in the Halti cumulate sequence, occurring on both sides of the dunite unit as well as in the

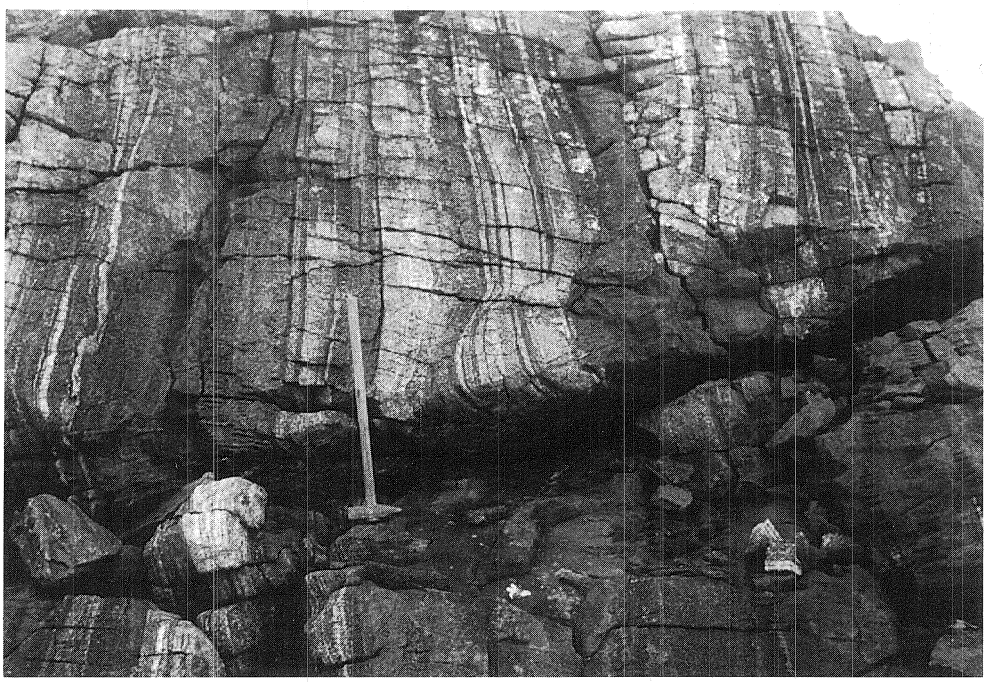

Fig. 6. Rhythmic layering in troctolite. Locality 113, Halti.

southwestern horn-like protrusion of the complex and in the northwesterly outlier (Fig. 2).

The distinct rhythmic layering in the troctolite (Fig. 6) is due to modal variations in the abundances of olivine and plagioclase, such that some layers may strictly be anorthositic and others dunitic. Individual layers may vary from several centimeters to many meters in thickness and persist laterally for tens of meters. A linear alignment of plagioclase laths is evident in some places and a magmatic erosional discordance in the troctolite at the eastern margin of the dunite horizon indicates that base of the sequence is to the east, and hence the complex is upward younging. In contrast, the western contact between the dunite horizon and the troctolites shows the effects of synmagmatic brecciation (Fig. 4). Fragments of both dunite and anorthosite are present, the largest being many cubic meters in size, with plagioclase in the matrix commonly being concordantly aligned around their margins. Adjacent to the Ridnitsohkka sills, the troctolites show some evidence of shearing parallel to imbricate fault zones.

Olivine gabbros

The transition from troctolite to olivine gabbro is related to an increase in the abundance of clinopyroxene. Olivine gabbro outcrops around the summit of Halti and its western flanks and in general forms the uppermost part of the cumulate sequence. Where clinopyroxene is particularly abundant, olivine gabbros can be readily distinguished in the field from troctolites because of their distinctly darker color. The olivine gabbros at the summit of Halti are massive but further west they are layered, with layers typically between 10 and 30 cm thick. The layered olivine gabbros at the western margin of the complex display synmagmatic brecciation structures.

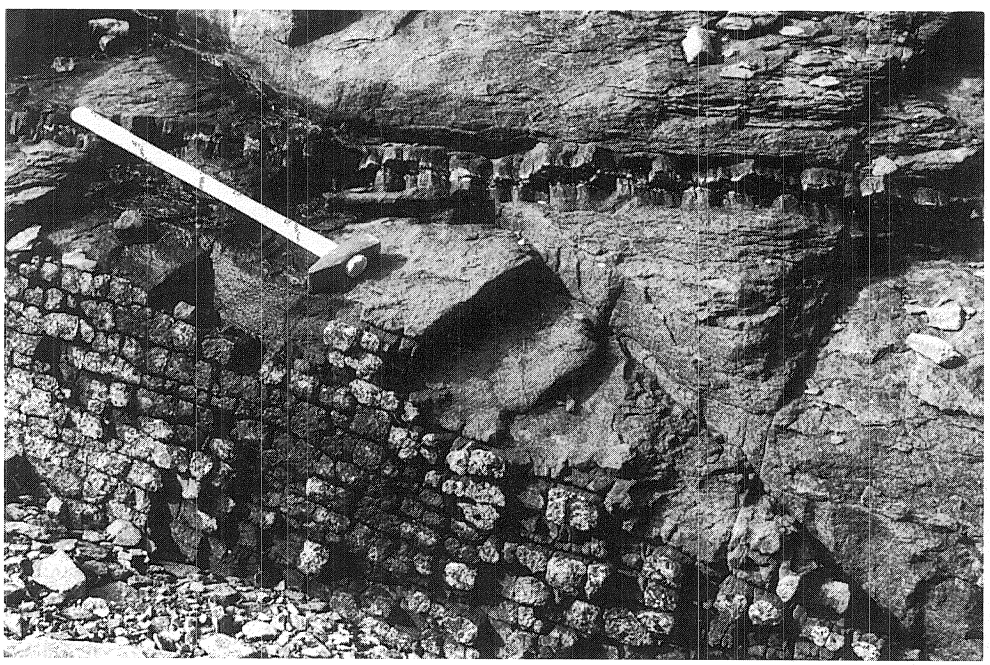

Fig. 7. Gabbro pegmatite dykes in dunite. Lower dyke shows typical reticulate joint and fracture pattern while both margins of upper dyke show reaction selvages against the dunite. Locality 20, Halti.

Coarse-grained gabbro pegmatite dykes

The latest stage differentiates within the Halti cumulate sequence are coarse-grained gabbro pegmatoid dykes that are both mineralogically and chemically very similar to the olivine gabbros. They are most abundant in the dunites and troctolites of the eastern part of the cumulates, occurring only rarely within the olivine gabbro unit. No equivalents of these dykes have been found outside the cumulates, nor within the Ridnitsohkka area. The dykes are sharply discordant across host rocks and do not show any preferred or systematic orientation (Fig. 7). They are typically 5—20 cm thick but lenses many meters thick have also been found. In outcrop they are characteristically fractured, producing brick-shaped fragments (cf. Fig. 7).

Individual minerals within the gabbro pegmatoids are very coarse-grained, sometimes attaining 10 cm in diameter. In such cases reaction rims between olivine and plagioclase grains are discernible with the naked eye. Likewise reaction rims at the margins of the dykes are typical where they intrude olivine-rich country rocks.

Augite augen gabbro

The contact between the Halti cumulate sequence and the Ridnitsohkka gabbro sill unit to the east is marked by a distinctive and continuous gabbro horizon which varies between 20 and 50 m in thickness and is characterized by augite megacrysts. It shows gradational boundaries in both directions and several lenses of the same lithology are in fact present within the marginal part of the cumulate sequence. The augite megacryst gabbro appears to have formed by the replacement of troctolite, since relict troctolitic layering can still be discerned in places. Olivine has been partially consumed during the formation of the augite megacrysts, so that the latter

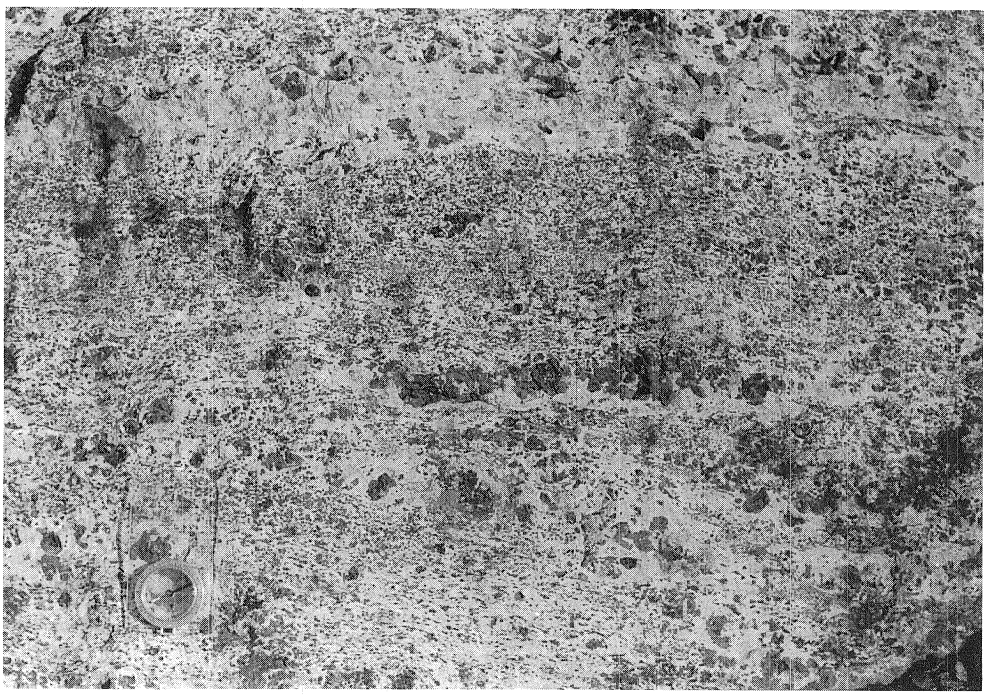

Fig. 8. Metasomatic augite augen gabbro replacing troctolite in contact zone between Halti cumulates and Ridnitsohkka gabbro sill unit. Augite megacrysts are surrounded by pale olivine-free rims. Locality 118, Halti.

are characteristically rimmed by a light colored zone devoid of olivine (Fig. 8). In general, particular layers of troctolite appear to have been altered to augite megacryst gabbro by the preferential growth of augite in olivine-rich layers. Alteration across troctolite layering has also apparently taken place, presumably due to the presence of early fractures. Augite megacrysts may be 5—7 cm across and are also present, though less abundant, within the Ridnitsohkka sill unit as well.

Due to intense shearing along the boundary zone between the Halti cumulates and the Ridnitsohkka sill unit, the augite megacryst gabbro has developed an augen texture. Due to the presence of disseminated sulfides (principally pyrrhotite), weathered surfaces of the augite augen gabbro are typically rusty. Gabbro pegmatoid dykes have not been found cutting across the augite augen gabbro.

Carbonate breccias

In the vicinity of the Finnish-Norwegian border the augite augen gabbros lying between the Halti cumulates and the Ridnitsohkka sill unit contain a number of carbonate breccia lenses several meters in thickness. Country rock in proximity to the breccias is strongly sheared, as are clasts in the breccia itself. Clasts consist predominantly of schistose augite gabbro and are up to one meter in diameter, set in a matrix of coarse-grained carbonate. A number of lenses of bluish quartz several meters thick are also present within the brecciated zone, which evidently represents the most intensely deformed part of the already mylonitic augite augen gabbro. Similar quartz- and carbonate-rich mylonite zones have been found along the basal contacts of ophiolite nappes (Davies, 1980).

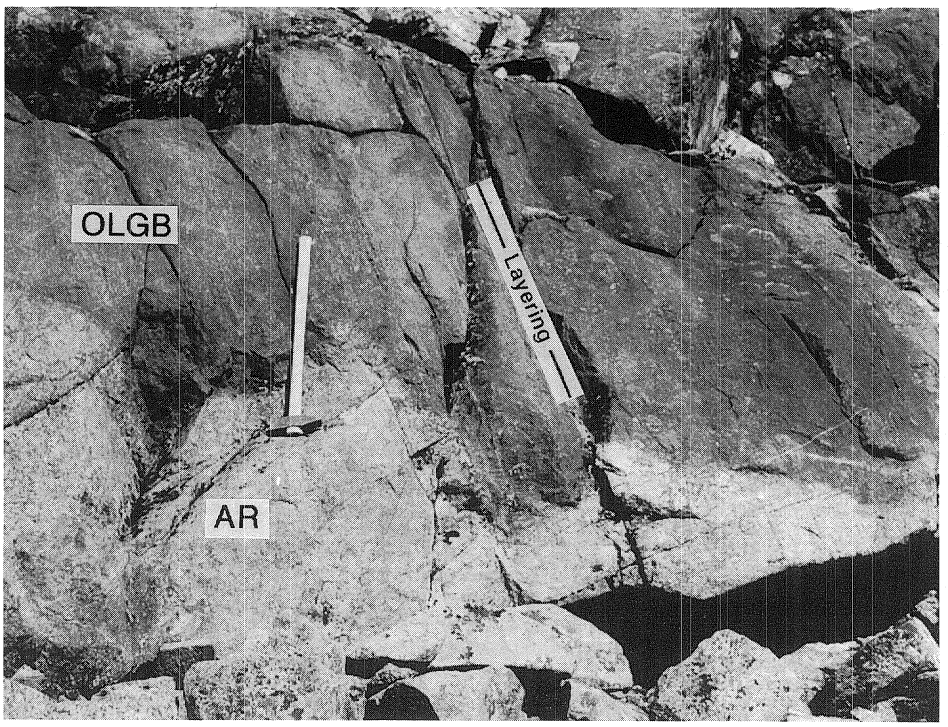

Fig. 9. Partial replacement of troctolite by amphibole rock; relict magmatic layering is still however, discernible. AR = amphibole rock, OLGB = olivine gabbro. Locality 41, Halti.

Amphibole rocks

Plagioclase-bearing lithologies in the western and central parts of the Halti cumulate sequence have been widely altered to amphibole rock. Amphibole rocks are also present in a narrow zone along the southeast margin and form the predominant rock type in the most southerly cumulate outlier (Fig. 2). Amphibole alteration truncates primary magmatic layering (Fig. 9), but nevertheless predates nappe emplacement since amphibole rocks are foliated only in proximity to the thrust surface. The degree of alteration is highly variable on a local scale, such that relict enclaves of unaltered rock are found within amphibole rock and conversely, amphibole rock may occur as narrow anastomosing seams in otherwise pristine country rock. The amphibole rocks weather to a greenish gray color and are thus readily distinguished in the field from other lithologies.

Along the western margin of the cumulate sequence, and also in the most southerly of the three outliers, amphibole rocks are in direct contact with the gneisses of the underlying Nabar Nappe and are intensely sheared, making precise determination of the contact difficult. The sheared amphibole rocks contain isolated concordant lenses, up to ten meters in length, of metatroctolite and metadunite which are elongate parallel to the thrusting direction. Further away from the basal contact the amphibole rock is massive and resembles a coarse-grained homogeneous gabbro.

Granitic dykes

Granites are most abundant in the contact metamorphic aureole of the Ridnitsohkka sill unit, although narrow alkali granite dykes are also present in the eastern and southern parts of the Halti cumulate sequence. A number of alkali granite dykes several cm in thickness have also been found within the central part of the Ridnitsohkka sill unit.

Ridnitsohkka gabbro sill unit

An extensive, clearly defined unit of gabbroic sills with gneiss interlayers outcrops to the east of the Halti cumulate sequence in Finland (Fig. 2) and can be followed beyond the confines of the study area at least as far as Guolasjavri, some 4 km northwest of the northernmost exposure of the Halti cumulates (Zwaan, pers. comm., 1989).

Gabbro sills

The trend of the Ridnitsohkka gabbro sills is effectively parallel to the eastern and northern margin of the Halti cumulate sequence and furthermore, gneiss interlayers between the sills dip everywhere between 20—50° towards the cumulates. The sills vary in thickness from several centimeters (Fig. 10) to many tens of meters and are generally homogeneous and even grained, although some plagioclase porphyritic variants have been noted. They usually display a weak foliation parallel to that in the enclosing gneisses, with the most intense deformation occurring in the contact zone with the Halti cumulates. No chilled margins have been found. A weakly developed rhythmic layering is also present in sills near the contact with the cumulates, along with a number of lenticular units several meters in thickness that contain graphite and disseminated sulfides, including pyrrhotite and pyrite.

Gneiss interlayers

Banded felsic garnet-sillimanite gneisses are common as concordant interlayers between, or fragments within the gabbro sills. They range in thickness from several centimeters up to tens of

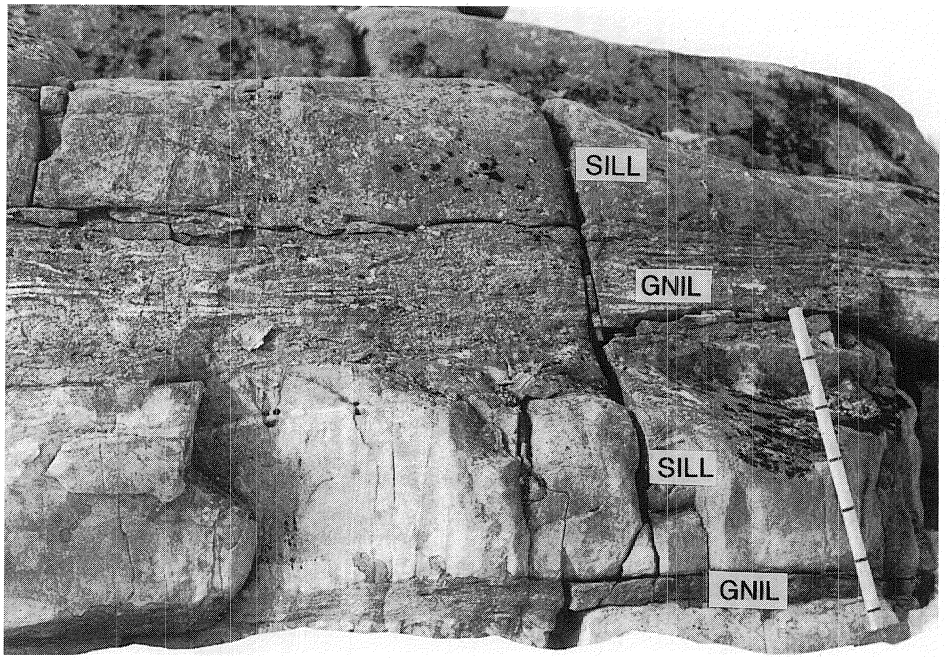

Fig. 10. Isoclinally folded gneiss interlayers between gabbro sills. SILL = gabbro sill, GNIL = gneiss interlayer. Locality 356, Ridnitsohkka.

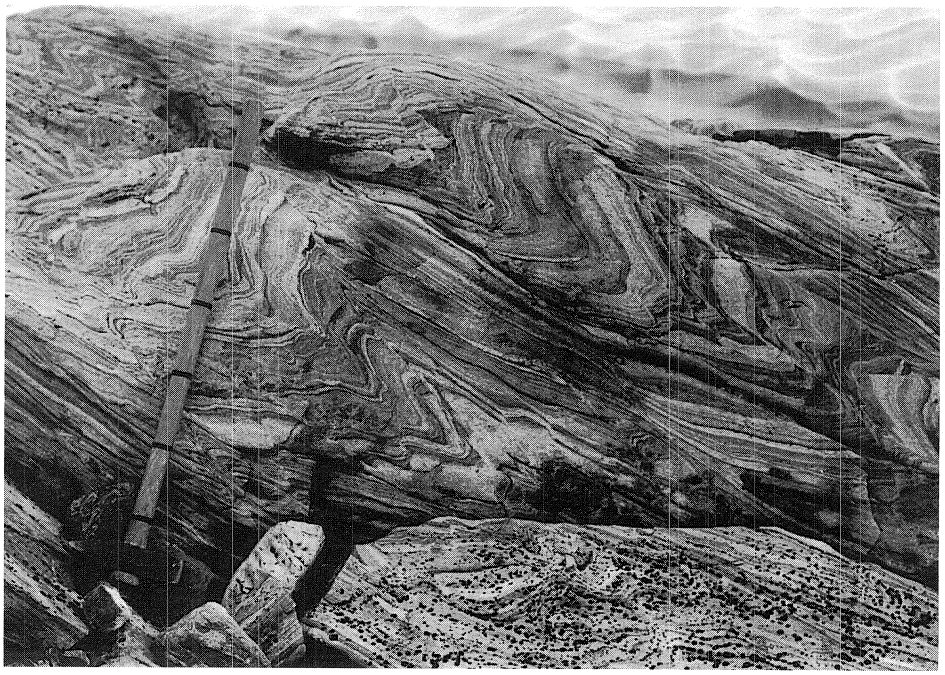

Fig. 11. Intensely folded garnet-biotite-muscovite gneiss in the outer part of the Ridnitsohkka contact metamorphic aureole. Small scale faulting is common and fold axial planes dip towards the sill area, approximately parallel to sill trend. Locality 504E, Ridnitsohkka.

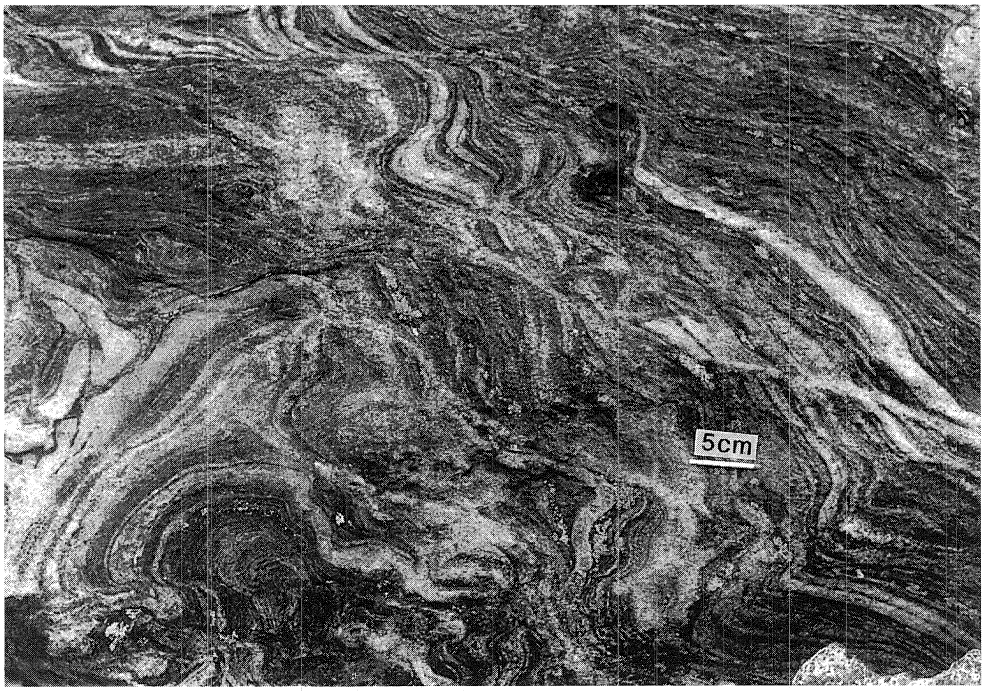

Fig. 12. Disharmonic folding of garnet-biotite-muscovite gneiss in Ridnitsohkka contact metamorphic aureole. Locality 504D, Ridnitsohkka.

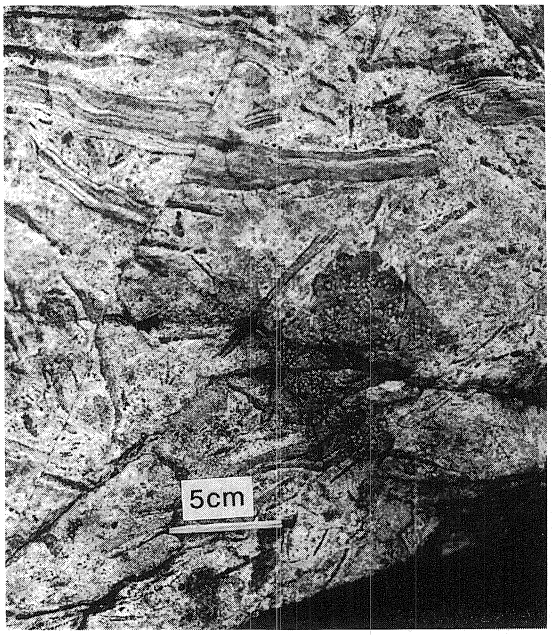

Fig. 13. Agmatite with platy and angular gneiss fragments in a granitic matrix. Locality 504C, Ridnitsohkka.

meters and commonly show intrafolial isoclinal folds with subhorizontal fold axes (Fig. 10). They are very uncommon near the Halti cumulates, but become progressively more abundant away from the contact, until they comprise up to 30—40 % of the sequence by volume. All primary features have been obliterated, so that the nature of their protolith remains uncertain. In addition to the dominant felsic compositions some narrow metabasalt and diopside skarn layers are present.

Contact metamorphic aureole

A contact metamorphic aureole is present in gneisses of the Nabar Nappe for a distance of up to 500 m from its contact with the Ridnitsohkka sill unit. The gneisses outside the aureole contain a garnet — biotite — muscovite assemblage and dip gently towards the sill area. In the outer part of the aureole however, the gneisses have been intensely folded (Fig. 11), with axial planes be-

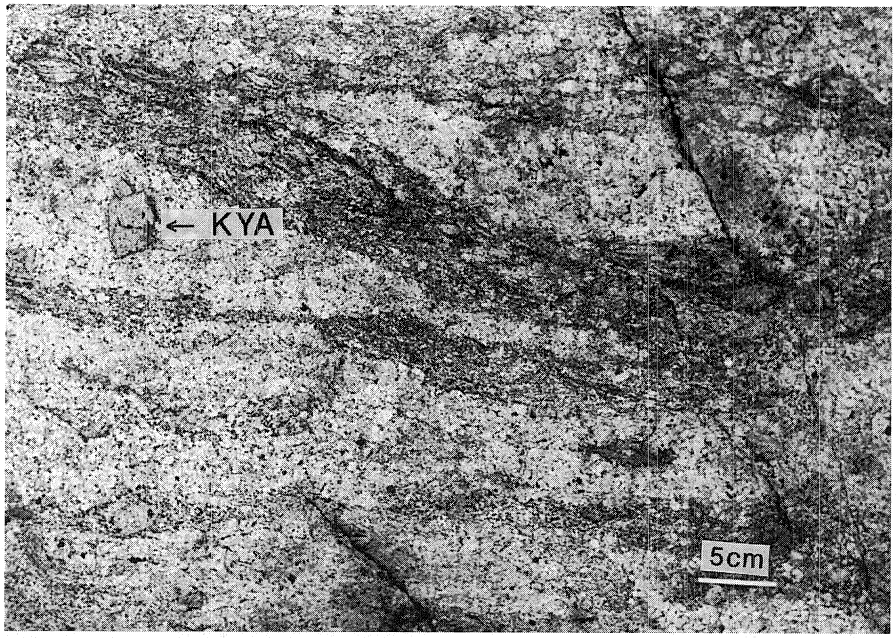

Fig. 14. Kyanite porphyroblasts in anatectic granite within Ridnitsohkka contact aureole. Strongly modified gneiss relicts are present as enclaves in granite. KYA = kyanite. Locality 504B, Ridnitsohkka.

ing subparallel to those within the isoclinally folded gneiss interlayers between Ridnitsohkka sills. Closer to the sill area the intensity of disharmonic folding increases, as does grain size and the degree of migmatization (Fig. 12), culminating in the development of lenses of anatectic granite several tens of meters thick. The innermost parts of the aureole are agmatitic, with a granitic matrix containing disoriented angular and platy fragments of gneiss (Fig. 13) and in some instances, almost wholly assimilated relict enclaves (Fig. 14). Both the granitic matrix and the gneiss fragments contain porphyroblasts of garnet and kyanite, crystals of the latter sometimes being 5—7 cm in length (Fig. 14).

TEXTURE

Halti cumulates

The most common minerals in the Halti cumulates are olivine, plagioclase, clinopyroxene and Cr-spinel. With the exception of olivine, which has to some extent been replaced by serpentine, they are effectively unaltered. Due to intense deformation, plagioclase twin lamellae may be distorted and deformation lamellae have formed in olivine. With increasing strain both plagioclase and olivine show the effects of grain size reduction and have dynamically recrystallized to fine-grained granular mosaics and olivine subgrains are separated by a ramifying network of serpentine. Many of these small olivine grains are optically contiguous, indicating that they are

relicts of larger phenocrysts that were originally up to 1 cm in diameter. Secondary metamorphic olivine forms coronas around ilmenomagnetite grains in the olivine gabbro and contains distinctly less Mg (Fo_{48}) than cumulus olivine in the same rock (Fo_{72}). The more strongly granulized dunites have apparently undergone further recrystallization, and may tend to contain less serpentine. Sulfide minerals are not common in either troctolites or dunites. Pentlandite is the most common phase but pyrrhotite, chalcopyrite and pyrite are also sporadically present, while olivine gabbros may additionally contain small amounts of cumulate ilmenomagnetite.

Intercumulus phases form only a minor proportion of the dunites and troctolites, so that according to the classification scheme of Irvine (1982), they may be regarded as either olivine — Cr-spinel or plagioclase — olivine — Cr-spinel adcumulates. In the olivine gabbros clinopyroxene is either a cumulus mineral, in which case the rock is a plagioclase — clinopyroxene — olivine adcumulate, or a poikilitic intercumulus phase, in which case the rock is a poikilitic plagioclase — olivine — orthocumulate.

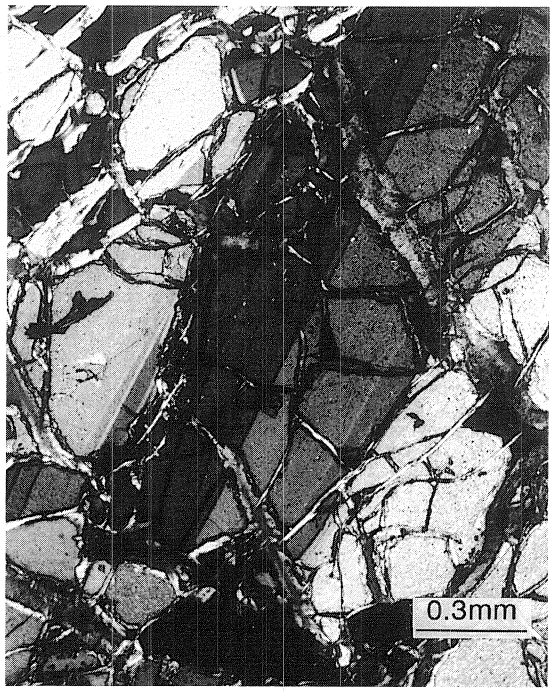

Fig. 16. Deformation lamellae in olivine in dunite. Sample 15, Halti.

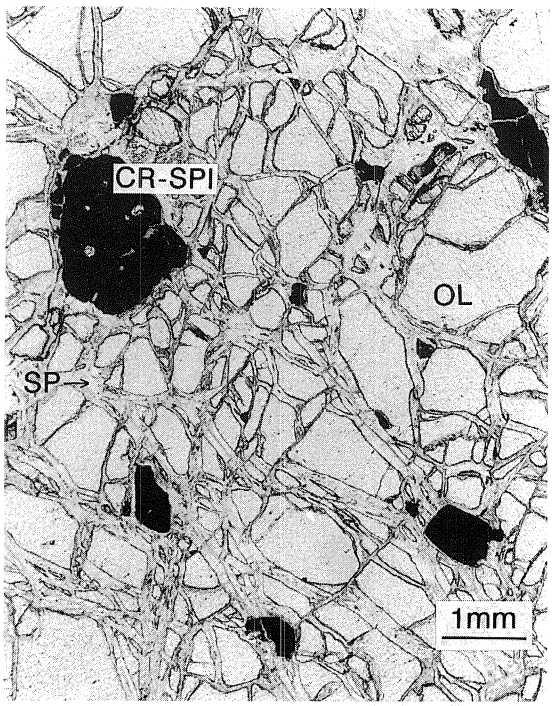

Fig. 15. Moderately serpentinized olivine — Cr-spinel cumulate (dunite). CR-SPI = Cr-spinel, OL = olivine, SP = serpentine. Sample 32, Halti.

Olivine and Cr-spinel occur as cumulus minerals in the dunites and plagioclase clearly forms an accessory intercumulus phase. Dunites have generally been somewhat serpentinized (Fig. 15), with serpentine typically comprising 20—40 % of the rock by volume. The larger olivine grains have deformation lamellae (Fig. 16). Cr-spinel is generally an accessory phase occurring either as subhedral to euhedral grains or inclusions within olivine. However it can also form massive layers of cumulus grains, either containing isolated olivine grains or alternating with layers of cumulus olivine (Fig. 17).

In the transition zone between dunite and troctolite, plagioclase abundances steadily increase,

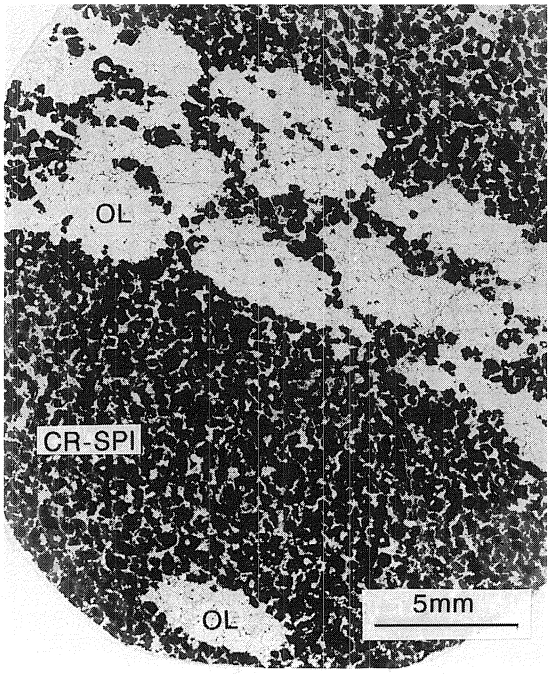

Fig. 17. Cr-spinel — olivine cumulate. Massive Cr-spinel layer is composed of small cumulate Cr-spinel grains and contains isolated grains of cumulate olivine. Olivine also forms massive layers. CR-SPI = Cr-spinel, OL = olivine. Sample 380, Halti.

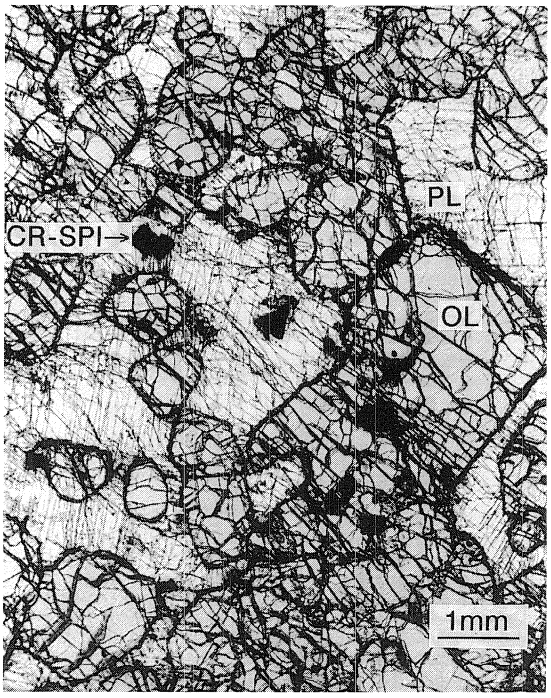

Fig. 18. Olivine — Cr-spinel cumulate with intercumulus plagioclase (troctolite). CR-SPI = Cr-spinel, OL = olivine, PL = plagioclase. Sample 154, Halti.

although at first it is an intercumulus phase (Fig. 18). At higher levels in the troctolites and in the olivine gabbros however it is clearly a cumulus mineral. Troctolites also contain cumulus Cr-spinel and olivine, although the latter tends to form ramifying networks enclosing plagioclase laths and may thus be considered as an intercumulus phase (Fig. 19). A similar kind of 'amoeboid' structure is evidently ubiquitous in troctolites of the Stillwater Complex (McCallum et al., 1980) and has been attributed to the breakdown and subsequent recrystallization of cumulus oli-

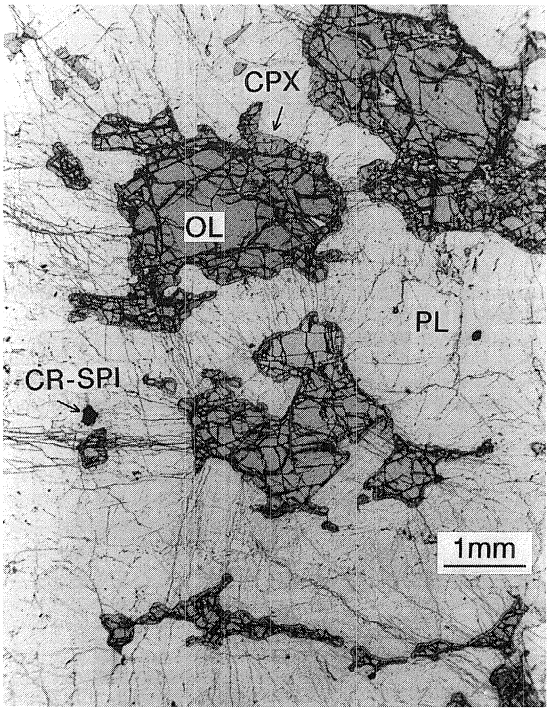

Fig. 19. Plagioclase — olivine — Cr-spinel cumulate (troctolite), with a small amount of intercumulus clinopyroxene. Note amoeboidal structure (McCallum et al. 1990), where ramifying protusions of olivine have grown between plagioclase grains. A narrow corona between olivine and plagioclase is also present. CPX = clinopyroxene, CR-SPI = Cr-spinel, OL = olivine, PL = plagioclase. Sample 72, Halti.

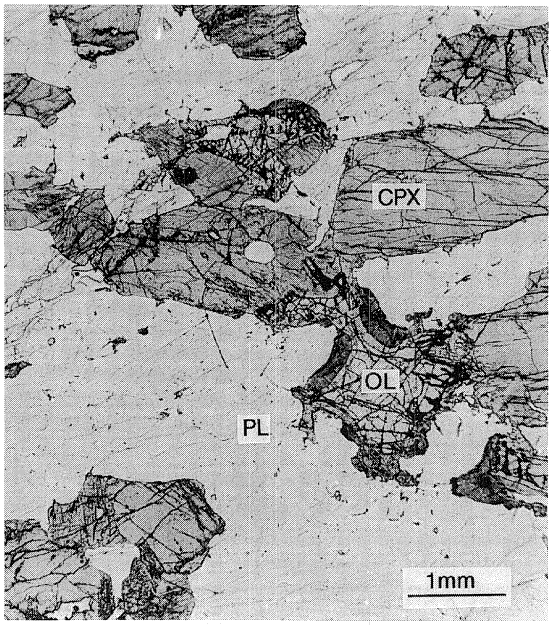

Fig. 20. Plagioclase — clinopyroxene — olivine cumulate (olivine gabbro) showing distinct coronas between olivine and plagioclase grains. CPX = clinopyroxene, OL = olivine, PL = plagioclase. Sample 50, Halti.

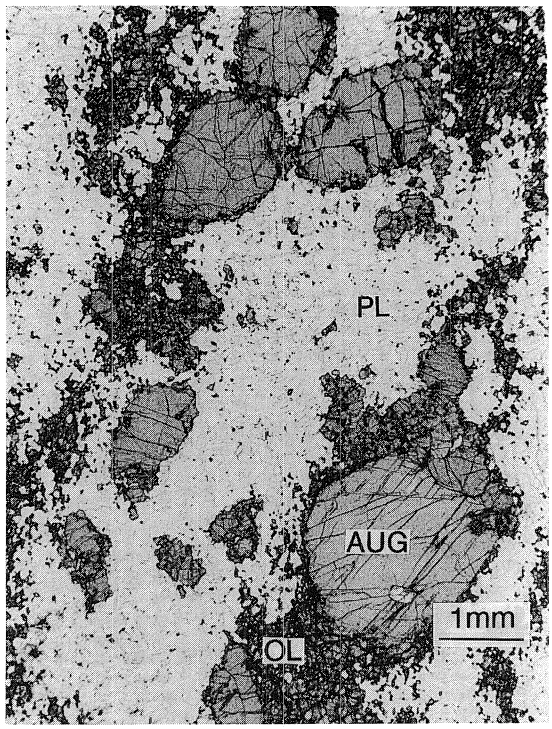

Fig. 22. Augite augen gabbro in which augite is well preserved but olivine and plagioclase are strongly granulized. AUG = augite, OL = olivine, PL = plagioclase. Sample 22A, Halti-Ridnitsohkka contact zone.

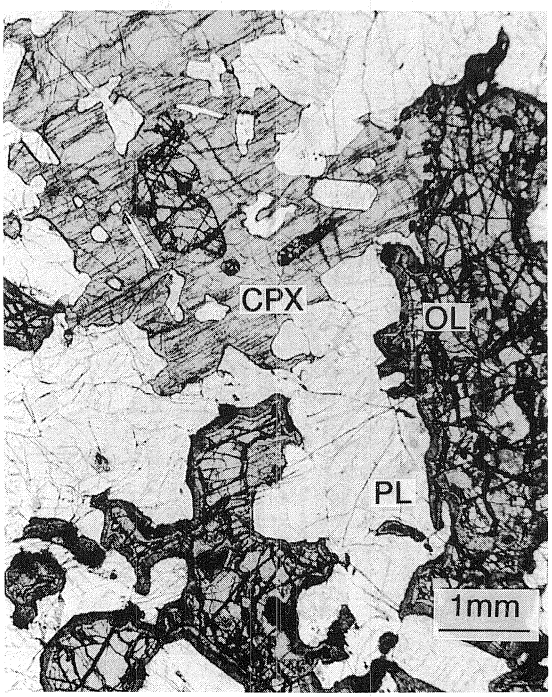

vine grains. Thin films of intercumulus augitic clinopyroxene are also characteristic along olivine and plagioclase grain boundaries in troctolites. Corona textures are invariably present between plagioclase and olivine grains and in some instances may have developed to such an extent that one or other of the phases has been totally consumed.

In the olivine gabbros, clinopyroxene is generally a cumulus phase, along with plagioclase and olivine (Fig. 20). However textures similar to

Fig. 21. Plagioclase — olivine cumulate containing poikilitic clinopyroxene (olivine gabbro). Olivine and plagioclase are distinctly smaller where present as inclusions in clinopyroxene than elsewhere in the rock. A double corona is clearly developed between olivine and plagioclase grains. CPX = clinopyroxene, OL = olivine, PL = plagioclase. Sample 147, Halti.

those in the troctolites are also present, with clinopyroxene, olivine and plagioclase occurring as cumulus grains. Olivine typically has a ramifying amoeboid structure, while clinopyroxene is also as thin films between olivine and plagioclase grains. Olivine gabbros in the stratigraphically highest parts of the cumulate sequence contain poikilitic clinopyroxene, enclosing small cumulus grains of plagioclase and olivine (Fig. 21). Cr-spinel has not been found in the olivine gabbros, the only oxide phase present being ilmenomagnetite.

Augite in the augite augen gabbro is clearly coarser grained and better preserved than other minerals, even where the rock is highly strained (Fig. 22). Some large augite megacrysts contain inclusions of relict olivine.

Ridnitsohkka gabbro sills

The principal primary minerals in the Ridnitsohkka sills are plagioclase, clinopyroxene, orthopyroxene, biotite and amphibole. Clinopyroxene in the sills characteristically shows orthopyroxene exsolution lamellae along (100) planes, whereas no such features were observed in pyroxenes from the Halti cumulates. Ilmenite, apatite and zircon are typical as accessory minerals. Sulfides are rare and consist almost entirely of pyrrhotite, with only minor amounts of pyrite and chalcopyrite.

Microscopically, textures of the sills appear to be equigranular and massive (Fig. 23), porphyritic types containing plagioclase phenocrysts being rather rare (Fig. 24).

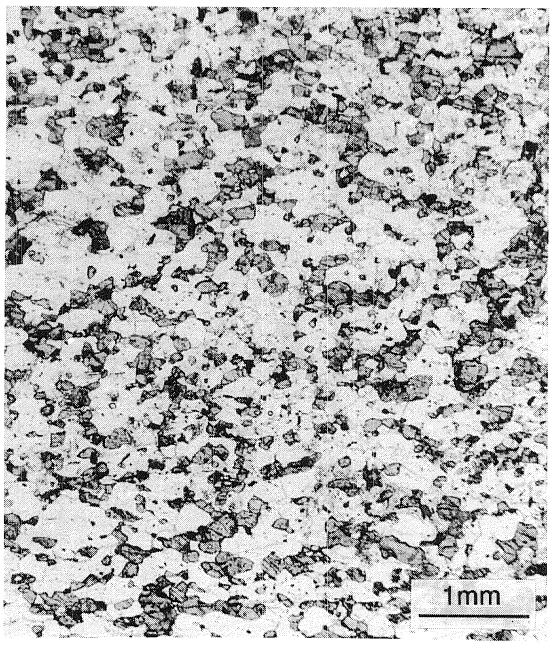

Fig. 23. Equigranular plagioclase — orthopyroxene — clinopyroxene — ilmenite assemblage in gabbro sill. Sample 26, Ridnitsohkka.

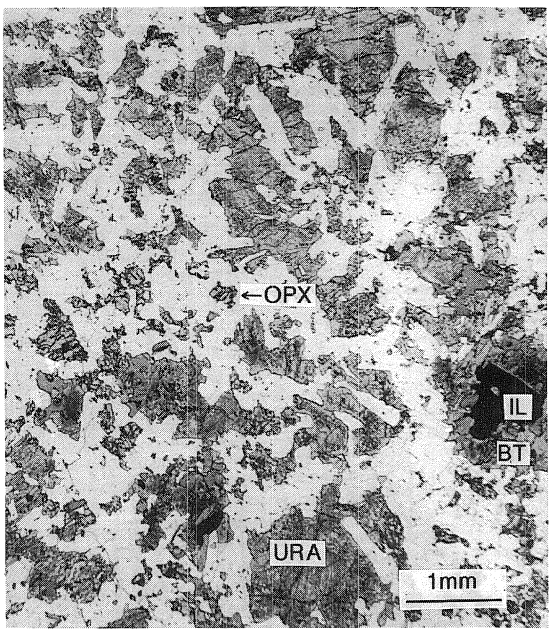

Fig. 24. Gabbro sill containing plagioclase phenocrysts. Poikilitic clinopyroxene has been altered to to uralite and biotite reaction rims surround ilmenite grains. BT = biotite, IL = ilmenite, OPX = orthopyroxene, URA = uralite. Sample 89, Ridnitsohkka.

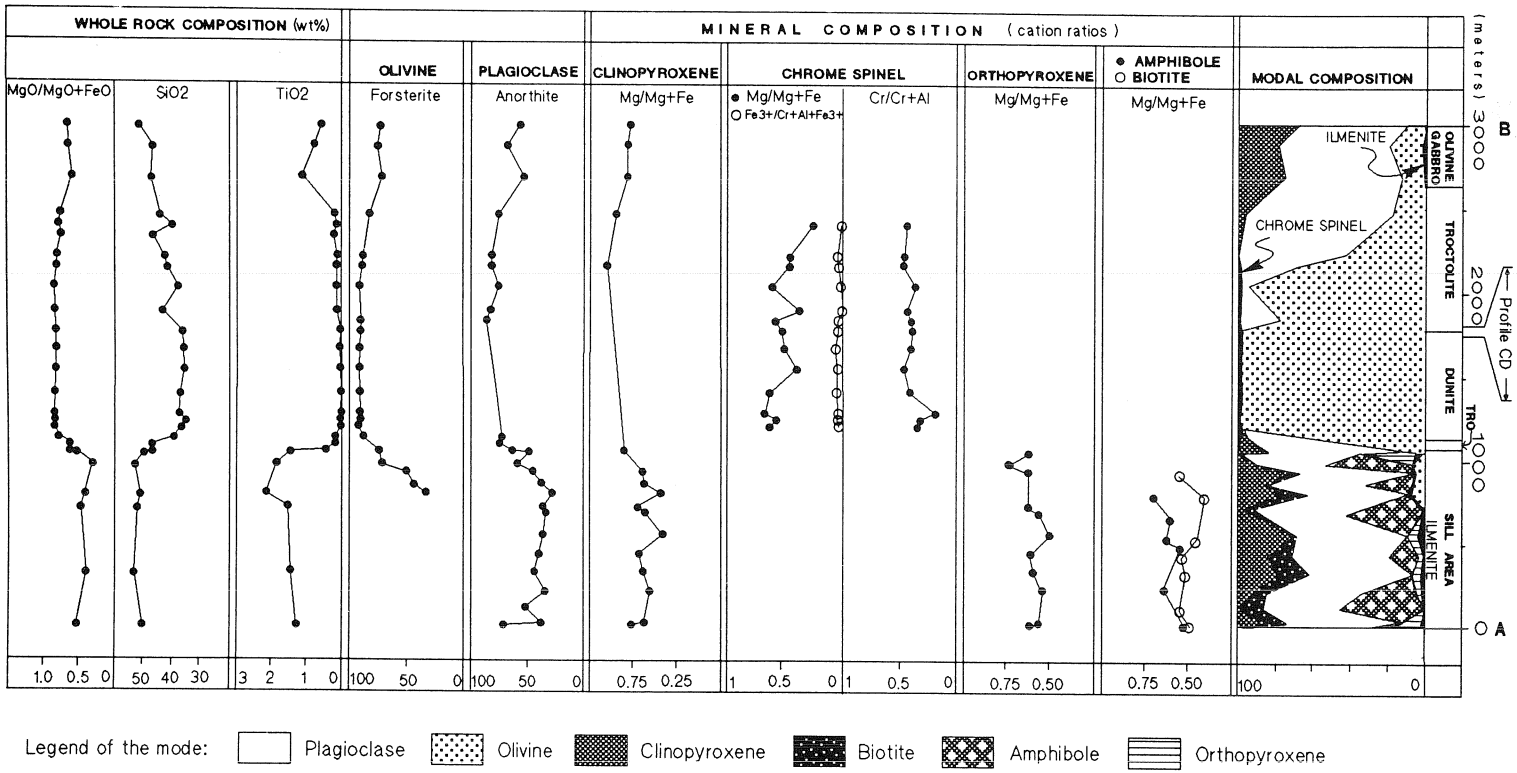

Fig. 25. Variation of the whole rock (wt%), mineral (olivine and plagioclase in mol%; other cation ratios) and modal compositions in the Ridnitsohkka and Halti areas. Location of line AB is shown in Fig.2. For profile CD, see Fig.26.

MINERAL CHEMISTRY

Olivine

Olivines in the Halti cumulates are typically Mg-rich (Appendix 1), with compositions of Fo_{90-92} in dunites, Fo_{76-92} in the troctolites, Fo_{72-82} in olivine gabbros and Fo_{69-82} in the pegmatitic gabbro dykes (Figs. 25, 26). The pegmatitic gabbro dykes have caused a lowering of forsterite contents in country rocks immediately adjacent to their contacts (Appendix 1, sample 31). Cumulus olivine in the massive Cr-spinel horizons has an exceptionally high Mg content of Fo_{92-93}. The lowest forsterite values for the Halti cumulates are Fo_{63-72} in the augite augen gabbro. The unusually high Fo-values of olivines in the Cr-spinel layers may be ascribed to post-cumulus or even subsolidus processes. Cameron (1975) for example observed that the Mg/Fe ratio in olivine as well as Cr-spinel increases sympathetically with increasing modal abundances of Cr-spinel. Lehmann (1983) has demonstrated that during subsolidus diffusion between olivine and Cr-spinel, Mg and Ni migrate preferentially from Cr-spinel into olivine, whereas the converse applies to Fe and Mn. The compositions of individual olivine grains in the Halti cumulates

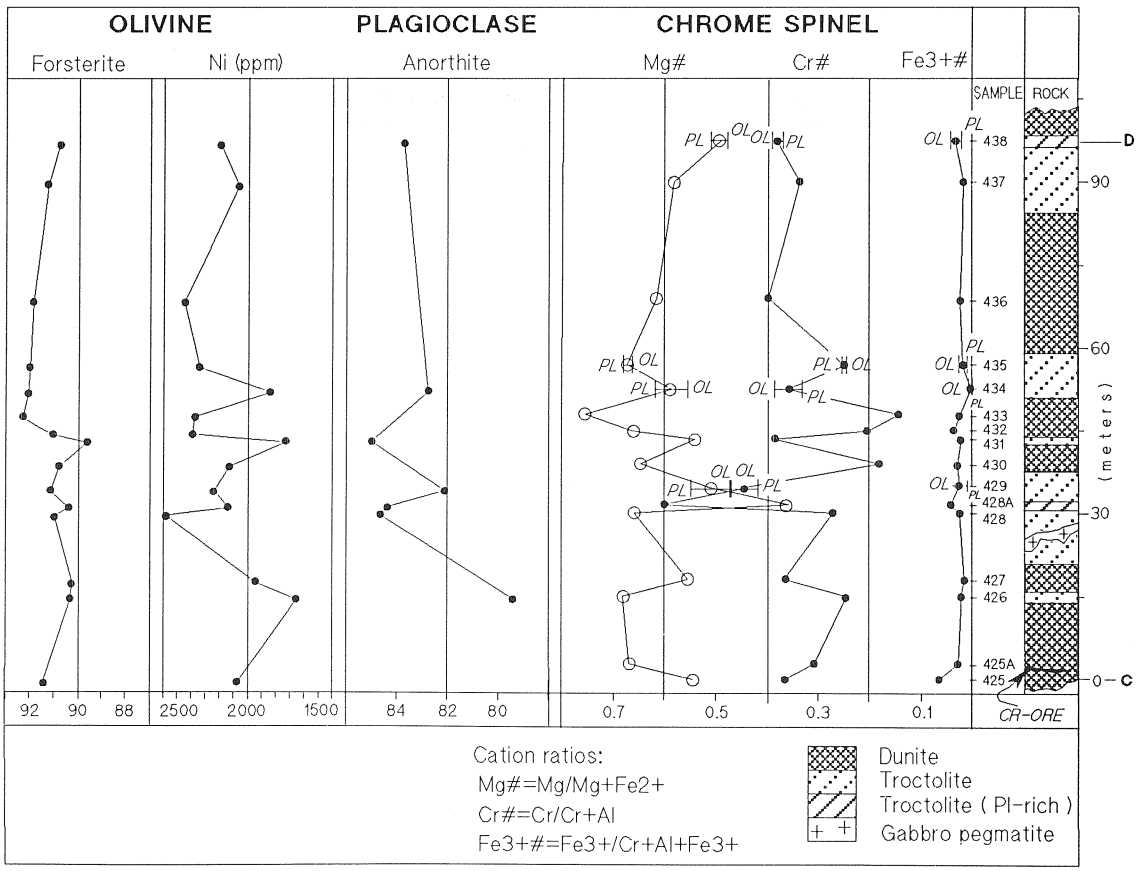

Fig. 26. Variation in olivine (mol%), plagioclase (mol%) and chrome spinel (cation ratios) compositions along profile CD, across the contact zone between dunite and troctolite. See also Fig.25. Compositions of chrome spinel inclusions in plagioclase (PL) and in olivine (OL) in the same sample are shown.

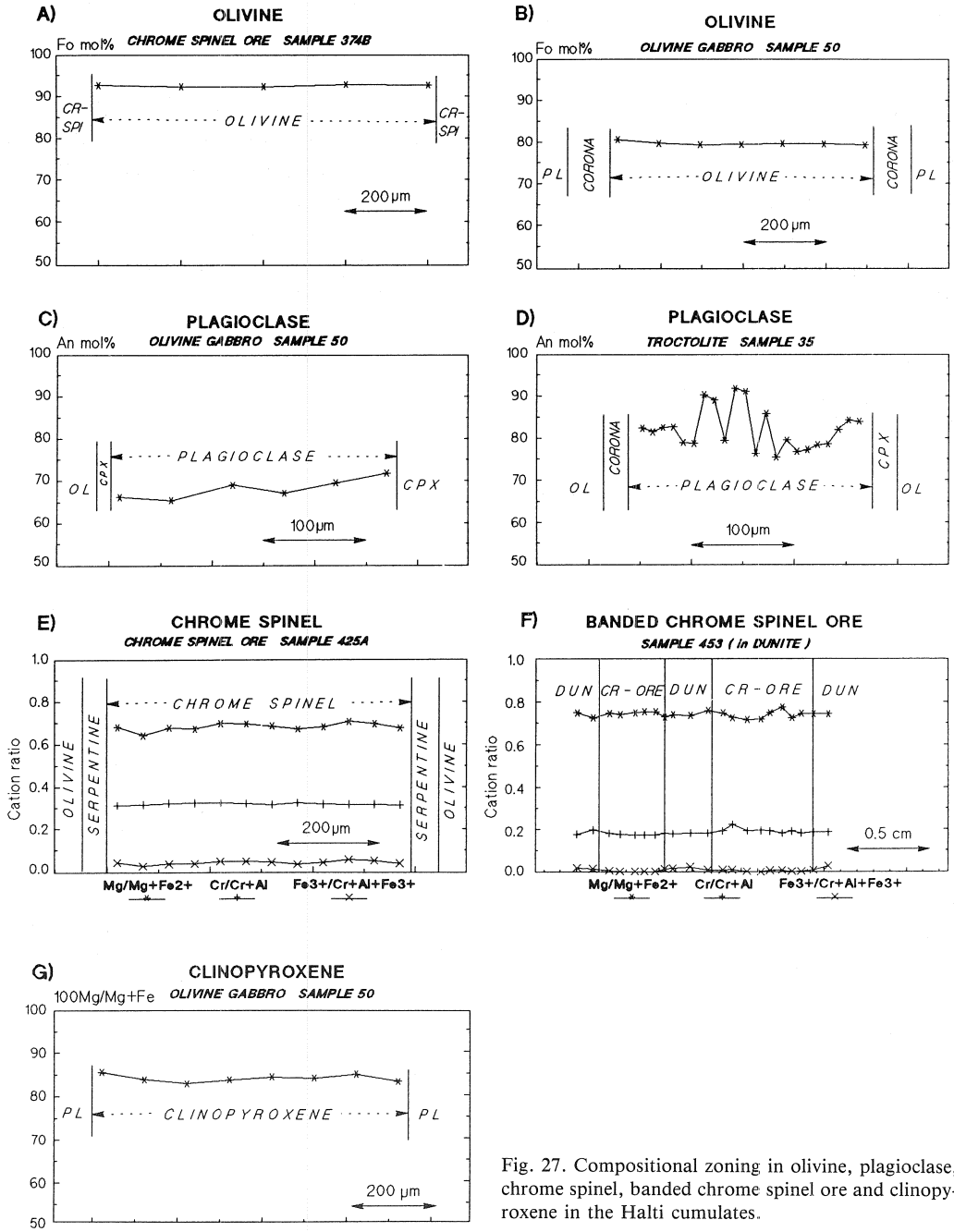

Fig. 27. Compositional zoning in olivine, plagioclase, chrome spinel, banded chrome spinel ore and clinopyroxene in the Halti cumulates.

have evidently homogenized under subsolidus conditions since there is no evidence for compositional zoning (Figures 27a, 27b, Table 1).

The Ni contents of olivines in the dunites and troctolites is around 1500—2500 ppm but falls rapidly with decreasing Fo-values (Fig. 28). In the olivine gabbro olivines Ni abundances are independent of Fo-values and are distinctly less than 1000 ppm. The presence of even a small amount of sulphide melt significantly reduces the abundance of chalcophile elements in silicate magmas since they are preferentially incorporated into the sulfide melt (Duke and Naldrett, 1978). The rapid decrease in Ni content in olivines in the Halti cumulates thus indicates that sulphide melt was present in the magma during the crystallization of the dunites and troctolites. Although there are no major concentrations of massive sulfides in these cumulates, disseminated pentlandite is present, particularly in the dunites.

Mn abundances in olivine show a positive correlation with Fe such that Mn is at its lowest

Table 1. Compositional zoning in olivine, plagioclase and chrome spinel from the Halti area. Dm = grain diameter in μm. Cation ratios: Mg # = Mg/Mg + Fe2 +, Cr # = Cr/Cr + Al and Fe3 + # = Fe3 + /Cr + Al + Fe3 +.

OLIVINE

Sample	Dm	Lithology		Fo
374B	800	Chromitite	Rim	92.6
			Core	92.3
			Rim	92.6
154	800	Troctolite	Rim	89.9
			Core	89.9
			Rim	89.8
39	700	Troctolite	Rim	82.6
			Core	82.7
			Rim	83.2
51	60	Troctolite	Rim	78.2
			Core	77.7
			Rim	77.3
43	1000	Olivine gabbro	Rim	73.8
			Core	74.1

PLAGIOCLASE

Sample	Dm	Lithology		An
39	1600	Troctolite	Rim	76.6
			Core	75.3
			Rim	75.2
51	80	Troctolite	Rim	65.8
			Core	66.1
			Rim	67.5
426	700	Troctolite	Rim	80.8
			Core	81.2
			Rim	79.8
43	650	Olivine gabbro	Rim	67.9
			Core	69.6
			Rim	66.6

CHROME SPINEL

Sample	Dm	Lithology		Mg#	Cr#	Fe3+#
15	500	Dunite	Rim	0.65	0.38	0.06
			Core	0.65	0.38	0.05
			Rim	0.60	0.41	0.05
20	300	Dunite	Rim	0.51	0.37	0.07
			Core	0.50	0.38	0.08
49	300	Troctolite	Rim	0.37	0.58	0.02
			Core	0.36	0.56	0.05
			Rim	0.38	0.56	0.03
154	300	Troctolite	Rim	0.55	0.38	0.05
			Core	0.56	0.39	0.06
			Rim	0.56	0.37	0.03
31	300	Gabbro pegmatite	Rim	0.37	0.42	0.09
			Core	0.37	0.41	0.07
			Rim	0.37	0.41	0.10
21	130	Amphibole rock	Rim	0.26	0.44	0.02
			Core	0.28	0.42	0.02
			Rim	0.24	0.44	0.01

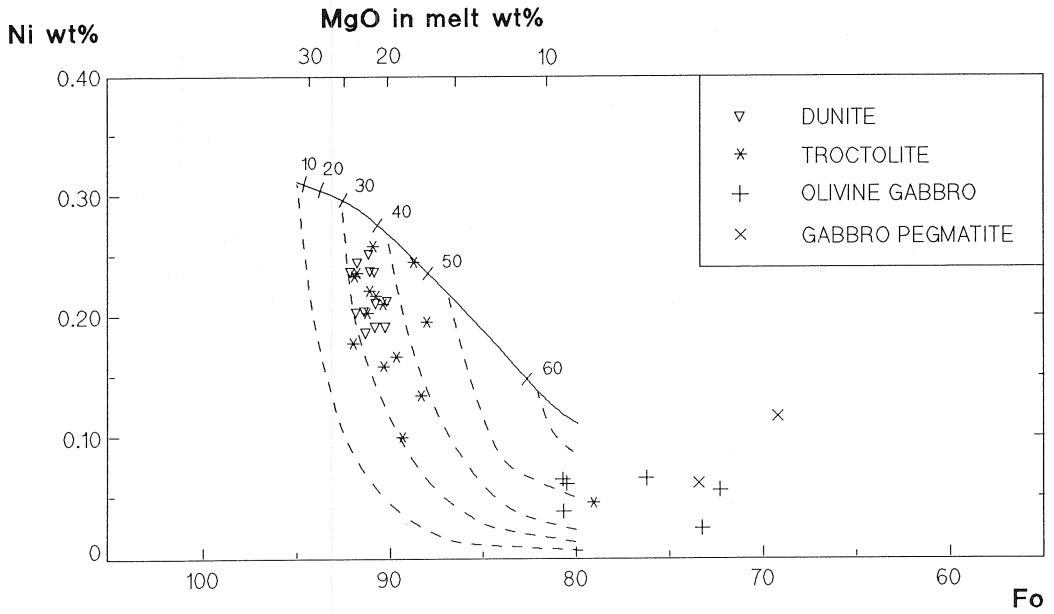

Fig. 28. Variation of nickel with forsterite in olivines from Halti cumulate rocks. Compositions of fractionating olivine for sulfide-undersaturated case (solid curve) and for sulfide saturated case (dashed curves) where silicate liquid becomes saturated at various MgO concentrations are shown. Numbers on solid curve indicate mol% olivine fractionation. Modified from Duke & Naldrett (1978).

in the dunites (<0.12 wt% MnO) and highest in the pegmatitic gabbro dykes (0.35—0.40 wt% MnO). The Ca content of olivine in the Halti cumulates is generally low, and typically less than 0.1 wt% CaO, if not below detection limits. This positive correlation between Mn and Fe and relatively low Ca content is typical of magmatic olivine (Simkin and Smith, 1970).

During the recrystallization of olivine, primary structures are obliterated and compositions become progressively more forsteritic, although these differences are not usually detectable at the initial stages of the process (Hoffman and Walker, 1978). Recrystallization at Halti has generally not resulted in the destruction of cumulus olivine, neither has the composition altered significantly during metamorphism. This is also apparent from the Ni vs. Fo diagram (Duke and Naldrett, 1978) for olivine from the Halti cumulates, on which the variations in Ni content closely resemble those of the magmatic trend (Fig. 28).

Olivine in the Ridnitsohkka sills shows an opposite trend and more rapid change in composition compared to that in the Halti cumulates, with values ranging from Fo_{35-72}. This is clearly evident from the olivine variation diagram in Fig. 25 and also in Fig. 29. Manganese contents are distinctly higher than in olivines from the Halti cumulates, at around 0.50—0.94 wt% MnO but Ca contents in olivines from the Ridnitsohkka sills are low, just as in the cumulate olivines.

Chrome spinel

The compositions of Cr-spinels from the Halti cumulates are given in Appendix 2. Low $Cr/Cr+Al$ and $Mg/Mg+Fe^{2+}$ ratios and low Fe^{3+} abundances are typical for the Halti cumu-

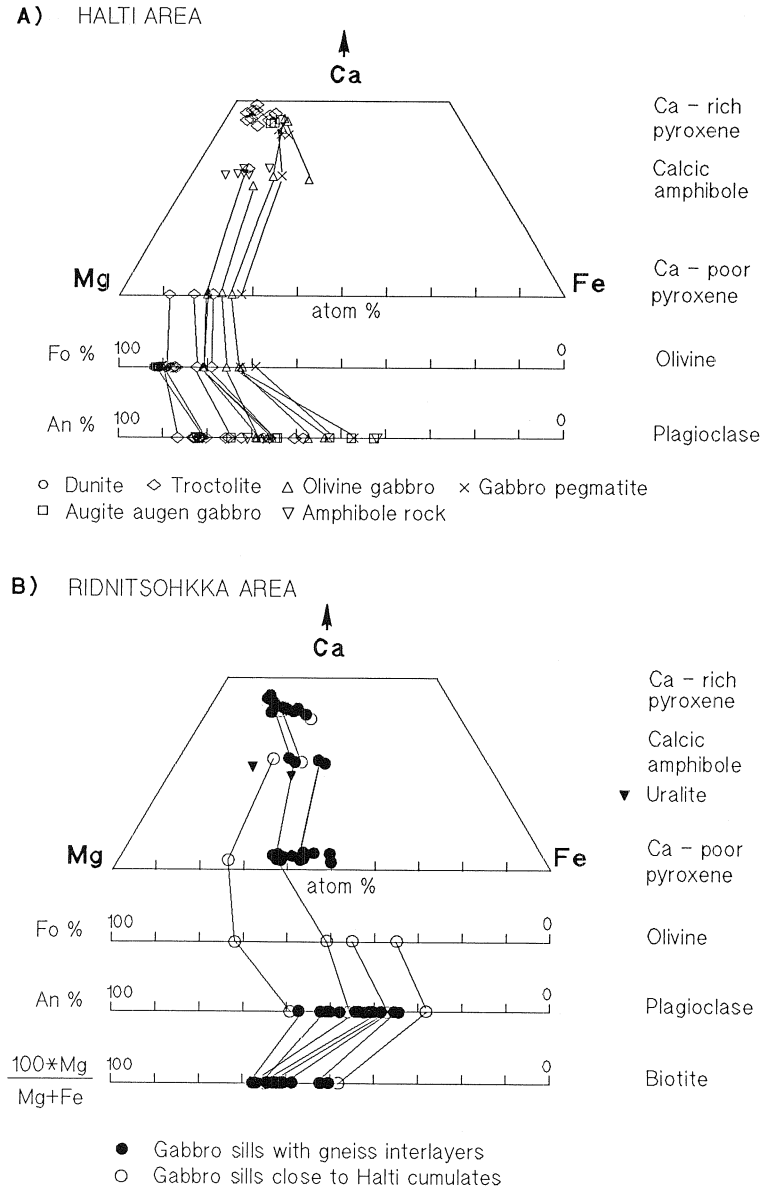

Fig. 29. Compositional variations of the major coexisting silicates in the Halti-Ridnitsohkka igneous rocks.

late Cr-spinels and they tend to plot towards the Cr-Al side of the Cr-spinel field on the Cr-Al-Fe^{3+} triangular diagram (Fig. 30a). The lowest Cr abundances in Cr-spinels are found in the dunites and the highest in the troctolites, although some overlap does occur. The massive Cr-spinel layers are Al-rich and there is no tendency for Fe^{3+} abundances to increase with increasing Cr. The Fe^{3+} contents of Cr-spinels in the amphibole rock are also consistently rather low and, because Fe^{3+} is sensitive to alteration (Hoffman and Walker, 1978), presumably indi-

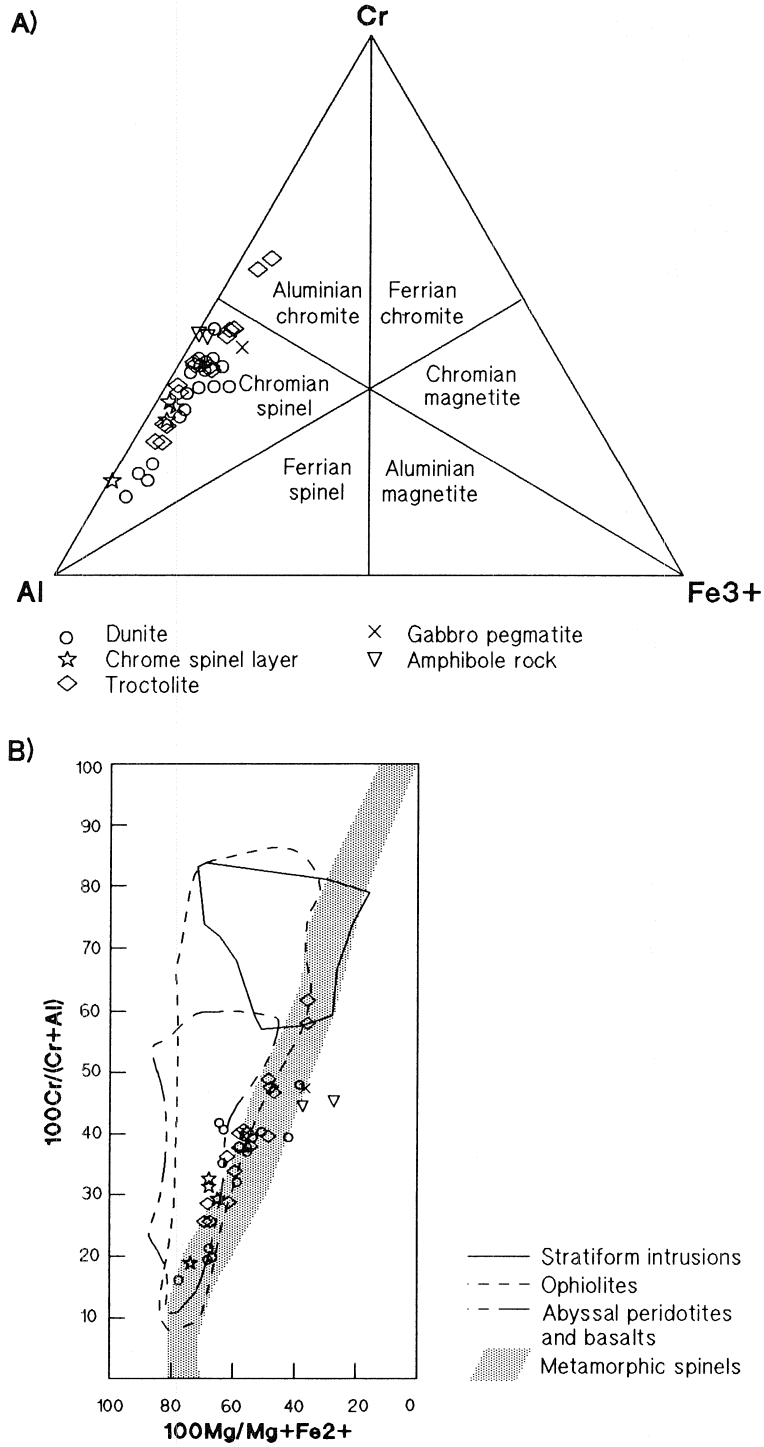

Fig. 30. (A) Atomic proportions of Cr,Al and Fe^{3+} for chrome spinels from the Halti area. (B) Chrome spinel compositions in the Halti area, with compositional fields after Pober & Faupl (1988). Fe^{2+} and Fe^{3+} are calculated from total Fe by assuming spinel stoichiometry.

cate that there have been no major changes in composition. The low Cr/Cr + Al and Mg/Mg + Fe^{3+} ratios of the Halti Cr-spinels are readily apparent from Fig. 30b, with data points falling along the boundary between the metamorphic and ophiolitic fields.

There is no compositional zoning within individual Cr-spinel grains in the Halti cumulates (Fig. 27e, Table 1). Neither do spinels in the massive Cr-spinel layers or the olivine-rich layers show significant differences in composition. Figure 27f nevertheless does show that the massive Cr-spinel layers have slightly higher Mg/Mg + Fe^{2+} ratios and lower Fe^{3+}/Cr + Fe^{3+} ratios when compared to Cr-spinel layers containing cumulus olivine. A similar compositional change is also apparent in Cr-spinel grains occurring as inclusions in plagioclase and olivine in the troctolites, with inclusions in olivine tending to have slightly lower Mg/Mg + Fe^{3+} ratios and conversely, higher Fe^{3+}/Cr + Al + Fe^{3+} ratios (Fig. 26). This phenomenon may be attributed to subsolidus diffusion between olivine and plagioclase, as Lehmann (1983) has experimentally demonstrated.

Plagioclase

Plagioclase compositions in the Halti cumulates become distinctly more albitic as differentiates become more felsic (Fig. 25, Appendix 3). Anorthite contents are highest in the intercumulus plagioclase occurring in the transition zone between the troctolites and the underlying dunites, being around An_{73-86}. In the olivine gabbros values range from An_{54-68} and in the pegmatitic gabbro dykes from An_{47-53}. Anorthite contents in the augite augen gabbro vary considerably, from An_{43-75}, as do those of the amphibole rocks ranging from An_{42-83}. The anorthite contents of plagioclase in the Ridnitsohkka gabbro sills are clearly lower (An_{28-60}) than in the cumulate lithologies, and in both cases the overall trends are similar to respective changes in Mg/Fe ratios in olivines and clinopyroxenes (Fig. 25). An contents fall gradually at first until the olivine-bearing sills, after which the trend is reversed and values increase rapidly towards the contact with the Halti cumulates. This wide variation in plagioclase compositions in both the Halti cumulates and the Ridnitsohkka gabbro sills is well displayed in Figs. 29a and 29b.

Plagioclase compositions vary markedly in the transition zone between the dunite and troctolite units (Fig. 26). Individual plagioclase grains also show compositional zoning (Figs. 27c, 27d, Table 1). Although in some instances distinct, this zoning is typically weak, with An contents increasing towards the cores.

Clinopyroxene

The clinopyroxenes present in the cumulates consist of diopside and Ca-rich augite (Appendix 4). Mg/Mg + Fe ratios are highest in intercumulus clinopyroxenes in the troctolites and lowest in clinopyroxenes in the pegmatitic gabbro dykes (Fig. 29a). The overall range in composition is nevertheless relatively limited, En values in the troctolite clinopyroxenes varying between En_{44-48}, compared with En_{43-44} for the clinopyroxenes from pegmatitic gabbro dykes. In both the troctolites and the olivine gabbros the Mg/Mg + Fe ratio for clinopyroxenes decreases

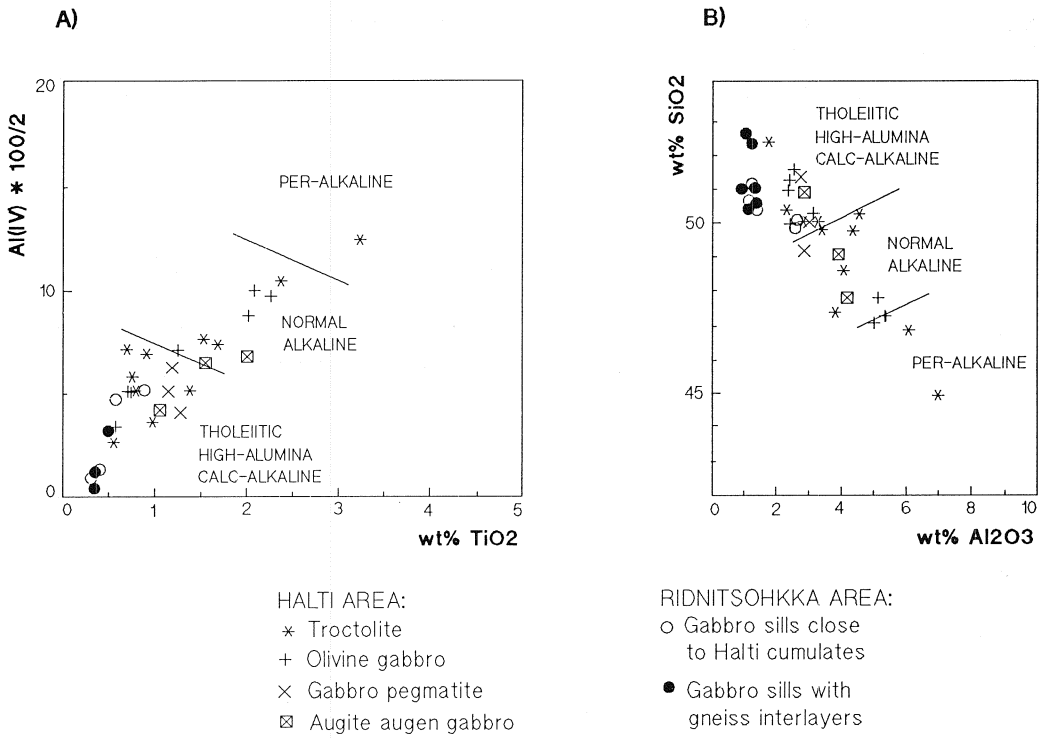

Fig. 31. Clinopyroxene compositions for the Halti and Ridnitsohkka rocks. Compositional fields are from LeBAS (1962).

in a linear fashion (Fig. 25), while in the augite augen gabbro, En values for clinopyroxenes are approximately the same as those in the pegmatitic gabbro dykes, varying between En_{42-45}. In the Ridnitsohkka sills, clinopyroxene is present as Ca-rich augite having En values between En_{35-43}, and is markedly richer in Fe than that in the Halti cumulates. Mg/Mg+Fe ratios in clinopyroxenes are variable in the gabbro sills containing gneiss interlayers, but then show a steady linear increase in olivine sills approaching the contact with the Halti cumulates. Clinopyroxenes within the metabasaltic interlayers have high En values, between En_{44-48}. Clinopyroxenes within the cumulates have consistently higher Al_2O_3, Cr_2O_3 and TiO_2 than those in the sills, although clinopyroxenes in sills nearer the cumulates do tend to be somewhat transitional in composition. There is no significant systematic difference in TiO_2 and Al_2O_3 abundances between the cumulus and intercumulus clinopyroxene phases within the Halti cumulates. This contrasts with Cr_2O_3, which has higher abundances in troctolite intercumulus clinopyroxenes than in the olivine gabbro cumulates. This is a consequence of the melt having been strongly depleted in Cr due to the crystallization of Cr-spinel as a cumulus phase during the formation of the dunite and troctolite units.

Kushiro (1960) and LeBAS (1962) showed that the Al and Ti contents of clinopyroxene decrease as the SiO_2 content of a magma increases. This is clearly evident in the Halti and Ridnitsohkka clinopyroxenes. On the diagrams of LeBAS (1962), the Ridnitsohkka clinopyroxenes all fall within the non-alkaline field (Fig. 31), whereas

the Halti clinopyroxenes plot in both the non-alkaline and alkaline fields, with a few samples lying in the peralkaline side as well.

Internal compositional zoning within individual cumulate clinopyroxene grains is neither common nor well developed (Fig. 27g).

Orthopyroxene

Primary orthopyroxene is only present within the Ridnitsohkka gabbro sills; in the Halti cumulates it is secondary, occurring in coronas as a result of reactions between olivine and plagioclase. Corona orthopyroxenes in the cumulates have high En values (En_{72-89}) and low Wo values, being everywhere below $Wo_{1.3}$, contrasting with respective values of En_{49-62} and Wo_{2-3} for the primary Ridnitsohkka orthopyroxenes (Appendix 5). These differences are clearly shown in Figs. 30a and 30b. The highest Mg/Mg + Fe ratios in the Ridnitsohkka orthopyroxenes occur in the olivine-bearing sills nearest the Halti cumulates. Compositional changes are not linear (Fig. 25). Comparisons between the compositions of orthopyroxenes in the sills and metamorphic pyroxenes in the intervening remnants of country rock gneisses are made in a subsequent section, dealing with metamorphism.

Amphibole

Primary amphibole has only been recorded from the Ridnitsohkka gabbro sills and is pargasitic in composition (Fig. 32, Appendix 6). The Mg/Mg + Fe ratio of the primary amphiboles in the sill area increases gradually towards, and is at its highest, in the olivine-bearing sills (Fig. 25). Primary amphibole differs compositionally from secondary amphibole in its higher TiO_2 and K_2O abundances, an observation also made by Augé (1987) when studying cumulates in the Oman ophiolite.

The secondary amphiboles in the Halti cumulates are compositionally distinct from those occurring in the Ridnitsohkka sills (Fig. 32), the uralitic amphibole in the sills being hornblende, whereas that in the amphibole rock in the Halti cumulates is Fe-tchermackite. The amphibole in the corona between plagioclase and olivine grains is anomalously high in Al (IV).

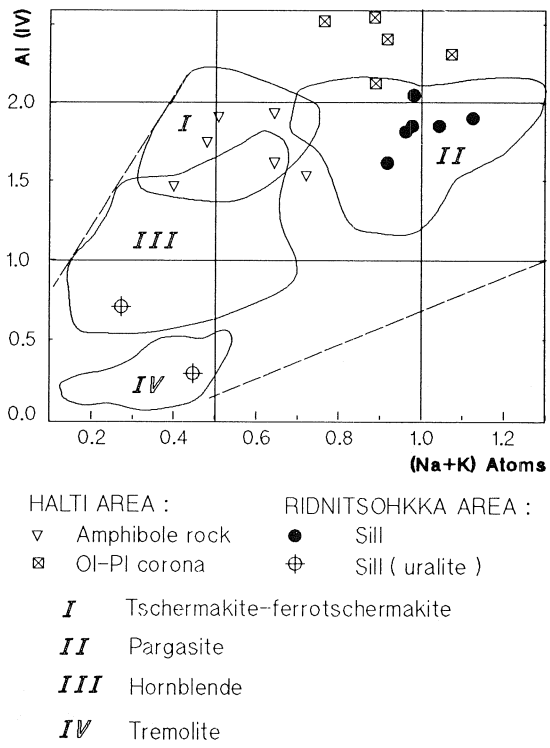

Fig. 32. Chemical variation of calcium-rich amphiboles from the Halti and Ridnitsohkka areas expressed as number of (Na + K) and Al (IV) atoms per formula unit. Assumption: wt% H_2O = 100 — wt% total. Fields I — IV are according to Deer et al. (1963).

Biotite

The Mg/Mg + Fe ratio for biotites in the Ridnitsohkka sills falls gradually towards the olivine-bearing sills, after which it rises distinctly (Fig. 25). The compositions of biotites from the Ridnitsohkka sills are given in Appendix 7. Compositions for biotites from the sills, from intervening country rock gneisses, from the contact metamorphic aureole and from gneisses outside the aureole are compared in the section dealing with metamorphism.

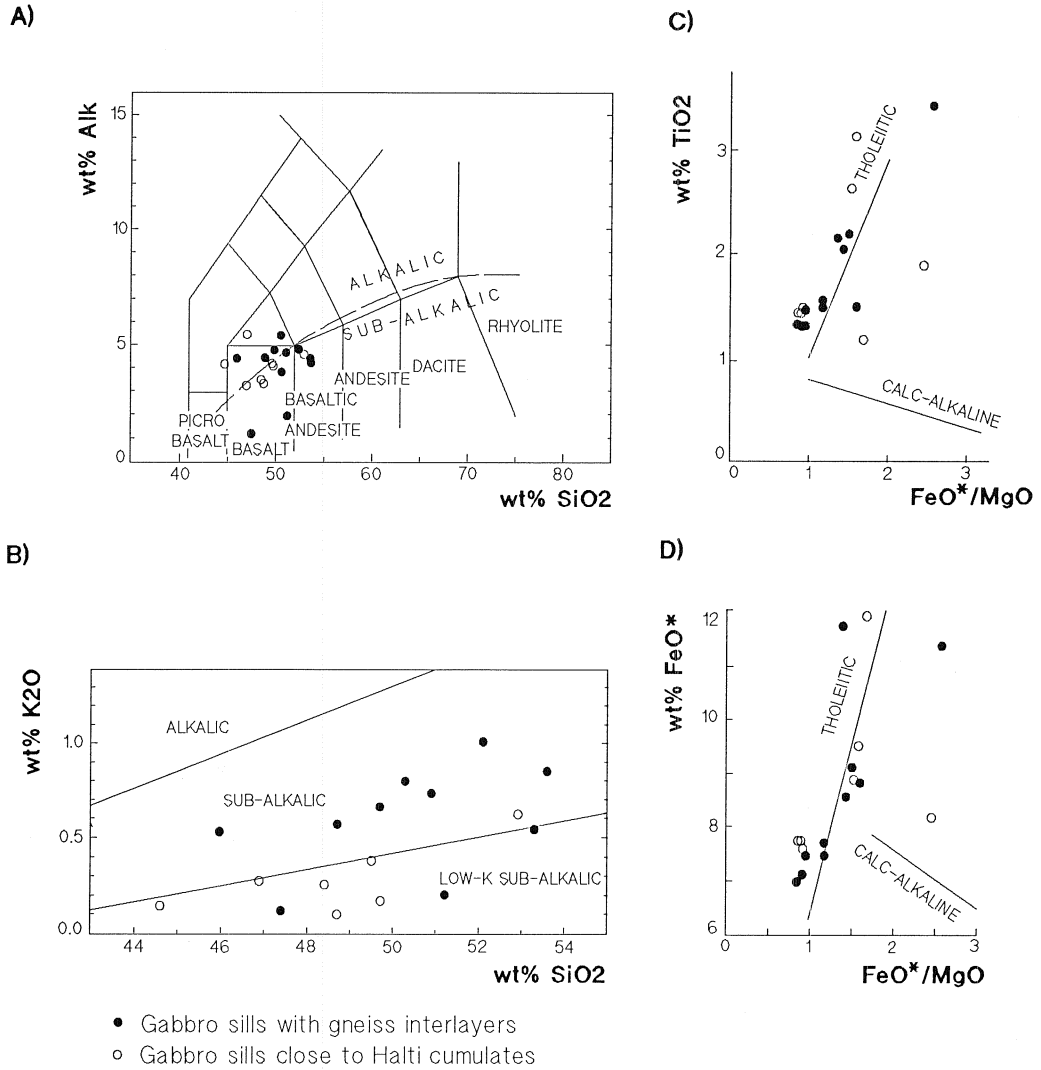

Fig. 33. Compositions of the Ridnitsohkka gabbro sills plotted on a variety of diagrams. (A) SiO_2 vs. $Na_2O + K_2O$ (LeBAS et al. 1986). The dividing line between alkalic and sub-alkalic magma series is from Miyashiro (1978). (B) SiO_2 vs. K_2O (Middlemost 1975). (C) FeO^*/MgO vs. TiO_2 (Miyashiro 1978). (D) FeO^*/MgO vs. FeO^* (Miyashiro 1975). (E) $(Na_2O + K_2O)$-FeO^*-MgO (Irvine & Baragar 1971). (F) Al_2O_3-$(FeO^* + TiO_2)$-MgO cation diagram (Jensen 1976). (G) MgO-FeO^*-Al_2O_3 (Pearce et al. 1977). (H) Al_2O_3 vs. A.I. (Middlemost 1975). FeO^* — total iron calculated as FeO.

WHOLE ROCK GEOCHEMISTRY

Geochemistry of the Ridnitsohkka gabbro sills

The character and geotectonic setting of volcanic rocks is to some extent reflected in their geochemistry, with the trace elements Ti, P, Zr, Nb, Y, Hf, Nb, Ta, Th and Cr as well as the lanthanide series elements being the most useful for discriminating between different associations. The distribution of these elements is also effective in discriminating between different kinds of undifferentiated dykes and sills. Analytical data for Ti and Cr were available for the majority of the Ridnitsohkka sills examined in this study but lanthanide abundances were determined for only two samples.

It is difficult to determine the original composition of the Ridnitsohkka gabbro sills because of the assimilation of country-rock gneisses during emplacement, reflected in the presence of hydrous primary phases such as biotite and hornblende. Concentrations of plagioclase in particular layers and the presence of rhythmic layer-

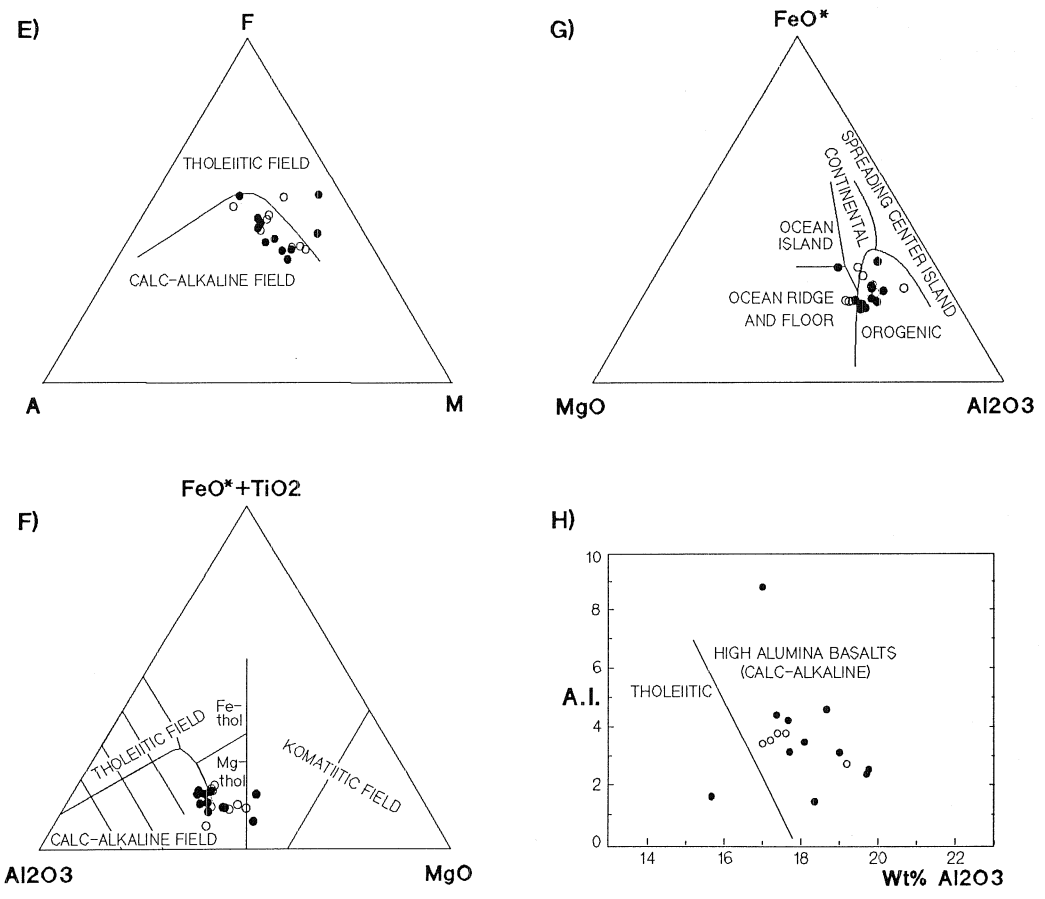

• Gabbro sills with gneiss interlayers
○ Gabbro sills close to Halti cumulates

Fig. 33. cont.

ing near the Halti cumulates indicates that the accumulation of different mineral phases took place. Variation diagrams for both mineral and whole-rock compositions (Fig. 25) representing samples from Profile A — B in Fig. 2 show, that differentiation was insignificant in those sills that contain abundant interlayers of country rock gneisses. In contrast, the olivine-bearing sills nearer the Halti cumulates contain fewer country rock interlayers and accordingly have distinctly more primitive and regressive mineral and whole rock compositions. The diagrams in Fig. 33 demonstrate a moderate degree of scatter between data for sills occurring in different locations throughout the sill area. On the LeBAS et al. (1986) diagram (Fig. 33a) most data points plot in the basaltic field while in the classification of Miyashiro (1978) they fall on both sides of the alkaline — subalkaline boundary. Contamination due to assimilation of gneissic material is evident from the large scatter on the K_2O vs. SiO_2 diagram (Middlemost, 1975), shown in Figure 33b. According to the Miyashiro (1978) plots of TiO_2 vs. FeO_{tot}/MgO (Figure 33c) and FeO_{tot} vs. FeO_{tot}/MgO (Figure 33d), the Ridnitsohkka sills are clearly tholeiitic, whereas on the Irvine and Baragar (1971) AFM diagram (Figure 33e), the data lie principally in the calc-alkaline field, even though the differentiation trend is tholeiitic. On the Jensen (1976) cation plot (Figure 33f) data points fall in both the calc-alkaline and Mg-tholeiite fields. The high Al_2O_3 contents of the gabbro sills is clearly evident in both the Pearce et al.(1977) diagram (Figure 33g), in which most of the data lie within the orogenic field, and in the Middlemost (1975) Alkali Index (A.I.) vs. Al_2O_3 diagram (Figure 33h), in which they fall entirely within the calc-alkaline (high-Al) basalt field. This is at least partly due to the accumulation of plagioclase phenocrysts, as also indicated by the positive Eu anomaly in the REE distributions (Figure 36). TiO_2 contents are also high, averaging 1.5—2.0 wt%, but in some instances attaining 3.5 wt%. This is unusual for basalts in convergent plate margin settings, which generally have TiO_2 contents of 0.8—1.1 wt% (Pearce, 1976) and is instead more reminiscent of abundances (1.4—3.0 wt% TiO_2) in rifted

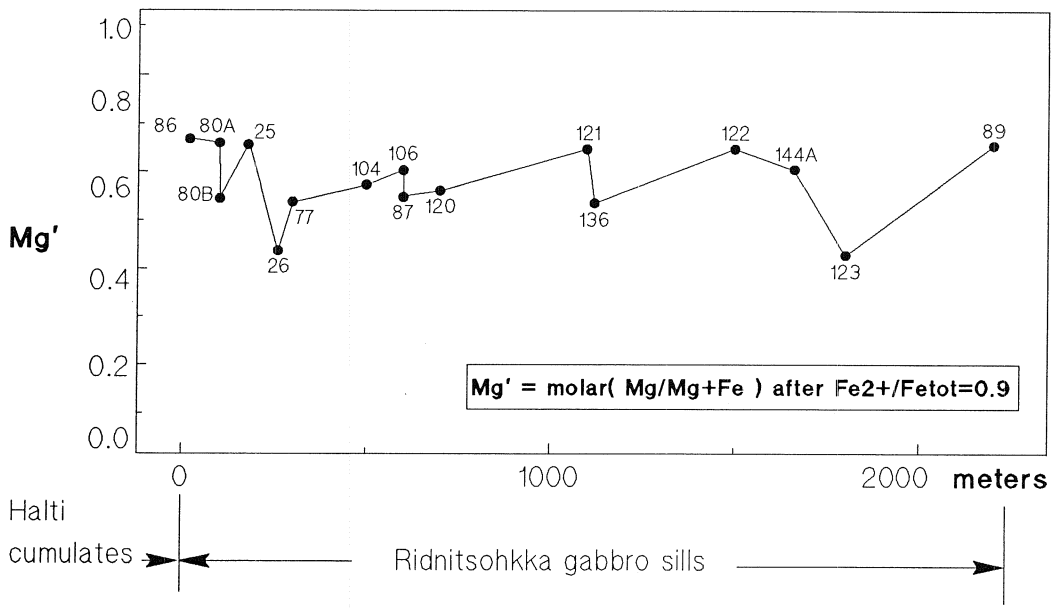

Fig. 34. Variation of Mg' in Ridnitsohkka gabbro sills. Sample locations are shown in Appendix 13.

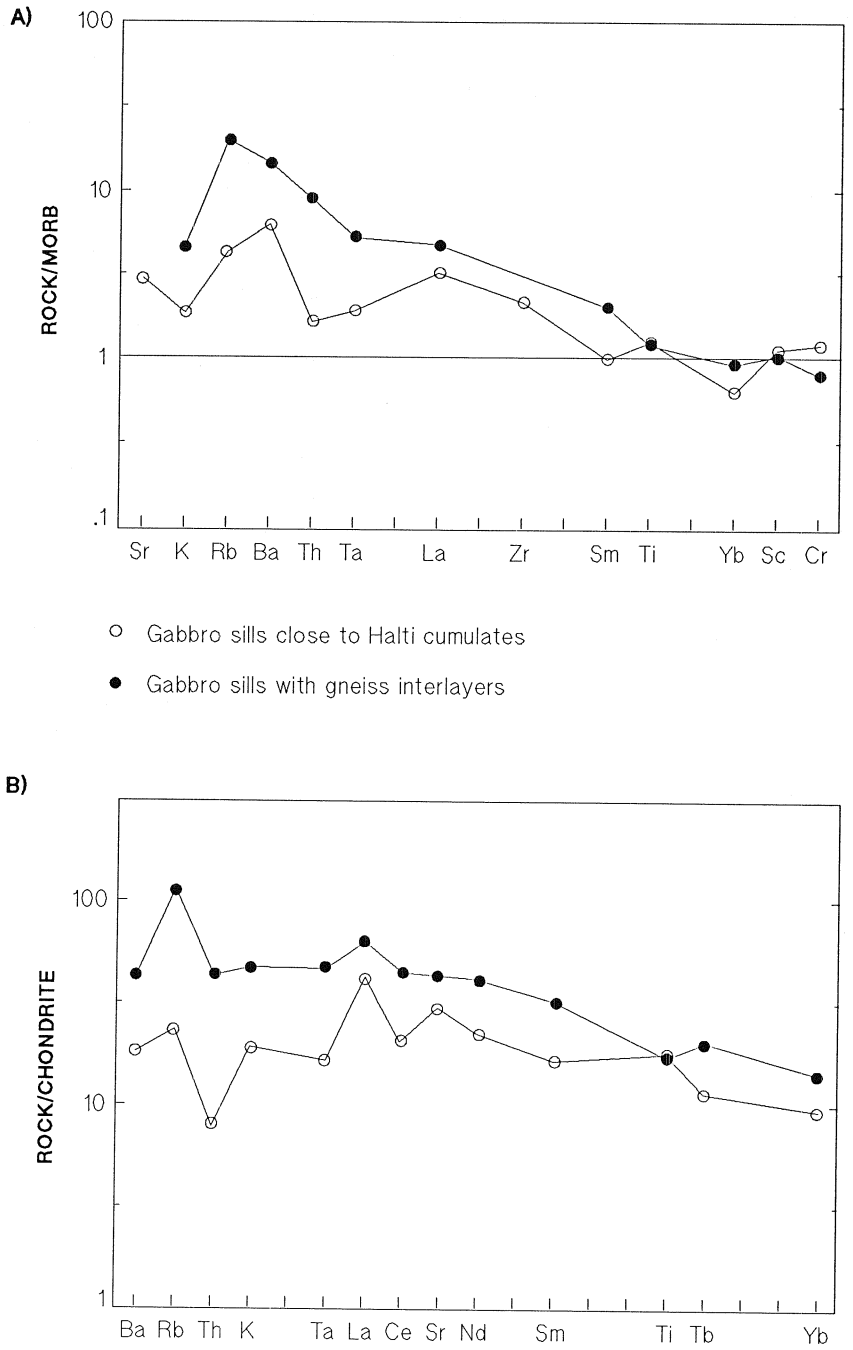

Fig. 35. MORB-normalized (Fig. A) and chondrite-normalized (Fig. B) trace element patterns for average values of Ridnitsohkka gabbro sills. The MORB-normalizing constants are from Pearce (1983) and the chondrite-normalizing constants are from Thompson et al. (1984).

margin or intracontinental settings.

The variation diagrams in Fig. 25 indicate that SiO_2 and TiO_2 contents of the sills increase slightly when traversing westwards towards the olivine-bearing sills, while MgO/MgO + FeO ratios concomitantly decrease. However, these trends are reversed when traversing towards the Halti cumulates through the olivine-bearing sills themselves, which is consistent with the overall trend observed for Mg' numbers of the Ridnitsohkka sills (Fig. 34).

The chondrite- and MORB-normalized trace element distribution diagrams in Fig. 35 clearly distinguish between sills containing abundant gneiss interlayers and those nearer the Halti cumulates, with incompatible elements being enriched in the former with respect to the latter. From these variation diagrams it is possible to infer the degree of contamination. In general, when basalt is affected by crustal contamination, Ti, Tb, Y, Tm and Yb remain unchanged but abundances of other elements increase depending on the degree of assimilation and composition of the contaminating material (Wilson, 1989). Thus positive Ba, Rb, Th and K anomalies are typical on chondrite-normalized diagrams where contamination has taken place in the upper crust, whereas lower crustal contamination results in somewhat smaller enrichments in Rb and especially Th. Strong contamination by upper crustal material also correlates with a distinct Nb-Ta minimum (Wilson, 1989). With two exceptions, characterized by relatively high Ba values, all samples from the Ridnitsohkka sills containing abundant gneiss interlayers display distinct Rb maxima on the chondrite-normalized ratio diagrams. The Ba enrichment may be explained by the relative abundance of plagioclase, whereas the absence of any Nb-Ta minimum may result from an unusually high degree of assimilation and mixing of acid gneiss material within the mafic melt, an effect different from contamination. Some diagrams show a distinct Th minimum, with the lowest values being close to the

Table 2. Rare earth element data for the Halti cumulates and Ridnitsohkka gabbro sills (in ppm).

	1	2	3	4	5
La	1.07	1.18	2.3	9.5	21
Ce	<3	<3	3.2	17.9	39
Nd	<3	<3	<3	13.8	26
Sm	0.17	1.15	0.63	3.8	7
Eu	0.21	0.62	0.6	2.1	2.89
Tb	0.05	0.22	0.12	0.6	1.04
Yb	0.3	0.77	0.34	2.1	3.1
Lu	0.04	0.12	0.08	0.29	0.42
Eu/Sm	1.24	0.54	0.95	0.55	0.41
(Eu/Sm)CN	3.24	1.41	2.50	1.45	1.08
(La/Lu)CN	2.76	1.01	3.48	3.38	5.15

1. 74 Troctolite,Halti.
2. 44 Olivine gabbro,Halti.
3. 18 Augite augen gabbro,Halti.
4. 25 Gabbro sill close to Halti cumulates,Ridnitsohkka.
5. 87 Gabbro sill with gneiss interlayers,Ridnitsohkka.

detection limit and this is probably an indication of the originally primitive character of the melt. The great degree of variation amongst the Ridnitsohkka data generally reflects the varying extent of assimilation, with the highest Rb and K abundances representing the greatest amounts of contamination. In contrast, the highest Cr abundances are found in sills adjacent to the Halti cumulates (Fig. 35a), attesting to their primitive nature.

Lanthanum, Ce, Nd, Sm, Eu, Tb, Yb and Lu were determined by Instrumental Neutron Activation Analysis for five samples from the Halti-Ridnitsohkka complex (Table 2), while many additional samples were analyzed for Sm and Lu using X-ray fluorescence (Appendix 12). Lanthanide abundances are distinctly higher in the Ridnitsohkka sills than in the Halti cumulates. Chondrite-normalized REE patterns for sills containing abundant gneiss interlayers are similar in form to those for the olivine-bearing sills located nearer the contact with the Halti cumulates and both show a similar degree of LREE enrichment (Fig. 36). This latter phenomenon is due to the occurrence of apatite, even though it is present in only small concentrations (Henderson, 1984). Positive Eu anomalies in both kinds of sills is a result of enrichment in plagioclase by crystal fractionation processes. The abundances of HREE are generally considered to be unaffected by metamorphic processes but there is a lack of consensus concerning the behavior of the LREE. For example, Ludden and Thompson (1979) consider LREE to be mobile to some extent whereas Dungan et al. (1983) maintain that they are immobile. According to Grauch (1989), the mobility

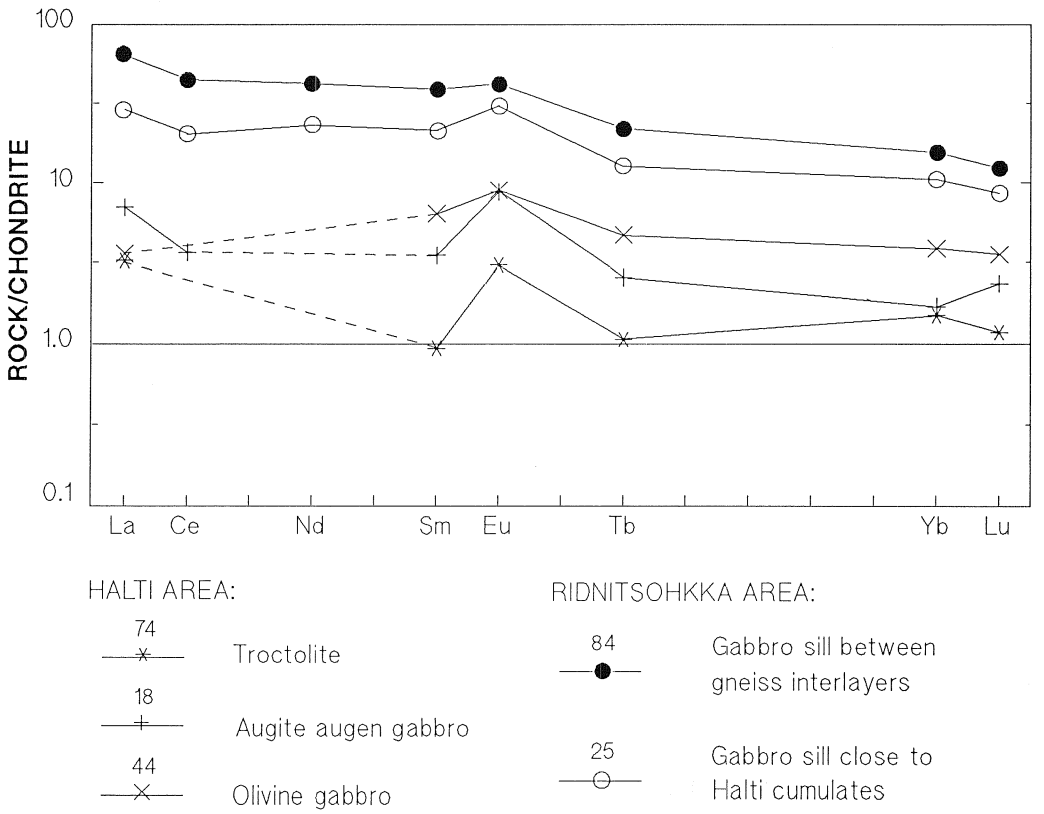

Fig. 36. Chondrite normalized REE-plot for Halti cumulates and Ridnitsohkka gabbro sills. Normalizing values are those used by Haskin et al. (1968).

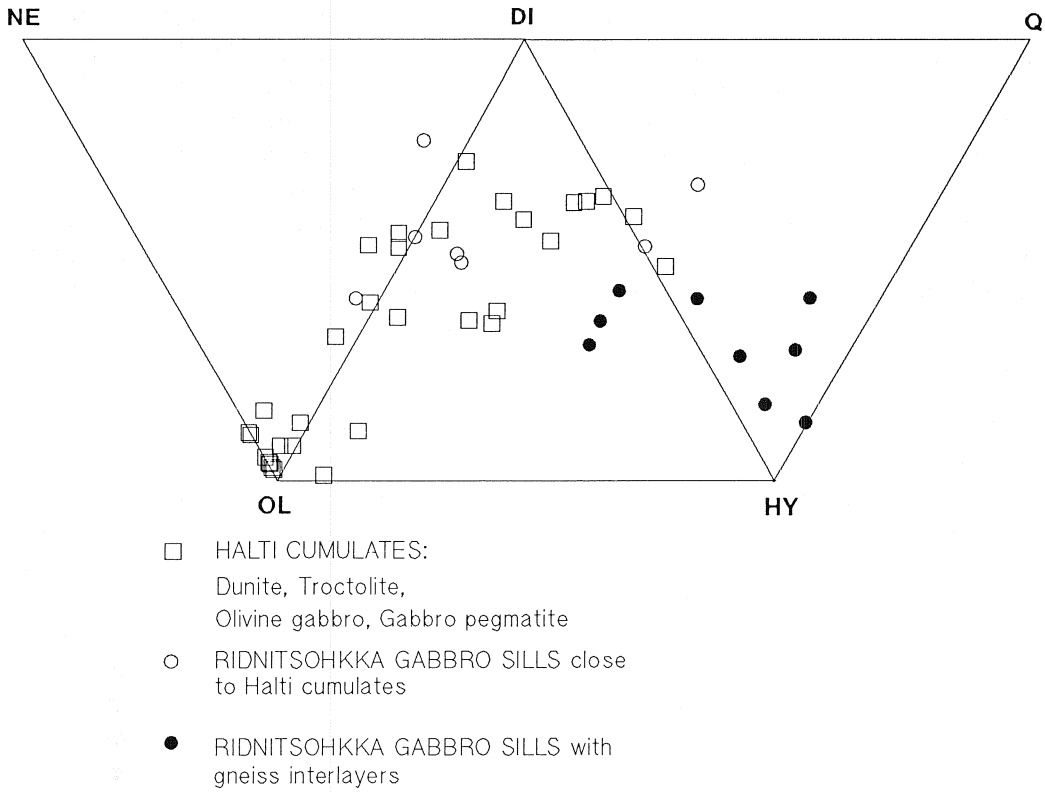

Fig. 37. Normative compositions of Halti cumulates and Ridnitsohkka gabbro sills on the Ne-Ol-Di-Hy-Q -diagram.

of REE in general during metamorphism has not been studied in sufficient detail as to allow confident interpretation of REE patterns and abundances of either metamorphic derivatives or their inferred protoliths.

On the Ne-Ol-Di-Hy-Qz diagram (Fig. 37), sills containing gneiss interlayers plot closer to the hypersthene apex than the olivine-bearing sills, which fall among the data for the Halti cumulates.

The geochemical characteristics of the Ridnitsohkka gabbro sills that contain abundant gneiss interlayers are clearly distinctive. The marked increase in Fe and Ti in the more felsic differentiates attest to their tholeiitic nature, as does evidence for the coeval crystallization of Ca-rich and Ca-poor pyroxene and the presence of orthopyroxene lamellae in clinopyroxene (Deer et al., 1978). On the other hand, their high Al_2O_3 abundances and the enrichment of incompatible elements and LREE are reminiscent of high-Al basalts belonging to the calc-alkaline series. Moreover some sills are quartz normative while others contain normative olivine.

A similar tholeiitic trend is discernible with respect to Fe and Ti in the sills nearer the Halti cumulates, containing fewer gneiss interlayers. Al_2O_3 abundances are also high but incompatible element and lanthanide enrichments are distinctly less than for the other sills. Normative compositions are also different, more closely resembling the late stage differentiates of the Halti cumulate sequence.

The gabbro sills adjacent to the Halti cumulates are associated with several graphite-bearing lenses containing disseminated sulfides, which are

typically several meters in thickness. These contain distinctly more orthopyroxene than the adjacent gabbro sills and are also preferentially enriched in LREE (Appendix 12, samples 25A and 116A). These sulfide-bearing lenses have La/Sm ratios of 30—40 and Lu abundances below detection limits whereas La/Sm ratios for the other sills are <4 and Lu abundances are in excess of the detection limit, ranging between 0.29—0.64. Evidently the lenses represent intense assimilation of gneissic country rock material. According to Irvine (1975), the addition of silica and alkali elements (either through contamination or magma mixing) decreases the solubility of sulfides in magma and results in the formation of an immiscible sulfide melt component. This causes polymerization of the silicate melt, leading to the precipitation of pyroxene instead of olivine.

Geochemistry of the Halti cumulates

The chemical composition of the Halti cumulates is controlled by the relative abundances of olivine, Cr-spinel, plagioclase and clinopyroxene, which vary considerably as a result of the presence of rhythmic layering.

On the basis of their SiO_2 contents, the Halti cumulates can be described as both ultramafic and mafic; the former, with SiO_2 less than 45 wt%, include all the dunites and most of the troctolites analyzed. These have correspondingly high MgO contents, in the case of the dunites, 43—48 wt%, while troctolite MgO values range from 10—43 wt%. Plagioclase-rich troctolites, olivine gabbros and coarse-grained pegmatitic gabbro dykes contain 45—52 wt% SiO_2. Dunite and troctolite samples lie near the olivine-diopside line on the Ne-Ol-Di-Hy-Qz diagram, while olivine gabbro and pegmatitic gabbro dykes are located nearer the Di-Hy side, due to their higher SiO_2 contents (Fig. 37).

Whole-rock MgO/MgO + FeO ratios decrease while SiO_2 increases slightly as differentiation progresses (Fig. 25). Dunites have MgO/MgO + FeO ratios between 0.78—0.84, troctolites between 0.61—0.82 and olivine gabbros 0.57—0.70. TiO_2 contents are very low in both the dunites and the troctolites but rises distinctly in the olivine gabbros, in proportion to the abundance of clinopyroxene and ilmenomagnetite.

Of the trace elements analyzed, only Cr, Co, Ni, Sc and Sm are consistently in excess of detection limits and hence useful in assessing variations and trends within the cumulate sequence as a whole (Appendix 12). Scandium and Sm are lowest in the dunites and troctolites (Sc <10 ppm, Sm <0.4 ppm) and somewhat higher in the olivine gabbros and pegmatitic gabbro dykes (Sc = 20—70 ppm, Sm = 0.5—5 ppm). The metasomatic amphibole rocks in the troctolite unit have distinctly lower Sc contents than their counterparts in the olivine gabbro unit, thus indicating that amphibole-forming processes did not cause any remobilization of Sc; this is less certain in the case of Sm. High Cr abundances in the troctolites and dunites are due to the presence of Cr-spinel. Nickel and Co contents are also higher in the dunites and troctolites than elsewhere, and occur principally within olivine, since sulfides are rare in these lithologies.

Lanthanide abundances are lowest in the dunites, and a few samples having Sm up to 0.03 ppm are the only ones to have values in excess of the detection limit (Table 2). The troctolites and olivine gabbros also have low REE abundances, with both Ce and Nd being below their detection limits of around 3 ppm. Likewise Nd is below the detection limit in the augite augen gabbro. The cumulus character of plagioclase is readily apparent from the positive Eu anomaly, particularly for the troctolites and augite augen gabbro. These in general exhibit REE patterns reminiscent of plagioclase crystallized from an

andesitic or basaltic melt (Henderson, 1984). This indicates that only a small amount of intercumulus material is present, an inference supported by microscopic observation. The REE patterns of the olivine gabbros reflect the influence of cumulus clinopyroxene, with characteristic LREE depletion and a somewhat smaller positive Eu anomaly. Even though the augite augen gabbro contains about 20 % of modal augite, it has an almost identical REE distribution to that of the troctolites, and thus clearly differs from that of the olivine gabbros. This implies an effectively isochemical process with respect to lanthanides for the formation of the augite augen gabbro from a troctolitic protolith.

Gold, Re and PGE (= platinum group elements) were determined from two massive Cr-spinel layers, since chromite-rich layers in layered mafic intrusions have been shown to be anomalous with respect to enrichments in the PGE (e.g. Alapieti and Lahtinen, 1986). The Cr-spinel layers in the Halti cumulates contain accessory

Table 3. Concentration of PGE, Au and Re (ppb) and Cu, Ni, Co, and S (ppm) in two banded chrome spinel layers from the Halti cumulate sequence.

	374	380
Os	<3	<4
Ir	0.8	0.8
Ru	3	12
Rh	7	40
Pt	6	6
Pd	29	11
Au	7	5
Re	<1	2
Cu	1090	1080
Ni	3740	2940
Co	197	183
S	3280	4370
Pd/Ir	36.3	13.8

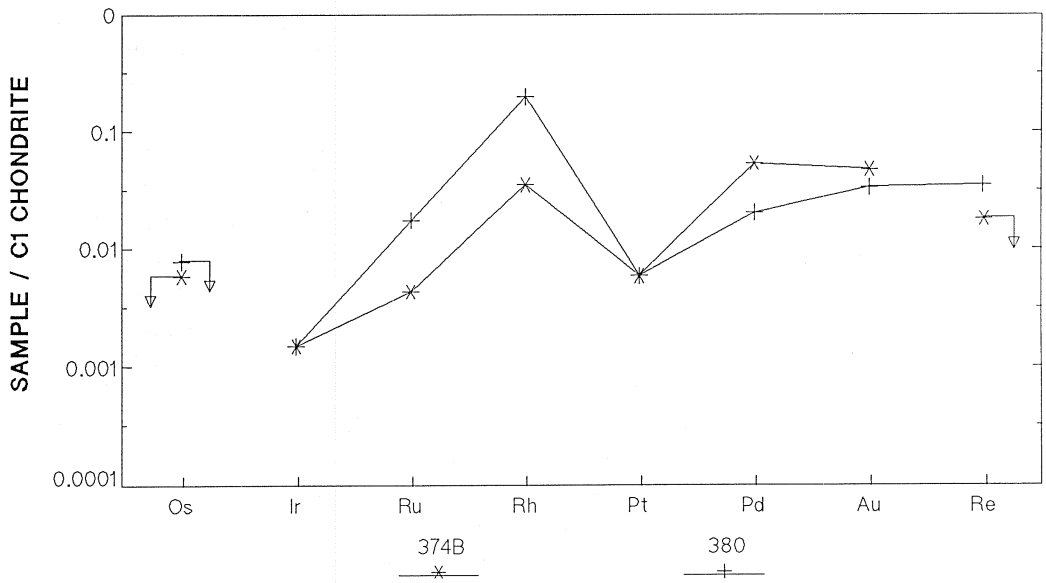

Fig. 38. Chondrite normalized PGE, Au and Re distribution diagram for Halti banded chrome spinel layers. Normalizing values for PGE and Au are from Cabri & Naldrett (1984) and for Re from Morris & Short (1978). Detection limits for Os and Re are shown.

amounts of pentlandite and chalcopyrite, but PGE-bearing minerals have not been identified. PGE concentrations are accordingly very low (Table 3), such that Os was below the detection limit for both samples and Re was below the detection limit for one sample. Chondrite-normalized abundances are shown in Fig. 38. There is little evidence for PGE fractionation in either sample (Pd/Ir = 13.6 and 36.6 respectively) and both samples show a negative Pt anomaly. The slope of the curve is a result of fractionation processes at an early stage in the parent magma, since Os, Ir and Ru tend to be more lithophile than Rh, Pt and Pd, and hence Pt and Pd are preferentially concentrated in residual melt phases (Naldrett, 1981). The negative Pt anomaly is presumably due to alteration and remobilization of sulfides during metamorphism, as has been demonstrated for some metamorphosed Ni-Cu occurrences in Finland (Papunen, 1989). The small degree of PGE fractionation in the Halti cumulate sequence further attests to the primitive nature of its parent magma.

METAMORPHISM AND DEFORMATION

Structural — metamorphic evolution

The Scandinavian Caledonides record two major tectonometamorphic events, the earlier being known as the Finnmarkian phase, which took place at 540—530 Ma (Sturt et al., 1978; Pedersen et al., 1989), while the younger, known as the Scandian phase, occurred between 440—410 Ma (Gee, 1975). The Finnmarkian phase is best developed in the northernmost parts of Scandinavia, although its effects are recognized as far south as the Sulitjelma area in the central part of the orogen (Boyle et al., 1985). Barker (1989) has identified four stages of deformation within Scandian phase nappe sequences in the Tromsö and northern Norrbotten districts, to the west of the Finnish portion of the Caledonides. D_1 is only represented by epidote and chlorite inclusions within garnet porphyroblasts, from which it is inferred that S_1 formed under greenschist facies conditions. D_2 structures are related directly to the Scandian phase since they deform Middle Ordovician and Silurian fossils in, amongst other places, the Guolasjavri area immediately to the west of Halti (Binns and Gayer, 1980). During D_2 an intense foliation developed parallel to the axial planes of F_2 folds, transposing and obliterated earlier structures. This stage of penetrative deformation represents ductile shearing associated with southeastwards translation of deformed crust during the collision between Fennoscandia and Laurentia. Towards the end of D_2 and during D_3, strain became progressively partitioned into narrow thrust zones, while folding changed in style from recumbent isoclinal to upright and more open. Recumbent folds are best developed in proximity to thrust planes and both S_2 and S_3 are subparallel to thrusts. Thrust planes were deformed, along with other structural elements, into broad open folds during D_4. According to Barker (1989), this tectonometamorphic sequence can be recognized throughout all the nappes in the Tysfjord — Tromsö region and S_2 is everywhere the dominant fabric.

The Ridnitsohkka sills were intruded at about 430 Ma (Vaasjoki et al., in prep.) and are hence Scandian in age, thus enabling the tectonostratigraphic history of the Halti-Ridnitsohkka complex with that of the Tromsö region. An additional feature present in the Halti-Ridnitsohkka area is metamorphism due to the intrusion itself. This resulted at first in intense thermal metamorphism of relict gneiss interlayers between the Rid-

nitsohkka sills and the development of a widespread contact metamorphic aureole in the gneisses adjacent to the sill area, with local migmatization and brecciation by anatectic alkali granite material. The Halti ultramafic magma subsequently caused strong metasomatic and thermal reworking of the sill unit adjacent to the cumulate sequence. After the cessation of magmatism the whole complex was deformed, resulting in small scale isoclinal folding within the gneiss interlayers and finally producing a strong foliation in the cumulates and the sill unit at the contact zone between them. The metasomatic megacrystic clinopyroxene gabbro at the contact between the sills and the Halti cumulates also developed its characteristic augen texture during this deformational stage.

The contact between the Halti cumulates and the underlying gneisses is a flatlying thrust zone which clearly truncates the rhythmic layering of the cumulates. No contact metamorphic effects are present in the gneisses below the thrust.

The isoclinal folding of the gneiss interlayers between the Ridnitsohkka sills evidently correlates with the earliest stages of Scandian D_2 deformation, whereas the intense foliation in the contact zone between the cumulates and the sill area presumably represents later D_2 deformation. This implies that the main stage of Halti-Ridnitsohkka magmatism pre-dates the peak of the Scandian orogenic phase. The detachment beneath the Halti cumulates is a D_3 structure. In the contact zone between the cumulates and the sill unit S_2 and S_3 are mutually discordant, the latter being virtually horizontal and restricted to the vicinity of the detachment surface, while the former is more penetrative and dips steeply westwards. East of the Ridnitsohkka aureole there is no clearly defined thrust zone and S_2 and S_3 are probable subparallel, both dipping gently towards the northwest. The gneisses beneath the cumulates belong to the Nabar Nappe, which was considered by Lehtovaara (1986a) to be Finnmarkian. Although the contact between the Nabar gneisses and the cumulates is clearly tectonic, the same gneisses occurring immediately to the east of the Ridnitsohkka sills were contact metamorphosed at 430 Ma. Hence the uppermost parts of the Nabar Nappe can be considered as Scandian in age.

Metamorphic textures in the Ridnitsohkka contact metamorphic aureole and in the gneiss interlayers

Outside the contact aureole the prevailing lithology is a granoblastic muscovite — biotite gneiss containing garnet and K-feldspar porphyroblasts. It is stringly foliated parallel to the direction of thrusting and quartz in particular has undergone extensive dynamic recrystallization. Garnet is invariably almandine of homogeneous composition and usually forms idiomorphic porphyroblasts that show fracturing only in the more strongly mylonitized zones. None of the minerals in the gneisses show any evidence of alteration.

K-feldspar porphyroblasts tend to be larger in the outermost parts of the aureole than outside the aureole while quartz and muscovite are both stable and garnet is unzoned. In the inner parts of the aureole however, quartz, muscovite and plagioclase have reacted to form kyanite and sillimanite plus a melt phase. Muscovite remains only in leucosomes. Kyanite porphyroblasts may be several cm in length and sillimanite is usually fibrolitic. Sillimanite porphyroblasts are however rare, occurring only near the contact with gabbro sills. Both kyanite and sillimanite contain small inclusions of hercynite spinel. In the inner parts of the aureole and in gneiss remnants between sills, almandine garnet is typically zoned, with an idiomorphic, relatively inclusion-free

core surrounded by an Mg-rich rim commonly containing inclusions of fibrolitic sillimanite. Xenomorphic porphyroblasts of garnet having similar compositions and containing fibrolite inclusions are also present elsewhere. An almandine garnet reaction zone is present at the boundary between the kyanite porphyroblastics and biotite in the aureole rocks.

K-feldspar and plagioclase in the anatectic granites usually are 0.5—0.8 mm in diameter and are extensively recrystallized at their margins. Quartz has however recrystallized entirely, forming mosaics of subgrains. Muscovite and biotite in the granites occur either as small interstitial grains deflected around feldspar or as larger flaky aggregates while almandine garnet is typically homogeneous and idiomorphic.

The gneiss interlayers between sills clearly display internal banding at the macroscopic scale, primarily due to the alternation of bands containing coarse-grained K-feldspar blasts with those containing finer grained quartz, plagioclase and K-feldspar; the latter also contain abundant fine-grained intergrowth of sillimanite and biotite and sillimanite and orthopyroxene. Sporadic layers rich in garnet or orthopyroxene are also present, the latter occurring as poikiloblasts containing inclusions of plagioclase and K-feldspar. Fibrolitic sillimanite is common between feldspar grains. Ilmenite, zircon, rutile and various sulfides, including pyrite and pyrrhotite occur as accessory phases in both gneiss interlayers and the aureole.

The gneiss interlayers between sills adjacent to the Halti cumulates are fine-grained cordierite-plagioclase rocks. They do not contain any quartz or K-feldspar nor, apart from the cordierite, any Fe- or Mg-bearing silicate phases. Interstitial sulfide minerals (pyrrhotite ± pyrite ± chalcopyrite) are nevertheless present, either disseminated or defining distinct bands. Accessory minerals include ilmenite, sillimanite, rutile and zircon.

Skarn layers occurring between gabbro sills are generally even-grained, granoblastic diopside-plagioclase rocks, with plagioclase usually being anorthitic; minor amounts of biotite and titanite are also present.

Metabasaltic units occurring within the gneiss interlayers are fine-grained and granoblastic, with abundant ortho- and clinopyroxene and showing intense submicroscopic shear band development.

Metamorphic mineral reactions, mineral compositions and pressure-temperature determinations for the Ridnitsohkka sill unit

Mineral reactions in the contact metamorphic aureole

The contact aureole, which coincides broadly with the presence of kyanite porphyroblasts, is best developed on the eastern slopes of Ridnitsohkka, where it is about 500 m thick. Outside the aureole the gneisses consist of the assemblage garnet — biotite — K-feldspar — muscovite — plagioclase — quartz.

Kyanite is thus only present within the aureole and formed by the breakdown of muscovite during anatexis:

(1) plagioclase + muscovite + quartz + H_2O = Al_2SiO_5 + melt

Reaction (1) takes place at temperatures between 600—700 °C, depending on the composition of plagioclase and also whether or not K-feldpar is present. If plagioclase is albitic and K-feldspar is present, then Reaction (1) occurs at lower temperatures and at a minimum pressure (with aH_2O = 1) of 4—5 kbar. If pressure remains constant at 6 kbar, then kyanite forms in the lower range of temperatures and sillimanite at higher temperatures (Fig. 40). In the presence

of K-feldspar however there is a tendency for melt to form at the expense of aluminosilicates (Thompson and Tracy, 1979). Anatectic melts consist of components K-feldspar, albite-rich plagioclase and quartz and of water. The kyanite porphyroblasts in the Ridnitsohkka aureole have evidently formed according to Reaction (1), although thermal effects were not evenly distributed throughout the aureole, since sillimanite has also formed in some gneisses situated further from the sills. Furthermore, there is evidence for the partial replacement of kyanite by sillimanite, indicating a general rise in temperature in the inner part of the aureole.

If biotite is also present, then at slightly higher temperatures the following reaction takes place:

(2) biotite + sillimanite/kyanite + quartz = K-feldspar + garnet + H_2O

Garnet rims around kyanite porphyroblasts in the Ridnitsohkka aureole and the Mg-rich almandine porphyroblasts containing sillimanite needles have formed through this reaction. At lower pressures cordierite would be expected instead of or in addition to garnet in Reaction (2) (Winkler, 1979), but no cordierite has been found in the aureole.

Kyanite is not usually found as a contact metamorphic mineral because its formation requires high pressures. Within the Scandinavian Caledonides however, kyanite has also been described from the surroundings of at least the Artfjäll gabbro (Senior and Otten, 1985) and the Reinfjord ultramafite (Bennett et al., 1986).

Mineral reactions in the gneiss interlayers

Remnants of country rock gneisses were subjected to high temperatures during the intrusion of the Ridnitsohkka sills and typically have mineral assemblages such as:

garnet + orthopyroxene + K-feldspar + plagioclase + sillimanite ± quartz ± biotite ± cordierite ± ilmenite ± spinel ± rutile

garnet + K-feldspar + plagioclase + quartz + sillimanite ± biotite ± ilmenite ± rutile

According to Reaction (1) above, coarse-grained sillimanite formed instead of kyanite in the gneiss interlayers as well as in the inner part of the aureole. Sillimanite porphyroblasts did not form in the innermost part of the gabbro sill area however, because temperatures during the peak of magmatism were higher than in the aureole, and led to the formation of garnet + cordierite + K-feldspar assemblages instead of biotite + sillimanite + quartz. Gneiss enclaves within the sills subsequently underwent retrogressive alteration such that cordierite has almost totally been replaced either by intergrowths of biotite + sillimanite + quartz:

(3) cordierite + K-feldspar + H_2O = biotite + sillimanite + quartz

or orthopyroxene + sillimanite + quartz:

(4) cordierite = orthopyroxene + sillimanite + quartz

The breakdown of cordierite via Reaction (4) requires an increase in pressure and, according to Newton (1972) the assemblage hypersthene + sillimanite + quartz is the high pressure equivalent of cordierite and is stable at pressures exceeding 8—11 kbar, depending upon the water content of cordierite. The intergrowth aggregates of orthopyroxene + sillimanite + quartz are exceedingly fine-grained, so that it was only possible to identify them as such using the electron microprobe (Appendix 8). Biotite is also present in these intergrowths as are, according to the probe data, both K-feldspar and plagioclase. Cordierite was only identified in one thin section, where it occurs with orthopyroxene and also as inclusion within it. In this case too, the cordierite has undergone retrograde alteration.

Sillimanite is invariably fibrolitic in the gneiss interlayers within the sill area.

In addition to its occurrence with sillimanite as fine-grained intergrowths, orthopyroxene also forms large poikiloblasts whose presence indi-

cates that the activity of water during sill intrusion was significantly less than the total pressure. In other words, hypersthene formed during the breakdown of biotite, thus:

(5) biotite + quartz = hypersthene + almandine + K-feldspar + H_2O

The orthopyroxene-bearing gneisses within the Ridnitsohkka sill area generally have only small amounts of quartz because it was apparently largely consumed during Reaction (5) which can take place over a wide range of temperatures, depending upon the composition of biotite. Orthopyroxene could not form in the aureole rocks via Reaction (5) however, because the partial pressure of water was too high. In the Ridnitsohkka gneiss interlayer orthopyroxenes tend to be aluminium-rich (3—4 wt% Al_2O_3, see Appendix 5), and these too have been in places strongly retrogressed to form biotite-sillimanite intergrowths:

(6) orthopyroxene + K-feldspar + H_2O = biotite + sillimanite

The final prograde reaction in the gneiss interlayers, as in the aureole, involved the formation of Mg-rich garnet. This took place via Reaction (2), forming rims around earlier garnets as well as elsewhere in the rock, at the expense of biotite-bearing aggregates.

The abundance of K-feldspar in the gneiss interlayers indicates that they are not merely restitic in origin, but rather that some additional melt component was present. The paucity of migmatite in these units nevertheless requires either that much of the partial melt was physically removed, or that the partial pressure of water was significantly less than in the aureole and that temperatures were insufficient to cause widespread anatexis. Winkler (1979) observed that at medium pressures in the absence of free water, the temperatures necessary to form melts are 100 °C higher. If pressures are also increased significantly, then this temperature difference may be as high as 150 °C.

Gneiss remnants between the sills nearest the Halti cumulates have a very distinctive appearance and mineralogy, being massive and completely lacking migmatites. They generally contain cordierite, while K-feldspar, quartz, biotite and orthopyroxene are absent. Typical assemblages are:

cordierite + plagioclase + ilmenite + spinel + sulfides, and

cordierite + plagioclase + sillimanite + ilmenite + rutile + quartz + sulfides

These assemblages formed metasomatically due to thermal effects from the adjacent cumulate source magmas, and subsequent increases in pressure were not sufficient to make cordierite unstable.

Retrograde effects in the sills themselves are minimal, the most widespread being uralitization of clinopyroxene in those sills near the contact aureole. The composition of uralitic amphibole is clearly distinct from that of primary amphibole (Appendix 6, Fig. 32). Orthopyroxene and spinel — amphibole coronas formed between olivine and plagioclase grains in the olivine bearing sills at the same time as corona textures in the Halti cumulates.

Compositions of metamorphic minerals

For each mineral analyzed from the Ridnitsohkka aureole gneisses and gneiss interlayers 3—4 determinations were made, including both margins and cores, from which means were calculated. No systematic determinations of zonation were undertaken, but in cases where the cores and rims of garnets were distinctly different, the data have been listed separately (Appendix 9).

Garnet. Garnets in the Ridnitsohkka area may be subdivided into three groups on the basis of their chemical compositions (Fig. 39, Appendix 9). Garnets in the aureole and interlayer gneisses are zoned, with their central parts having a pyrope component (Prp = Mg/Mg + Fe + Mn +

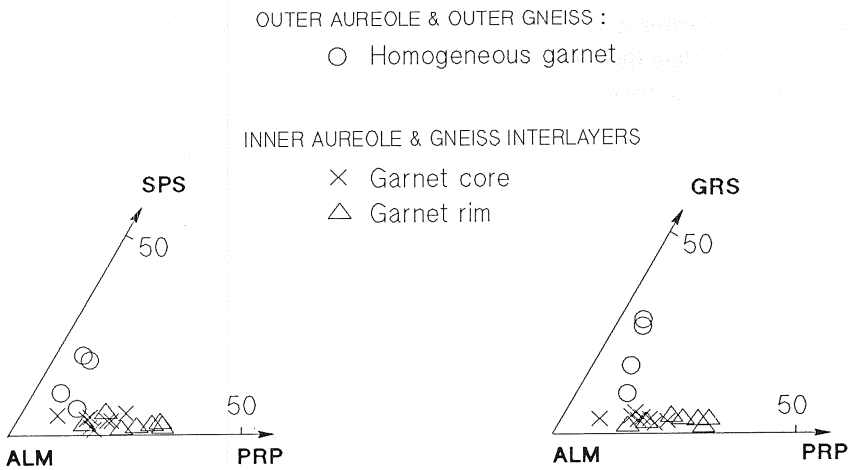

Fig. 39. Garnet compositions in the Ridnitsohkka area. ALM = almandine, SPS = spessartite, PYR = pyrope, GRS = grossularite.

Ca) of 0.14—0.22, which is appreciably less than that in the sillimanite-bearing rims (Prp = 0.15—0.31). The third group of garnets occur in the isoclinally folded outer parts of the aureole and in the gneisses outside the aureole. These have markedly higher spessartine and grossular contents and the pyrope component is correspondingly less (Prp = 0.04—0.10). The highest pyrope abundances in these rocks (Prp = 0.10) are found in mylonite zone outside the aureole.

Biotite. Biotites outside the contact aureole clearly have the lowest X_{Mg} values (X_{Mg} = Mg/Mg + Fe + Mn + Ti + Al^{VI}), with a mean value of 0.25 and a standard deviation of 0.02 (Appendix 7). In the mylonite zone east of the aureole, X_{Mg} = 0.33 and in the isoclinally folded gneisses in the outer aureole, X_{Mg} = 0.25. The mean value of X_{Mg} for the aureole as a whole is 0.39, with a standard deviation of 0.04. The highest X_{Mg} values occur in the biotite within the gneiss interlayers and the gabbro sills themselves; the former have a mean X_{Mg} of 0.52 and a standard deviation of 0.08, while respective values for the sills are 0.52 and 0.05. The highest X_{Mg} value obtained, of 0.75, was from a strongly recrystallized metabasalt interlayer between the sills. There is no detectable difference in biotite composition between the inner and outer parts of the aureole. Likewise, compositions within the whole of the sill area are very uniform.

Orthopyroxene. Metamorphic orthopyroxene in the gneiss interlayers is typically poikiloblastic, containing abundant plagioclase and K-feldspar inclusions, and may be up to 3—4 mm in diameter. They have a great scatter of En values (En = 100Mg/Mg + Fe + Ca), ranging between 40 and 60 (Appendix 5). The same applies to orthopyroxene in the sills En_{49-61}, with one exceptional sample at En_{73}. Calcium contents, measured by the wollastonite component (Wo = 100Ca/Ca + Mg + Fe), are much lower in the interlayer gneiss orthopyroxenes (Wo = $Wo_{0.4-0.5}$ and two samples below detection limit) than in those from the gabbro sills (Wo = $Wo_{1.3-3.1}$). The interlayer gneiss orthopyroxenes differ from the sill orthopyroxenes most clearly in having much higher Al_2O_3 contents (3.38—3.45 wt% for the gneisses and < 1.18 wt% for the sills).

Plagioclase. Plagioclases in the gneisses beyond and in the outermost parts of the Ridnitsohkka aureole clearly have the lowest anorthite contents (An_{26-28}). The highest anorthite values in the

aureole occur in proximity to the sills (An_{44}) and within the gneiss interlayers in general, vary from An_{29-42}. Plagioclase compositions are presented in Appendix 3.

Cordierite. A single, partly altered cordierite grain from the central part of the sill area was analyzed and has an X_{Mg} value (X_{Mg} = Mg/Mg+Fe) of 0.84 (Appendix 10). Cordierite in gneiss interlayers near the Halti cumulates have not been altered and have X_{Mg} values of 0.73—0.80. These high Mg values indicate that cordierite formed at high pressures in the upper part of the cordierite-almandine stability field (Thompson, 1976).

Spinel. Spinel is only present in gneiss interlayers and within the inner parts of the aureole and occurs either as inclusions within aluminosilicates or together with plagioclase. Spinel is typically present as greenish hercynite, with X_{Mg} (X_{Mg} = $Mg/Mg+Fe^{2+}$) varying between 0.71—0.85 (Appendix 10). A notable exception to this is the occurrence of brownish Cr-bearing spinel in gneiss interlayers adjacent to the Halti cumulates, which have X_{Mg} = 0.66 (not listed in Appendix 11).

Ilmenite. Ilmenite is a common accessory mineral in the Ridnitsohkka sills, the contact aureole and the gneiss interlayers. Appendix 10 lists compositions of samples from the aureole and interlayer gneisses, demonstrating that there is no appreciable difference between them, although Mn, Mg and V are slightly higher in the interlayer ilmenites than in those in the aureole.

Muscovite. Muscovite is abundant in the gneisses outside the Ridnitsohkka aureole and also within the aureole but is absent from the gneiss interlayers in the sill area. The X_{Fe} value (X_{Fe} = Fe/Fe+Mg) increases in a linear fashion from 0.31 to 0.52 progressing towards the outer part of the aureole and attains a maximum of 0.60 in the gneisses beyond it. In the mylonitic gneisses outside the contact aureole muscovite X_{Mg} = 0.45 (Appendix 11).

Pressure and temperature determinations

The analytical precision of the measurements was, using the SEM-EDS system, below 0.5 wt% and the abundances of many elements were so small as to remain below detection limits. Therefore thermobarometric estimations that involve elements occurring at very small concentrations should be treated with caution. The PT estimations derived here are hence rather qualitative, particularly since, with the exception of garnet, mean values for individual grains have been used in the calculations.

Metamorphic temperatures have been calculated using the garnet — biotite, garnet — orthopyroxene and K-feldspar — plagioclase geothermometers. Pressures were estimated with the garnet — orthopyroxene — plagioclase — quartz and garnet — plagioclase — sillimanite — quartz geobarometers. The Mg-rich rims of garnets containing sillimanite inclusions have been used in calculations involving garnet because they are considered to have crystallized or equilibrated at the peak of prograde metamorphism. Because biotite is susceptible to retrograde alteration, it is inferred that it too equilibrated under peak metamorphic conditions, before undergoing compositional changes during retrogression.

Table 4 lists the temperatures calculated for two samples from gneiss interlayers, using the garnet — orthopyroxene geothermometer. Temperatures using the calibration by Harley (1984), between 911—950 °C compare favourably with those calculated according to the Perchuk et al. (1985) calibration, 924—970 °C. These are both distinctly higher than temperature estimations obtained from other geothermometers, but evidently represent the thermal peak associated with sill intrusion.

Garnet — biotite geothermometry (Table 4) has been carried out using the methods suggested by Ferry and Spear (1978), Perchuk and Lavrenteva (1983) and Hodges and Spear (1982). Calculated temperatures are highest for gneiss interlayers in the inner part of the sill area, being

Table 4. Garnet — biotite, garnet — orthopyroxene and plagioclase — K-feldspar temperature determinations for the Ridnitsohkka area. Garnet — biotite temperatures according to F&S = Ferry & Spear 1978, P&L = Perchuck & Lavrentera 1983, H&S = Hodges & Spear 1982. Garnet — orthopyroxene temperatures according to H = Harley 1984, P = Perchuck et al. 1985. Plagioclase — K-feldspar temperatures according to S = Stormer 1975, Ha = Haselton et al. 1983. Lithol. = lithologies: GNIL = gneiss intrlayer between Ridnitsohkka gabbro sills, GNAU = metamorphic aureole in outer gneiss, GN = outer gneiss. Location: S/AU = distance in meters westward (+)/eastward (—) from the contact between sill area and metamorphic aureole at Ridnitsohkka, C/S = distance in meters away (—) from the Halti cumulates in the sill area, C/GN = distance in meters away (—) from the Halti cumulates in the outer gneiss area.

			T(C) Garnet–Biotite			T(C) Garnet–Opx		T(C) Plg–(K–Fs)	
Sample	Lithol.	Location	F&S	P&L	H&S	H	P	S	Ha
361A	GNIL	S/AU+1380 =C/S–450	–	–	–	–	–	765	885
88	GNIL	S/AU+800 =C/S–1300	1061	795	1074	950	970	675	722
357A	GNIL	S/AU+750 =C/S–1100	–	–	–	–	–	604	638
355C	GNIL	S/AU+360 =C/S–1500	737	664	749	911	924	–	–
89A	GNIL	S/AU+20 =C/S–2100	592	591	605	–	–	–	–
504A	GNAU	S/AU–20	685	639	698	–	–	–	–
504F	GNAU	S/AU–100	661	627	676	–	–	643	673
505	GNAU	S/AU–100	640	616	646	–	–	–	–
504B	GNAU	S/AU–140	609	600	625	–	–	–	–
504C	GNAU	S/AU–230	621	607	641	–	–	–	–
504D	GNAU	S/AU–450	782	685	791	–	–	–	–
504E	GNAU	S/AU–580	602	596	688	–	–	–	–
134A	GN	S/AU–820	616	604	653	–	–	–	–
133	GN	S/AU–1840	585	587	683	–	–	–	–
40	GN	C/GN–100	676	634	732	–	–	–	–

around 660—800 °C according to the calibration of Perchuk and Lavrenteva. They are nevertheless lower than temperature estimations for the same samples made using the garnet — orthopyroxene method (with the exception of several unrealistically high values in excess of 1000 °C). Temperatures between 600—690 °C determined for the aureole using the garnet — biotite geothermometer (as calibrated by Perchuk and Lavrenteva) appear to systematically decrease towards its outer margin. Temperatures in the gneisses outside the aureole appear to be rather low, between 590—600 °C using the Perchuk and Lavrenteva method. The gneisses beneath the Halti cumulates yield somewhat higher temperatures (634 °C according to the Perchuk and Lavrenteva calibration), presumably due to downwards migration of heat from the cumulate sequence. The systematically lower temperatures obtained from garnet — biotite pairs

Table 5. Garnet — plagioclase — sillimanite — quartz (G-P-S-Q) and garnet -orthopyroxene — plagioclase — quartz (G-O-P-Q) pressure estimates for Ridnitsohkka gneiss interlayers. G-P-S-Q: Pressures calculated according to NH = Newton & Haselton 1981, KN = Kozoil & Newton 1988. G-O-P-Q: Pressures calculated according to (PC-Mg, PC-Fe) = Perkins & Chipera 1985, NP = Newton & Perkins 1982, PH = Powell & Holland 1988. Temperatures are based on the garnet — orthopyroxene thermometer after Harley 1984 (from Table 4). Lithol. = lithology: GNIL = gneiss interlayer between Ridnitsohkka gabbro sills.

			P(kbar) G-P-S-Q		P(kbar) G-O-P-Q			
Sample	Lithol.	T(C)	NH	KN	PC-M	PC-Fe	NP	PH
88	GNIL	950	8.3	8.9	5.9	5.0	6.8	6.0
355C	GNIL	911	6.7	7.3	4.7	4.6	5.6	4.8

compared to those from garnet — orthopyroxene geothermometry result from retrogressive alteration of biotite.

Temperatures calculated using the K-feldspar — plagioclase geothermometer represent retrogressive stages of metamorphism. Table 4 lists results according to the calibrations by Stormer (1975) and Haselton et al. (1983). Values are highest (765 °C according to the Stormer calibration) for gneiss interlayers nearest the contact zone with the Halti cumulates. Temperatures do not however systematically decrease across the sill unit since values obtained from the aureole (643 °C using the Stormer calibration) are similar to those obtained from gneiss interlayers between the sills (604—675 °C). Temperatures for sample 88 were also determined using the garnet — orthopyroxene and garnet — biotite geothermometers and the resultant values were significantly higher than those obtained using the K-feldspar — plagioclase method.

Pressures were determined using the garnet — plagioclase — sillimanite — quartz (Newton and Haselton, 1981; Koziol and Newton, 1988) and garnet — orthopyroxene — plagioclase — quartz (Newton and Perkins, 1982; Perkins and Chipera, 1985; Powell and Holland, 1988) geobarometers.

The garnet — plagioclase — sillimanite — quartz geobarometer is very sensitive to changes in temperature. Therefore the pressure estimates in Table 5 were determined using the temperatures determined by the Harley (1984) calibration for garnet — orthopyroxene pairs from two samples of interlayer gneisses. However, because the temperatures determined for garnet — biotite pairs represent retrogressive metamorphism and are hence too low, garnet — plagioclase — sillimanite — quartz pressure estimates using these temperatures are likewise too low, with values (not listed in Table 5) variously ranging from 1.8—6.0 kbar (according to Newton and Haselton) and 2.6—6.7 kbar (according to Kozoil and Newton). Pressure estimates using the garnet — orthopyroxene geothermometer are distinctly greater, ranging between 6.7—8.3 kbar (for the Newton and Haselton calibration) and 7.3—8.9 kbar (according to the Kozoil and Newton calibration).

Pressures determined using the garnet — orthopyroxene — plagioclase — quartz geobarometer are clearly lower than corresponding values using the garnet — plagioclase — sillimanite — quartz geobarometer. This difference is probably a consequence of the garnet + orthopyroxene + plagioclase + quartz assemblage not being in strict equilibrium. Of the various garnet — orthopyroxene — plagioclase — quartz geobarometers available, the Fe-reaction of Perkins and Chipera (1985) gives a distinctly lower pressure (4.6—5.0 kbar) than do the others (4.7—6.8 kbar). This particular barometer is not very temperature dependent, so that for example, a change of ± 100 °C results in a change in press-

ure of only ±0.1—0.3 kbar. Temperatures calculated according to the calibration of Harley (1984) have been used in determining the garnet — orthopyroxene — plagioclase — quartz pressures listed in Table 5.

Metamorphic mineral reactions, mineral compositions and pressure-temperature determinations for the Halti cumulate sequence

The metamorphic history of the cumulates can be determined by studying corona textures between olivine and plagioclase grains and also by the mineral assemblages in the amphibole rock.

Coronas between olivine and plagioclase grains

Corona reactions in the forsterite-anorthite system are particularly sensitive to changes in pressure (Kushiro and Yoder, 1966; Green and Ringwood, 1967) and, depending on the temperatures involved, plagioclase and olivine are in equilibrium with one another up to pressures of 6—9 kbar. At higher pressures they react to form orthopyroxene and clinopyroxene — spinel intergrowths, which are stable up to pressures of 9—11 kbar, again depending upon ambient temperatures. If water is present however, amphibole forms instead of clinopyroxene (Grieve and Gittings, 1975):

(7) olivine + plagioclase + H_2O = orthopyroxene + amphibole + spinel

At still higher pressures garnet forms at the expense of the spinel-bearing aggregates. Corona textures between olivine and plagioclase in the Halti cumulates invariably consist of orthopyroxene and spinel — amphibole intergrowth, with the exception of sporadic occurrences of Ca-rich plagioclase — clinopyroxene and orthopyroxene — spinel — anorthite intergrowths (Sipilä, 1988).

The temperatures at which coronas form has been investigated by Wells (1977) and Nickel and Brey (1984), using pyroxene geothermometry and assuming equilibrium between corona orthopyroxene and any primary clinopyroxene in the rock (Table 6). Wells (1977) determined temperatures of between 870—990 °C and Nickel and Brey (1984) obtained values in the range 750—930 °C, when one anomalously low result was excluded from consideration. The thermometry of Wells (1977) is independent of pressure and the pressure dependence of the Nickel and Brey (1984) geothermometer is also small. The variation between the two studies is nevertheless large and the values of Nickel and Brey are 60—120 °C lower than those determined by Wells. The scatter in temperatures between different samples is partly attributed to the fact that the Fe/Mg ratio of the corona pyroxene is not always in equilibrium during corona formation. However, the main reason for the scatter is that at low temperatures, relatively small variations in pyroxene Mg/Mg + Fe values cause major changes in calculated temperatures. The general temperature range over which corona textures form nevertheless appears to be between 800—900 °C, correlating with pressures of 7—10 kbar (Kushiro and Yoder, 1966; Green and Ringwood, 1967).

The Mg contents of the corona orthopyroxenes between olivine — plagioclase are high (En_{63-89}) while the abundances of Ca ($Wo_{0.3-1.3}$) and Al_2O_3 (< 1.6 wt%) are low (Appendix 5). Corona amphibole corresponds to pargasite in composition (Appendix 6), while because of its exceedingly fine grain size, reliable determinations of corona spinel composition could not be made.

In addition to the spinel occurring within intergrowths in the coronas between olivine and plagioclase grains, the Halti cumulate olivine gabbros also contain metamorphic green her-

Table 6. Orthopyroxene — clinopyroxene temperatures for the Halti cumulates and Ridnitsohkka gabbro sills calculated according to W = Wells 1977 and N = Nickel and Brey 1984. Lithol. = lithologies: SILL = Ridnitsohkka gabbro sill, MBIL = metabasalt interlayer between sills, GBPG = gabbro pegmatite, TRO = troctolite, OLGB = olivine gabbro. * = orthopyroxene is from the corona between olivine and plagioclase.

Ridnitsohkka area					Halti area			
Sample	Lithol.		W	N	Sample	Lithol.	W	N
26	SILL		1238	1202	31	GBPG*	966	894
87	SILL		1249	1212	39	TRO*	871	752
144A	SILL		1196	1161	43	OLGB*	718	476
352	SILL		1225	1190	44	OLGB*	947	868
353	SILL		1241	1204	48	OLGB*	989	926
355A	SILL		1301	1258				
356	SILL		1242	1205				
357	SILL		1239	1202				
358	SILL		1312	1267				
359	SILL		1262	1224				
360	SILL		1311	1266				
363	SILL		1257	1219				
		AVG	1256	1218				
		std	34	31				
362A	MBIL		1104	1066				
25	SILL*		1075	1032				

cynite inclusions in ilmenomagnetite. McSween et al., (1984) described similar metamorphic ilmenomagnetite from the Piedmont gabbro -metagabbro association, which evidently represent temperatures of 500—550 °C and pressures of 5 kbar.

Amphibole rocks

Amphibole rocks formed when the plagioclase-bearing lithologies of the Halti cumulate sequence underwent intense hydrothermal alteration at about the same time as, if not somewhat later than the development of the corona textures (Bøe, 1976). These rocks generally lack primary mafic minerals, such as olivine and clinopyroxene, whereas primary plagioclase is usually present. Typical assemblages consist of:

plagioclase + amphibole + zoisite + kyanite ± corundum ± quartz ± paragonite

The mineral pair zoisite — kyanite appears, on the basis of microscopic observations, to have formed by plagioclase breakdown:

(8) anorthite + H_2O = zoisite + kyanite + quartz

Most of the quartz generated by Reaction (8) was evidently consumed during the subsequent formation of other minerals, such as amphibole and mica. According to Goldsmith (1981), Reaction (8) terminates at an invariant point at 725 °C and 10.2 kbar, after which anorthite begins to melt (Fig. 40). Reaction (8) has nevertheless taken place below the invariant point in the Halti amphibole rocks since there is no evidence for partial melting in outcrop or in thin section. Goldsmith (1981) concluded that corundum may also be present in this mineral assemblage, but its pressure and temperature dependency is not precisely known. However, in the absence of

quartz and at pressures equalling or exceeding 10 kbar, corundum is probably stable in the anorthite + H_2O and zoisite + kyanite + H_2O + melt fields (Fig. 40).

Amphibole compositions from the Halti amphibole rock correspond to those of tchermackite and ferrotchermackite on the Deer et al. (1963) classification diagram (Fig. 32, Appendix 6). They also have alkali and Al(IV) contents that are markedly lower than those of the corona amphiboles. According to the classification by Leake (1978), and calculating Fe^{3+}/Fe^{2+} ratios by the method of Droop (1987), amphiboles in the amphibole rocks belong principally to the tchermackitic hornblende and magnesio-hornblende groups whereas the corona amphiboles are pargasitic. Plagioclase compositions in the amphibole rocks vary between An_{42-83} (Appendix 3). In addition the amphibole rock contains a colorless mica which proved to be paragonite (Appendix 11), although margarite too is present (R. Alviola, pers. comm. 1991). Appendix 11 also lists some zoisite compositions for the Halti amphibole rocks.

P-T evolution of the Halti-Ridnitsohkka complex

The Ridnitsohkka gabbro sills intruded their pelitic gneiss host rocks during the Scandian phase of the Caledonian Orogeny at about 430 Ma. Pressures during intrusion were around 7—8 kbar and the temperature of the sill magma was calculated by orthopyroxene — clinopyroxene thermometry to have been in excess of 1200 °C (Table 6). This caused intense thermal metamorphism of the gneisses and led to anatexis in the aureole proper, since this was where the partial pressure of water was greatest. Because of the high pressures, the breakdown of muscovite led to the formation of kyanite where aureole temperatures were below 660—750 °C and sillimanite where temperatures were higher, such as in the inner part of the aureole and within the gneiss interlayers close to the aureole. Temperatures were so high in the central part of the sill area that the assemblage garnet + cordierite + K-feldspar was stable in preference to sillimanite + biotite + quartz. Heat from the sill magma also caused the breakdown of biotite in some gneisses, with the formation of orthopyroxene instead. High pressures nevertheless promoted the relatively rapid and complete hydration of cordierite and orthopyroxene, forming intergrowths containing biotite and sillimanite, which in turn reacted with quartz to form K-feldspar and Mg-rich almandine garnet. The partial pressure of water in the gneiss interlayers was relatively low and any anatectic melt that may have formed was to some extent assimilated into the sill magmas. That this took place is shown by the abundances of alkalis in the sills and the presence hydrous primary minerals such as hornblende and biotite. The pressure maximum of 8—10 kbar in the sill area was attained during the peak of D_2 deformation, during which the last remaining cordierite in the gneiss interlayers reacted to form fine-grained aggregates of orthopyroxene + sillimanite + quartz. Regional pressures in the gneiss interlayers immediately adjacent to the Halti cumulates did not however, exceed that of the stability field for cordierite.

The metamorphic evolution of the Halti cumulate sequence was controlled not only by the amount of water present but also by the high ambient pressures. Orthopyroxene and spinel — amphibole coronas developed between olivine and plagioclase grains in the troctolites and olivine gabbros at temperatures of 800—900 °C and at pressures of 7—10 kbar. Where water was abun-

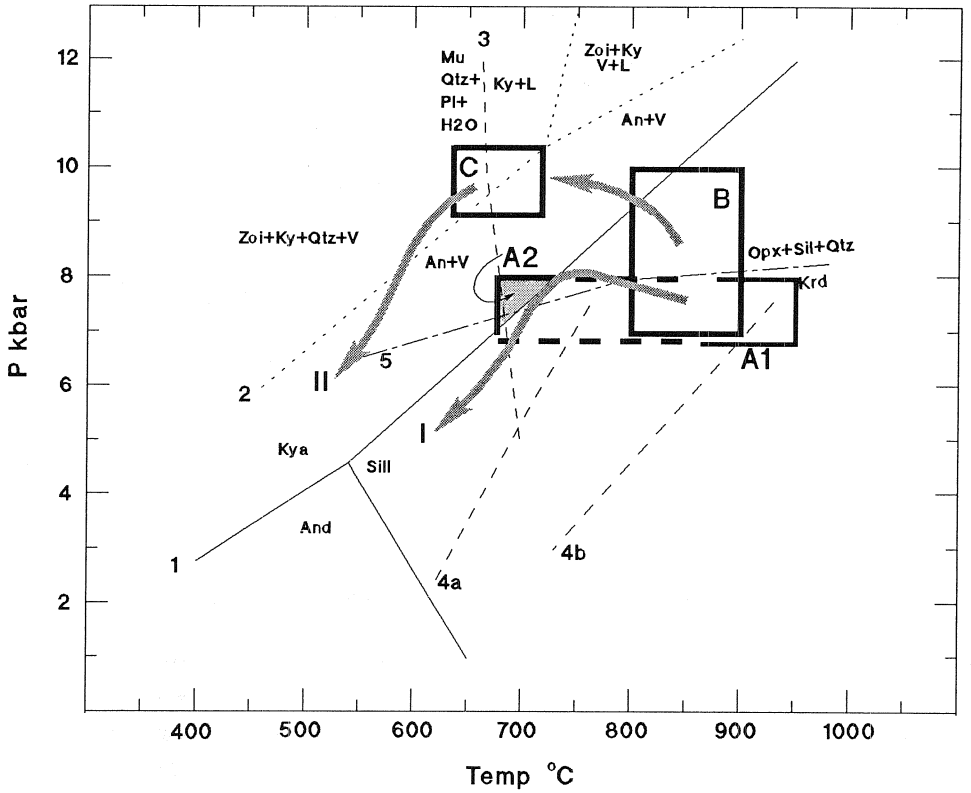

Fig. 40. P-T diagram and possible P-T paths for the Ridnitsohkka gneiss interlayers (I) and Halti cumulate rocks (II). Box A1-A2 = intrusion of Ridnitsohkka gabbro sills (A1) and formation of the kyanite bearing metamorphic aureole (A2, darker area). Box B = formation of the olivine-plagioclase corona. Box C = formation of Halti amphibole rock. Metamorphic conditions are based on: Box A1-A2; Gar-Opx temperature and Grt-Pl-Sil-Qtz & Grt-Opx-Pl-Qtz barometers (A1), reaction Ms + Qtz + Pl + H2O = Ky + L (A2, darker area) (Thompson & Tracy 1979). Box B; Opx-Cpx thermometer and pressure from the corona mineralization (Grieve & Gittins 1975). Box C; corundum bearing plagioclase breakdown reaction (Goldsmith 1981). P-maximum in path I is based on cordierite breakdown: Crd = Opx + Sil + Qtz (Newton 1972). Stability curves: (1) Kya-And-Sill (Salje 1986). (2) An + V = Zoi + Ky + Qtz + V; An + V = Zoi + Ky + V + L; Zoi + Ky + V + L = Zoi + Ky + Qtz + V (Goldsmith 1981). (3) Mu + Qtz + Pl + H2O = Ky + L (Thompson & Tracy 1979). (4a) Bt + Sil + Qtz = Grt + Crd + Kfs (XH2O = 0.4 (Holdaway & Lee 1977)). (4b) Bt + Sil + Qtz = Grt + Crd + Kfs (XH2O = ptot (Holdaway & Lee 1977)). (5) Crd = Opx + Sil + Qtz (Newton 1972).

dant, the mineralogy of plagioclase-bearing cumulates was radically altered, with Ca-rich plagioclase breaking down to form zoisite + kyanite + quartz, and tchermackitic amphibole being the only stable mafic phase. Corundum formed during plagioclase breakdown is consistent with pressures around 10 kbars. The temperature at which the amphibole rocks formed must have been below 700 °C, because at higher temperatures the breakdown of plagioclase is associated with the onset of melting, for which there is no evidence in the Halti cumulates. Corona and amphibole rock formations were essentially isobaric, with the coronas developing at temperatures 150—200 °C higher than the amphibole rocks.

The pressure maximum in both the sill area and within the cumulates was attained after the climax of magmatic activity. The intense shearing of all lithologies, including the amphibole rock,

in the contact zone between the cumulate sequence and the sill unit indicates that they were tectonically juxtaposed or displaced after the peak of metamorphism. This explains the preservation of cordierite-bearing, lower pressure assemblages in gneiss interlayers in close proximity to the cumulates.

Approximate P-T paths for the Halti-Ridnitsohkka rocks and reaction curves used in their determination are shown in Fig. 40.

PETROGENESIS OF THE HALTI-RIDNITSOHKKA COMPLEX

The parent magma for the Halti cumulate sequence

No chilled margin or apophyses to the Halti cumulate sequence have been found, from which it might have been possible to determine the primary composition of the parent magma. The lower contact against the gneisses of the Nabar Nappe is tectonic, while the contact with the Ridnitsohkka sill unit is obscured by the metasomatic augite megacryst gabbro. Because contacts are thus tectonic, and because much of the complex has been removed by erosion, it is not feasible to use the relative proportions of presently exposed lithologies to calculate a mean composition for the cumulates, and hence estimate the bulk composition of the parent magma.

However, the MgO/MgO + FeO molar ratio (Mg') can be determined using the composition of the most Mg-rich olivine present, assuming it to have been in equilibrium with the parent magma. Using a distribution coefficient value of $K_D = 0.33$ (Bickle, 1982; Duke, 1986), Mg' for the parent magma can be determined according to the formula $Fo = Mg'/Mg' + K_D(1\text{-}Mg')$ (Kaula et al., 1981). The highest forsterite contents in the olivines of the Halti dunites are in the range Fo_{92-90}, which would be in equilibrium with a melt having a calculated Mg' of 0.75—0.79.

The partitioning of Mg between olivine and a silicate melt depends on both the composition of the melt and temperature (Leeman, 1978; Roeder and Emslie, 1970). Application of the correlations presented by Duke and Naldrett (1978) for komatiitic magmas indicates that the Halti olivines having compositions of Fo_{92-90} would have crystallized from a melt containing on average 20—25 wt% MgO (Fig. 28).

When determining the MgO content of a melt from the forsterite composition of olivine, it is essential to establish that the olivine is primary and has not been subjected to any alteration processes. Metamorphic olivines formed via the dehydration of serpentine minerals tend to be anomalously Mg-rich (Evans, 1977; Dymek et al., 1988). However, during the initial stages of recrystallization, there is no significant difference between the Mg contents of primary and recrystallizing olivine (Hoffman and Walker, 1988). Although olivine in the Halti cumulate lithologies is indeed Mg-rich, it is nevertheless primary and not metamorphic, as is demonstrated for example, by the presence of cumulus textures and the lack of strong recrystallization. Variations in the Ni/Fo ratio of olivine (Fig. 28) follow the magmatic trend defined by Duke and Naldrett (1978). Likewise, the positive correlation between Mn and Fe and the generally low Ca abundances are characteristic of magmatic, or more specifically plutonic olivine (Simkin and Smith, 1970).

Cr-spinel, which has the general formula $(Mg,Fe^{2+})(Cr,Al,Fe^{3+})_2O_4$ is a typical accessory mineral in basalts and peridotites. Except for the Cr_2O_3 component, it has no significant influence on the bulk composition of rocks or parent magmas (Irvine, 1965, 1975; Dick, 1977; Dick and Bullen, 1984). Cr-spinel is thus an extremely sen-

sitive indicator of petrogenesis with the extra advantage of not causing any significant change in major element distributions. The composition of Cr-spinel is dependent upon factors such as concentration ratios, pressure, temperature and oxygen fugacity. Allan et al., (1988) showed that for MORB type volcanics there is a strong positive correlation between the MgO, FeO and Al_2O_3 abundances of groundmass glass and Cr-spinel phenocrysts; for Cr_2O_3 however, positive correlation is weak. Cr-spinel having high alumina contents were formerly considered to represent crystallization at high pressures (Jaques and Green, 1979; Dick and Bullen, 1984). However, according to experimental investigations carried out by Allan et al. (1988) and Thy (1991a), the Cr/Cr + Al ratio is more dependent on the concentrations of these elements in the melt. The partitioning of Mg and Fe^{2+} between spinel and melt is very temperature dependent, while the Fe^{2+}/Fe^{3+} ratio is very sensitive to changes in oxygen fugacity (Dick and Bullen, 1984; Allan et al., 1988). High Fe contents are indicative of alteration processes during which MgO and Al_2O_3 are replaced by FeO and Fe_2O_3 (Beeson and Jackson, 1969; Hoffman and Walker, 1978). A high Al_2O_3 content in Cr-spinel may also indicate a metamorphic origin since during the prograde metamorphism of serpentinite, in the presence of chlorite and any two other Mg-silicate phases, the Cr/Cr + Al ratio of Cr-spinel decreases systematically with increasing metamorphic grade (Evans and Frost, 1975). Brown Al-rich chromite is characteristic of the upper amphibolite facies, while green Mg-Al spinel is typical of the granulite facies, when chlorite is also replaced by amphibole.

The low Cr/Cr + Al and Mg/Mg + Fe^{2+} ratios of the Halti Cr-spinels indicates that they do not have typical magmatic compositions and on the Cr/Cr + Al vs. Mg/Mg + Fe^{2+} diagram (Fig. 30b) they accordingly plot along the boundary between the metamorphic and ophiolitic spinel fields. The lowest Mg/Mg + Fe^{2+} values and highest Fe abundances occur in the corroded Cr-spinel grains in the amphibole rock and although Fe^{3+} is very low, these spinels probably represent the highest degree of alteration.

The composition of the Halti cumulate Cr-spinel can nevertheless be considered to be primary, since the presence of cumulus textures demonstrates that they are not metamorphic in origin. Moreover an origin by prograde secondary replacement of metamorphic chlorite can be discounted because there is no compelling evidence for chlorite ever having existed in the rocks. The serpentinization of olivine in the Halti cumulates was a relatively late stage process and in many places serpentine veins truncate Cr-spinel grains, again attesting to their early origin. None of the larger cumulate Cr-spinel grains show any evidence of a systematic decrease in Cr/Cr + Al ratios from core to rim, which would have been expected had they grown during prograde metamorphism (Evans and Frost, 1975; Trommsdorf and Evans, 1974). Moreover, the later stage serpentinization has apparently not affected Cr-spinel compositions since they have not become more Fe-rich towards their rims. During serpentinization it is possible for chromite to be overgrown by a rim of magnetite (Bliss and McLean, 1975; Vuollo, 1988; Vuollo and Piirainen, 1990). An increase in the Cr/Cr + Al ratio and concomitant decrease in the Mg/Mg + Fe^{2+} ratio in Cr-spinels with increasing SiO_2 abundances in host rock (Fig. 25) is a characteristic feature of primary magmatic Cr-spinel (Dick and Bullen, 1984). The low Cr/Cr + Al ratio of Cr-spinel in the Halti cumulates thus implies that the corresponding ratio in the source magma was also low (Allan et al., 1988; Thy, 1991a).

Kushiro (1960) and LeBAS (1962) showed that the composition of pyroxene provides some constraints on the composition of the basaltic magmas from which they have crystallized. Clinopyroxenes from the Halti cumulates cover a broad compositional range, lying predominantly in the fields for clinopyroxenes from non-alkaline basalts and normal alkaline basalts on the LeBAS (1962) diagram (Fig. 31).

The fact that the Halti cumulate sequence structurally overlies the Ridnitsohkka sill unit may suggest that the sill magma may represent the parent magma of the cumulates. The Mg' of the magma in equilibrium with the cumulate olivines, based on their forsterite contents, was 0.75—0.79, which corresponds to a MgO content of 20—25 wt%. The maximum Mg' determined for the Ridnitsohkka sills was 0.70, with a mean value of 0.61, while the highest MgO content in the sills is 9.0 wt%, with a mean of 6.7—6.8 wt%. Thus, the parent magma for the Halti cumulates was clearly much richer in MgO than the Ridnitsohkka sill magma. Furthermore, the positive Eu anomalies in the sills shows that their parent magma cannot have been a residual melt following fractionation of the plagioclase-rich Halti cumulates. Likewise the growth of metasomatic clinopyroxene porphyroblasts in the contact zone between the Halti cumulates and the sills is clear confirmation that the sills cannot represent a cumulate residue, since they had clearly crystallized before the last residual differentiates from the cumulates. Further evidence for their separate origin is the absence of dykes resembling the Ridnitsohkka sills that might have cut across the cumulate sequence.

The composition of the parent magma for the Halti cumulates may also be estimated by making comparisons with other similar, well studied magmatic complexes. The layered peridotites and gabbros of the Rhum magmatic complex (Wager and Brown, 1968; Emeleus, 1987; Bédard et al., 1988) closely resemble those at Halti in terms of lithology, mineralogy and both whole-rock and mineral chemistry. The parent magma for the dunitic peridotites of the Rhum complex were previously regarded as basalts rich in alumina (Wager and Brown, 1968), but more recently it has been interpreted as picritic (Emeleus, 1987; Bédard et al., 1988). The composition of the Rhum parent magma is assumed to have been equivalent to that of cross-cutting picritic dykes, which have MgO contents in excess of 20 wt% (Emeleus, 1987).

According to Bennett et al. (1986), the ultramafic rocks of the Seiland petrographic province, consisting of wehrlites and dunites, crystallized from a mantle-derived, possibly picritic parent magma that contained about 20 wt% MgO. Such magmas are best represented by certain picrite — ankaramite dykes which cut the main ultramafic complex. Robins et al. (1987) considered that the Honningsvåg dunite — troctolite — olivine gabbro cumulates crystallized from a number of separate pulses of subalkaline basalt or picritic magma.

The fact that Ca-poor pyroxene is missing from the Halti cumulate olivine + plagioclase + clinopyroxene assemblage suggests that the primary magma may have been silica undersaturated. However, the magma did fractionate towards more felsic differentiates, even if this process was relatively weak. The composition of the parent magma must therefore have been on the SiO_2 side of the critical plane of silica undersaturation as defined by Yoder and Tilley (1962). The absence of primary hydrous minerals and the appearance of plagioclase early during the cumulus stage indicates that the water activity in the melt was low (Biggar, 1983). In summary it may be concluded that the parent magma for the Halti cumulate sequence was picritic and contained in excess of 20 wt% MgO. It was also evidently slightly oversaturated with respect to silica, water activity was low and its Al/Cr ratio was high.

Conditions of crystallization of the Halti cumulate sequence

On the basis of the cumulus minerals present, the Halti cumulates appear to have formed by simple progressive fractionation of a primitive magma. The order of cumulus mineral crystalli-

zation, namely olivine + Cr-spinel + plagioclase + clinopyroxene, is typical of low pressure environments. Numerous experimental studies have shown that the mineral pair olivine-plagioclase is unstable in many basaltic systems at pressures greater than 9 — 12 kbar (Cohen et al., 1967; Green and Ringwood, 1967; Thy, 1991a,b). Thy (1991a) in particular showed that in weakly alkaline and transitional tholeiitic lavas, clinopyroxene crystallizes before olivine when pressures exceed 14 kbar, while between 12.5—14 kbar the crystallization sequence is olivine + clinopyroxene + plagioclase. At pressures below 12.5 kbar, the sequence of crystallization changes to olivine + plagioclase + clinopyroxene. According to Presnall et al. (1978), olivine and plagioclase cannot be in equilibrium with an Mg- and Ca-rich melt at pressures in excess of 5 kbar. Thy (1991a) demonstrated experimentally that at low pressures, alkalic and transitional basalt melts will crystallize Cr-spinel having Cr/Cr + Al ratios below 0.50, Mg/Mg + Fe ratios between 0.40—0.65 and relatively low estimated Fe^{3+}. The Al content of the Halti chrome spinels supports the hypothesis that the cumulates crystallized at relatively low pressures. Similarly, high Ti/Al ratios in clinopyroxenes are indicative of crystallization at pressures below 10 kbar (Thy, 1991a). The low Fe^{3+} contents of the Halti chrome spinels and the relative scarcity of oxide phases in the later differentiates further indicates that both oxygen fugacity and primary water contents of the magmas were low (Sato and Valencia, 1980).

Fractional crystallization of the Halti cumulates can be understood in terms of the low pressure pseudo-ternary Fo-Di-An system (Presnall et al., 1978). The composition of the parent magma for the cumulates was in the 'spinel area' of the forsterite field (Morse, 1980) and with progressive fractionation moved via the Fo-An cotectic towards the Fo-Di-An ternary pseudo-eutectic, with the last residual melt fraction crystallizing at temperatures of around 1300 °C. This fractionation coincided with the formation of cumulus layers, at first Cr-spinel dunites, followed by troctolites and olivine gabbros, with the pegmatitic gabbro dykes crystallizing from the last residual melt fraction.

Pressure exerts a major control on the stability fields of various mineral phases in the Fo-Di-An system. As pressure increases the stability fields of spinel and clinopyroxene enlarge at the expense of the olivine and plagioclase fields. As a consequence of this, further pressure increases lead to progressively more restricted magmatic compositions, with plagioclase being the first phase to crystallize after olivine. When pressures exceed 5 kbar however, only clinopyroxene and spinel can crystallize after olivine. Thus, a single parent magma can give rise to either dunite -troctolite cumulates at lower pressures or dunite — wehrlite cumulates under high pressure conditions. The widespread occurrence of olivine — plagioclase cumulates in the Halti sequence indicates that pressures were relatively low during their crystallization.

Intrusive environment of the Halti-Ridnitsohkka complex

According to Hausen (1942a), the Halti massif represents a phacolith, that had not yet crystallized at the time of nappe emplacement, with the magma acting as a kind of lubricant facilitating slip on thrust surfaces. He attributed the heterogeneity of the sequence to tectonic movements within the magma and surrounding gneisses and contended that only the olivine gabbro had crystallized under peaceful conditions.

The uncertain tectonostratigraphic setting of the Halti-Ridnitsohkka complex and the lack of precise age determinations has resulted in much speculation concerning its origin. Generally it has been correlated with the upper part of the Kalak

Nappe Complex and was assumed to have been emplaced into a rift in latest Precambrian time, during the earliest stages of opening of Iapetus (Lehtovaara and Sipilä, 1987; Lehtovaara, 1989; Mattson and Lindqvist, 1990; Sipilä, 1989; Zwaan and Roermund, 1990). Reservations concerning its position amongst the upper Scandian phase allochthons were expressed by Lehtovaara (1984), and correlation has been made with the Seve Nappe Complex (Lehtovaara, 1989). The Halti cumulates have also been interpreted as a remnant of an ophiolitic cumulate sequence (Lehtovaara, 1984; Sipilä, 1987; Lehtovaara and Sipilä, 1987), because ophiolites typically contain abundant dunite — troctolite — olivine gabbro cumulates (Coleman, 1977).

New U-Pb age determinations for zircon and baddeleyite from the Ridnitsohkka sills and associated contact aureole (445—425 Ma) clearly indicate however, that the sills were intruded during the Scandian orogenic phase (Vaasjoki et al., in prep.). Preliminary paleomagnetic data indicate an age of around 400 Ma for the Ridnitsohkka sills, in spite of their low remanence intensity and directional instability (Mertanen et al., 1990). The Scandian was the main phase of the Caledonian orogeny, related to the closure of Iapetus during the Late Ordovician and Silurian, when Fennoscandia and Laurentia collided. During collision the margin of Fennoscandia was telescoped and tectonically thickened, with the emplacement of nappes onto the foreland far from the suture. The closure of Iapetus was of an oblique (Phillips et al., 1976), strike-slip nature (Gayer, 1989) and most of the ophiolites obducted were already emplaced by Early Ordovician time (Dunning and Pedersen, 1988). In contrast, the Halti-Ridnitsohkka complex should be correlated with other Caledonian mafic intrusive complexes ((Artfjället (Senior and Otten, 1985; Otten and Senior, 1985), Fongen-Hyllingen (Habekost and Wilson, 1989; Wilson, 1985; Wilson et al., 1981), Honningsvåg (Robins et al., 1987), Råna (Tucker et al., 1990; Boyd and Nixon, 1985; Boyd and Mathiesen, 1979) and possibly Vaddas (Stevens, 1982)), that were likewise emplaced at the peak of orogenic activity. Ridnitsohkka sills are surrounded by a distinct contact metamorphic aureole. Because gneisses in the outer part of the aureole as well as between the sills have disharmonic folding, it is clear that the sills were intruded syntectonically. The earliest intrusions in the Halti-Ridnitsohkka complex were tholeiitic gabbro sills and it is possible that during the closure of Iapetus, deep-reaching transform faults tapped and facilitated the emplacement of mantle-derived ultramafic magmas from which the Halti cumulates also crystallized. The P-T paths determined for the Halti cumulates and the Ridnitsohkka gneiss interlayers indicate that maximum pressures were attained after the peak of magmatic activity.

Causes of regressive magmatism

A distinctive feature of the Halti-Ridnitsohkka magmatic complex is the gradual transition in magma type from a quartz-normative tholeiitic basalt through transitional olivine- and hypersthene-normative basalts to very primitive MgO-rich magmas form which the ultramafic and mafic Halti cumulates differentiated.

A similar development, from tholeiitic through transitional to weakly alkaline is observed within the Icelandic rift (Thy, 1991a,b). Tholeiitic magmatism is concentrated within the main rift zone while transitional and alkaline volcanism takes place in more marginal or distal areas. According to Thy (1991a,b), the tholeiitic magmas were erupted from relatively shallow (2—3 kbar) magma chambers, whereas the marginal zone magmas were from greater depths, corresponding to pressures of (3—8 kbar). The alkali affinity of

the latter magmas is a function of relatively high water activities as well as their higher pressures, enabling plagioclase to occur as a liquidus phase. In this case, the marginal zone lavas would be located on the alkali side of the thermal divide in the basalt tetrahedron and thus become nepheline saturated under hydrous conditions. The tholeiitic lavas are in contrast located on the opposite side of the thermal divide and become silica saturated under relatively anhydrous conditions.

Irvine (1974) presented a number of possible explanations to account for the regressive magmatism observed in the Duke Island ultramafic complex:

(1) Heating of wall rocks by successive pulses of magma results in slower cooling and fractionation of subsequent melts.
(2) Later magmas assimilate or are mixed with cumulate olivine that crystallized in the feeder channel from earlier magma pulses.
(3) Successive magma pulses are derived from progressively deeper sources, or are from regions that are progressively more and more anhydrous.
(4) The mantle source becomes progressively enriched in olivine as a consequence of repeated melt extraction.

Bennett et al. (1986) ascribe regression in the mafic and ultramafic sequences of the Seiland province to spasmodic sealing of a very deep magma chamber that was,as a result of density contrasts, strongly vertically zoned.

The simplest explanation for the origin of regressive magmatism in the Halti-Ridnitsohkka complex is the fourth possibility suggested by Irvine (1974), namely progressive olivine enrichment of the source due to melt extraction. Otherwise it would be difficult to account for the gradual change towards more primitive compositions in the Ridnitsohkka sills, clearly shown in Figures 26 and 34, until they eventually approaching those of the Halti cumulates. If the parent magma for the cumulates had indeed been derived from deeper in the mantle than that of the parent magma for the sills, then it would have been necessary for increasingly larger amounts of the cumulate magma to mix with the sill magma, in order to produce regressive compositional trends in the resultant hybrid rock. The following model calculation, made using the program IGPET 2 (Carr, 1987), shows how such a hybrid composition could be obtained by magma mixing.

The calculations require a number of assumptions to be made and only take major element concentrations into account. Two samples from the Ridnitsohkka sills are needed, one of which (sample 86 in this case) is taken to be of hybrid composition, while the other (sample 89, from the eastern margin of the sill area) is considered to represent the primary sill composition. The

Table 7. Magma mixing calculations. Picrite = groundmass of picrite dyke in Rhum Complex (McClurg 1982). SILL 89 = Ridnitsohkka gabbro sill at eastern margin of sill area, SILL 86 = Ridnitsohkka gabbro sill close to Halti cumulates.

	%								
	0.119	Picrite							
	0.881	SILL 89							
	SiO2	TiO2	Al2O3	FeO	MnO	MgO	CaO	Na2O	K2O
Picrite	45.29	1.08	11.27	10.54	0.16	20.71	9.51	1.32	0.11
SILL 89	50.87	1.31	19.27	7.21	0.14	7.89	9.45	3.05	0.81
Hybride SILL 86									
Obs	49.78	1.45	17.38	7.91	0.15	9.22	10.73	3.28	0.09
Calc	50.60	1.30	18.46	7.67	0.14	9.49	9.53	2.87	0.73
Dif	-0.82	0.15	-1.08	0.24	0.01	-0.27	1.20	0.41	-0.64

Sum of squares of residuals = 3.589

composition of the parental cumulate magma is assumed to be equivalent to that published for the groundmass of picritic dykes within the Rhum complex (Bédard et al., 1988, after McClurg, 1982). A reasonable hybrid composition is achieved using a 10 % picritic component (Table 7). The residual sum of squares is rather small, at 3.6, with the greatest departures from calculated compositions being upwards for K and downwards for Ca. However, since these are rather mobile elements, it is possible that this merely reflects changes that took place during metamorphism. Abundances of other elements correspond reasonably well with calculated values, even though respective contents in the source materials differ considerably, particularly for Si, Al, Fe and Mg.

Replacement structures and processes

On the basis of their primary structures the Halti dunites principally represent olivine — Cr-spinel adcumulates which crystallized to form rhythmic layers at the margins and on the floor of the magma chamber. The amount of interstitial plagioclase present is small. The dunite unit is nearly a kilometer thick and does not represent crystallization from a single batch of magma. Rather, the magma chamber would have been repeatedly replenished by successive pulses of primitive, Mg-rich magma, from which olivine and Cr-spinel were continually precipitated. Presumably this magma contained olivine crystals that were in equilibrium under mantle conditions since the Fo contents of olivine are high (around Fo_{90}) throughout all dunites. These magmas evidently intruded the already crystalline troctolite unit as well, since discontinuous layers of dunite several meters in thickness occur within the troctolites and the much denser picrite magma caused widespread brecciation of plagioclase-rich troctolite. Hot ultramafic magma may also have corroded and assimilated the plagioclase-rich lithologies, which have partially, or even totally changed to dunite (Fig. 4).

Similar replacement structures are common within the Rhum complex (Bédard et al., 1988), in which successive pulses of picritic magma intruded troctolitic layers. The high temperature ultramafic complexes within the Seiland province also show the same kind of features (Bennett et al., 1986). These complexes represent numerous mantle-derived magmapulses in which successively intruded primitive Mg-rich magmas have metasomatically enriched the surrounding rocks in olivine. These processes however are spatially restricted to a zone several meters wide in immediate proximity to the ultramafic magmas. The resultant effect on the olivine gabbros is that they become coarse-grained olivine-rich troctolites, while the troctolites become altered to dunite. In the Melkvann and Kvalfjord complexes, secondary wehrlite has formed in addition to dunite. Similar secondary dunites have been described from elsewhere, including the Duke Island ultramafic sequence (Irvine, 1974, 1985) and the Honningsvåg intrusion (Robins et al., 1987).

Origin of the augite augen gabbro

The contact zone between the Halti cumulate sequence and the Ridnitsohkka sill unit is characterized by a coarse-grained augite megacrysts gabbro, with individual megacrysts exceeding

5 cm in diameter. The same lithology is also present as discontinuous lenses up to 20 m thick within the cumulate sequence itself. The augen structure is a consequence of intense shearing of the contact zone, whereas within the cumulates strain is much less. Textures indicate that the rock is derived by metasomatic alteration of troctolites and the augite megacrysts are invariably surrounded by a rim free of olivine. Alteration is typically pervasive, although in some places it is patchy or transects layering and transitions to unaltered troctolites are gradual. Augite occurs as scattered megacrysts less than 1 cm in size and as larger aggregates several centimeters in diameter also in the olivine-bearing Ridnitsohkka sills against the highly deformed contact zone.

This alteration phenomenon was caused by the same magma which produced the pegmatitic gabbro dykes within the cumulate sequence. Although these pegmatites generally have sharp contacts against the troctolites, there are a number of instances where the contact between the two lithologies is gradational, in which case coarse augite augen are developed in the troctolites. Thus the relatively low temperature three phase (plagioclase + olivine + clinopyroxene) pegmatite magma, which was saturated with respect to pyroxene, has reacted with troctolite and continuously equilibrated to maintain a cotectic assemblage amongst these minerals. According to Bédard et al. (1988), the heterogeneous clinopyroxene gabbros in the Rhum complex were formed in an analogous fashion when porous troctolites and a lower temperature basaltic melt reacted together.

The contact zone between the Halti cumulates and Ridnitsohkka gabbro sills was active at an early stage and promoted the movement of gabbroic pegmatite magma which led to widespread pyroxene metasomatism. Amphibole metasomatism was a distinctly younger process which also affected the augite augen gabbros.

SUMMARY AND CONCLUSIONS

The Halti-Ridnitsohkka magmatic complex was intruded shortly before the climax of the Scandian phase of the Caledonian orogeny around 430 Ma. Magmatism commenced with the intrusion of the Ridnitsohkka gabbro sills into metapelitic gneisses at depths equivalent to pressures of 7—8 kbar. The high temperature of the sill magma (>1200 °C) caused significant thermal metamorphism of gneiss interlayers and produced a wide contact metamorphic aureole in which local anatexis and granite formation took place. Cordierite and orthopyroxene crystallized in the gneiss interlayers but were replaced by biotite — sillimanite aggregates during subsequent hydration processes. Any remaining cordierite reacted to form sillimanite and orthopyroxene, since pressures were also continually increasing. The last prograde event in the gneiss interlayers and in the aureole resulted in the formation of garnet at the expense of biotite and sillimanite.

The gabbro sills have a distinctive chemistry. Although the marked increase in Fe and Ti abundances with increasing Fe/Mg ratios attests to their tholeiitic nature, assimilation of partially melted country rock gneisses led to the anomalous enrichments in incompatible and lanthanide elements and, in addition, the crystallization of primary hydrous minerals and presence of normative quartz. Fractionation also took place, especially of cumulus plagioclase, resulting in distinct positive Eu anomalies. The alumina content of the sills is also higher than is typical for tholeiites and although it appears to be a primary feature, it may instead be a consequence of plagioclase accumulation.

The composition of the sill magma gradually became more primitive before the formation of the Halti cumulates; this was caused either by mixing of the picritic Halti cumulate magmas with the gabbroic sill magma or else by an increasing degree of mantle partial melting.

The Halti dunite — troctolite — olivine gabbro cumulate sequence differentiated from a picritic parent magma at rather low pressures. The high Fo content of olivine in all dunites and the replacement of plagioclase-rich units by dunite indicate the successive intrusion of separate pulses of primitive magma. The presently exposed remnants of the complex have features consistent with the final stages of crystallization having taken place at the ternary pseudoeutectic of the forsterite — diopside — plagioclase system. Pegmatitic gabbros crystallized from the last residual melts, which also caused metasomatic alteration of troctolites to megacrystic olivine gabbros; this process was most manifest in the contact zone between the sills and the cumulate sequence.

Metamorphism of the cumulates was controlled by water activity at pressures up to 10 kbar. Where water contents were low, orthopyroxene and spinel — amphibole corona textures formed between olivine and plagioclase grains. Where water was more abundant, Ca-plagioclase broke down to zoisite, quartz and kyanite, with tchermackitic amphibole being the only mafic mineral present. Corundum formed where silica was deficient.

The peak of Halti-Ridnitsohkka magmatism coincided with the collision between Fennoscandia and Laurentia. The oblique geometry of convergence produced extensional zones of weakness into which the Ridnitsohkka gabbro sills and the Halti picritic magmas were intruded. The earlier stages of deformation resulted in isoclinal folding within the gneiss interlayers and outer part of the aureole. During subsequent deformation was the metasomatic augite gabbro developed an augen texture and a strong foliation formed in the sills and gneiss interlayers. Amphibole formation in the cumulates took place after this and the main stage of nappe emplacement must have postdated this since the amphibole rock is also intensely foliated adjacent to the basal thrust plane. Thus the present allochthonous position of the Halti-Ridnitsohkka complex within the Caledonides results from the final stages of collision between the Fennoscandian and Laurentian plates.

ACKNOWLEDGMENTS

This study forms part of a mapping program in the Finnish Caledonides being carried out jointly by the University of Turku and the Geological Survey of Finland.

I wish firstly to express my gratitude to my teacher, Professor Heikki Papunen at Turku University for his interest, encouragement and support throughout the various stages of the project.

I am grateful to the project leader, Dr Jyrki Lehtovaara for his many enthusiastic discussions, in the midst of the arctic wilds as well as in the bustling city. I would also like to thank my colleague from the Norwegian Geological Survey, Bouke Zwaan for his expert advice concerning the Caledonian geology of northern Scandinavia.

Assistant Professors Jyrki Lehtovaara and Tauno Piirainen were the official examiners of the manuscript, and I have endeavoured to put their constructive criticism to good use.

I also sincerely thank the many other people who have provided stimulating discussions and

valuable ideas relating to the study, particularly Professor Kalle Neuvonen and my colleagues Timo Kilpeläinen, Ari Linna, Jyri Rastas, Markku Sutinen and Kari Yli-Kyyny at Turku University and Pentti Hölttä at Geological Survey of Finland. Jyrki Juhanoja assisted greatly with mineral analyses, and Turkka Puisto prepared thin sections, while Tuula Wan and Ritva Ääri helped in numerous additional ways.

I wish to express my appreciation to Professor Atso Vorma, Acting Research Director of the Geological Survey of Finland, for approving the publication of the manuscript as a Survey Bulletin, and to Dr Veli Suominen for his assistance in many practical matters during the final stages of the work.

Weather in the study area can be fickle and freezing even in the middle of summer and I am accordingly very grateful to the Lapland Frontier Guard, the Posts and Telecommunications of Finland and the Finnish Customs for providing me with accommodation and protection against the elements in their excellent mountain huts.

The manuscript was translated into English by Peter Sorjonen-Ward.

I finally acknowledge financial support from the Foundation of the University of Turku and the Aarne and Anna-Liisa Laitakari Foundation.

REFERENCES

Alapieti, T. & Sivonen, S.J., 1983. Use of the electron microprobe in the investigation of the Early Proterozoic Koillismaa layered igneous complex, NE Finland. Geol. Surv. Finland Rep. Invest. 61, 22 p.

Alapieti, T. & Lahtinen, J., 1986. Stratigraphy, Petrology, and Platinum-Group Element Mineralization of the Early Proterozoic Penikat Layered Intrusion, Northern Finland. Econ. Geol. 81, 1126—1136.

Allan, J.F., Sack, R.O. & Batiza, R., 1988. Cr-rich spinels as petrogenetic indicators: MORB-type lavas from the Lamont seamount chain, eastern Pacific. Am. Mineral. 73, 741—753.

Andreasson, P.G., 1987. Early evolution of the Late Proterozoic Baltoscandian margin: inferences from rift magmatism. Geol. För. Stockh. Förh. 109, 336—367.

Andresen, A., Fareth, E., Bergh, S., Kristensen, S.E. & Krogh, E., 1985. Review of Caledonian lithotectonic units in Troms, north Norway. Pp. 569—579 in: Gee, D.G. & Sturt, B.A., (eds.) The Caledonide Orogen—Scandinavia and Related Areas 1. John Wiley & Sons, Chichester, 619 p.

Augé, T., 1987. Chromite deposits in the northern Oman ophiolite: Mineralogical constrains. Miner. Deposita 22, 1—10.

Barker, A.J., 1989. Metamorphic evolution of the Caledonian nappes of north central Scandinavia. Pp. 193—204 in: Gayer, R.A., (ed.) The Caledonide Geology of Scandinavia. Graham & Trottman, London, 312 p.

Bédard, J.H., Sparks, R.S.J., Renner, R., Chedale, M.J. & Hallworth, M.A., 1988. Peridotite sills and metasomatic gabbros in the Eastern Layered Series of the Rhum complex. J. geol. Soc. London 145, 207—224.

Beeson, M.H. & Jackson, E.D., 1969. Chemical composition of altered chromites from Stillwater Complex, Montana. Am. Mineral. 54, 1084—1100.

Bennett, M.C., Emblin, S.R., Robins, B. & Yeo, W.J.A., 1986. High-temperature ultramafic complexes in the North Norwegian Caledonides: I—Regional setting and field relationships. Norges Geol. Unders. 405, 1—40.

Bickle, M.J., 1982. The magnesium contents of komatiitic liquids. Pp. 479—495 in: Arndt, N.T. & Nisbet, E.G. (eds.) Komatiites. George Allen & Unwin., London, 526 p.

Biggar, G.M., 1983. Crystallization of plagioclase, augite and olivine in synthetic systems and in tholeiites. Mineral. Mag. 47, 161—176.

Binns, R.E. & Gayer, R.A., 1980. Silurian or Upper Ordovician fossils of Guolasjavri, Norway. Nature 284, 53—54.

Bliss, N.W. & MacLean, W.H., 1975. The paragenesis of zoned chromite from central Manitoba. Geochim. Cosmochim. Acta 39, 973—990.

Bøe, P., 1976. Geology of the Troctolite Complex of Raisduoddar-Hal'di, Troms, Northern Norway. Norges Geol. Unders. 324, 29—49.

Boyd, R. & Mathiesen, C.O., 1979. The nickel mineralization of the Råna mafic intrusion, Norland, Norway. Canadian Mineralogist 17, 287—298.

Boyd, R. & Nixon, F., 1985. Norwegian nickel deposits: A review. pp. 363—394 in: Papunen H. & Gorbunov, G.I. (eds.) Nickel-copper deposits of the Baltic Shield and Scandinavian Caledonides. Contribution to IGCP projects 91 and 161. Geol. Surv. Finland, Bull. 333, 394 p.

Boyle, A.P., Hansen, T.S. & Mason, R. 1985. A new tectonic perspective of the Sulitjelma Region. Pp. 529—542 in: Gee, D.G. & Sturt, B.A., (eds.) The Caledonide Orogen—Scandinavia and Related Areas 1. John Wiley & Sons, Chichester, 619 p.

Cabri, L.J. & Naldrett, A. J., 1984. The nature of the distribution and concentration of platinum-group elements in various geological environments. Proc. 27th Int. Geol. Congr., Moscow 10, 17—46.

Cameron, E.N., 1975. Postcumulus and subsolidus equilibration of chromite and coexisting silicates in the Eastern Bushveld Complex. Geochim. et Cosmochim. Acta 39, 1021—1033.

Carr, M.J., 1987. IGPET-II. Terra Softa Inc. Princeton, USA.

Cohen, L.H., Ito, K. & Kennedy, G.C., 1967. Melting and phase relations in an anhydrous basalt to 40 kilobars. Amer. J. Sci. 265, 475—518.

Coleman, R.G., 1977. Ophiolites — Ancient Oceanic Lithosphere? Springer-Verlag, Berlin, 229 p.

Cowie, J.W. & Basett, M.G., 1989. International Union of Geological Sciences 1989. Global Stratigraphic Chart with geochronometric and magnetostratigraphic calibration. Episodes 12 (2).

Davies, H.L., 1980. Folded thrust fault and associated metamorphics in the Suckling-Dayman massif, Papua New Guinea. Amer. J. Sci. 280-A, 171—191.

Deer, W.A., Howie, R.A. & Zussman, J., 1963. Rock-Forming Minerals 2, Chain Silicates. Longmans, London, 379 p.

Deer, W.A., Howie, R.A. & Zussman, J., 1978. Rock-Forming Minerals 2A, 2nd edition, Single-Chain Silicates. Longmans, London, 668 p.

Dick, H.J.B., 1977. Partial melting in the Josephine Peridotite I, The effect on mineral composition and its consequence for geobarometry and geothermometry. Amer. J. Sci. 277, 801—832.

Dick, H.J.B. & Bullen, T., 1984. Chromian spinel as a petrogenetic indicator in abyssal and alpine-type perido-

tites and spatially associated lavas. Contr. Mineral. Petrol. 86, 54—76.

Droop, G.T.R.,1987. A general equation for estimating Fe^{3+} concentrations in ferromagnesian silicates and oxides from microprobe analyses, using stoichiometric criteria. Mineral. Mag. 51, 4431—435.

Duke, J.M., 1986. Petrology and economic geology of the Dumont sill: an Archean intrusion of komatiitic affinity in Northwestern Quebec. Geol. Surv. Can. Econ. Geol. Rep. 35, 56 p.

Duke, J.M. & Naldrett, A.J., 1978. A numerical model of the fractionation of olivine and molten sulfide from komatiite magma. Earth Planet. Sci. Lett. 39, 255—266.

Dungan, M.A., Vance, J.A. & Blanhard, D.P., 1983. Geochemistry of the Shuksan greenschist and blueschists, North Cascades, Washington: variably fractionated and altered metabasalts of oceanic affinity. Contr. Mineral. Petrol. 82, 131—146.

Dunning, G.R. & Pedersen, R.B., 1988. U/Pb ages of ophiolites and arc related plutons of the Norwegian Caledonides: implications for the development of Iapetus. Contr. Mineral. Petrol. 98, 13—23.

Dymek, R.F., Boak, J.L. & Brothers, S.C., 1988. Titanian chondrotite- and titanian clinohumite-bearing metadunite from the 3800 Ma Isua supracrustal belt, West Greenland: Chemistry, petrology and origin. Am. Min. 73, 547—558.

Emeleus, C.H., 1987. The Rhum layered complex, inner Herbides, Scotland. Pp. 263—286 in: Parson, I. (ed.) Origins of Igneous Layering. Nato Asi Series C: Mathematical and Physical Sciences 196. D. Reidel Publishing Company, Dodrrecht, Holland, 666 p.

Evans, B.W., 1977. Metamorphism of alpine peridotite and serpentine. Ann. Rev. Earth Planet. Sci. 5, 397—447.

Evans, B.W. & Frost, R.B., 1975. Chrome spinel in progressive metamorphism—a preliminary analysis. Geochim. Cosmochim. Acta 39, 959—972.

Fareth, E., Gjelsvik, T. & Lindahl, I., 1977. Cier'te. Beskrivelse til det berggrunnsgeologiske kart 1733 II 1 : 50000. Norges Geol. Unders. 331, 1—28.

Ferry, J.M. & Spear, F.S., 1978. Experimental calibration of the partitioning of Fe and Mg between biotite and garnet. Contrib. Mineral. Petrol. 66, 113—117.

Føyn, S., 1967. Dividal-gruppen (»Hyolitus-sonen») i Finnmark og dens forhold til de eokambrisk-kambriske formasjoner. Norges Geol. Unders. 249 I, 1—84.

Gayer, R.A., 1989. The Caledonide Geology of Scandinavia (ed.). Graham & Trotman, London, 312 p.

Gayer, R.A., Humphreys, R.I., Binns, R.E. & Chapman, T.J., 1985. Tectonic modelling of the Finnmark and Troms Caledonides based on high level igneous rock geochemistry. Pp. 931—952 in: Gee, D.G. & Sturt, B.A., (eds.) The Caledonide Orogen—Scandinavia and Related Areas 2. John Wiley & Sons, Chichester, 1266 p.

Gee, D.G., 1975. A tectonic model for the central part of the Scandinavian Caledonides. Am. J. Sci. 275a, 468—515.

Goldsmith, J.R., 1981. The join $CaAl_2Si_2O_8$-H_2O (anorthite-water) at elevated pressures and temperatures. Am. Mineral. 66, 1183—1188.

Grauch, R.I., 1989. Rare earth elements in metamorphic rocks. Pp. 147—167 in: Lipin, B.R. & McKay, G.A. (eds.) Geochemistry and mineralogy of rare earth elements. Mineralogy Society of America, Reviews in Mineralogy, Special Paper 21, 348 p.

Green, D.H. & Ringwood, A.E., 1967. An experimental investigation of the gabbro to eclogite transformation and its petrological applications. Geochim. Cosmochim. Acta 31, 767—833.

Grieve, R.A.F. & Gittings, J., 1975. Composition and Formation of Coronas in the Hadlington Gabbro, Ontario, Canada. Can. J. Earth Sci. 12, 289—299.

Habekost, E.M. & Wilson, R., 1989. Raft-like Metabasaltic Inclusions in the Fongen-Hyllingen Layered Intrusive Complex, Norway, and their Implications for Magma Chamber Evolution. Journal of Petrology 30 (6), 1415—1441.

Harley, S.L., 1984. An experimental study of the partitioning of Fe and Mg between garnet and orthopyroxene. Contribut. Mineral. Petrol. 86, 359—373.

Haselton, H.T.Jr., Hovis, G.L., Hemingway, B.S. & Robie, R.A., 1983. Calorimetric investigation of the excess entropy of mixing in analbite-sanidine solid solutions: lack of evidence for Na,K short-range order and implications for two-feldspar thermometry. Am. Mineral. 68, 369—413.

Haskin, L.A., Haskin, M.A. & Frey, F.A., 1968. Relative and Absolute Terrestrial Abundances of the Rare Earths. Pp. 889—912 in: Ahrens, L.H., (ed.) Origin and Distribution of the Elements. Pergamon, Oxford, 1178 p.

Hausen, H., 1936. Halditjokkomassivet och dess differentiat. Pohjoismainen (19. skandinaavinen) luonnontutkijain kokous Helsingissä 1936. Nordiska (19. skandinaviska) naturforskarmötet i Helsingfors 1936. Eripainos. — Särtryck, 3 p.

Hausen, H., 1941. Das Halditjokko-Massiv. Ein basischer Phakolith im finnischen Abschnitt der kaledonischen Ueberschiebungszone. Geol. Rundsch. 32, 508—534.

Hausen, H., 1942a. Das Halditjokkomassiv. Ein phacolitischer Intrusionskörper. Basischer differentiate im Abschnitt Finnlands der Kaledoniden. Acta Acad. Aboen., Mathem. et Physica XIII (14), 83 p.

Hausen, H., 1942b. Der Abschnitt Finnlands der kaledonischen Ueberschiebungzone. Soc, Scient. Fennica. Comm. Phys. — Math. XI, 115 p.

Henderson, P., 1984. General geochemical properties and abundances of the rare earth elements. Pp. 1—29 in: Henderson, P., (ed.) Rare earth element geochemistry. Elsevier, Amsterdam, 510 p.

Hodges, K.V. & Spear, F.S., 1982. Geothermometry, geobarometry and the Al_2SiO_5 triple point at Mt. Moosilauke, New Hampshire. Am. Mineral. 67, 1118—1134.

Hoffman, M.A. & Walker, D., 1978. Textural and chemical variations of olivine and chrome spinel in the East Dover ultramafic bodies, south-central Vermont. Geol. Soc. Amer. Bull. 89, 699—710.

Holdaway, M.J. & Lee, S.M., 1977. Fe-Mg Cordierite Stability in High- Grade Pelitic Rocks Based on Experimental, Theoretical and Natural Observations. Contr. Mineral. Petrol. 63, 175—198.

Idman, H. & Eilu, P., 1988. Granitoidien muuttuminen varhaisproterotsooisen vihreäkivikompleksin länsireunalla Enontekiöllä — esimerkki kemiallisesta rapautumisesta. Pp. 31—37 in: Lappalainen, V. & Papunen, H. (eds.) Tutkimuksia geologian alalta. Annales Universitatis Turkuensis, Ser. C, 67, 194 p.

Irvine, T.N., 1965. Chromian spinel as a petrogenetic indicator, Part 1. Theory. Can. J. Earth Sci. 2, 648—672.

Irvine, T.N., 1967. Chromian spinel as a petrogenetic indicator, Part 2. Petrologic applications. Can. J. Earth Sci. 4, 71—103.

Irvine, T.N., 1974. Petrology of the Duke Island Ultramafic Complex, Southeastern Alaska. Geol. Soc America Mem. 138, 240 p.

Irvine, T.N., 1975. Crystallization sequences in the Muskox intrusion and other layered intrusions-II. Origin of chromitite layers and similar deposits of other magmatic ores. Geochim. Cosmochim. Acta 39, 991—990.

Irvine, T.N., 1982. Terminology for Layered Intrusions. Jour. Petrol. 23, 127—162.

Irvine, T.N., 1985. Notes of the Geology of the Duke Island Ultramafic Complex, Southeastern Alaska. A Contribution of IGCP Project 161 Sulfide deposits in mafic and ultramafic rocks. 33 p.

Irvine, T.N. & Baragar, W.R.A., 1971. A Guide to the Chemical Classification of the Common Volcanic Rocks. Can. J. Earth Sci. 8, 523—548.

Jaques, A.L. & Green, D.H., 1979. Anhydrous Melting of Peridotite at 0—15 kb Pressure and the Genesis of Tholeiitic Basalts. Contr. Mineral. Petrol. 73, 287—310.

Jensen, L.S., 1976. A new cation plot for classifying subalkalic volcanic rocks. Ontario Division of Mines, Misc. Paper no. 66, 22 p.

Kathol, B., 1987. The Vaivvancohkka Nappe, Torneträsk area, northern Swedish Caledonides. Geol. För. Stockh. Förh. 109, 350—353.

Kaula, W.M., Heard, III, J.W., Meririll, R.B., Pepin, R.O., Solomon, S.C., Walker, D. & Wood, C.A. (eds.), 1981. Basaltic volcanism on the terrestrial planets. Pergamon Press, Inc., New York, 1286 p.

Koziol. A.M. & Newton, R.C., 1988. Redetermination of the anorthite breakdown reaction and improvement of the plagioclase-garnet-Al_2SiO_5-quartz geobarometer. Am. Mineral. 73, 216—223.

Krill, A.G. & Zwaan, B., 1987. Reinterpretation of Finnmarkian deformation on western Sørøy, northern Norway. Nor. Geol. Tidsskr. 67, 15—24.

Kulling, O., 1964. Översikt över norra Norbottensfjällens kaledonberggrund. Sver. Geol. Unders. Ba 19, 166 p.

Kushiro, I., 1960. Si-Al Relations in Clinopyroxenes from Igneous Rocks. Amer. J. Sci. 258, 548—554.

Kushiro, I. & Yoder, H.S., 1966. Anorthite-Forsterite and Anorthite-Enstatite Reactions and their bearing on the Basalt-Eclogite Transformation. J. Petrol. 7, 337—362.

LeBAS, M. J., 1962. The role of aluminum in igneous clinopyroxenes with relation to their parentage. Amer. J. Sci. 260, 267—288.

LeBAS, M.J., Le Maitre, R.W., Streckeisen, A. & Zanettin, B., 1986. A Chemical Classification of Volcanic Rocks Based on the Total Alkali-Silica Diagram. Jour. Petrol. 27, 745—750.

Leake, B.E., 1978. Nomenclature of amphiboles. Am. Mineral. 63, 1023—1052.

Leeman, W.P., 1978. Distribution of Mg^{2+} between olivine and silicate melt, and its implications regarding melt structure. Geochim. Cosmochim. Acta 42, 789—800.

Lehmann, J., 1983. Diffusion between olivine and spinel: application to geothermometry. Earth Planet. Sci. Lett. 64, 123—138.

Lehtovaara, J.J., 1984. Suomen Kaledonidien rakenteesta. (Summary: Features of the structure of the Finnish Caledonides in the northwesternmost corner of the Finnish Lapland). Geologi 36, 1—9.

Lehtovaara, J.J., 1985. Re-evaluating the sub-Caledonian erosion surface at the border of the Caledonides in Enontekiö Lapland, northwestern Finland. Fennia 163, 365—368.

Lehtovaara, J.J., 1986a. Tectonostratigraphical outline of the Finnish Caledonides. Geol. För. Stockh. Förh. 108, 291—294.

Lehtovaara, J.J., 1986b. Traces of alum shale in the Finnish Caledonides of the Enontekiö Lapland. Fennia 164 (1), 95—103.

Lehtovaara, J.J., 1987. Enontekiön Ridnitsohkkan emäksinen juoniparvi. Basic dyke swarm at Ridnitsohkka fell in northwesternmost Enontekiö. (Abstract: Basic dyke swarm at Ridnitsohkka fell in northwesternmost Enontekiö). Pp. 199—203 in: Aro, K. and Laitakari, A. (eds.) Suomen diabaasit ja muut mafiset juonikivilajit. Diabases and other mafic dyke rocks in Finland. Geol. Surv. Finland, Rep. Invest. 76, 254 p.

Lehtovaara, J.J., 1988. The paleosedimentology of the autochthon of the Finnish Caledonides. Geol. Surv. Finland, Spec. Paper 5, 255—264.

Lehtovaara, J.J., 1989. Tectonostratigraphic position of the Finnish Caledonides at the Fennoscandian margin of the Northern Scandes. Bull. Geol. Soc. Finland 61 (2), 189—195.

Lehtovaara, J.J. & Sipilä, P., 1987. Revisions to tectonostratigraphy and magmatism of the Finnish Caledonides. Geol. För. Stockh. Förh. 109, 354—357.

Lindström, M., Bax, G., Dinger, M., Dworatzek, M., Erdtmann, W., Fricke, A., Kathol, B., Klinge, H., von Pape, H. & Stumpf, U., 1985. Geology of a part of the Torneträsk section of the Caledonian front, northern Sweden. Pp. 507—513 in: Gee, D.G. & Sturt, B.A., (eds.) The Caledonide Orogen—Scandinavia and Related Areas 1. John Wiley & Sons, Chichester, 619 p.

Ludden, J.N. & Thompson, G., 1979. An evaluation of the behaviour of the rare earth elements during the weathering of sea-floor basalts. Earth Planet. Sci. Lett. 43, 85—92.

Matisto, A., 1959. General geological map of Finland, Sheet B-8, Enontekiö, 1:400 000. Geol. Surv. Finland, Espoo.

Matisto, A., 1969. General geological map of Finland, 1:400 000, Sheet B-8, Enontekiö, Kivilajikartan selitys, 78 p.

Mattson,I. & Lindqvist, J.E., 1990. Sm-Nd isotope data on the amphibolite to granulite facies rocks of the Halti massif. Geonytt 1, 78 p.

McCallum, I.S., Raedeke, L.D. & Mathez, E.A., 1980. Investigations of the Stillwater complex: Part 1. Stratigraphy and structure of the banded zone. Amer. J. Sci 280-A, 59—87.

McClurg, J., 1982. Geology and structure of the northern part of the Rhum ultrabasic complex. Unpublished Ph.D. thesis, University of Edinburgh.

McSween Jr, H.Y., Sando, T., Clark, S.R., Harden, J.T, & Strange, E.A., 1984. The gabbro-metagabbro association of the southern Appalachian Piedmont. Amer. J. Sci. 284, 437—461.

Mertanen, S., Pesonen, L.J., & Leino, M., 1990. Uusia paleomagneettisia tuloksia Fennoskandian diabaaseista. (Summary: New paleomagnetic results of diabase dykes in Fennoscandia). Geologi 42, 55—56.

Middlemost, E.A.K., 1975. The Basalt Clan. Earth Sci. Rev. 11, 337—364.

Minsaas, O., & Sturt, B.A., 1985. The Ordovician-Silurian clastic sequence overlying the Lyngen Gabbro Complex and its environmental significance. Pp. 379—395 in: Gee, D.G. & Sturt, B.A., (eds.) The Caledonide Orogen—Scandinavia and Related Areas 1. John Wiley & Sons, Chichester, 619 p.

Miyashiro, A., 1975. Classification, characteristics, and origin of ophiolites. J. Geol. 83, 249—281.

Miyashiro, A., 1978. Nature of Alkalic Volcanic Rock Series. Contr. Mineral. Petrol. 66, 91—104.

Morris, D.F.C. & Short, E.L., 1978. Rhenium abundances in meteorites, tektites, cosmos and lunar materials. In: Wedepohl, E. (ed.) Handbook of geochemistry II (5). Springer, Berlin.

Morse, S.A., 1980. Basalts and Phase Diagrams. An introduction to the Quantitative Use of Phase Diagrams in Igneous Petrology. Springer-Verlag, New York, 493 p.

Munday, R.J.C., 1974. The geology of the northern half of the Lyngen peninsula, Troms, Norway. Norsk. Geol. Tidsskr. 54, 49—62.

Naldrett, A.J., 1981. Platinum-group element deposits. Pp. 197—231 in: Cabri, L.J., (ed.) Platinum group elements: mineralogy, geology, recovery. Canadian Institute of Mining and Metallurgy. Montreal. (CIM Spec. vol. 23), 267 p.

Newton, R.C., 1972. An experimental determination of the high-pressure stability limits of magnesian cordierite under wet and dry conditions. J. Geol. 80, 398—420.

Newton, R.C. & Haselton, H.T.I., 1981. Thermodynamics of the garnet-plagioclase-Al_2SiO_5-quartz geobarometer. Pp. 131—147 in: Newton, R.C., Navrotsky, A. & Wood, B.J. (eds.) Thermodynamics of Minerals and Melts. Springer, New York.

Newton, R.C. & Perkins, D., 1982. Thermodynamic calibration of geobarometers based on the assemblages garnet-plagioclase-orthopyroxene(clinopyroxene)-quartz. Am. Mineral. 67, 203—222.

Nickel, K.G. & Brey, G., 1984. Subsolidus orthopyroxene-clinopyroxene systematics in the system CaO-MgO-SiO_2 to 60 kb: a re-evaluation of the regular solution model. Contrib. Mineral. Petrol. 87, 35—42.

Otten, M. & Senior, A., 1985. Mineral chemistry and crystallization conditions of the Artfjället gabbro and dolerites (Central Swedish Caledonides). Lithos 18, 295—310.

Padget, P., 1955. The Geology of the Caledonides of the Birtavarre Region, Troms, Northern Norway. Norges Geol. Unders. 192, 106 p.

Papunen, H., 1989. Platinum-group elements in metamorphosed Ni-Cu deposits in Finland. Pp. 165—176 in: Magmatic sulfides-the Zimbabwe volume. The Institution of Mining and Metallurgy, London, 1989.

Pearce, J.A., 1976. Statistical Analysis of Major Element Patterns in Basalts. Jour. Petrol. 17, 15—43.

Pearce, J.A., 1983. The role of sub-continental lithosphere in magma genesis at destructive plate margins. Pp. 230—249 in: Hawkesworth, C.J. & Norry, M.J. (eds.) Continental basalts and mantle xenoliths. Shiva, Nantwich, 272 p.

Pearce, J.A., Gorman, B.E. & Birkett, T.C., 1977. The relationship between major element chemistry and tectonic environment of basic and intermediate volcanic rocks. Earth Planet. Sci. Lett. 36, 121—132.

Pedersen, R.B., Dunning, G.R. & Robins, B., 1989. U-Pb ages of nepheline syenite pegmatites from Seiland Magmatic Province, N Norway. Pp. 3—8 in: Gayer, R.A. (ed.) The Caledonide Geology of Scandinavia. Graham & Trotman, London, 312 p.

Perchuck, L.I. & Lavrenteva, I.V., 1983. Experimental investigation on exchange equilibria in the system cordierite-garnet-biotite. Pp 199—239 in: Saxena, S.K. (ed.) Kinetics and equilibrium in mineral reactions. Springer-Verlag, New York, 273 p.

Perchuck, L.I., Aranovich, L.Ya., Podlesskii. K.K., Lavrant'eva, I.V., Gerasimov, V.Yu., Fed'kin, V.V., Kitsul, V.I., Karsakov, L.P., & Berdnikov, N.V., 1985. Precambrian granulites of the Aldan Shield, eastern Siberia, USSR. J. Metam. Geol. 3, 265—310.

Perkins, D. & Chipera, S.J., 1985. Garnet-orthopyroxene-plagioclase-quartz barometry: refinement and application to the English River subprovince and the Minnesota River Valley. Contrib. Mineral. Petrol. 89, 69—80.

Pettersen, K., 1870. Geol. Undersögelser inden Tromsö Amt. II. Det Kongl. Norske Vidensk. Selsk. Skr. 6 Bind. Trondhj. 41—166.

Pettersen, K., 1876a. Olivinförekomster i det nordlige Norge. Geol. För. Stockh. Förh. 3 (6). 198—205.

Pettersen, K., 1876b. Über das Vorkommen des Serpentins und Olivinfels im nördlichen Norwegen. Neues Jahrb. für Mineral., Geol. und Palaeontol., 613—622.

Phillips, W.E.A., Stillman, C.J. & Murphy, T., 1976. A Caledonian plate tectonic model. J. geol. Soc. London 132, 579—609.

Piper, J.D.A., 1985. Palaeomagnetism in the Caledonian-Appalachian orogen: a review. Pp. 35—49 in: Gee, D.G. & Sturt, B.A., (eds.) The Caledonide Orogen—Scandinavia and Related Areas 1. John Wiley & Sons, Chichester, 619 p.

Pober, E. & Faupl, P., 1988. The chemistry of detrital chromian spinels and its implications for the geodynamic evolution of the Eastern Alps. Geol. Rundschau 77 (3), 641—670.

Powell, R. & Holland, T.J.B., 1988. An internally consistent dataset with uncertainties and correlations: 3. Ap-

plications to geobarometry, worked examples and a computer program. J. Metam. Geol. 6, 173—204.

Presnall, D.C., Dixon, S.A., Dixon, J.R., O'Donell, T.H., Brenner,, N.L., Schrock, R.L. & Dycus, D.W., 1978. Liquidus Phase Relations on the Join Diopside-Forsterite-Anorthite From 1 atm to 20 kbar: Their Bearing on the Generation and Crystallization of Basaltic Magma. Contrib. Mineral. Petrol. 66, 203—220.

Ramsay, D.M., & Sturt, B.A., 1977. A Sub-Caledonian Unconformity within the Finnmarkian Nappe Sequence and Its Regional Significance. Norges Geol. Unders. 334, 107—116.

Ramsay, D.M., Sturt, B.A., Zwaan, K.B. & Roberts, D., 1981. Caledonides of northernmost Norway. Terra cognita 1, 67—68.

Ramsay, D.M., Sturt, B.A., Zwaan, K.B. & Roberts, D., 1985. Caledonides of northern Norway. Pp. 163—184 in: Gee, D.G. & Sturt, B.A., (eds.) The Caledonide Orogen—Scandinavia and Related Areas 1. John Wiley & Sons, Chichester, 619 p.

Roberts, D., 1974. Hammerfest. Beskrivelse til det 1:250 000 bergrunnsgeologiske kart. Norges Geol. Unders. 301, 1—66.

Roberts, D., 1988. Reinterpretation of Finnmarkian deformation on western Sørøy, northern Norway: some comments. Nor. Geol. Tidsskr. 68, 309—312.

Roberts, D., 1990. Geochemistry of mafic dykes in the Corrovarre Nappe, Troms, North Norway. Norges Geol. Unders. 419, 45—53.

Roberts, D., & Gee, D.G., 1985. An introduction to the structure of the Scandinavian Caledonides. Pp. 55—68 in: Gee, D.G. & Sturt, B.A., (eds.) The Caledonide Orogen—Scandinavia and Related Areas 1. John Wiley & Sons, Chichester, 619 p.

Robins, B. & Gardener, P.M., 1975. The magmatic evolution of the Seiland province, and Caledonian plate boundaries in Northern Norway. Earth Planet. Sci. Lett. 26, 167—178.

Robins, B., Haukvik, L. & Jansen, S., 1987. The organization and internal structure of cyclic units in the Honningsvåg intrusive suite, North Norway: Implications for intrusive mechanisms, double-diffusive convection and pore magma infiltration. Pp. 287—312 in: Parson,I. (ed.) Origins of Igneous Layering. Nato Asi Series C: Mathematical and Physical Sciences 196. D. Reidel Publishing Company, Dordrecht, Holland, 666 p.

Roeder, P.L. & Emslie, R.F., 1970. Olivine-Liquid Equilibrium. Contr. Mineral. Petrol. 29, 275—289.

Salje, E., 1986. Heat capacities and entropies of andalusite and sillimanite: The influence of fibrolitization on the phase diagram of Al_2SiO_5 polymorphs. Amer. Mineral. 71, 1366—1371.

Sato, M., & Valenza, M., 1980. Oxygen fugacities of the layered series of the Skaergaard intrusion, East Greenland. Amer. J. Sci. 280-A. 134—158.

Senior, A. & Otten, M.T., 1985. The Artfjället gabbro and its bearing on the evolution of the Storfjället Nappe, central Swedish Caledonides. Pp. 725—734 in: Gee, D.G. & Sturt, B.A., (eds.) The Caledonide Orogen—Scandinavia and Related Areas 2. John Wiley & Sons, Chichester, 1266 p.

Simkin, T. & Smith, J.V., 1970. Minor element distribution in olivine. J. Geol. 78, 304—325.

Sipilä, P., 1987. Haltitunturin alueen magmakivet. Unpubl. licentiate-thesis, Dept. of Geology, Univ. of Turku, 74 p.

Sipilä, P., 1988. Plagioklaasi-oliviinikorona Haltitunturin troktoliitti-oliviinigabrokivissä. Pp. 31—37 in: Lappalainen, V. & Papunen, H. (eds.) Tutkimuksia geologian alalta. Annales Universitatis Turkuensis, Ser. C, 67, 194 p.

Sipilä, P., 1989. Mafic and ultramafic rocks of the Raisduoddar-Halti area in the Finnish Caledonides — probably a part of the Iapetus rift zone. Terra abs. 1, 7—8.

Sipilä, P., 1990. Ridnitsohkkan gabbrosillit Suomen Kaledonideilla. Geologi 42, 40—43.

Sipilä, P., 1991. Mafic and ultramafic igneous rocks of the Raisduoddar-Halti area in the Finnish-Norwegian Caledonides. Petrography, mineralogy and geochemistry. Bull. Geol. Soc. Finland 63 (1), 15—24.

Skiöld, T., 1979. Zircon ages from an Archaean gneiss province in northern Sweden. Geol. För. Stockh. Förh. 103, 169—171.

Solyom, Z., Andreasson, P.G. & Johansson, I., 1979a. Geochemistry of amphibolites from Mt. Sylarna, Central Scandinavian Caledonides. Geol. För. Stockh. Förh. 101, 17—25.

Solyom, Z., Gorbatschev, R. & Johansson, I., 1979b. The Ottfjället dolerites: geochemistry of the dyke swarm in relation to the geodynamics of the Caledonide orogen of Central Swedish Scandinavia. Sver. Geol. Unders. C756, 111 p.

Stevens, B., 1982. The Vaddasgaissa Metagabbro, Nordreisa, Nord-Troms. Unpubl. rep. Norges Geol. Unders., 137 p.

Stephens, M.B., Furnes, H., Robins, B. & Sturt, B.A., 1985. Igneous activity within the Scandinavian Caledonides. Pp. 623—657 in: Gee, D.G. & Sturt, B.A., (eds.) The Caledonide Orogen—Scandinavia and Related Areas 2. John Wiley & Sons, Chichester, 1266 p.

Stjernvall, H.J., 1892. Lisiä Suomen Lapin Geognosiaan.II. Koe Könkämäenon ja Norjan rajan välisen seudun geologisten suhteiden esitykseksi. Suomen Teollisuushallituksen tiedonantoja. 17. vihko. 93—149.

Stormer, J.C., 1975. A Practical Two-Feldspar Geothermometer. Am. Mineral. 60, 667—674.

Sturt, B.A., Pringle, I.R. & Roberts, D., 1975. Caledonian Nappe Sequence of Finnmark, Northern Norway, and the Timing of Orogenic Deformation and Metamorphism. Geol. Soc. Am. Bull. 86, 710—718.

Sturt, B.A., Pringle, I.R. & Ramsay, D.M., 1978. The Finnmarkian phase of the Caledonian Orogeny. J. geol. Soc. London 135, 547—610.

Sturt, B.A. & Ramsay, D.M., 1988. Reinterpretation of Finnmarkian deformation on western Sørøy, northern Norway: a comment. Nor. Geol. Tidsskr. 68, 213—220.

Tanner, V., 1914. Studier över Kvartärsystemet i Fennoskandias nordliga delar. III. Bull. Comm. geol. Finlande 38, 667 p.

Thompson, A.B., 1976. Mineral reactions in pelitic rocks. II. Calculation of some P-T-X(Fe-Mg) phase reactions. Am. Mineral. 69, 88—97.

Thompson, A.B. & Tracy, R.J., 1979. Model Systems for

Anatexis of Pelitic Rocks. Facies Series Melting and Reactions in the System $CaO—KAlO_2—NaAlO_2—Al_2O_3—SiO_2—H_2O$. Contrib. Mineral. Petrol. 70, 429—438.

Thompson, R.N., Morrison, M.A., Hendry, G.L. & Parry, S.J., 1984. An assessment of the relative roles of a crust and mantle in magma genesis: an elemental approach. Phil. Trans. R. Soc. Lond. A310, 549—590.

Thy, P., 1991a. High and low pressure phase equilibria of mildly alkalic lava from the 1965 Surtsey eruption: Implications for the evolution of mildly alkalic and transitional basalts in the south-eastern propagating rift zone of Iceland. Lithos 26, 253—269.

Thy, P., 1991b. High and low pressure phase equilibria of mildly alkalic lava from the 1965 Surtsey eruption: Experimental results. Lithos 26, 223—243.

Trommsdorff, V. & Evans, B.W., 1974. Progressive metamorphism of antigorite schist in the Bergell tonalite aureole (Italy). Amer. J. Sci. 272, 423—437.

Tucker, R.D., Boyd, R. & Barnes, S.-J., 1990. A U-Pb zircon age for the Råna intrusion, N. Norway: New evidence of basic magmatism in the Scandinavian Caledonides in Early Silurian time. Nor. Geol. Tidsskr. 70, 229—239.

Tynni, R., 1980. Fossiileja Porojärven alueella kaledonialaisen ylityöntölaatan alaisissa ala-kambrisissa sedimenteissä. (Summary: Fossils in lower Cambrian sedimentary sequences below thrust planes of Caledonian age in the Porojärvi area, Northern Finland). Geologi 32, 17—22.

Vaasjoki, M., Sipilä, P., Lehtovaara, J.J. & Sakko, M., (in prep.). U-Pb isotopic determinations on baddeleyite and zircon from the Halti-Ridnitsohkka intrusion in Finnish Lapland: A further constraint on Caledonide evolution.

Vuollo, J.I., 1988. Kolin kerrosjuonen petrologia — Kaunisniemen profiili. Raportti No. 16, Oulun yliopisto, Pohjois-Karjalan malmiprojekti. 122 p.

Vuollo, J.I. & Piirainen T., 1989. Mineralogical evidence for an ophiolite from the Outokumpu serpentinites in North Karelia. Bull. Geol. Soc. Finland 61 (1), 95—112.

Wager, L.R. & Brown, G.M., 1968. Layered Igneous Rocks. Oliver & Boyd. Edinburgh, 588 p.

Welin, E., Christiansson, K. & Nilsson, Ö., 1971. Rb-Sr radiometric ages of extrusive and intrusive rocks in northern Sweden.I. Sver. Geol. Unders. C 666, 38 p.

Wells, P.R.A., 1977. Pyroxene Thermometry in Simple and Complex Systems. Contr. Mineral. Petrol. 62, 129—139.

Wilson, J.R., 1985. The synorogenic Fongen-Hyllingen layered basic complex, Trondheim region, Norway. Pp. 717—725 in: Gee, D.G. & Sturt, B.A., (eds.) The Caledonide Orogen—Scandinavia and Related Areas 2. John Wiley & Sons, Chichester, 1266 p.

Wilson, J.R., Esbensen, K.H., & Thay, P., 1981. Igneous Petrology of the Synorogenic Fongen-Hyllingen Layered Basic Complex, South-Central Scandinavian Caledonides. Jour. Petrol. 22, 584—627.

Wilson, M., 1989. Igneous petrogenesis. A global tectonic approach. Academic Division of Unwin Hyman Ltd. London, 466 p.

Winkler, H.G.F., 1979. Petrogenesis of Metamorphic Rocks, Fifth Edition. Springer-Verlag, New York, 348 p.

Yoder, H.S., Jr, & Tilley, C.E., 1962. Origin of Basaltic Magmas: An Experimental Study of Natural and Synthetic Rock Systems. Jour. Petrol. 3, 342—532.

Zachrisson, E., 1986. Scandinavian Caledonides: Stratabound Sulphide Deposits. Sver. Geol. Unders. Ba 42.

Zwaan, K.B., 1988. Nordreisa. Berggrunnsgeologisk kart 1:250 000. Norges Geol. Unders., Trondheim.

Zwaan, K.B. & Roberts, D., 1978. Tectonostratigraphic Succession and Development of the Finnmarkian Nappe Sequence, North Norway. Norges Geol. Unders. 343, 53—71.

Zwaan, K. & van Roermund, B.L.M., 1989. The intrusion mechanism and Caledonian tectono-metamorphic history of a rift-related diabase swarm, preserved in the Corrojavre mega-lens, northern Norway. Terra abstracts 1, 8.

Zwaan, K. & van Roermund H.L.M., 1990. A rift-related mafic dyke swarm in the Corrovarre Nappe of the Caledonian Middle Allochthon, Troms, North Norway, and its tectonometamorphic evolution. Norges Geol. Unders. 419, 25—44.

Appendix 1. Olivine compositions for the Halti and Ridnitsohkka rocks. Lith. = lithologies: DUN = dunite, TRO = troctolite, OLGB = olivine gabbro, GBPG = gabbro pegmatite, ORE = banded chrome spinel ore, AAUG = augite augen gabbro, SIL* = gabbro sill close to Halti cumulates. Type: PgCont = olivine in dunite on the contact of gabbro pegmatite, Cor = corona between ilmenite and plagioclase. Ni-bearing analyses made at the University of Oulu, others at the University of Turku. n.d. = not detected.

	Halti area															
Sample	15	17	20	30	31	32	33	81	374A	374C	425	427	430	432	433	436
Lith.	DUN	DUN	DUN	DUN	DUN	DUN	DUN	DUN	DUN	DUN	DUN	DUN	DUN	DUN	DUN	DUN
Type					PgCont											
SiO2	40.94	43.50	43.09	42.58	38.14	42.20	42.68	42.13	38.58	38.69	43.29	42.48	42.90	42.36	43.21	43.19
Al2O3	–	0.01	–	0.01	–	–	0.03	0.01	–	–	0.04	–	0.01	–	–	0.01
FeO	8.89	8.09	9.11	9.56	24.81	8.61	9.58	8.75	9.36	13.28	8.45	9.53	9.15	8.80	7.83	8.16
MnO	–	0.12	0.17	0.15	0.41	0.13	0.13	0.12	–	–	0.13	0.13	0.14	0.15	0.10	0.16
MgO	49.47	51.09	50.50	50.46	38.42	50.61	49.26	50.34	47.27	45.52	50.20	49.50	50.38	50.42	51.65	50.85
CaO	–	0.14	0.05	0.03	–	0.12	0.33	0.02	–	–	0.30	0.02	0.05	0.03	0.07	0.06
NiO	0.30	0.26	0.24	0.30	n.d.	0.24	0.27	0.32	n.d.	n.d.	0.26	0.24	0.27	0.30	0.30	0.31
Total	99.60	103.21	103.17	103.09	101.78	101.90	102.27	101.69	95.21	97.49	102.67	101.90	102.90	102.05	103.15	102.73
Ox	4	4	4	4	4	4	4	4	4	4	4	4	4	4	4	4
Si	1.004	1.021	1.017	1.009	0.987	1.008	1.019	1.009	0.993	0.991	1.024	1.017	1.016	1.011	1.015	1.019
Al	0.000	0.000	0.000	0.000	0.000	0.000	0.001	0.000	0.000	0.000	0.001	0.000	0.000	0.000	0.000	0.000
Fe	0.182	0.159	0.180	0.190	0.536	0.172	0.191	0.175	0.201	0.284	0.167	0.191	0.181	0.176	0.154	0.161
Mn	0.000	0.002	0.003	0.003	0.009	0.003	0.003	0.002	0.000	0.000	0.003	0.003	0.003	0.003	0.002	0.003
Mg	1.805	1.788	1.777	1.782	1.480	1.802	1.753	1.797	1.812	1.735	1.769	1.767	1.778	1.793	1.808	1.789
Ca	0.000	0.003	0.001	0.001	0.000	0.003	0.009	0.000	0.000	0.000	0.008	0.001	0.001	0.001	0.002	0.001
Ni	0.006	0.005	0.005	0.006	0.000	0.005	0.005	0.006	0.000	0.000	0.005	0.005	0.005	0.006	0.006	0.006
Total	2.996	2.978	2.983	2.991	3.013	2.993	2.981	2.989	3.007	3.009	2.977	2.984	2.984	2.990	2.987	2.979
Fo	90.84	91.83	90.80	90.37	73.40	91.29	90.17	91.13	90.00	85.94	91.37	90.25	90.76	91.06	92.15	91.74

Appendix 1. cont.

	Halti area															
Sample	18S	18T	18U	18V	28	34	35A	39	49	51	100	154	426	428	428A	429
Lith.	TRO	TRO	TRO	TRO	TRO	TRO	TRO	TRO	TRO	TRO	TRO	TRO	TRO	TRO	TRO	TRO
Type																
SiO2	37.08	38.44	39.53	38.69	42.51	42.29	41.56	38.02	42.46	40.35	43.58	40.48	42.19	42.32	42.30	42.31
Al2O3	–	–	–	–	–	0.01	–	–	0.01	0.01	–	–	0.01	0.01	0.00	0.01
FeO	19.16	16.32	10.10	21.79	11.71	8.10	11.36	16.01	10.86	19.33	10.58	9.93	9.35	8.88	9.32	8.80
MnO	–	–	–	–	0.20	0.11	0.16	0.34	0.14	0.25	0.17	–	0.14	0.14	0.12	0.14
MgO	39.99	42.91	47.15	40.69	48.18	50.44	48.15	43.13	48.18	40.99	49.56	49.30	49.06	50.12	49.11	50.50
CaO	–	–	–	–	0.01	0.04	0.04	–	0.05	0.01	0.04	–	0.05	0.03	0.02	0.02
NiO	n.d.	n.d.	n.d.	n.d.	0.25	0.30	0.17	0.35	0.31	0.06	0.13	0.37	0.20	0.33	0.27	0.28
Total	96.23	97.67	96.77	101.17	102.86	101.27	101.44	97.85	102.01	100.99	104.05	100.08	100.99	101.82	101.14	102.06
Ox	4	4	4	4	4	4	4	4	4	4	4	4	4	4	4	4
Si	0.991	0.996	1.003	0.991	1.018	1.013	1.009	0.986	1.022	1.020	1.024	0.994	1.019	1.012	1.020	1.010
Al	0.000	0.000	0.000	0.000	0.000	0.000	0.000	0.000	0.000	0.000	0.000	0.000	0.000	0.000	0.000	0.000
Fe	0.428	0.353	0.214	0.466	0.234	0.162	0.231	0.347	0.219	0.409	0.208	0.204	0.189	0.178	0.188	0.176
Mn	0.000	0.000	0.000	0.000	0.004	0.002	0.003	0.007	0.003	0.005	0.003	0.000	0.003	0.003	0.003	0.003
Mg	1.591	1.655	1.781	1.552	1.720	1.802	1.743	1.666	1.728	1.544	1.737	1.801	1.766	1.787	1.765	1.796
Ca	0.000	0.000	0.000	0.000	0.000	0.001	0.001	0.000	0.001	0.000	0.001	0.000	0.001	0.001	0.000	0.000
Ni	0.000	0.000	0.000	0.000	0.005	0.006	0.003	0.007	0.006	0.049	0.002	0.007	0.004	0.006	0.005	0.005
Total	3.009	3.004	2.997	3.009	2.981	2.986	2.990	3.014	2.979	3.027	2.975	3.006	2.982	2.987	2.981	2.990
Fo	78.82	82.42	89.28	76.90	88.02	91.75	88.30	82.76	88.75	79.06	89.31	89.85	90.33	90.94	90.37	91.08

Appendix 1. cont.

	Halti area															
Sample	431	434	435	437	438	37A	37A	43	44	47	48	50	368	31	366A	374B
Lith.	TRO	TRO	TRO	TRO	TRO	OLGB	OLGB	OLGB	OLGB	OLGB	OLGB	OLGB	OLGB	GBPG	GBPG	ORE
Type							Cor									
SiO2	42.08	43.64	43.65	43.51	42.86	36.38	33.94	41.25	40.42	42.10	41.74	41.77	38.70	38.83	40.83	40.12
Al2O3	0.00	0.00	0.00	0.00	0.01	–	–	0.01	0.01	–	–	0.01	–	–	–	–
FeO	10.17	8.05	8.07	8.75	9.10	24.19	40.95	22.03	24.67	18.77	18.13	18.42	17.16	27.58	24.42	7.19
MnO	0.17	0.15	0.15	0.15	0.15	0.32	0.42	0.36	0.33	0.25	0.22	0.24	0.41	0.40	0.35	–
MgO	49.40	51.50	51.31	50.85	49.91	35.33	21.12	39.68	37.79	43.44	42.57	42.98	43.11	34.79	37.93	50.54
CaO	0.02	0.04	0.11	0.08	0.03	–	–	0.01	0.01	0.03	0.01	0.01	–	0.02	0.01	–
NiO	0.21	0.23	0.30	0.26	0.28	0.07	–	0.08	0.03	0.08	0.08	0.05	n.d.	0.15	0.08	n.d.
Total	102.04	103.60	103.59	103.60	102.34	96.29	96.42	103.42	103.27	104.67	102.76	103.47	99.39	101.77	103.62	97.85
Ox	4	4	4	4	4	4	4	4	4	4	4	4	4	4	4	4
Si	1.010	1.020	1.021	1.020	1.020	0.998	1.014	1.028	1.022	1.021	1.028	1.023	0.991	1.015	1.027	0.994
Al	0.000	0.000	0.000	0.000	0.000	0.000	0.000	0.000	0.000	0.000	0.000	0.007	0.000	0.000	0.000	0.000
Fe	0.204	0.157	0.158	0.172	0.181	0.554	1.022	0.459	0.522	0.381	0.374	0.377	0.367	0.602	0.514	0.149
Mn	0.003	0.003	0.003	0.003	0.003	0.007	0.011	0.008	0.007	0.005	0.005	0.005	0.009	0.009	0.007	0.000
Mg	1.768	1.794	1.789	1.778	1.770	1.443	0.939	1.474	1.425	1.570	1.563	1.570	1.643	1.354	1.422	1.863
Ca	0.000	0.001	0.003	0.002	0.001	0.000	0.000	0.000	0.000	0.001	0.000	0.000	0.000	0.001	0.000	0.000
Ni	0.004	0.004	0.006	0.005	0.005	0.001	0.000	0.002	0.001	0.002	0.002	0.001	0.000	0.003	0.002	0.000
Total	2.989	2.979	2.980	2.980	2.980	3.003	2.986	2.971	2.977	2.980	2.972	2.983	3.009	2.984	2.972	3.006
Fo	89.66	91.95	91.88	91.18	90.72	72.26	47.90	76.25	73.19	80.47	80.69	80.64	81.75	69.22	73.45	92.61

Appendix 1. cont.

	Halti area							Ridnitsohkka area			
Sample	380	425A	18	18R	333	375	423	361	362	363	364
Lith.	ORE	ORE	AAUG	AAUG	AAUG	AAUG	AAUG	SIL*	SIL*	SIL*	SIL*
Type											
SiO2	40.45	40.64	40.23	38.97	34.79	37.09	36.24	34.52	32.30	36.71	35.62
Al2O3	–	–	0.00	0.00	–	–	–	–	–	0.02	–
FeO	7.99	6.51	23.91	25.07	31.46	24.72	28.02	50.13	42.82	40.89	24.18
MnO	–	–	0.41	0.41	0.63	–	0.52	0.94	0.55	0.50	0.61
MgO	50.39	51.20	38.91	36.29	29.56	36.30	33.43	14.86	19.39	23.26	35.31
CaO	–	–	0.02	0.02	–	–	–	0.01	–	0.02	–
NiO	n.d.	n.d.	0.07	0.10	n.d.	n.d.	n.d.	n.d.	n.d.	n.d.	n.d.
Total	98.83	98.35	103.54	100.87	96.44	98.11	98.21	100.45	95.06	101.40	95.73
Ox	4	4	4	4	4	4	4	4	4	4	4
Si	0.995	0.998	1.013	1.016	0.991	0.997	0.992	1.031	0.996	1.029	0.986
Al	0.000	0.000	0.000	0.000	0.000	0.000	0.000	0.000	0.000	0.001	0.000
Fe	0.164	0.133	0.503	0.547	0.748	0.555	0.641	1.252	1.103	0.958	0.559
Mn	0.000	0.000	0.009	0.009	0.015	0.000	0.012	0.024	0.014	0.012	0.014
Mg	1.845	1.871	1.460	1.410	1.254	1.452	1.363	0.662	0.890	0.971	1.455
Ca	0.000	0.000	0.000	0.001	0.000	0.000	0.000	0.000	0.000	0.000	0.000
Ni	0.000	0.000	0.001	0.002	0.000	0.000	0.000	0.000	0.000	0.000	0.000
Total	3.005	3.002	2.986	2.985	3.009	3.003	3.008	2.969	3.004	2.971	3.014
Fo	91.84	93.35	74.38	72.05	62.62	72.36	68.02	34.59	44.66	50.34	72.25

Appendix 2. Chrome spinel compositions in the Halti area. Lith. = lithologies: DUN = dunite, TRO = troctolite, GBPG = gabbro pegmatite, ORE = banded chrome spinel ore, AR = amphibole rock. Type: chrome spinel inclusion in olivine (= Ol), plagioclase (= Pl), sulfide (= Sulf) (others are interstitial). Type number in ore samples show the number of analysis, from which the mean is calculated. Fe^{3+} is calculated by assuming spinel stoichiometry. Cation ratios: XMg = Mg/Mg + Fe^{2+}, XAl = Al/Al + Cr + Fe^{3+}, XCr = Cr/Al + Cr, XFe^{3+} = Fe^{3+}/Al + Cr + Fe^{3+}.

Sample	15	17	20	20	28	30	32	32	32	33	81	374A	374C	425	427	430
Lith.	DUN	DUN	DUN	DUN	DUN	DUN	DUN	DUN	DUN	DUN	DUN	DUN	DUN	DUN	DUN	DUN
Type				Sulf			Ol	Pl				Ol	Ol	Ol	Ol	Ol
Al2O3	30.79	35.61	30.55	36.66	32.86	46.56	28.80	26.87	31.51	32.42	34.30	36.15	28.73	32.82	35.60	46.31
Cr2O3	32.23	28.15	30.75	26.97	31.32	15.83	36.38	35.02	32.12	30.67	29.20	25.61	26.58	29.22	31.86	16.15
Fe2O3	4.74	3.47	6.31	4.87	2.98	4.69	1.09	4.30	3.99	3.69	4.71	4.35	8.37	6.80	2.46	3.63
FeO	14.68	14.95	19.87	18.62	18.25	14.09	24.53	23.85	18.97	19.18	18.37	17.56	22.81	17.84	18.34	14.66
MnO	–	–	–	–	–	–	0.49	–	–	–	–	–	–	–	–	–
MgO	14.30	14.55	11.26	12.43	12.84	16.19	8.30	8.92	11.92	11.94	12.76	13.20	9.18	12.43	13.28	15.71
TiO2	0.61	0.51	0.58	–	1.02	0.30	1.02	1.29	0.57	0.81	0.57	0.86	1.44	–	0.42	0.43
Total	97.35	97.23	99.33	99.54	99.26	97.66	100.61	100.25	99.09	98.71	99.91	97.72	97.11	99.11	101.97	96.90
Ox	32	32	32	32	32	32	32	32	32	32	32	32	32	32	32	32
Al	8.756	9.925	8.730	10.130	9.205	12.292	8.343	7.846	8.942	9.193	9.517	10.111	8.554	9.250	9.641	12.348
Cr	6.149	5.263	5.896	4.999	5.887	2.804	7.069	6.859	6.116	5.834	5.436	4.805	5.308	5.526	5.788	2.889
Fe3+	0.874	0.629	1.163	0.870	0.544	0.803	0.211	0.812	0.735	0.678	0.846	0.777	1.591	1.224	0.425	0.618
Fe2+	2.952	2.947	4.022	3.644	3.620	2.630	5.036	4.936	3.813	3.852	3.608	3.485	4.818	3.569	3.525	2.774
Mn	0.000	0.000	0.000	0.000	0.000	0.000	0.103	0.000	0.000	0.000	0.000	0.000	0.000	0.000	0.000	0.000
Mg	5.158	5.144	4.083	4.356	4.562	5.421	3.050	3.305	4.291	4.295	4.492	4.668	3.456	4.431	4.548	5.298
Ti	0.110	0.091	0.106	0.000	0.182	0.051	0.189	0.241	0.104	0.147	0.100	0.153	0.273	0.000	0.073	0.073
XMg	0.636	0.636	0.504	0.545	0.558	0.673	0.377	0.401	0.529	0.527	0.555	0.573	0.418	0.554	0.563	0.656
XAl	0.555	0.627	0.553	0.633	0.589	0.773	0.534	0.506	0.566	0.585	0.602	0.644	0.554	0.578	0.608	0.779
XCr	0.413	0.347	0.403	0.330	0.390	0.186	0.459	0.466	0.406	0.388	0.364	0.322	0.383	0.374	0.375	0.190
XFe3+	0.055	0.040	0.074	0.054	0.035	0.050	0.013	0.052	0.047	0.043	0.054	0.050	0.103	0.077	0.027	0.039

Appendix 2. cont.

Sample	432	432	433	436	18U	18U	34	35A	49	100	154	426	428	428A	429	429
Lith.	DUN	DUN	DUN	DUN	TRO	TRO	TRO	TRO	TRO	TRO	TRO	TRO	TRO	TRO	TRO	TRO
Type	Ol	Ol	Ol	Ol	Ol	Pl								Pl	Ol	Pl
Al2O3	36.93	45.02	50.97	32.31	41.21	44.42	36.08	27.52	19.81	26.88	31.57	42.70	41.18	18.51	25.76	30.81
Cr2O3	24.18	18.23	13.65	33.07	24.30	21.69	30.11	34.69	41.49	35.45	31.71	21.76	23.99	43.58	35.26	34.32
Fe2O3	4.91	4.44	3.33	2.99	2.78	0.64	1.52	3.84	2.87	3.52	4.24	3.01	3.30	4.14	3.96	1.18
FeO	16.97	13.92	10.31	15.22	16.40	16.28	15.82	21.39	24.44	20.78	18.14	13.08	14.10	23.84	19.79	17.72
MnO	–	–	–	–	–	–	–	–	0.64	–	–	–	–	–	–	–
MgO	12.73	15.95	18.83	14.23	14.24	14.34	14.10	10.28	7.94	10.24	12.80	16.39	15.98	7.77	10.25	12.56
TiO2	–	–	–	0.46	–	–	0.34	1.22	2.43	0.97	1.01	0.31	0.41	1.21	0.81	0.92
Total	95.71	97.56	97.08	98.28	98.92	97.36	97.96	98.94	99.62	97.84	99.48	97.25	98.96	99.05	95.83	97.51
Ox	32	32	32	32	32	32	32	32	32	32	32	32	32	32	32	32
Al	10.498	11.988	13.100	9.069	11.121	11.969	10.001	8.030	6.027	7.937	8.881	11.460	10.999	5.703	7.779	8.841
Cr	4.611	3.257	2.354	6.229	4.400	3.921	5.599	6.791	8.472	7.023	5.983	3.918	4.298	9.006	7.144	6.608
Fe3+	0.891	0.754	0.546	0.537	0.479	0.110	0.281	0.726	0.558	0.674	0.774	0.515	0.563	0.815	0.764	0.215
Fe2+	3.424	2.630	1.880	3.031	3.140	3.112	3.102	4.422	5.277	4.348	3.614	2.490	2.673	5.211	4.242	3.609
Mn	0.000	0.000	0.000	0.000	0.000	0.000	0.000	0.000	0.140	0.000	0.000	0.000	0.000	0.000	0.000	0.000
Mg	4.576	5.370	6.120	5.051	4.860	4.888	4.957	3.805	3.054	3.835	4.567	5.563	5.397	3.027	3.915	4.558
Ti	0.000	0.000	0.000	0.082	0.000	0.000	0.059	0.227	0.471	0.183	0.181	0.053	0.070	0.238	0.157	0.168
XMg	0.572	0.671	0.765	0.625	0.607	0.611	0.615	0.462	0.367	0.469	0.558	0.691	0.669	0.367	0.480	0.558
XAl	0.656	0.749	0.819	0.573	0.695	0.748	0.630	0.516	0.400	0.508	0.568	0.721	0.693	0.367	0.496	0.564
XCr	0.305	0.214	0.152	0.407	0.283	0.247	0.359	0.458	0.584	0.469	0.403	0.255	0.281	0.612	0.479	0.428
XFe3+	0.056	0.047	0.034	0.034	0.030	0.007	0.018	0.047	0.037	0.043	0.049	0.032	0.035	0.053	0.049	0.014

Appendix 2. cont.

Sample	431	434	434	435	435	437	438	438	31	374B	380	425A	453	21	153
Lith.	TRO	TRO	TRO	TRO	TRO	TRO	TRO	TRO	GBPG	ORE	ORE	ORE	ORE	AR	AR
Type	Pl	Ol	Pl	Ol	Pl	Ol	Ol	Pl		6	5	12	21		
Al2O3	31.83	32.38	37.95	42.62	43.64	35.44	30.47	32.29	25.19	38.36	41.31	39.68	50.97	29.46	29.82
Cr2O3	30.94	31.94	29.24	21.74	22.96	27.96	30.04	29.73	31.47	28.74	25.08	27.55	17.26	34.42	34.35
Fe2O3	2.70	2.23	0.23	3.64	1.93	2.48	4.46	2.34	7.00	2.23	2.99	3.62	0.34	1.20	-1.72
FeO	17.77	17.53	15.55	14.08	13.10	16.52	19.90	19.55	24.54	14.46	15.38	13.99	11.84	28.50	24.16
MnO	-	-	-	-	-	-	-	-	0.51	-	-	-	-	-	-
MgO	12.22	12.75	14.65	16.19	16.48	13.39	10.63	11.78	8.16	15.86	15.86	16.56	18.61	5.56	8.07
TiO2	0.71	0.75	0.55	0.55	-	0.61	0.65	1.49	2.13	0.62	0.74	0.50	0.44	0.47	1.15
Total	96.16	97.58	98.17	98.83	98.10	96.39	96.16	97.19	98.99	100.26	101.36	101.90	99.46	99.61	95.83
Ox	32	32	32	32	32	32	32	32	32	32	32	32	32	32	32
Al	9.225	9.222	10.395	11.321	11.584	10.026	8.978	9.287	7.530	10.254	10.836	10.389	12.879	8.739	8.958
Cr	6.014	6.101	5.373	3.873	4.088	5.307	5.939	5.735	6.312	5.155	4.414	4.839	2.925	6.850	6.922
Fe3+	0.499	0.406	0.041	0.618	0.327	0.447	0.840	0.429	1.346	0.381	0.500	0.606	0.056	0.235	-0.322
Fe2+	3.653	3.543	3.022	2.654	2.467	3.316	4.161	3.990	5.202	2.743	2.862	2.599	2.123	5.996	5.146
Mn	0.000	0.000	0.000	0.000	0.000	0.000	0.000	0.000	0.110	0.000	0.000	0.000	0.000	0.000	0.000
Mg	4.478	4.593	5.073	5.440	5.533	4.793	3.961	4.284	3.095	5.362	5.262	5.484	5.947	2.092	3.075
Ti	0.131	0.135	0.095	0.094	0.000	0.109	0.122	0.274	0.406	0.105	0.125	0.083	0.070	0.088	0.221
XMg	0.551	0.565	0.627	0.672	0.692	0.591	0.488	0.518	0.373	0.662	0.648	0.679	0.737	0.259	0.259
XAl	0.586	0.586	0.658	0.716	0.724	0.635	0.570	0.601	0.089	0.649	0.688	0.656	0.812	0.552	0.576
XCr	0.395	0.398	0.341	0.255	0.261	0.346	0.398	0.382	0.456	0.335	0.289	0.318	0.185	0.439	0.436
XFe3+	0.032	0.026	0.003	0.039	0.020	0.028	0.053	0.028	0.496	0.024	0.032	0.038	0.004	0.015	-0.021

Appendix 3. Plagioclase compositions for the Halti-Ridnitsohkka complex. Lith. = lithologies: TRO = troctolite, OLGB = olivine gabbro, GBPG = gabbro pegmatite, AAUG = augite augen gabbro, AR = amphibole rock, SIL* = gabbro sill close to Halti cumulates, SIL = gabbro sill between gneiss interlayers, GNIL = gneiss interlayer between gabbro sills, MBIL = metabasalt interlayer between gabbro sills, SKARN = diopside skarn layer between gabbro sills, GNAU = metamorphic aureole in outer gneiss, GN = outer gneiss. Type: Cent = central part of a 10 meters thick sill, Marg = margin of the same sill, Phen = plagioclase phenocryst, Myl = mylonite.

	Halti area															
Sample	18S	18T	18U	18V	28	34	35A	39	49	51	100	154	426	428	428A	429
Lith.	TRO	TRO	TRO	TRO	TRO	TRO	TRO	TRO	TRO	TRO	TRO	TRO	TRO	TRO	TRO	TRO
Type																
SiO2	48.28	49.26	46.55	52.19	49.98	48.68	47.01	47.78	51.11	50.95	44.80	46.07	44.92	44.41	46.06	45.18
Al2O3	31.48	30.41	34.38	30.90	32.23	32.57	33.39	31.82	29.89	30.67	32.24	34.32	34.26	34.34	35.20	35.56
CaO	13.54	12.43	16.27	12.44	15.52	15.90	17.01	15.89	13.46	13.99	16.23	18.45	16.26	16.54	16.82	16.90
Na2O	3.64	4.53	2.08	4.91	3.26	2.75	2.06	2.85	4.24	4.01	1.94	1.57	2.14	1.83	1.88	2.04
K2O	–	–	–	–	–	–	–	–	–	–	–	–	–	–	–	–
Total	96.94	96.64	99.27	100.43	100.99	99.90	99.47	98.34	98.70	99.63	95.21	100.42	97.57	97.12	99.96	99.68
Ox	32	32	32	32	32	32	32	32	32	32	32	32	32	32	32	32
Si	9.092	9.290	8.612	9.447	9.067	8.936	8.698	8.927	9.438	9.332	8.661	8.485	8.478	8.426	8.478	8.359
Al	6.949	6.722	7.454	6.556	6.853	7.009	7.243	6.969	6.471	6.586	7.304	7.409	7.579	7.636	7.595	7.712
Ca	2.730	2.510	3.222	2.411	3.014	3.126	3.370	3.178	2.660	2.744	3.360	3.637	3.285	3.359	3.315	3.348
Na	1.327	1.654	0.745	1.721	1.144	0.977	0.739	1.030	1.516	1.424	0.725	0.561	0.783	0.672	0.670	0.732
K	0.000	0.000	0.000	0.000	0.000	0.000	0.000	0.000	0.000	0.000	0.000	0.000	0.000	0.000	0.000	0.000
Total	20.097	20.176	20.033	20.136	20.078	20.048	20.050	20.104	20.085	20.087	20.049	20.091	20.125	20.092	20.059	20.151
An	67.30	60.28	81.23	58.35	72.49	76.18	82.02	75.53	63.69	65.83	82.26	86.63	80.74	83.33	83.19	82.07

Appendix 3. cont.

	Halti area															
Sample	431	434	438	37A	43	44	47	48	50	368	31	366A	18	18R	22	333
Lith.	TRO	TRO	TRO	OLGB	OLGB	OLGB	OLGB	OLGB	OLGB	OLGB	GBPG	GBPG	AAUG	AAUG	AAUG	AAUG
Type																
SiO2	43.38	45.21	43.83	53.05	50.38	53.79	50.67	51.19	50.13	49.44	54.00	54.44	51.92	49.45	48.93	53.08
Al2O3	34.15	34.43	33.89	29.19	30.62	29.40	29.32	30.61	30.94	32.80	28.32	29.21	30.77	31.34	32.80	29.03
CaO	16.27	16.41	16.56	11.12	14.41	11.89	13.28	13.85	14.54	14.10	11.06	10.31	13.48	12.46	16.05	9.88
Na2O	1.78	1.94	1.89	5.26	3.74	4.87	4.11	3.90	3.76	4.07	5.49	6.35	4.18	3.82	2.96	5.88
K2O	–	–	–	–	–	–	–	–	–	–	–	0.22	–	–	–	–
Total	95.57	97.98	96.17	98.62	99.15	99.96	97.38	99.56	99.38	100.40	98.87	100.54	100.35	97.07	100.74	97.87
Ox	32	32	32	32	32	32	32	32	32	32	32	32	32	32	32	32
Si	8.365	8.491	8.409	9.733	9.284	9.740	9.477	9.371	9.226	9.011	9.877	9.811	9.417	9.252	8.918	9.791
Al	7.720	7.578	7.619	6.277	6.614	6.240	6.429	6.568	6.675	7.006	6.071	6.170	6.542	6.872	7.007	6.277
Ca	3.358	3.299	3.401	2.184	2.843	2.305	2.659	2.715	2.865	2.752	2.166	1.989	2.618	2.496	3.131	1.950
Na	0.664	0.705	0.703	1.869	1.337	1.709	1.489	1.384	1.340	1.435	1.946	2.218	1.469	1.385	1.044	2.102
K	0.000	0.000	0.000	0.000	0.000	0.000	0.000	0.000	0.000	0.000	0.000	0.051	0.000	0.000	0.000	0.000
Total	20.107	20.073	20.133	20.063	20.077	19.994	20.053	20.037	20.107	20.204	20.061	20.239	20.046	20.005	20.101	20.121
An	83.50	82.39	82.86	53.89	68.02	57.42	64.11	66.23	68.13	65.73	52.67	46.72	64.05	64.32	74.99	48.13

Appendix 3. cont.

	Halti area					Ridnitsohkka area									
Sample	375	423	45	46	153	25	26	361	362	363	364	87	89	106	144
Lith.	AAUG	AAUG	AR	AR	AR	SIL*	SIL*	SIL*	SIL*	SIL*	SIL*	SIL	SIL	SIL	SIL
Type															
SiO2	52.44	54.12	50.31	57.24	46.19	55.54	55.78	60.23	54.78	53.94	49.51	55.55	53.74	57.43	54.54
Al2O3	29.85	27.72	31.65	27.16	33.43	28.39	27.40	25.47	26.32	27.82	30.28	26.15	28.70	25.81	27.99
CaO	11.23	9.13	14.82	9.04	17.05	10.73	9.14	5.92	7.64	9.26	12.31	9.23	11.80	8.08	10.54
Na2O	5.63	6.66	3.42	6.86	1.93	5.86	6.17	8.26	6.89	6.04	4.60	6.00	4.94	7.00	5.64
K2O	–	–	–	–	–	–	0.43	1.17	0.25	0.32	–	0.23	–	0.15	–
Total	99.14	97.63	100.20	100.30	98.61	100.53	98.91	101.06	95.88	97.39	96.70	97.16	99.18	98.48	98.71
Ox	32	32	32	32	32	32	32	32	32	32	32	32	32	32	32
Si	9.599	10.000	9.176	10.258	8.629	9.975	10.156	10.688	10.261	9.991	9.325	10.280	9.807	10.455	9.971
Al	6.403	6.003	6.767	5.706	7.321	5.978	5.847	5.298	5.779	6.040	6.686	5.672	6.139	5.508	5.998
Ca	2.200	1.805	2.895	1.733	3.410	2.063	1.781	1.124	1.532	1.836	2.482	1.829	2.304	1.575	2.062
Na	1.994	2.382	1.207	2.382	0.699	2.040	2.176	2.840	2.498	2.168	1.679	2.150	1.746	2.468	1.998
K	0.000	0.000	0.000	0.000	0.000	0.000	0.099	0.265	0.060	0.074	0.000	0.055	0.000	0.035	0.000
Total	20.196	20.190	20.045	20.079	20.060	20.056	20.058	20.216	20.129	20.110	20.172	19.986	19.997	20.042	20.029
An	52.45	43.11	70.56	42.13	82.99	50.28	43.92	26.58	37.45	45.02	59.66	45.35	56.88	38.62	50.80

Appendix 3. cont.

	Ridnitsohkka area															
Sample	352	353	354	355A	355B	356	357	358	359	360	360	503	88	89A	188G	341
Lith.	SIL	SIL	SIL	SIL	SIL	SIL	SIL	SIL	SIL	SIL	SIL	SIL	GNIL	GNIL	GNIL	GNIL
Type				Cent	Marg					Phen						
SiO2	48.42	57.88	52.52	57.48	56.28	55.03	54.45	56.72	57.37	54.70	57.97	52.82	56.99	55.09	55.94	57.69
Al2O3	32.71	27.75	29.81	26.57	27.47	28.67	27.57	26.43	26.41	30.24	28.44	28.41	24.03	25.42	25.60	24.45
CaO	14.15	8.09	10.87	7.15	8.34	9.07	8.35	7.54	7.18	10.54	8.30	9.65	5.97	7.71	7.06	5.79
Na2O	3.02	7.22	5.35	7.38	6.58	6.25	6.75	7.12	7.54	5.73	7.85	5.63	6.91	6.28	6.82	7.70
K2O	–	–	–	0.27	–	–	–	–	–	0.20	0.19	0.26	0.24	–	0.41	0.42
Total	98.30	100.93	98.54	98.85	98.67	99.01	97.11	97.82	98.49	101.41	102.75	96.78	94.14	94.50	95.83	96.04
Ox	32	32	32	32	32	32	32	32	32	32	32	32	32	32	32	32
Si	8.987	10.278	9.644	10.412	10.224	9.992	10.080	10.379	10.421	9.750	10.162	9.853	10.761	10.418	10.449	10.716
Al	7.115	5.776	6.416	5.642	5.848	6.102	5.982	5.669	5.623	6.318	5.844	6.212	5.319	5.635	5.606	5.322
Ca	2.812	1.538	2.136	1.387	1.623	1.763	1.655	1.477	1.397	2.011	1.557	1.927	1.207	1.561	1.412	1.151
Na	1.086	2.483	1.903	2.590	2.315	2.199	2.421	2.524	2.651	1.977	2.664	2.035	2.527	2.299	2.467	2.770
K	0.000	0.000	0.000	0.062	0.000	0.000	0.000	0.000	0.000	0.045	0.043	0.062	0.058	0.000	0.096	0.098
Total	19.999	20.075	20.099	20.093	20.010	20.056	20.139	20.049	20.093	20.102	20.270	20.089	19.872	19.913	20.030	20.057
An	72.14	38.25	52.89	34.35	41.21	44.49	40.60	36.92	34.51	49.86	36.51	47.89	31.82	40.45	35.52	28.63

Appendix 3. cont.

	Ridnitsohkka area												
Sample	355C	357A	361A	362A	362B	504B	504C	504D	504E	504F	505	40	134A
Lith.	GNIL	GNIL	GNIL	MBIL	SKARN	GNAU	GNAU	GNAU	GNAU	GNAU	GNAU	GN	GN
Type													Myl
SiO2	54.50	55.79	54.51	51.92	41.95	58.66	57.01	58.77	59.81	53.32	55.28	59.27	58.12
Al2O3	25.38	26.35	28.17	30.11	37.26	25.97	26.94	25.78	25.01	26.62	26.67	24.20	24.69
CaO	7.37	7.56	8.94	11.46	19.23	6.23	7.62	5.70	5.61	8.76	7.31	5.52	5.65
Na2O	7.31	7.38	6.65	5.33	–	8.29	7.37	7.72	8.97	6.11	7.34	7.57	7.87
K2O	–	0.37	0.21	–	–	–	–	0.33	–	0.23	0.23	0.25	0.27
Total	94.57	97.45	98.48	98.82	98.44	99.15	98.94	98.32	99.39	95.03	96.84	96.80	96.59
Ox	32	32	32	32	32	32	32	32	32	32	32	32	32
Si	10.344	10.297	9.985	9.537	7.897	10.564	10.326	10.645	10.736	10.103	10.252	10.87	10.720
Al	5.647	5.700	6.048	6.483	8.221	5.483	5.718	5.474	5.261	5.912	5.798	5.50	5.338
Ca	1.498	1.495	1.754	2.253	3.875	1.201	1.477	1.106	1.078	1.776	1.452	1.08	1.115
Na	2.686	2.637	2.358	1.895	0.000	2.891	2.587	2.710	3.117	2.243	2.638	2.69	2.812
K	0.000	0.086	0.049	0.000	0.000	0.000	0.000	0.077	0.000	0.056	0.055	0.06	0.064
Total	20.175	20.215	20.194	20.169	19.993	20.140	20.108	20.012	20.192	20.090	20.195	19.90	20.049
An	35.80	35.44	42.16	54.32	100.00	29.35	36.34	28.41	25.70	43.59	35.03	28.28	27.84

Appendix 4. Clinopyroxene compositions for the Halti-Ridnitsohkka complex. Lith. = lithologies: TRO = troctolite, OLGB = olivine gabbro, GBPG = gabbro pegmatite, AAUG = augite augen gabbro, SIL* = gabbro sill close to Halti cumulates, SIL = gabbro sill between the gneiss interlayers, MBIL = metabasalt interlayer between gabbro sills, SKARN = diopside skarn layer between gabbro sills.

	Halti area															
Sample	18T	18U	18V	39	49	100	428	428A	429	431	434	37	37A	43	44	47
Lith.	TRO	TRO	TRO	TRO	TRO	TRO	TRO	TRO	TRO	TRO	TRO	OLGB	OLGB	OLGB	OLGB	OLGB
SiO2	50.39	50.29	50.07	48.61	49.81	47.37	49.76	52.39	50.07	44.92	46.82	47.24	47.03	47.79	50.28	50.96
TiO2	0.97	0.70	1.38	1.54	1.68	0.91	0.76	0.55	0.82	3.24	2.36	2.08	2.02	2.26	1.25	0.78
Cr2O3	0.59	1.24	0.49	0.73	1.43	1.09	0.70	0.70	0.81	0.91	1.20	0.25	–	–	0.42	0.27
Al2O3	2.32	4.56	2.83	4.08	3.41	3.84	4.33	1.77	3.30	6.99	6.09	5.36	5.04	5.15	3.14	2.37
FeO	4.12	2.61	4.85	4.71	3.28	2.81	2.46	2.58	2.43	2.46	2.48	6.72	7.29	6.77	8.19	5.92
MnO	–	–	–	–	–	–	–	–	–	–	–	–	–	–	–	–
MgO	15.93	15.62	15.09	15.14	16.10	14.81	15.49	17.10	16.09	13.61	14.37	13.72	13.35	13.66	14.99	15.88
CaO	21.15	22.56	21.40	20.97	23.05	21.84	22.56	22.58	22.47	21.83	22.34	21.64	21.06	21.85	22.47	23.22
Na2O	–	1.66	1.04	1.36	–	0.66	–	–	–	–	–	0.81	–	1.33	0.58	–
Total	95.47	99.24	97.16	97.13	98.76	93.32	96.07	97.67	96.00	93.95	95.66	97.82	95.79	98.80	101.32	99.40
Ox	6	6	6	6	6	6	6	6	6	6	6	6	6	6	6	6
Si	1.928	1.859	1.899	1.848	1.854	1.863	1.885	1.948	1.899	1.753	1.793	1.802	1.827	1.807	1.860	1.899
Ti	0.028	0.019	0.039	0.044	0.047	0.027	0.022	0.015	0.023	0.095	0.068	0.060	0.059	0.064	0.035	0.022
Al	0.104	0.198	0.126	0.182	0.149	0.177	0.192	0.077	0.147	0.320	0.273	0.240	0.229	0.228	0.136	0.103
Cr	0.018	0.036	0.015	0.022	0.042	0.034	0.021	0.021	0.024	0.028	0.036	0.007	0.000	0.000	0.012	0.008
Fe	0.132	0.081	0.154	0.150	0.102	0.092	0.078	0.080	0.077	0.080	0.079	0.214	0.237	0.214	0.253	0.184
Mn	0.000	0.000	0.000	0.000	0.000	0.000	0.000	0.000	0.000	0.000	0.000	0.000	0.000	0.000	0.000	0.000
Mg	0.907	0.860	0.852	0.857	0.892	0.867	0.874	0.946	0.909	0.790	0.819	0.779	0.772	0.769	0.825	0.881
Ca	0.866	0.893	0.869	0.854	0.918	0.920	0.915	0.899	0.912	0.912	0.916	0.883	0.876	0.885	0.890	0.926
Na	0.000	0.119	0.076	0.100	0.000	0.050	0.000	0.000	0.000	0.000	0.000	0.060	0.000	0.097	0.041	0.000
Total	3.983	4.064	4.029	4.056	4.004	4.030	3.987	3.987	3.992	3.978	3.985	4.045	3.999	4.064	4.052	4.023
En	47.63	46.90	45.44	46.06	46.64	46.15	46.81	49.15	47.87	44.34	45.15	41.51	40.97	41.17	41.93	44.24
Wo	45.47	48.70	46.36	45.89	48.03	48.95	49.03	46.70	48.07	51.17	50.48	47.08	46.47	47.38	45.22	46.51
Fs	6.91	4.40	8.20	8.05	5.33	4.90	4.16	4.15	4.06	4.49	4.37	11.40	12.55	11.46	12.86	9.25

Appendix 4. cont.

	Halti area										Ridnitsohkka area				
Sample	48	50	368	31	366A	423	18	18R	333	375	25	26	361	362	363
Lith.	OLGB	OLGB	OLGB	GBPG	GBPG	GBPG	AAUG	AAUG	AAUG	AAUG	SIL*	SIL*	SIL*	SIL*	SIL*
SiO2	51.58	51.25	49.98	50.05	51.37	49.20	47.77	49.06	49.15	50.92	50.12	49.83	51.14	50.41	50.67
TiO2	0.74	0.71	0.58	1.19	1.28	1.15	2.01	1.56	1.22	1.05	0.89	0.58	–	0.41	0.32
Cr2O3	0.38	0.67	0.30	–	–	–	–	–	–	0.58	–	–	–	–	–
Al2O3	2.55	2.41	2.42	3.02	2.76	2.88	4.18	3.91	3.72	2.88	2.64	2.58	1.24	1.40	1.14
FeO	5.68	5.60	4.68	7.96	8.16	8.74	5.82	6.25	7.80	5.86	8.63	12.68	14.70	10.88	10.50
MnO	–	–	–	–	–	–	–	–	–	–	0.32	0.39	0.50	–	–
MgO	16.11	16.55	15.83	14.91	15.11	14.24	13.72	14.68	13.61	15.12	14.15	12.93	11.98	13.32	13.47
CaO	23.37	22.34	20.72	21.63	20.32	19.12	20.97	21.32	20.41	21.25	22.11	20.17	19.31	19.07	19.41
Na2O	–	–	–	0.87	–	1.32	–	–	1.66	–	–	–	0.94	–	–
Total	100.41	99.52	94.51	99.64	98.99	96.66	94.46	96.78	97.55	97.64	98.86	99.17	99.81	95.49	95.50
Ox	6	6	6	6	6	6	6	6	6	6	6	6	6	6	6
Si	1.899	1.900	1.933	1.876	1.919	1.899	1.866	1.872	1.880	1.918	1.898	1.906	1.960	1.974	1.982
Ti	0.021	0.020	0.017	0.034	0.036	0.033	0.059	0.045	0.035	0.030	0.025	0.017	0.000	0.012	0.009
Al	0.110	0.105	0.110	0.133	0.121	0.130	0.192	0.175	0.167	0.127	0.117	0.116	0.056	0.064	0.052
Cr	0.011	0.020	0.009	0.000	0.000	0.000	0.000	0.000	0.000	0.017	0.000	0.000	0.000	0.000	0.000
Fe	0.175	0.173	0.151	0.249	0.254	0.282	0.190	0.199	0.249	0.184	0.273	0.405	0.470	0.356	0.343
Mn	0.000	0.000	0.000	0.000	0.000	0.000	0.000	0.000	0.000	0.000	0.010	0.013	0.016	0.000	0.000
Mg	0.883	0.913	0.911	0.832	0.841	0.818	0.797	0.834	0.775	0.847	0.798	0.736	0.683	0.776	0.784
Ca	0.921	0.887	0.858	0.868	0.813	0.790	0.877	0.871	0.835	0.857	0.896	0.826	0.792	0.800	0.813
Na	0.000	0.000	0.000	0.063	0.000	0.098	0.000	0.000	0.123	0.000	0.000	0.000	0.069	0.000	0.000
Total	4.020	4.018	3.990	4.055	3.984	4.052	3.980	3.996	4.063	3.980	4.018	4.019	4.047	3.982	3.983
En	44.61	46.28	47.45	42.69	44.06	43.29	42.79	43.79	41.67	44.87	40.56	37.43	35.12	40.18	40.43
Wo	46.56	44.94	44.67	44.52	42.60	41.81	47.04	45.75	44.94	45.37	45.57	41.99	40.71	41.40	41.89
Fs	8.83	8.78	7.87	12.79	13.34	14.90	10.18	10.46	13.39	9.75	13.87	20.58	24.17	18.42	17.68

Appendix 4. cont.

	Ridnitsohkka area												
Sample	87	106	144A	352	353	355A	356	357	358	359	360	362A	362B
Lith.	SIL	SIL	SIL	SIL	SIL	SIL	SIL	SIL	SIL	SIL	SIL	MBIL	SKARN
SiO2	50.59	51.04	51.01	53.46	51.96	51.60	50.31	52.35	50.79	50.42	52.62	51.86	52.43
TiO2	–	0.51	–	0.28	–	–	0.36	–	0.58	0.35	0.35	–	–
Cr2O3	–	–	–	–	–	–	–	–	–	–	–	–	–
Al2O3	1.39	1.35	0.91	–	–	–	–	1.24	–	1.14	1.05	1.03	–
FeO	10.19	11.41	9.23	7.89	10.65	12.14	10.55	9.99	14.80	10.74	9.86	4.68	4.24
MnO	–	0.41	–	0.37	0.38	0.47	0.00	–	0.51	0.45	0.28	–	–
MgO	13.57	13.83	13.68	13.86	13.11	12.97	13.25	14.16	11.49	12.92	14.50	16.64	15.64
CaO	19.40	20.98	20.65	20.81	20.18	19.26	19.77	20.77	18.67	19.66	19.44	21.65	23.97
Na2O	–	–	–	–	–	–	–	–	–	–	–	–	–
Total	95.14	99.52	95.48	96.66	96.28	96.43	94.23	98.51	96.84	95.69	98.08	95.87	96.28
Ox	6	6	6	6	6	6	6	6	6	6	6	6	6
Si	1.983	1.937	1.989	2.041	2.020	2.015	2.000	1.981	2.000	1.977	1.992	1.977	1.999
Ti	0.000	0.014	0.000	0.008	0.000	0.000	0.011	0.000	0.017	0.010	0.010	0.000	0.000
Al	0.064	0.060	0.041	0.000	0.000	0.000	0.000	0.055	0.000	0.052	0.046	0.046	0.000
Cr	0.000	0.000	0.000	0.000	0.000	0.000	0.000	0.000	0.000	0.000	0.000	0.000	0.000
Fe	0.334	0.361	0.300	0.252	0.345	0.396	0.351	0.316	0.487	0.352	0.312	0.149	0.135
Mn	0.000	0.013	0.000	0.012	0.012	0.015	0.000	0.000	0.017	0.015	0.009	0.000	0.000
Mg	0.792	0.781	0.794	0.788	0.760	0.754	0.785	0.798	0.674	0.754	0.817	0.944	0.888
Ca	0.814	0.852	0.863	0.851	0.841	0.805	0.842	0.842	0.788	0.826	0.788	0.884	0.979
Na	0.000	0.000	0.000	0.000	0.000	0.000	0.000	0.000	0.000	0.000	0.000	0.000	0.000
Total	3.986	4.019	3.988	3.951	3.978	3.985	3.989	3.991	3.983	3.986	3.974	4.000	4.001
En	40.83	39.15	40.57	41.67	39.06	38.57	39.69	40.81	34.58	39.05	42.63	47.76	44.36
Wo	41.97	42.73	44.09	45.02	43.22	41.18	42.57	43.05	40.43	42.74	41.11	44.70	48.90
Fs	17.20	18.12	15.34	13.32	17.72	20.25	17.75	16.14	24.99	18.21	16.26	7.54	6.74

Appendix 5. Orthopyroxene compositions for the Halti-Ridnitsohkka complex. Lith = lithologies: TRO = troctolite, OLGB = olivine gabbro, GBPG = gabbro pegmatite, SIL* = gabbro sill close to Halti cumulates, SIL = gabbro sill between gneiss interlayers, GNIL = gneiss interlayer between gabbro sills, MBIL = metabasalt interlayer between gabbro sills. Cor = corona between olivine and plagioclase. Cent = central part of 10 meter thick sill, Marg = margin of the same sill.

	Halti area								Ridnitsohkka area						
Sample	39	51	100	43	44	48	50	31	25	26	363	364	87	89	144A
Lith.	TRO	TRO	TRO	OLGB	OLGB	OLGB	OLGB	GBPG	SIL*	SIL*	SIL*	SIL*	SIL	SIL	SIL
Type	Cor	Cor	Cor	Cor	Cor	Cor	Cor	Cor	Cor						
SiO2	54.96	54.78	52.97	54.98	53.90	54.36	54.99	53.47	53.18	50.51	50.70	51.91	50.37	52.65	51.25
TiO2	–	–	–	–	–	–	–	–	–	0.38	–	–	–	–	–
Al2O3	0.75	–	0.55	1.12	–	1.62	0.71	0.83	–	1.18	–	1.14	–	0.61	–
FeO	11.45	13.45	6.93	15.53	16.99	12.91	13.37	18.03	23.63	26.13	22.62	16.28	22.08	24.23	23.66
MnO	0.37	–	0.28	0.40	0.42	–	0.32	0.43	0.57	0.53	0.53	0.53	0.66	0.76	0.53
MgO	31.10	30.10	31.30	28.88	27.41	29.51	30.28	26.21	23.08	18.90	21.05	25.89	21.46	21.52	21.12
CaO	0.22	0.18	–	0.23	0.16	0.65	–	0.20	0.20	1.47	1.38	0.92	1.29	0.79	0.96
Na2O	0.70	–	–	–	–	–	–	–	–	–	–	–	–	–	–
Total	99.55	98.50	92.03	101.15	98.87	99.04	99.67	99.17	100.65	99.09	96.29	96.67	95.86	100.56	97.53
Ox	6	6	6	6	6	6	6	6	6	6	6	6	6	6	6
Si	1.959	1.983	1.992	1.958	1.980	1.954	1.967	1.968	1.980	1.947	1.981	1.954	1.974	1.973	1.982
Ti	0.000	0.000	0.000	0.000	0.000	0.000	0.000	0.000	0.000	0.011	0.000	0.000	0.000	0.000	0.000
Al	0.031	0.000	0.024	0.047	0.000	0.068	0.030	0.036	0.000	0.053	0.000	0.050	0.000	0.027	0.000
Fe	0.341	0.406	0.218	0.462	0.521	0.387	0.399	0.554	0.735	0.841	0.738	0.512	0.723	0.758	0.764
Mn	0.011	0.000	0.009	0.012	0.013	0.000	0.010	0.013	0.018	0.017	0.017	0.017	0.022	0.024	0.017
Mg	1.650	1.621	1.752	1.531	1.499	1.578	1.612	1.436	1.279	1.085	1.225	1.450	1.252	1.200	1.215
Ca	0.008	0.007	0.000	0.009	0.006	0.025	0.000	0.008	0.008	0.061	0.058	0.037	0.054	0.032	0.040
Na	0.048	0.000	0.000	0.000	0.000	0.000	0.000	0.000	0.000	0.000	0.000	0.000	0.000	0.000	0.000
Total	4.049	4.017	3.996	4.018	4.020	4.012	4.018	4.014	4.020	4.015	4.019	4.021	4.026	4.014	4.018
En	82.53	79.69	88.95	76.49	73.98	79.28	80.15	71.88	63.28	54.60	60.61	72.55	61.72	60.31	60.19
Wo	0.41	0.34	0.00	0.44	0.31	1.26	0.00	0.39	0.38	3.05	2.86	1.86	2.67	1.59	1.98
Fs	17.05	19.97	11.05	23.08	25.71	19.46	19.85	27.73	36.34	42.35	36.53	25.59	35.62	38.09	37.84

Appendix 5. cont.

	Ridnitsohkka area														
Sample	352	353	355A	355B	356	357	358	359	360	503	88	355C	357A	361A	362A
Lith.	SIL	SIL	SIL	SIL	SIL	SIL	SIL	SIL	SIL	SIL	GNIL	GNIL	GNIL	GNIL	MBIL
Type			Cent	Marg											
SiO2	51.58	51.77	51.53	50.28	50.08	52.71	51.13	51.20	53.07	50.59	45.81	45.71	48.83	48.80	53.70
TiO2	–	–	–	–	–	–	–	–	–	0.35	0.34	–	0.33	–	–
Al2O3	–	–	–	1.02	–	–	–	–	–	–	3.80	4.35	3.38	3.68	–
FeO	22.95	26.57	27.05	29.94	23.79	23.50	29.99	26.51	22.98	22.34	34.09	31.05	24.80	23.62	12.22
MnO	0.47	0.81	1.03	0.58	0.61	0.73	0.86	1.04	0.69	0.49	0.66	0.87	1.44	0.40	–
MgO	20.27	19.31	17.95	16.76	19.54	20.99	16.80	19.00	21.46	20.69	12.71	14.34	18.83	20.39	27.61
CaO	0.90	0.82	1.32	0.63	1.16	1.16	1.39	0.87	1.10	1.36	–	–	0.19	0.24	0.80
Na2O	–	–	–	–	–	–	–	–	–	–	–	–	–	–	–
Total	96.17	99.29	98.89	99.21	95.18	99.08	100.17	98.61	99.30	95.82	97.40	96.32	97.80	97.13	94.34
Ox	6	6	6	6	6	6	6	6	6	6	6	6	6	6	6
Si	2.011	1.991	1.999	1.966	1.992	2.000	1.985	1.987	2.002	1.983	1.873	1.865	1.899	1.892	2.019
Ti	0.000	0.000	0.000	0.000	0.000	0.000	0.000	0.000	0.000	0.010	0.010	0.000	0.010	0.000	0.000
Al	0.000	0.000	0.000	0.047	0.000	0.000	0.000	0.000	0.000	0.000	0.182	0.208	0.154	0.167	0.000
Fe	0.747	0.853	0.876	0.977	0.790	0.744	0.972	0.859	0.724	0.731	1.164	1.058	0.805	0.765	0.384
Mn	0.016	0.026	0.034	0.019	0.021	0.023	0.028	0.034	0.022	0.016	0.023	0.030	0.047	0.013	0.000
Mg	1.177	1.105	1.037	0.975	1.156	1.185	0.971	1.097	1.205	1.208	0.773	0.871	1.090	1.177	1.545
Ca	0.038	0.034	0.055	0.027	0.049	0.047	0.058	0.036	0.044	0.057	0.000	0.000	0.008	0.010	0.032
Na	0.000	0.000	0.000	0.000	0.000	0.000	0.000	0.000	0.000	0.000	0.000	0.000	0.000	0.000	0.000
Total	3.989	4.009	4.001	4.011	4.008	4.000	4.015	4.013	3.998	4.006	4.025	4.031	4.014	4.024	3.981
En	59.98	55.48	52.68	49.28	57.95	59.97	48.53	55.07	61.08	60.50	39.92	45.15	57.26	60.31	78.79
Wo	1.92	1.70	2.79	1.34	2.47	2.38	2.89	1.82	2.25	2.87	0.00	0.00	0.42	0.50	1.65
Fs	38.10	42.83	44.52	49.38	39.58	37.66	48.58	43.11	36.68	36.64	60.08	54.85	42.31	39.18	19.56

Appendix 6. Amphibole compositions for the Halti-Ridnitsohkka complex. Lith. = lithologies: AR = amphibole rock, GBPG = gabbro pegmatite, OLGB = olivine gabbro, TRO = troctolite, SIL = gabbro sill between gneiss interlayers. SIL* = gabbro sill close to Halti cumulates. Type: Cor = corona between olivine and plagioclase, Ura = uralite. XMg = Mg/Mg + Fe.

	Halti area										
Sample	21	22	38	45	46	153	31	37A	43	44	51
Lith.	AR	AR	AR	AR	AR	AR	GBPG	OLGB	OLGB	OLGB	TRO
Type							Cor	Cor	Cor	Cor	Cor
SiO2	44.72	43.00	44.53	46.52	45.26	45.54	40.68	38.80	38.21	38.98	39.51
TiO2	–	–	0.27	0.37	–	–	–	–	–	–	0.24
Cr2O3	–	–	–	–	–	–	–	–	–	–	–
Al2O3	16.56	17.09	16.30	13.82	17.15	16.37	18.89	19.51	23.04	18.75	18.87
FeO	6.56	8.03	5.49	6.86	5.94	3.74	9.73	12.90	7.58	8.69	6.49
MnO	–	–	–	–	–	–	–	–	0.30	–	–
MgO	15.80	13.48	14.90	15.40	14.78	16.46	13.04	11.35	15.48	13.46	14.37
CaO	13.03	12.28	11.71	12.71	12.50	12.33	11.75	10.97	11.52	11.42	12.25
Na2O	2.43	2.08	1.91	1.49	2.35	1.80	2.95	3.79	3.14	2.99	2.52
K2O	0.21	0.44	–	–	–	–	0.36	–	0.15	0.41	0.48
Total	99.30	96.38	95.11	97.15	97.98	96.25	97.40	97.30	99.42	94.70	94.73
Ox	23	23	23	23	23	23	23	23	23	23	23
Si	6.273	6.250	6.431	6.622	6.375	6.448	5.931	5.758	5.424	5.836	5.854
Al4	1.727	1.750	1.569	1.378	1.625	1.552	2.069	2.242	2.576	2.164	2.146
Al6	0.995	1.161	1.190	0.927	1.206	1.166	1.159	1.152	1.258	1.128	1.132
Ti	0.000	0.000	0.030	0.039	0.000	0.000	0.000	0.000	0.000	0.000	0.027
Cr	0.000	0.000	0.000	0.000	0.000	0.000	0.000	0.000	0.000	0.000	0.000
Fe	0.768	0.974	0.662	0.815	0.698	0.442	1.184	1.599	0.898	1.086	0.803
Mn	0.000	0.000	0.000	0.000	0.000	0.000	0.000	0.000	0.036	0.000	0.000
Mg	3.299	2.916	3.202	3.262	3.099	3.469	2.829	2.507	3.271	3.000	3.170
Ca	1.956	1.910	1.810	1.938	1.885	1.869	1.833	1.743	1.751	1.831	1.942
Na	0.661	0.584	0.535	0.410	0.642	0.495	0.832	1.089	0.862	0.868	0.722
K	0.037	0.081	0.000	0.000	0.000	0.000	0.066	0.000	0.028	0.078	0.091
Total	15.715	15.627	15.428	15.391	15.530	15.440	15.904	16.089	16.104	15.991	15.887
XMg	0.811	0.750	0.829	0.800	0.816	0.887	0.705	0.611	0.785	0.734	0.798

Appendix 6. cont.

	Ridnitsohkka area							
Sample	355A	357	359	360	362	364	354	360
Lith.	SIL	SIL	SIL	SIL	SIL*	SIL*	SIL	SIL
Type							Ura	Ura
SiO2	41.87	42.40	41.55	43.68	41.09	41.65	53.19	51.48
TiO2	2.72	3.37	3.06	2.24	3.93	2.88	0.93	0.22
Cr2O3	–	–	–	–	–	–	0.39	–
Al2O3	10.91	12.26	11.69	12.89	11.53	12.71	5.15	3.62
FeO	16.33	11.80	15.34	12.60	13.30	10.77	9.97	14.54
MnO	–	–	–	–	–	–	–	0.25
MgO	10.08	11.84	10.21	11.77	11.14	13.56	17.14	13.77
CaO	10.62	10.98	10.85	10.81	10.47	11.41	11.75	10.72
Na2O	2.63	2.76	2.89	2.46	2.65	3.18	1.42	0.94
K2O	1.16	1.10	1.14	1.17	1.31	1.20	0.27	0.13
Total	96.31	96.49	96.72	97.62	95.42	97.37	100.20	95.66
Ox	23	23	23	23	23	23	23	23
Si	6.408	6.332	6.313	6.435	6.273	6.172	7.403	7.641
Al4	1.592	1.668	1.687	1.565	1.727	1.828	0.597	0.359
Al6	0.364	0.478	0.394	0.660	0.336	0.380	0.243	0.271
Ti	0.313	0.378	0.349	0.248	0.451	0.321	0.098	0.024
Cr	0.000	0.000	0.000	0.000	0.000	0.000	0.043	0.000
Fe	2.086	1.471	1.946	1.550	1.695	1.333	1.159	1.802
Mn	0.000	0.000	0.000	0.000	0.000	0.000	0.000	0.031
Mg	2.295	2.631	2.309	2.580	2.532	2.991	3.550	3.042
Ca	1.739	1.755	1.764	1.705	1.712	1.810	1.751	1.703
Na	0.779	0.797	0.849	0.702	0.782	0.912	0.382	0.269
K	0.226	0.209	0.220	0.220	0.254	0.226	0.048	0.024
Total	15.803	15.720	15.832	15.665	15.763	15.972	15.273	15.166
XMg	0.524	0.641	0.543	0.625	0.599	0.692	0.754	0.628

Appendix 7. Biotite compositions from the Ridnitsohkka area. Lith = lithologies: SIL = gabbro sill between the gneiss interlayers, SIL* = gabbro sill close to Halti cumulates, GNIL = gneiss interlayer between gabbro sills, MBIL = metabasalt interlayer between gabbro sills, GNAU = metamorphic aureole in outer gneiss, GN = outer gneiss. XMg = Mg/Mg + Fe + Mn + Ti + AlVI. Type: Myl = Mylonite.

Sample	87	89	106	144A	353	354	355B	356	357	358	361	363	88	89A
Lith.	SIL	SIL	SIL	SIL	SIL	SIL	SIL	SIL	SIL	SIL	SIL*	SIL*	GNIL	GNIL
Type														
SiO2	36.62	37.28	36.25	36.31	37.71	36.19	35.49	36.49	35.61	36.06	35.33	35.36	33.48	36.48
TiO2	4.66	4.13	4.57	4.93	4.94	3.99	4.17	5.10	5.13	4.56	6.92	6.75	4.78	3.35
Cr2O3	–	–	–	–	–	–	–	–	–	–	–	0.36	–	–
Al2O3	15.41	16.02	16.27	14.84	15.86	16.03	16.02	15.77	16.01	15.30	15.06	14.45	16.66	17.22
FeO	15.15	12.89	14.80	14.05	15.55	13.87	18.71	14.86	14.21	18.17	19.48	12.37	20.00	11.38
MnO	–	–	–	–	–	–	–	–	–	–	–	–	–	–
MgO	13.09	15.05	13.75	13.32	12.59	13.88	10.69	13.17	13.76	11.34	10.26	13.49	9.26	16.57
Na2O	–	–	–	–	–	1.47	–	–	–	–	–	–	–	–
K2O	9.65	9.58	9.41	9.45	10.42	10.02	9.88	10.27	10.15	9.51	10.17	10.02	10.40	10.55
Total	94.58	94.94	95.06	92.89	97.06	95.47	94.96	95.66	94.86	94.94	97.23	92.80	94.58	95.55
Ox	22	22	22	22	22	22	22	22	22	22	22	22	22	22
Si	5.532	5.535	5.433	5.559	5.565	5.430	5.451	5.464	5.370	5.510	5.340	5.421	5.241	5.381
Al4	2.468	2.465	2.567	2.441	2.435	2.570	2.549	2.536	2.630	2.490	2.660	2.579	2.759	2.619
Al6	0.261	0.322	0.291	0.222	0.308	0.250	0.335	0.232	0.200	0.250	0.009	0.018	0.297	0.357
Ti	0.529	0.461	0.515	0.567	0.548	0.450	0.482	0.574	0.581	0.524	0.787	0.778	0.563	0.372
Cr	0.000	0.000	0.000	0.000	0.000	0.000	0.000	0.000	0.000	0.000	0.000	0.044	0.000	0.000
Fe	1.911	1.598	1.852	1.797	1.916	1.737	2.399	1.858	1.789	2.318	2.458	1.584	2.614	1.401
Mn	0.000	0.000	0.000	0.000	0.000	0.000	0.000	0.000	0.000	0.000	0.000	0.000	0.000	0.000
Mg	2.944	3.325	3.066	3.035	2.766	3.100	2.443	2.935	3.088	2.578	2.307	3.078	2.157	3.638
Na	0.000	0.000	0.000	0.000	0.000	0.428	0.000	0.000	0.000	0.000	0.000	0.000	0.000	0.000
K	1.858	1.811	1.796	1.843	1.958	1.916	1.934	1.958	1.949	1.852	1.958	1.957	2.073	1.982
Total	15.503	15.516	15.521	15.464	15.495	15.881	15.592	15.557	15.608	15.522	15.518	15.459	15.705	15.751
XMg	0.521	0.583	0.536	0.540	0.500	0.560	0.432	0.524	0.546	0.455	0.415	0.564	0.383	0.631

Appendix 7. cont.

Sample	188G	355C	357A	362A	504A	504B	504C	504D	504E	504F	505	40	133	134A
Lith.	GNIL	GNIL	GNIL	MBIL	GNAU	GNAU	GNAU	GNAU	GNAU	GNAU	GNAU	GN	GN	GN
Type														Myl
SiO2	35.64	35.15	35.52	38.32	35.11	35.12	35.60	34.44	35.17	35.26	34.32	34.42	33.00	33.53
TiO2	8.68	4.16	4.29	3.82	4.08	3.07	3.60	4.36	3.50	5.06	3.99	3.87	3.85	3.67
Cr2O3	–	–	–	–	–	–	–	–	–	–	–	–	–	–
Al2O3	15.72	16.99	15.43	15.21	18.46	18.73	19.12	18.04	17.17	17.60	19.43	16.10	16.53	16.60
FeO	12.95	14.48	14.08	5.89	18.65	18.74	18.36	18.73	23.91	14.68	17.28	23.89	22.71	19.40
MnO	–	–	–	–	–	–	–	–	–	–	–	0.30	–	–
MgO	11.58	13.25	13.88	19.45	9.01	9.64	9.54	8.60	5.93	11.78	8.34	6.36	5.10	7.48
Na2O	–	–	–	–	–	–	–	–	–	–	1.39	–	1.31	–
K2O	10.73	10.18	10.00	10.73	10.00	9.56	10.18	9.89	9.79	10.51	9.60	10.04	9.36	9.66
Total	95.30	94.22	93.20	93.42	95.33	94.85	96.39	94.07	95.46	94.89	94.34	94.98	91.85	90.33
Ox	22	22	22	22	22	22	22	22	22	22	22	22	22	22
Si	5.339	5.343	5.449	5.627	5.357	5.371	5.356	5.340	5.495	5.329	5.277	5.446	5.393	5.455
Al4	2.661	2.657	2.551	2.373	2.643	2.629	2.644	2.660	2.505	2.671	2.723	2.554	2.607	2.545
Al6	0.100	0.371	0.224	0.245	0.659	0.728	0.728	0.619	0.639	0.447	0.777	0.433	0.558	0.619
Ti	0.977	0.475	0.495	0.422	0.468	0.352	0.407	0.508	0.411	0.575	0.461	0.461	0.473	0.449
Cr	0.000	0.000	0.000	0.000	0.000	0.000	0.000	0.000	0.000	0.000	0.000	0.000	0.000	0.000
Fe	1.620	1.838	1.804	0.723	2.377	2.392	2.306	2.425	3.119	1.852	2.218	3.157	3.099	2.635
Mn	0.000	0.000	0.000	0.000	0.000	0.000	0.000	0.000	0.000	0.000	0.000	0.040	0.000	0.000
Mg	2.582	2.997	3.168	4.250	2.047	2.195	2.135	1.984	1.379	2.651	1.909	1.498	1.240	1.811
Na	0.000	0.000	0.000	0.000	0.000	0.000	0.000	0.000	0.000	0.000	0.413	0.000	0.415	0.000
K	2.048	1.972	1.953	2.006	1.944	1.862	1.950	1.954	1.948	2.024	1.879	2.024	1.948	2.001
Total	15.327	15.654	15.645	15.646	15.496	15.529	15.526	15.490	15.495	15.549	15.658	15.612	15.733	15.515
XMg	0.489	0.528	0.557	0.754	0.369	0.387	0.383	0.358	0.249	0.480	0.356	0.268	0.231	0.328

Appendix 8. Compositions of fine grained intergrowths and minerals in gneiss interlayers between Ridnitsohkka gabbro sills. Mineral: SIL = sillimanite, OPX = orthopyroxene, BIT = biotite, PLG = plagioclase. Cation ratio XMg in Biotite: XMg = Mg/Mg + Fe + Mn + Ti + AlVI.

Sample	355C				357A						361A			
Mineral	SIL	OPX	BIT	OPX+BIT	SIL	OPX	OPX	PLG	BIT	OPX+SIL	OPX	OPX+SIL	OPX+SIL	OPX+SIL
Beam diam.	Spot	Spot	Spot	20um	Spot	Spot	Spot	Spot	Spot	20um	Spot	30um	20um	20um
SiO2	34.02	43.98	35.03	39.76	34.74	45.24	48.08	60.63	33.65	47.34	43.34	40.74	38.82	42.91
TiO2	–	–	1.30	0.50	–	–	–	–	0.41	–	1.18	–	–	–
Al2O3	62.30	6.30	15.85	14.20	62.32	6.05	3.79	23.87	15.61	33.22	9.48	38.56	47.91	23.53
FeO	0.57	25.58	17.80	20.42	1.11	22.77	22.34	–	11.58	10.27	18.28	9.30	8.56	16.15
MnO	–	1.11	0.33	0.54	–	1.13	1.13	–	–	–	–	–	–	–
MgO	–	14.99	12.37	12.54	–	17.77	19.60	–	14.59	7.44	18.53	10.05	7.72	14.75
CaO	–	–	–	–	–	–	–	4.40	–	0.18	–	–	–	–
Na2O	–	–	–	–	–	–	–	9.37	–	–	–	–	–	–
K2O	–	1.47	8.84	4.54	–	–	–	–	9.47	–	2.35	0.91	–	0.52
Total	96.89	93.43	91.54	92.48	98.16	92.96	94.95	98.27	85.29	98.45	93.15	99.56	103.02	97.87
Ox	5	6	22	6	5	6	6	32	22	6	6	6	6	6
Si	0.955	1.825	5.541	1.653	0.965	1.840	1.903	10.961	5.576	1.643	1.740	1.416	1.290	1.580
Ti	0.000	0.000	0.155	0.015	0.000	0.000	0.000	0.000	0.051	0.000	0.036	0.000	0.000	0.000
Al	2.051	0.306	2.939	0.692	2.029	0.288	0.176	5.058	3.032	1.351	0.446	1.571	1.867	1.015
Fe	0.013	0.886	2.351	0.709	0.026	0.773	0.738	0.000	1.602	0.297	0.613	0.270	0.238	0.497
Mn	0.000	0.039	0.044	0.019	0.000	0.039	0.038	0.000	0.000	0.000	0.000	0.000	0.000	0.000
Mg	0.000	0.926	2.913	0.776	0.000	1.076	1.155	0.000	3.598	0.384	1.107	0.520	0.382	0.809
Ca	0.000	0.000	0.000	0.000	0.000	0.000	0.000	0.851	0.000	0.007	0.000	0.000	0.000	0.000
Na	0.000	0.000	0.000	0.000	0.000	0.000	0.000	3.282	0.000	0.000	0.000	0.000	0.000	0.000
K	0.000	0.078	1.781	0.240	0.000	0.000	0.000	0.000	1.998	0.000	0.120	0.040	0.000	0.024
Total	3.019	4.061	15.725	4.105	3.020	4.016	4.009	20.151	15.856	3.682	4.061	3.818	3.776	3.925
Opx:														
En		51.09				58.19	61.00			55.82	64.37	65.84	61.64	61.95
Wo		0.00				0.00	0.00			0.97	0.00	0.00	0.00	0.00
Fs		48.91				41.81	39.00			43.21	35.63	34.16	38.36	38.05
Bit:														
Al IV			2.459						2.424					
Al VI			0.480						0.608					
XMg			0.490						0.614					
Plg:														
An								20.59						

Appendix 9. Garnet compositions from the Ridnitsohkka area. Distance 1 = distance westward (+)/eastward (—) from the contact between the sill area and metamorphic aureole in Ridnitsohkka. Distance 2 = distance away from the Halti cumulates. Myl = mylonite.

	Gneiss interlayers in sill area						
Sample	88 Core	88 Rim	357A Rim	355C Core	355C Rim	89A Core	89A Rim
Distance 1	+800m		+750m	+360m		+20m	
Distance 2	−1300m		−1100m	−1500m			
SiO2	35.51	36.22	34.85	35.89	36.08	35.89	36.28
Al2O3	21.46	21.60	22.63	21.34	21.30	21.23	22.42
FeO	34.29	32.79	28.96	32.61	30.38	34.27	30.08
MnO	1.42	0.49	1.54	2.17	0.81	1.50	0.60
MgO	5.00	6.65	7.45	5.56	7.26	4.58	8.03
CaO	0.85	1.15	0.40	1.04	1.05	1.16	1.12
K2O	–	–	–	–	–	–	–
Total	98.53	98.90	95.83	98.62	96.86	98.63	98.53
Ox	24	24	24	24	24	24	24
Si	5.801	5.821	5.709	5.830	5.868	5.857	5.776
Al	4.108	4.069	4.346	4.062	4.060	4.061	4.183
Fe	4.677	4.400	3.962	4.423	4.125	4.670	3.999
Mn	0.197	0.066	0.213	0.299	0.111	0.207	0.081
Mg	1.215	1.591	1.818	1.345	1.757	1.113	1.902
Ca	0.148	0.198	0.070	0.181	0.182	0.203	0.191
K	0.000	0.000	0.000	0.000	0.000	0.000	0.000
Total	16.145	16.144	16.118	16.139	16.102	16.112	16.132
Alm	0.750	0.703	0.653	0.708	0.668	0.754	0.648
Sps	0.032	0.011	0.035	0.048	0.018	0.033	0.013
Prp	0.195	0.254	0.300	0.215	0.285	0.180	0.308
Grs	0.024	0.032	0.012	0.029	0.029	0.033	0.031

Appendix 9. cont.

	Metamorphic aureole in outer gneiss									Outer gneiss		
Sample	504A Core	505 Core	505 Rim	504F Core	504F Rim	504B Core	504C Core	504D Rim	504E	134A Myl	133	40
Distance 1	−20m	−100m		−100m		−140m	−230m	−450m	−580m	−820m	−1840m	
Distance 2												−100m
SiO2	36.24	35.76	34.99	36.40	35.92	35.23	36.87	36.27	36.31	35.49	35.32	34.39
Al2O3	22.16	21.62	20.94	21.91	21.57	20.59	22.60	21.61	21.58	21.24	20.91	20.49
FeO	35.14	35.33	36.18	35.52	32.72	33.52	34.51	33.66	24.96	31.62	26.30	27.84
MnO	0.74	1.82	0.86	0.52	0.43	1.50	1.79	2.17	6.47	2.40	3.19	6.87
MgO	3.96	1.79	3.65	4.23	5.77	3.31	3.56	4.42	1.17	2.39	1.06	1.69
CaO	1.10	1.11	0.51	1.34	1.36	1.34	1.76	0.81	7.59	3.08	8.67	4.82
K2O	–	–	–	–	–	–	–	–	–	–	–	0.18
Total	99.34	97.43	97.12	99.92	97.78	95.50	101.09	98.94	98.08	96.21	95.44	96.28
Ox	24	24	24	24	24	24	24	24	24	24	24	24
Si	5.858	5.943	5.844	5.857	5.845	5.942	5.860	5.885	5.939	5.931	5.932	5.827
Al	4.199	4.211	4.099	4.132	4.114	4.071	4.212	4.109	4.137	4.160	4.115	4.069
Fe	4.743	4.902	5.045	4.772	4.445	4.720	4.580	4.560	3.408	4.412	3.687	3.939
Mn	0.101	0.256	0.122	0.071	0.059	0.214	0.242	0.298	0.896	0.340	0.454	0.985
Mg	0.952	0.443	0.906	1.014	1.398	0.831	0.842	1.067	0.284	0.594	0.265	0.426
Ca	0.190	0.198	0.091	0.231	0.238	0.242	0.299	0.141	1.329	0.551	1.558	0.875
K	0.000	0.000	0.000	0.000	0.000	0.000	0.000	0.000	0.000	0.000	0.000	0.038
Total	16.043	15.952	16.107	16.077	16.098	16.022	16.034	16.060	15.993	15.989	16.011	16.158
Alm	0.792	0.845	0.818	0.784	0.724	0.786	0.768	0.752	0.576	0.748	0.618	0.633
Sps	0.017	0.044	0.020	0.012	0.010	0.036	0.041	0.049	0.151	0.058	0.076	0.158
Prp	0.159	0.076	0.147	0.167	0.228	0.138	0.141	0.176	0.048	0.101	0.044	0.068
Grs	0.032	0.034	0.015	0.038	0.039	0.040	0.050	0.023	0.225	0.093	0.261	0.141

Appendix 10. Cordierite, spinel and ilmenite compositions from the Halti-Ridnitsohkka complex. Lith. = lithologies: GNIL = gneiss interlayer between gabbro sills, OLGB = olivine gabbro, GNAU = metamorphic aureole in outer gneiss. Cation ratios: Cordierite XMg = Mg/Mg + Fe; Spinel XMg = Mg/Mg + Fe^{2+}, XAl = Al/Al + Cr + Fe^{3+}, XCr = Cr/Al + Cr, XFe^{3+} = Fe^{3+}/Al + Cr + Fe^{3+}, Fe^{3+} is calculated by assuming spinel stoichiometry.

Cordierite			
	Ridnitsohkka area		
Sample	188G	341	361A
Lith.	GNIL	GNIL	GNIL
SiO2	47.39	45.48	47.54
Al2O3	33.67	33.17	34.39
FeO	4.45	6.04	3.85
MgO	10.16	8.97	11.34
Na2O	1.03	–	–
K2O	0.22	–	–
Total	96.92	93.66	97.13
Ox	18	18	18
Si	4.903	4.882	4.872
Al	4.084	4.174	4.131
Fe	0.385	0.542	0.329
Mg	1.565	1.433	1.730
Na	0.207	0.000	0.000
K	0.028	0.000	0.000
Total	11.172	11.031	11.063
XMg	0.803	0.726	0.840

Spinel						
	Ridnitsohkka area					Halti
Sample	88	89A	188G	355C	504F	43
Lith.	GNIL	GNIL	GNIL	GNIL	GNIL	OLGB
Al2O3	54.69	59.57	54.57	57.27	57.08	52.86
Cr2O3	0.28	–	6.94	–	–	9.79
Fe2O3	4.80	0.46	1.09	3.12	2.50	3.96
FeO	33.26	32.67	27.55	28.89	34.91	23.50
MnO	–	–	0.52	0.61	0.33	–
MgO	4.25	5.34	7.94	6.88	3.42	11.31
Total	97.28	98.04	98.61	96.77	98.24	101.42
FeO tot	37.59	33.09	28.54	31.71	37.18	27.07
Ox	32	32	32	32	32	32
Al	15.084	15.905	14.552	15.444	15.549	13.631
Cr	0.052	0.000	1.246	0.000	0.000	1.700
Fe3+	0.848	0.079	0.186	0.539	0.436	0.654
Fe2+	6.535	6.214	5.233	5.550	6.774	4.317
Mn	0.000	0.000	0.100	0.119	0.065	0.000
Mg	1.489	1.811	2.689	2.356	1.183	3.704
Total	24.008	24.008	24.007	24.008	24.007	24.007
XMg	0.186	0.226	0.339	0.298	0.149	0.462
XCr	0.003	0.000	0.085	0.000	0.000	0.119
XAl	0.944	0.995	0.910	0.966	0.973	0.853
XFe3+	0.053	0.005	0.012	0.034	0.027	0.041

Appendix 10. cont.

Ilmenite									
	Ridnitsohkka area								
Sample	88	89A	188G	504A	504B	504F	504D	504C	505
Lith.	GNIL	GNIL	GNIL	GNAU	GNAU	GNAU	GNAU	GNAU	GNAU
SiO2	–	–	–	–	0.36	0.32	–	0.32	–
TiO2	46.97	51.33	50.49	49.75	49.47	51.13	51.19	49.58	49.58
Cr2O3	0.39	–	–	–	–	–	–	–	–
Al2O3	–	–	–	–	–	–	–	–	–
V2O3	0.60	0.77	0.85	–	–	0.46	0.64	0.60	0.56
FeO	48.13	45.92	43.84	45.09	44.38	44.36	44.90	45.80	44.17
MnO	0.42	–	0.92	–	–	–	–	–	–
MgO	0.98	1.11	0.99	–	0.56	0.96	–	–	0.68
CaO	–	–	0.22	–	–	–	–	–	–
Na2O	–	–	–	–	0.88	–	–	–	–
Total	97.49	99.14	97.30	94.84	95.65	97.23	96.73	96.29	95.00
Ox	6	6	6	6	6	6	6	6	6
Si	0.000	0.000	0.000	0.000	0.019	0.016	0.000	0.017	0.000
Ti	1.862	1.960	1.963	1.995	1.960	1.979	2.004	1.959	1.977
Cr	0.016	0.000	0.000	0.000	0.000	0.000	0.000	0.000	0.000
Al	0.000	0.000	0.000	0.000	0.000	0.000	0.000	0.000	0.000
V	0.025	0.031	0.035	0.000	0.000	0.019	0.027	0.025	0.024
Fe	2.119	1.948	1.893	2.009	1.953	1.907	1.952	2.010	1.956
Mn	0.019	0.000	0.040	0.000	0.000	0.000	0.000	0.000	0.000
Mg	0.077	0.084	0.076	0.000	0.044	0.074	0.000	0.000	0.054
Ca	0.000	0.000	0.012	0.000	0.000	0.000	0.000	0.000	0.000
Na	0.000	0.000	0.000	0.000	0.090	0.000	0.000	0.000	0.000
Total	4.118	4.024	4.020	4.005	4.066	3.995	3.983	4.011	4.011

Appendix 11. Muscovite, K-feldspar, zoisite and paragonite compositions from the Halti-Ridnitsohkka complex. Lith. = lithologies: GNAU = metamorphic aureole in outer gneiss, GN = outer gneiss, GNIL = gneiss interlayer between gabbro sills, AR = amphibole rock. Type: Myl = mylonite. Cation ratio: Muscovite XFe = Fe/Fe + Mg.

	Ridnitsohkka area							
	Muscovite							
Sample	504A	504B	504C	504D	504E	505	133	134A
Lith.	GNAU	GNAU	GNAU	GNAU	GNAU	GNAU	GN	GN
Type								Myl
SiO2	43.98	44.57	44.08	43.44	46.34	44.93	44.33	44.56
TiO2	1.35	1.09	–	0.79	1.40	–	1.12	1.17
Al2O3	35.23	34.85	35.81	34.77	30.88	36.10	30.27	32.99
FeO	1.34	1.56	1.27	1.51	3.47	0.84	3.35	1.89
MgO	1.13	1.08	–	0.79	1.80	1.04	1.27	1.32
Na2O	–	–	–	–	–	1.01	–	–
K2O	10.78	10.77	11.23	10.95	11.03	10.39	11.04	10.66
Total	93.82	93.92	92.40	92.24	94.92	94.32	91.39	92.59
Ox	23	23	23	23	23	23	23	23
Si	5.987	6.059	6.086	6.025	6.306	6.057	6.280	6.157
Al IV	2.013	1.941	1.914	1.975	1.694	1.943	1.720	1.843
Al VI	3.609	3.612	3.882	3.679	3.231	3.762	3.307	3.499
Ti	0.138	0.111	0.000	0.083	0.143	0.000	0.119	0.122
Fe	0.153	0.177	0.146	0.175	0.394	0.095	0.397	0.218
Mg	0.229	0.219	0.000	0.162	0.365	0.209	0.269	0.272
Na	0.000	0.000	0.000	0.000	0.000	0.264	0.000	0.000
K	1.870	1.866	1.975	1.935	1.913	1.784	1.992	1.876
Total	13.999	13.986	14.004	14.033	14.045	14.115	14.084	13.988
XFe	0.400	0.447	1.000	0.518	0.519	0.312	0.596	0.445

	Ridnitsohkka area			
	K-feldspar			
Sample	88	357A	361A	504F
Lith.	GNIL	GNIL	GNIL	GNAU
SiO2	61.74	59.84	61.86	59.69
TIO2	0.29	0.27	0.36	–
Al2O3	18.70	18.91	18.98	18.10
FeO	–	–	–	–
MGO	–	–	–	0.68
CaO	0.33	–	–	0.22
Na2O	2.46	1.62	2.88	1.74
K2O	13.07	14.08	14.45	15.02
Total	96.58	94.73	98.53	95.44
Ox	32	32	32	32
Si	11.770	11.685	11.670	11.668
Ti	0.042	0.040	0.051	0.000
Al	4.179	4.329	4.197	4.147
Fe	0.000	0.000	0.000	0.000
Mg	0.000	0.000	0.000	0.197
Ca	0.066	0.000	0.000	0.045
Na	0.908	0.612	1.051	0.661
K	3.173	3.503	3.472	3.739
Total	20.139	20.169	20.442	20.458
K/K+Na	0.777	0.851	0.768	0.850

Appendix 11. cont.

	Halti area			
	Zoisite			Paragonite
Sample	46	45	38	38
Lith.	AR	AR	AR	AR
SiO2	39.66	39.14	38.69	44.12
TIO2	–	–	–	–
CR2O3	–	–	–	–
Al2O3	33.28	33.43	32.60	40.10
FeO	0.67	0.77	0.79	0.25
MNO	–	–	–	–
MGO	–	–	–	–
CaO	26.05	25.46	24.67	1.29
Na2O	–	–	–	6.62
K2O	–	–	–	0.30
Total	99.67	98.80	96.75	92.68
Ox	13	13	13	22
Si	3.101	3.084	3.109	5.815
Ti	0.000	0.000	0.000	0.000
Cr	0.000	0.000	0.000	0.000
Al	3.050	3.088	3.071	6.194
Fe	0.044	0.051	0.053	0.028
Mn	0.000	0.000	0.000	0.000
Mg	0.000	0.000	0.000	0.000
Ca	2.180	2.148	2.122	0.183
Na	0.000	0.000	0.000	1.690
K	0.000	0.000	0.000	0.050
Total	8.375	8.371	8.355	13.958

Appendix 12. Whole rock chemical data for the Halti-Ridnitsohkka complex. Oxides in weight %, elements in ppm. Lith. = lithologies: DUN = dunite, TRO = troctolite, OLGB = olivine gabbro, GBPG = gabbro pegmatite, AAUG = augite augen gabbro, AR = amphibole rock, SIL = gabbro sill between gneiss interlayers, SIL* = gabbro sill close to Halti cumulates, SIL** = sulfide bearing gabbro sill close to Halti cumulates, GR = granite. Comment 1 = oxide analyses determined at the University of Turku. SiO2, TiO2, Al2O3, FeO, CaO and K2O by XRF and MnO, MgO and Na2O by AAS. Minor elements, where determined, were analyzed at the Finnish National Technical Research Center at Espoo by XRF. Comment 2 = whole-rock analyses determined by XRF at the Outokumpu Laboratories. Comment 3 = as for 1, with REE determined by XRF at the Finnish National Technical Research Center at Espoo. Comment 4 = as for 1, with Bi, Cl, Nb, Pt, V and Y determined by XRF at the Outokumpu Laboratories. Comment 5 = as for 1, with Cu, Pb, S, Sr, Zr and P determined by XRF at the Outokumpu Laboratories. FeO* = total Fe as FeO; n.d. = not determined.

	Halti area													
Sample	15	17	20	30	32	33	54	81	84	314C	18T	28	34	35A
Lith.	DUN	DUN	DUN	DUN	DUN	DUN	DUN	DUN	DUN	DUN	TRO	TRO	TRO	TRO
SiO2	36.90	36.50	35.60	37.20	35.50	36.00	33.80	35.00	37.10	35.00	42.00	39.20	37.50	42.50
TiO2	0.02	0.03	0.06	0.03	0.03	0.03	0.06	0.03	0.02	0.03	0.18	0.19	0.15	0.14
Al2O3	0.22	0.25	0.31	0.49	0.27	0.27	0.38	0.22	0.24	0.68	8.65	9.73	2.64	16.64
FeO*	9.51	9.40	10.50	9.83	10.40	10.82	10.65	9.79	12.23	8.90	11.19	9.17	9.01	6.30
MnO	0.13	0.13	0.12	0.13	0.12	0.14	0.12	0.12	0.15	0.14	0.18	0.13	0.11	0.12
MgO	46.03	47.88	42.91	48.46	42.83	44.87	41.39	44.68	44.14	39.40	25.40	32.04	43.82	23.59
CaO	0.28	0.20	0.25	0.24	0.17	0.28	0.30	0.23	0.18	0.37	5.30	4.74	1.43	7.87
Na2O	0.27	0.27	0.20	0.26	0.33	0.24	0.30	0.07	–	–	0.82	1.52	0.70	0.85
K2O	0.01	0.01	0.08	0.01	–	–	0.02	0.01	–	–	0.02	–	0.16	–
LOI	5.39	5.19	5.18	1.93	4.57	3.82	8.84	4.95	1.63	n.d.	n.d.	1.00	1.84	1.17
P2O5	n.d.	n.d.	n.d.	n.d.	n.d.	n.d.	n.d.	n.d.	n.d.	0.01	0.01	n.d.	n.d.	n.d.
Total	98.76	99.86	95.21	98.58	94.22	96.47	95.86	95.10	95.69	84.52	93.76	97.72	97.36	99.18
Ag	<3.34	<3.15	<3.41	<3.02	n.d.	<3.19	<3.36	<3.26	n.d.	–	–	<3.12	<3.15	<2.81
As	<0.372	<0.342	<0.363	<0.331	n.d.	<0.338	3.380	<0.352	n.d.	3	3	<0.342	<0.341	<0.290
Au	0.0030	0.0150	0.0163	0.0028	n.d.	0.0043	0.0032	0.0228	n.d.	n.d.	n.d.	0.0052	0.0029	0.0106
Ba	<37.2	<35.0	<36.1	<32.5	n.d.	<34.1	<38.2	<35.2	n.d.	27	9	<34.3	34.0	<30.2
Bi	n.d.	n.d.	n.d.	n.d.	n.d.	n.d.	n.d.	n.d.	n.d.	–	–	n.d.	n.d.	n.d.
Br	0.554	0.770	1.750	0.785	n.d.	<0.264	6.250	0.996	n.d.	n.d.	n.d.	0.580	<0.263	0.931
Cl	n.d.	n.d.	n.d.	n.d.	n.d.	n.d.	n.d.	n.d.	n.d.	220	110	n.d.	n.d.	n.d.
Co	131.0	134.0	138.0	132.0	n.d.	130.0	124.0	145.0	n.d.	176	103	102.0	131.0	69.5
Cr	2910	3450	3970	2900	n.d.	3960	4480	3360	n.d.	3283	220	3650	3790	1160
Cs	<0.355	<0.331	<0.358	<0.317	n.d.	<0.341	<0.361	<0.347	n.d.	20	–	<0.340	<0.334	<0.298
Cu	n.d.	n.d.	n.d.	n.d.	n.d.	n.d.	n.d.	n.d.	n.d.	1000	95	n.d.	n.d.	n.d.
Mo	<0.941	<0.898	<0.964	<0.822	n.d.	<0.899	<0.991	<0.902	n.d.	–	–	<0.906	<0.892	<0.107
Nb	n.d.	n.d.	n.d.	n.d.	n.d.	n.d.	n.d.	n.d.	n.d.	6	7	n.d.	n.d.	n.d.
Ni	2120	2410	1980	1970	n.d.	2190	1950	2320	n.d.	3240	1230	1590	1980	575
Pb	n.d.	n.d.	n.d.	n.d.	n.d.	n.d.	n.d.	n.d.	n.d.	–	–	n.d.	n.d.	n.d.
Pt	n.d.	n.d.	n.d.	n.d.	n.d.	n.d.	n.d.	n.d.	n.d.	10	–	n.d.	n.d.	n.d.
Rb	<7.05	<6.51	<7.11	<6.34	n.d.	<6.52	<7.15	<6.90	n.d.	–	2	<6.82	<6.64	<6.24
S	n.d.	n.d.	n.d.	n.d.	n.d.	n.d.	n.d.	n.d.	n.d.	6370	1040	n.d.	n.d.	n.d.
Sb	<0.046	<0.044	<0.045	0.054	n.d.	<0.043	0.087	<0.044	n.d.	–	–	<0.043	<0.043	<0.036
Sc	7.61	7.45	7.61	7.97	n.d.	8.32	8.53	7.92	n.d.	n.d.	n.d.	10.40	7.53	5.34
Sn	<63.5	<60.9	<62.8	<56.3	n.d.	<58.9	<65.5	<60.4	n.d.	10	20	<60.2	<59.0	<52.7
Sr	n.d.	n.d.	n.d.	n.d.	n.d.	n.d.	n.d.	n.d.	n.d.	2	137	n.d.	n.d.	n.d.
Ta	0.0843	0.0782	0.0854	0.0763	n.d.	0.0778	0.0850	0.0820	n.d.	–	–	0.0975	0.0784	0.0821
Th	<0.218	<0.206	<0.215	<0.188	n.d.	<0.202	<0.225	<0.204	n.d.	–	–	<0.207	<0.202	<0.180
U	<0.140	<0.133	<0.141	<0.124	n.d.	<0.132	<0.146	<0.133	n.d.	4	3	<0.134	<0.132	<0.119
V	n.d.	n.d.	n.d.	n.d.	n.d.	n.d.	n.d.	n.d.	n.d.	29	70	n.d.	n.d.	n.d.
W	<0.704	<0.669	<0.697	<0.632	n.d.	<0.66	<0.713	<0.677	n.d.	–	–	<0.676	<0.655	<0.577
Zn	<26	<43	<46	<41	n.d.	43	72	45	n.d.	70	81	46	63	<40
Zr	n.d.	n.d.	n.d.	n.d.	n.d.	n.d.	n.d.	n.d.	n.d.	–	–	n.d.	n.d.	n.d.
Y	n.d.	n.d.	n.d.	n.d.	n.d.	n.d.	n.d.	n.d.	n.d.	–	3	n.d.	n.d.	n.d.
La	<0.175	<0.166	<0.170	<0.178	n.d.	<0.165	<0.203	<0.162	n.d.	10	–	0.568	<0.168	<0.251
Ce	n.d.	n.d.	n.d.	n.d.	n.d.	n.d.	n.d.	n.d.	n.d.	–	10	n.d.	n.d.	n.d.
Nd	n.d.	n.d.	n.d.	n.d.	n.d.	n.d.	n.d.	n.d.	n.d.	n.d.	n.d.	n.d.	n.d.	n.d.
Sm	<0.013	<0.013	0.032	0.026	n.d.	<0.012	0.020	<0.013	n.d.	n.d.	n.d.	0.196	0.041	0.113
Eu	n.d.	n.d.	n.d.	n.d.	n.d.	n.d.	n.d.	n.d.	n.d.	n.d.	n.d.	n.d.	n.d.	n.d.
Gd	n.d.	n.d.	n.d.	n.d.	n.d.	n.d.	n.d.	n.d.	n.d.	n.d.	n.d.	n.d.	n.d.	n.d.
Tb	n.d.	n.d.	n.d.	n.d.	n.d.	n.d.	n.d.	n.d.	n.d.	n.d.	n.d.	n.d.	n.d.	n.d.
Tm	n.d.	n.d.	n.d.	n.d.	n.d.	n.d.	n.d.	n.d.	n.d.	n.d.	n.d.	n.d.	n.d.	n.d.
Yb	n.d.	n.d.	n.d.	n.d.	n.d.	n.d.	n.d.	n.d.	n.d.	n.d.	n.d.	n.d.	n.d.	n.d.
Lu	<0.312	<0.298	<0.311	<0.275	n.d.	<0.294	<0.325	<0.295	n.d.	n.d.	n.d.	<0.297	<0.293	<0.265
Comments	1	1	1	1	1	1	1	1	1	2	2	1	1	1

Appendix 12. cont.

	Halti area													
Sample	39	49	51	69	70	71	72	73	74	75	76	100	130	37A
Lith.	TRO	TRO	TRO	TRO	TRO	TRO	TRO	TRO	TRO	TRO	TRO	TRO	TRO	OLGB
SiO2	43.90	41.40	47.10	46.70	45.20	40.70	44.90	44.20	39.10	40.30	47.40	41.50	41.10	47.00
TiO2	0.21	0.29	0.18	0.26	0.20	0.17	0.20	0.23	0.19	0.23	0.28	0.15	0.09	1.14
Al2O3	25.01	6.45	26.15	24.84	24.41	10.45	28.54	21.63	12.24	8.27	27.90	16.84	10.70	18.79
FeO*	3.60	9.59	4.09	4.63	3.86	8.90	2.66	5.11	7.74	8.49	3.49	7.57	9.57	7.23
MnO	0.06	0.15	0.06	0.09	0.06	0.14	0.05	0.10	0.14	0.15	0.06	0.10	0.15	0.09
MgO	9.82	34.80	8.16	9.40	13.50	29.88	8.72	13.00	27.19	29.48	5.47	27.66	32.12	9.63
CaO	11.62	4.27	10.36	11.23	10.84	5.42	12.63	10.46	5.97	5.52	11.78	6.10	4.97	11.46
Na2O	1.97	0.65	3.30	2.25	1.64	0.44	2.12	1.95	0.85	0.92	2.84	0.63	0.88	3.14
K2O	0.01	0.06	0.03	–	–	–	–	0.01	–	–	0.03	0.06	–	–
LOI	0.41	1.49	0.49	0.49	0.99	0.58	0.91	0.45	2.42	1.37	0.36	1.17	1.26	0.15
P2O5	n.d.	n.d.	n.d.	n.d.	n.d.	n.d.	n.d.	n.d.	–	n.d.	n.d.	n.d.	–	n.d.
Total	96.61	99.15	99.92	99.89	100.70	96.68	100.73	97.14	95.84	94.73	99.61	101.78	100.84	98.63
Ag	n.d.	<3.37	<2.84	n.d.	<2.74	n.d.	n.d.	n.d.	<3.50	n.d.	n.d.	<2.84	n.d.	<3.38
As	n.d.	<0.375	<0.282	n.d.	<0.270	n.d.	n.d.	n.d.	<0.353	n.d.	n.d.	<0.277	n.d.	<0.381
Au	n.d.	0.0033	0.0026	n.d.	0.0025	n.d.	n.d.	n.d.	0.0109	n.d.	n.d.	0.0028	n.d.	0.2600
Ba	n.d.	<37.9	<31.1	n.d.	<30.6	n.d.	n.d.	n.d.	<38.3	n.d.	n.d.	<29.4	n.d.	<39.1
Bi	n.d.	n.d.	n.d.	n.d.	n.d.	n.d.	n.d.	n.d.	n.d.	n.d.	n.d.	n.d.	n.d.	n.d.
Br	n.d.	<0.294	1.000	n.d.	<0.222	n.d.	n.d.	n.d.	0.656	n.d.	n.d.	0.726	n.d.	<0.307
Cl	n.d.	n.d.	n.d.	n.d.	n.d.	n.d.	n.d.	n.d.	n.d.	n.d.	n.d.	n.d.	n.d.	n.d.
Co	n.d.	99.1	30.0	n.d.	42.2	n.d.	n.d.	n.d.	87.1	n.d.	n.d.	85.5	n.d.	43.2
Cr	n.d.	3150	100	n.d.	852	n.d.	n.d.	n.d.	1910	n.d.	n.d.	1490	2593	383
Cs	n.d.	<0.370	<0.303	n.d.	<0.285	n.d.	n.d.	n.d.	<0.363	n.d.	n.d.	<0.291	n.d.	<0.390
Cu	n.d.	n.d.	n.d.	n.d.	n.d.	n.d.	n.d.	n.d.	240	n.d.	n.d.	n.d.	131	n.d.
Mo	n.d.	<0.243	<0.772	n.d.	<0.803	n.d.	n.d.	n.d.	<0.983	n.d.	n.d.	<0.732	n.d.	<0.048
Nb	n.d.	n.d.	n.d.	n.d.	n.d.	n.d.	n.d.	n.d.	n.d.	n.d.	n.d.	n.d.	n.d.	n.d.
Ni	n.d.	1650	81	n.d.	347	n.d.	n.d.	n.d.	1140	n.d.	n.d.	752	1820	117
Pb	n.d.	n.d.	n.d.	n.d.	n.d.	n.d.	n.d.	n.d.	4	n.d.	n.d.	n.d.	–	n.d.
Pt	n.d.	n.d.	n.d.	n.d.	n.d.	n.d.	n.d.	n.d.	n.d.	n.d.	n.d.	n.d.	n.d.	n.d.
Rb	n.d.	<7.06	<6.96	n.d.	<6.52	n.d.	n.d.	n.d.	<7.69	n.d.	n.d.	<5.90	n.d.	<6.89
S	n.d.	n.d.	n.d.	n.d.	n.d.	n.d.	n.d.	n.d.	847	n.d.	n.d.	n.d.	770	n.d.
Sb	n.d.	<0.047	0.054	n.d.	0.073	n.d.	n.d.	n.d.	<0.045	n.d.	n.d.	0.051	n.d.	<0.048
Sc	n.d.	19.00	4.73	n.d.	6.12	n.d.	n.d.	n.d.	7.66	n.d.	n.d.	6.30	n.d.	47.60
Sn	n.d.	<64.2	<54.4	n.d.	<53.2	n.d.	n.d.	n.d.	<67.0	n.d.	n.d.	<51.5	n.d.	<69.0
Sr	n.d.	n.d.	n.d.	n.d.	n.d.	n.d.	n.d.	n.d.	186	n.d.	n.d.	n.d.	144	n.d.
Ta	n.d.	0.0872	0.1040	n.d.	0.0969	n.d.	n.d.	n.d.	0.1000	n.d.	n.d.	0.0744	n.d.	0.1000
Th	n.d.	<0.216	<0.183	n.d.	<0.185	n.d.	n.d.	n.d.	<0.226	n.d.	n.d.	<0.170	n.d.	<0.214
U	n.d.	<0.143	<0.122	n.d.	<0.123	n.d.	n.d.	n.d.	<0.148	n.d.	n.d.	<0.114	n.d.	<0.147
V	n.d.	n.d.	n.d.	n.d.	n.d.	n.d.	n.d.	n.d.	n.d.	n.d.	n.d.	n.d.	n.d.	n.d.
W	n.d.	<0.756	<0.578	n.d.	<0.565	n.d.	n.d.	n.d.	<0.72	n.d.	n.d.	<0.56	n.d.	<0.878
Zn	n.d.	69	<46	n.d.	41	n.d.	n.d.	n.d.	53	n.d.	n.d.	<39	59	<48
Zr	n.d.	n.d.	n.d.	n.d.	n.d.	n.d.	n.d.	n.d.	37	n.d.	n.d.	n.d.	30	n.d.
Y	n.d.	n.d.	n.d.	n.d.	n.d.	n.d.	n.d.	n.d.	n.d.	n.d.	n.d.	n.d.	n.d.	n.d.
La	n.d.	0.663	0.977	n.d.	0.899	n.d.	n.d.	n.d.	1.07	n.d.	n.d.	<0.210	n.d.	1.030
Ce	n.d.	n.d.	n.d.	n.d.	n.d.	n.d.	n.d.	n.d.	<3	n.d.	n.d.	n.d.	n.d.	n.d.
Nd	n.d.	n.d.	n.d.	n.d.	n.d.	n.d.	n.d.	n.d.	<3	n.d.	n.d.	n.d.	n.d.	n.d.
Sm	n.d.	0.388	0.196	n.d.	0.294	n.d.	n.d.	n.d.	0.170	n.d.	n.d.	0.091	n.d.	1.890
Eu	n.d.	n.d.	n.d.	n.d.	n.d.	n.d.	n.d.	n.d.	0.21	n.d.	n.d.	n.d.	n.d.	n.d.
Gd	n.d.	n.d.	n.d.	n.d.	n.d.	n.d.	n.d.	n.d.	n.d.	n.d.	n.d.	n.d.	n.d.	n.d.
Tb	n.d.	n.d.	n.d.	n.d.	n.d.	n.d.	n.d.	n.d.	0.05	n.d.	n.d.	n.d.	n.d.	n.d.
Tm	n.d.	n.d.	n.d.	n.d.	n.d.	n.d.	n.d.	n.d.	n.d.	n.d.	n.d.	n.d.	n.d.	n.d.
Yb	n.d.	n.d.	n.d.	n.d.	n.d.	n.d.	n.d.	n.d.	0.3	n.d.	n.d.	n.d.	n.d.	n.d.
Lu	n.d.	<0.320	<0.260	n.d.	<0.270	n.d.	n.d.	n.d.	0.040	n.d.	n.d.	<0.250	n.d.	<0.325
Comments	1	1	1	1	1	1	1	1	3&5	1	1	1	2	1

Appendix 12. cont.

	Halti area													
Sample	43	44	47	48	50	63	64	65	66	67	68	68A	146	368
Lith.	OLGB	OLGB	OLGB	OLGB	OLGB	OLGB	OLGB	OLGB	OLGB	OLGB	OLGB	OLGB	OLGB	OLGB
SiO2	46.40	51.20	48.70	49.10	50.00	48.30	47.70	46.50	48.30	50.70	49.80	48.10	49.80	48.90
TiO2	0.80	0.59	0.38	0.37	0.37	0.38	0.24	0.27	0.31	0.18	0.37	0.30	0.22	0.24
Al2O3	16.99	17.99	19.00	18.50	18.53	17.22	21.33	20.29	22.28	23.00	23.52	21.28	21.40	18.70
FeO*	6.46	5.44	3.73	3.96	4.66	6.30	5.40	5.17	3.99	3.70	3.70	5.03	4.78	4.12
MnO	0.11	0.12	0.08	0.09	0.09	0.12	0.09	0.09	0.08	0.06	0.08	0.10	0.08	0.09
MgO	10.79	9.33	8.69	10.74	9.27	12.97	11.97	11.90	8.50	5.72	8.09	10.25	8.78	9.16
CaO	12.16	12.46	13.94	13.27	13.04	11.22	10.15	11.30	12.11	13.70	12.91	12.45	12.20	14.90
Na2O	2.51	2.76	2.22	2.40	1.69	2.14	2.57	2.43	2.84	2.71	2.51	2.32	2.60	1.60
K2O	–	0.01	0.02	–	0.03	0.03	0.03	0.02	0.02	0.03	0.02	–	0.03	0.03
LOI	0.08	0.55	0.38	0.40	0.25	0.13	0.22	1.28	0.37	n.d.	0.32	0.40	0.55	n.d.
P2O5	n.d.	n.d.	n.d.	n.d.	n.d.	n.d.	n.d.	n.d.	n.d.	–	n.d.	n.d.	–	0.01
Total	96.30	100.45	97.14	98.83	97.93	98.81	99.70	99.25	98.80	99.80	101.32	100.23	100.44	97.74
Ag	<3.40	<3.71	<3.15	<3.28	<2.22	<3.24	n.d.	<3.04	n.d.	n.d.	n.d.	n.d.	n.d.	–
As	<0.388	<0.423	<0.373	1.240	2.000	<0.358	n.d.	11.340	n.d.	n.d.	n.d.	n.d.	n.d.	6
Au	0.0032	0.0035	0.0340	0.0032	0.0032	0.0221	n.d.	0.0421	n.d.	n.d.	n.d.	n.d.	n.d.	n.d.
Ba	<38.1	30.6	<37.2	<38.8	<37.4	<36.6	n.d.	<34.1	n.d.	n.d.	n.d.	n.d.	n.d.	45
Bi	–	n.d.	n.d.	n.d.	n.d.	n.d.	n.d.	n.d.	n.d.	n.d.	n.d.	n.d.	n.d.	–
Br	<0.302	<0.340	<0.295	<0.301	0.498	1.100	n.d.	1.860	n.d.	n.d.	n.d.	n.d.	n.d.	n.d.
Cl	40	n.d.	n.d.	n.d.	n.d.	n.d.	n.d.	n.d.	n.d.	n.d.	n.d.	n.d.	n.d.	30
Co	45.0	36.8	29.6	33.7	36.0	49.9	n.d.	41.9	n.d.	n.d.	n.d.	n.d.	n.d.	39
Cr	437	689	543	596	1140	725	n.d.	830	n.d.	530	n.d.	n.d.	789	965
Cs	<0.393	<0.439	<0.375	<0.391	<0.377	<0.375	n.d.	<0.335	n.d.	n.d.	n.d.	n.d.	n.d.	2
Cu	n.d.	n.d.	n.d.	n.d.	n.d.	n.d.	n.d.	n.d.	n.d.	73	n.d.	n.d.	66	50
Mo	<0.889	<0.988	<0.830	0.462	<0.858	<0.865	n.d.	<0.845	n.d.	n.d.	n.d.	n.d.	n.d.	–
Nb	5	n.d.	n.d.	n.d.	n.d.	n.d.	n.d.	n.d.	n.d.	n.d.	n.d.	n.d.	n.d.	7
Ni	171	84	86	84	126	132	n.d.	182	n.d.	104	n.d.	n.d.	79	148
Pb	n.d.	n.d.	n.d.	n.d.	n.d.	n.d.	n.d.	n.d.	n.d.	–	n.d.	n.d.	–	–
Pt	10	n.d.	n.d.	n.d.	n.d.	n.d.	n.d.	n.d.	n.d.	n.d.	n.d.	n.d.	n.d.	–
Rb	<6.83	<7.70	<6.20	<6.48	<6.21	<6.69	n.d.	<6.52	n.d.	n.d.	n.d.	n.d.	n.d.	3
S	n.d.	n.d.	n.d.	n.d.	n.d.	n.d.	n.d.	n.d.	n.d.	182	n.d.	n.d.	361	370
Sb	0.105	<0.051	<0.046	<0.050	<0.046	<0.045	n.d.	0.367	n.d.	n.d.	n.d.	n.d.	n.d.	–
Sc	45.10	57.70	61.60	59.50	49.80	37.40	n.d.	24.00	n.d.	n.d.	n.d.	n.d.	n.d.	n.d.
Sn	<67.0	<74.3	<64.2	<66.9	72.0	<63.1	n.d.	<60.2	n.d.	n.d.	n.d.	n.d.	n.d.	10
Sr	n.d.	n.d.	n.d.	n.d.	n.d.	n.d.	n.d.	n.d.	n.d.	355	n.d.	n.d.	262	223
Ta	0.0912	0.1160	0.0904	0.0924	0.0857	0.0907	n.d.	0.0926	n.d.	n.d.	n.d.	n.d.	n.d.	–
Th	<0.206	<0.229	<0.198	<0.209	<0.206	<0.205	n.d.	<0.198	n.d.	n.d.	n.d.	n.d.	n.d.	–
U	<0.141	<0.157	<0.134	<0.142	<0.137	<0.136	n.d.	<0.132	n.d.	n.d.	n.d.	n.d.	n.d.	9
V	176	n.d.	n.d.	n.d.	n.d.	n.d.	n.d.	n.d.	n.d.	n.d.	n.d.	n.d.	n.d.	152
W	<0.86	<0.976	<0.884	<0.912	<0.464	<0.825	n.d.	<0.709	n.d.	n.d.	n.d.	n.d.	n.d.	–
Zn	<47	<53	<44	<45	<44	<46	n.d.	<43	n.d.	17	n.d.	n.d.	31	24
Zr	n.d.	n.d.	n.d.	n.d.	n.d.	n.d.	n.d.	n.d.	n.d.	59	n.d.	n.d.	52	–
Y	8	n.d.	n.d.	n.d.	n.d.	n.d.	n.d.	n.d.	n.d.	n.d.	n.d.	n.d.	n.d.	7
La	<0.289	1.18	<0.313	0.978	2.780	1.020	n.d.	1.660	n.d.	n.d.	n.d.	n.d.	n.d.	–
Ce	n.d.	<3	n.d.	n.d.	n.d.	n.d.	n.d.	n.d.	n.d.	n.d.	n.d.	n.d.	n.d.	10
Nd	n.d.	<3	n.d.	n.d.	n.d.	n.d.	n.d.	n.d.	n.d.	n.d.	n.d.	n.d.	n.d.	n.d.
Sm	1.130	1.15	0.798	0.724	1.050	0.829	n.d.	0.577	n.d.	n.d.	n.d.	n.d.	n.d.	n.d.
Eu	n.d.	0.62	n.d.	n.d.	n.d.	n.d.	n.d.	n.d.	n.d.	n.d.	n.d.	n.d.	n.d.	n.d.
Gd	n.d.	n.d.	n.d.	n.d.	n.d.	n.d.	n.d.	n.d.	n.d.	n.d.	n.d.	n.d.	n.d.	n.d.
Tb	n.d.	0.22	n.d.	n.d.	n.d.	n.d.	n.d.	n.d.	n.d.	n.d.	n.d.	n.d.	n.d.	n.d.
Tm	n.d.	n.d.	n.d.	n.d.	n.d.	n.d.	n.d.	n.d.	n.d.	n.d.	n.d.	n.d.	n.d.	n.d.
Yb	n.d.	0.77	n.d.	n.d.	n.d.	n.d.	n.d.	n.d.	n.d.	n.d.	n.d.	n.d.	n.d.	n.d.
Lu	<0.312	0.12	<0.300	<0.316	<0.306	<0.304	n.d.	<0.291	n.d.	n.d.	n.d.	n.d.	n.d.	n.d.
Comments	4	3	1	1	1	1	1	1	1	2	1	1	2	2

Appendix 12. cont.

	Halti area													
Sample	31	149	151	366A	423	18	18R	22A	27	29	116A	117	125	126
Lith.	GBPG	GBPG	GBPG	GBPG	GBPG	AAUG	AAUG	AAUG	AAUG	AAUG	AAUG	AAUG	AAUG	AAUG
SiO2	51.90	51.30	51.20	51.90	51.50	46.70	47.60	49.10	50.30	48.80	48.10	48.40	48.29	48.80
TiO2	0.52	0.53	0.63	0.51	0.62	0.46	0.44	0.41	1.08	1.09	1.70	0.45	1.09	0.49
Al2O3	19.32	17.47	17.78	19.70	17.60	18.80	20.20	18.66	14.04	6.48	17.45	19.36	18.63	19.48
FeO*	4.48	5.02	5.81	5.43	6.87	6.56	7.24	3.76	7.57	6.28	9.22	5.84	7.39	5.63
MnO	0.09	0.12	0.12	0.11	0.15	0.11	0.13	0.08	0.17	0.14	0.18	0.10	0.15	0.12
MgO	6.47	9.63	6.65	5.72	6.79	10.87	8.01	11.49	9.88	11.10	8.85	10.84	8.54	11.01
CaO	12.29	12.74	11.72	12.20	12.00	10.10	11.40	13.05	11.56	19.80	10.11	10.93	10.67	11.31
Na2O	3.81	2.83	3.07	3.42	3.27	3.19	2.25	2.25	3.10	0.73	3.14	2.79	3.74	2.56
K2O	0.08	0.02	0.06	0.11	0.11	0.06	0.12	–	0.11	0.02	0.10	0.02	0.03	0.05
LOI	0.48	0.38	1.00	n.d.	n.d.	0.05	n.d.	0.37	–	n.d.	0.27	0.22	–	0.32
P2O5	n.d.	n.d.	n.d.	0.01	0.02	n.d.	0.01	n.d.	n.d.	–	n.d.	n.d.	n.d.	n.d.
Total	99.44	100.04	98.04	99.11	98.92	96.90	97.39	99.17	97.81	94.45	99.12	98.95	98.53	99,77
Ag	<3.03	<2.66	<2.91	–	–	<3.19	–	<3.27	<3.46	–	<4.16	n.d.	n.d.	n.d.
As	<0.336	<0.310	2.820	4	7	<0.334	4	<0.381	<0.412	3	<0.454	n.d.	n.d.	n.d.
Au	0.0041	0.0025	0.0028	n.d.	n.d.	<0.003	–	0.0069	0.0034	n.d.	0.0038	n.d.	n.d.	n.d.
Ba	46.9	<31	105	36	45	60.6	81	<38.8	81.1	–	91.4	n.d.	n.d.	n.d.
Bi	n.d.	n.d.	n.d.	–	–	n.d.	–	n.d.	n.d.	–	n.d.	n.d.	n.d.	n.d.
Br	<0.266	<0.240	<0.267	n.d.	n.d.	<0.272	n.d.	<0.305	0.321	n.d.	<0.365	n.d.	n.d.	n.d.
Cl	n.d.	n.d.	n.d.	90	60	n.d.	60	n.d.	n.d.	120	n.d.	n.d.	n.d.	n.d.
Co	27.2	32.5	37.0	38	46	47.1	56	37.7	37.8	52	44.0	n.d.	n.d.	n.d.
Cr	280	1080	248	380	268	165	1189	1170	348	468	303	n.d.	n.d.	n.d.
Cs	0.356	<0.308	<0.355	10	–	<0.350	3	<0.391	<0.420	10	<0.479	n.d.	n.d.	n.d.
Cu	n.d.	n.d.	n.d.	47	31	n.d.	168	n.d.	n.d.	102	n.d.	n.d.	n.d.	n.d.
Mo	<0.772	<0.712	<0.757	–	–	<0.838	–	<0.895	<0.934	–	<1.110	n.d.	n.d.	n.d.
Nb	n.d.	n.d.	n.d.	6	6	n.d.	7	n.d.	n.d.	9	n.d.	n.d.	n.d.	n.d.
Ni	135	204	246	82	175	163	373	116	124	150	113	n.d.	n.d.	n.d.
Pb	n.d.	n.d.	n.d.	10	–	n.d.	10	n.d.	n.d.	–	n.d.	n.d.	n.d.	n.d.
Pt	n.d.	n.d.	n.d.	10	–	n.d.	–	n.d.	n.d.	–	n.d.	n.d.	n.d.	n.d.
Rb	29.00	<5.13	<5.83	5	4	<7.20	2	<6.51	<6.65	4	<8.75	n.d.	n.d.	n.d.
S	n.d.	n.d.	n.d.	640	1010	n.d.	3070	n.d.	n.d.	3860	n.d.	n.d.	n.d.	n.d.
Sb	<0.043	<0.039	<0.045	–	–	<0.041	–	0.141	<0.051	–	<0.057	n.d.	n.d.	n.d.
Sc	49.10	49.60	52.70	n.d.	n.d.	19.80	n.d.	54.80	67.20	n.d.	49.10	n.d.	n.d.	n.d.
Sn	<60.1	<52.1	<59.7	10	20	<59.5	10	<66.6	<70.8	20	<80.6	n.d.	n.d.	n.d.
Sr	n.d.	n.d.	n.d.	232	204	n.d.	468	n.d.	n.d.	117	n.d.	n.d.	n.d.	n.d.
Ta	0.0938	0.0737	0.0827	–	–	0.1070	–	0.0917	0.1520	10	0.4530	n.d.	n.d.	n.d.
Th	<0.184	<0.164	<0.184	–	–	<0.194	–	<0.213	<0.218	–	<0.248	n.d.	n.d.	n.d.
U	<0.124	<0.111	<0.122	6	6	<0.129	5	<0.143	<0.147	8	<0.172	n.d.	n.d.	n.d.
V	n.d.	n.d.	n.d.	186	207	n.d.	100	n.d.	n.d.	713	n.d.	n.d.	n.d.	n.d.
W	<0.799	<0.698	<0.782	–	–	<0.731	–	<0.886	<0.962	–	<1.03	n.d.	n.d.	n.d.
Zn	<44	<37	<41	37	51	53	55	<45	<50	44	<62	n.d.	n.d.	n.d.
Zr	n.d.	n.d.	n.d.	12	21	n.d.	14	n.d.	n.d.	35	n.d.	n.d.	n.d.	n.d.
Y	n.d.	n.d.	n.d.	10	16	n.d.	7	n.d.	n.d.	17	n.d.	n.d.	n.d.	n.d.
La	1.390	1.120	1.800	20	–	2.300	–	1.550	4.990	20	6.450	n.d.	n.d.	n.d.
Ce	n.d.	n.d.	n.d.	–	20	3.2	20	n.d.	n.d.	20	n.d.	n.d.	n.d.	n.d.
Nd	n.d.	n.d.	n.d.	n.d.	n.d.	<3	n.d.	n.d.	n.d.	n.d.	n.d.	n.d.	n.d.	n.d.
Sm	1.470	1.190	1.720	n.d.	n.d.	0.630	n.d.	0.874	4.830	n.d.	2.970	n.d.	n.d.	n.d.
Eu	n.d.	n.d.	n.d.	n.d.	n.d.	0.6	n.d.	n.d.	n.d.	n.d.	n.d.	n.d.	n.d.	n.d.
Gd	n.d.	n.d.	n.d.	n.d.	n.d.	n.d.	n.d.	n.d.	n.d.	n.d.	n.d.	n.d.	n.d.	n.d.
Tb	n.d.	n.d.	n.d.	n.d.	n.d.	0.12	n.d.	n.d.	n.d.	n.d.	n.d.	n.d.	n.d.	n.d.
Tm	n.d.	n.d.	n.d.	n.d.	n.d.	n.d.	n.d.	n.d.	n.d.	n.d.	n.d.	n.d.	n.d.	n.d.
Yb	n.d.	n.d.	n.d.	n.d.	n.d.	0.34	n.d.	n.d.	n.d.	n.d.	n.d.	n.d.	n.d.	n.d.
Lu	<0.279	<0.247	0.252	n.d.	n.d.	0.080	n.d.	<0.318	<0.335	n.d.	<0.379	n.d.	n.d.	n.d.
Comments	1	1	1	2	2	3	2	1	1	2	1	1	1	1

Appendix 12. cont.

	Halti area													
Sample	188F	334	333	21	21A	22	38	45	46	54D	62	97A	97B	148
Lith.	AAUG	AAUG	AAUG	AR	AR	AR	AR	AR	AR	AR	AR	AR	AR	AR
SiO2	49.77	51.20	48.10	39.70	38.60	46.90	46.40	47.60	45.70	42.50	48.60	42.80	42.40	43.50
TiO2	1.29	0.55	1.45	0.15	0.18	0.20	0.23	0.26	0.18	0.13	0.30	0.12	0.12	0.21
Al2O3	18.22	19.40	18.80	15.61	12.51	29.45	25.12	21.49	21.90	27.45	24.98	24.15	24.61	28.43
FeO*	7.31	5.12	8.28	6.71	9.13	1.53	3.10	4.14	5.03	2.04	4.00	2.97	2.47	2.07
MnO	0.12	0.11	0.15	0.09	0.11	0.03	0.05	0.08	0.09	0.03	0.06	0.04	0.04	0.03
MgO	7.16	7.04	6.38	21.41	30.48	2.53	8.22	9.46	12.14	9.05	7.56	13.61	13.13	7.46
CaO	10.45	12.80	10.50	8.12	3.92	12.93	11.89	12.37	10.06	13.22	11.16	11.29	10.98	12.95
Na2O	3.63	2.73	3.07	3.28	0.59	3.03	2.55	2.74	1.86	2.14	2.88	1.36	1.58	1.78
K2O	0.13	0.13	0.12	–	–	0.01	0.01	–	0.01	0.11	0.05	–	0.08	0.01
LOI	–	n.d.	n.d.	3.13	4.60	0.36	0.85	0.65	0.52	0.76	0.58	0.53	0.39	0.64
P2O5	n.d.	0.04	0.16	n.d.	n.d.	n.d.	n.d.	n.d.	n.d.	n.d.	n.d.	n.d.	n.d.	n.d.
Total	98.08	99.12	97.01	98.20	100.12	96.97	98.42	98.79	97.49	97.43	100.17	96.87	95.80	97.08
Ag	n.d.	–	–	<2.87	<3.07	<2.43	<2.55	<3.03	n.d.	<2.22	n.d.	<2.29	n.d.	n.d.
As	n.d.	7	2	<0.279	1.320	<0.24	3.320	2.690	n.d.	1.420	n.d.	1.310	n.d.	n.d.
Au	n.d.	n.d.	n.d.	0.0024	0.0027	0.0164	0.0025	0.0087	n.d.	0.0039	n.d.	0.0021	n.d.	n.d.
Ba	n.d.	54	80	<28.9	<31.9	<28.2	<29.4	<34.9	n.d.	<26.5	n.d.	<24.5	n.d.	n.d.
Bi	n.d.	–	–	n.d.	n.d.	n.d.	n.d.	n.d.	n.d.	n.d.	n.d.	n.d.	n.d.	n.d.
Br	n.d.	n.d.	n.d.	<0.223	1.200	0.682	<0.210	<0.270	n.d.	<0.183	n.d.	0.395	n.d.	n.d.
Cl	n.d.	20	40	n.d.	n.d.	n.d.	n.d.	n.d.	n.d.	n.d.	n.d.	n.d.	n.d.	n.d.
Co	n.d.	31	50	63.9	100.0	11.7	25.9	35.6	n.d.	27.7	n.d.	43.8	n.d.	n.d.
Cr	n.d.	1189	513	732	1350	94	536	616	n.d.	395	n.d.	1356	n.d.	n.d.
Cs	n.d.	20	–	<0.290	<0.327	0.223	<0.277	<0.345	n.d.	0.734	n.d.	<0.236	n.d.	n.d.
Cu	n.d.	33	56	n.d.	n.d.	n.d.	n.d.	n.d.	n.d.	n.d.	n.d.	n.d.	n.d.	n.d.
Mo	n.d.	–	–	<0.728	<0.785	<0.711	<0.745	<0.823	n.d.	<0.689	n.d.	<0.670	n.d.	n.d.
Nb	n.d.	7	8	n.d.	n.d.	n.d.	n.d.	n.d.	n.d.	n.d.	n.d.	n.d.	n.d.	n.d.
Ni	n.d.	74	105	346	587	51	143	158	n.d.	497	n.d.	375	n.d.	n.d.
Pb	n.d.	–	10	n.d.	n.d.	n.d.	n.d.	n.d.	n.d.	n.d.	n.d.	n.d.	n.d.	n.d.
Pt	n.d.	10	–	n.d.	n.d.	n.d.	n.d.	n.d.	n.d.	n.d.	n.d.	n.d.	n.d.	n.d.
Rb	n.d.	1	2	<6.28	<6.38	<5.97	<5.78	<6.30	n.d.	<5.41	n.d.	<5.23	n.d.	n.d.
S	n.d.	70	1260	n.d.	n.d.	n.d.	n.d.	n.d.	n.d.	n.d.	n.d.	n.d.	n.d.	n.d.
Sb	n.d.	–	–	0.230	0.206	0.064	0.410	0.221	n.d.	0.170	n.d.	0.439	n.d.	n.d.
Sc	n.d.	n.d.	n.d.	4.97	12.00	6.01	9.90	31.30	n.d.	2.49	n.d.	2.59	n.d.	n.d.
Sn	n.d.	10	10	<52.2	<56.5	<48.5	<51.4	<60.5	n.d.	<47.7	n.d.	<44.2	n.d.	n.d.
Sr	n.d.	254	344	n.d.	n.d.	n.d.	n.d.	n.d.	n.d.	n.d.	n.d.	n.d.	n.d.	n.d.
Ta	n.d.	–	–	0.0835	0.0776	0.0921	0.0898	0.0917	n.d.	0.0752	n.d.	0.0756	n.d.	n.d.
Th	n.d.	–	–	<0.173	<0.184	<0.171	<0.156	<0.197	n.d.	<0.165	n.d.	<0.156	n.d.	n.d.
U	n.d.	5	6	<0.115	<0.122	<0.114	<0.117	<0.131	n.d.	<0.110	n.d.	<0.103	n.d.	n.d.
V	n.d.	280	234	n.d.	n.d.	n.d.	n.d.	n.d.	n.d.	n.d.	n.d.	n.d.	n.d.	n.d.
W	n.d.	n.d.	10	<0.561	<0.646	<0.514	<0.566	<0.757	n.d.	<0.464	n.d.	<0.453	n.d.	n.d.
Zn	n.d.	36	65	<41	<44	<40	<39	<43	n.d.	<34	n.d.	<34	n.d.	n.d.
Zr	n.d.	15	24	n.d.	n.d.	n.d.	n.d.	n.d.	n.d.	n.d.	n.d.	n.d.	n.d.	n.d.
Y	n.d.	10	15	n.d.	n.d.	n.d.	n.d.	n.d.	n.d.	n.d.	n.d.	n.d.	n.d.	n.d.
La	n.d.	10	10	0.480	<0.209	0.915	1.530	0.666	n.d.	0.609	n.d.	<0.224	n.d.	n.d.
Ce	n.d.	30	20	n.d.	n.d.	n.d.	n.d.	n.d.	n.d.	n.d.	n.d.	n.d.	n.d.	n.d.
Nd	n.d.	n.d.	n.d.	n.d.	n.d.	n.d.	n.d.	n.d.	n.d.	n.d.	n.d.	n.d.	n.d.	n.d.
Sm	n.d.	n.d.	n.d.	0.168	0.198	0.330	0.420	0.475	n.d.	0.143	n.d.	0.080	n.d.	n.d.
Eu	n.d.	n.d.	n.d.	n.d.	n.d.	n.d.	n.d.	n.d.	n.d.	n.d.	n.d.	n.d.	n.d.	n.d.
Gd	n.d.	n.d.	n.d.	n.d.	n.d.	n.d.	n.d.	n.d.	n.d.	n.d.	n.d.	n.d.	n.d.	n.d.
Tb	n.d.	n.d.	n.d.	n.d.	n.d.	n.d.	n.d.	n.d.	n.d.	n.d.	n.d.	n.d.	n.d.	n.d.
Tm	n.d.	n.d.	n.d.	n.d.	n.d.	n.d.	n.d.	n.d.	n.d.	n.d.	n.d.	n.d.	n.d.	n.d.
Yb	n.d.	n.d.	n.d.	n.d.	n.d.	n.d.	n.d.	n.d.	n.d.	n.d.	n.d.	n.d.	n.d.	n.d.
Lu	n.d.	n.d.	n.d.	<0.249	<0.271	<0.247	<0.256	<0.291	n.d.	<0.239	n.d.	<0.222	n.d.	n.d.
Comments	1	2	2	1	1	1	1	1	1	1	1	1	1	1

Appendix 12. cont.

	Halti area		Ridnitsohkka area										
Sample	153	195	25	25A	26	77	80A	80B	86	116A	87	89	104
Lith.	AR	AR	SIL*	SIL*	SIL*	SIL*	SIL*	SIL*	SIL*	SIL*	SIL	SIL	SIL
SiO2	43.10	45.20	49.70	47.00	52.9	44.59	48.40	49.50	48.70	46.90	50.90	50.30	47.40
TiO2	0.14	0.06	1.47	1.73	1.87	3.12	1.42	2.61	1.42	1.16	2.17	1.30	2.13
Al2O3	23.54	29.77	17.21	21.08	19.2	16.04	17.39	17.61	17.00	17.79	18.06	19.05	15.61
FeO*	3.29	0.73	7.60	9.50	8.16	9.51	7.74	8.88	7.74	11.90	9.11	7.13	11.66
MnO	0.04	–	0.15	0.10	0.15	0.20	0.14	0.17	0.15	0.14	0.17	0.14	0.25
MgO	14.62	0.92	8.28	6.89	3.32	6.00	8.64	5.80	9.02	7.01	6.06	7.80	8.62
CaO	10.87	12.36	10.15	3.63	9.22	9.48	10.45	9.13	10.50	5.91	8.13	9.34	11.46
Na2O	1.21	4.62	3.84	4.72	3.94	3.99	3.21	3.79	3.21	2.94	3.92	3.02	1.08
K2O	0.10	0.24	0.17	0.69	0.63	0.14	0.25	0.38	0.09	0.27	0.74	0.80	0.12
LOI	0.49	0.85	0.07	3.79	–	–	0.03	–	0.50	5.45	0.38	0.44	0.10
P2O5	n.d.	n.d.	n.d.	n.d.	–	n.d.	n.d.	n.d.	n.d.	n.d.	n.d.	n.d.	n.d.
Total	97.40	94.75	98.64	99.13	99.39	93.07	97.67	97.87	98.33	99.47	99.64	99.32	98.43
Ag	n.d.	n.d.	<3.62	<3.92	n.d.	n.d.	n.d.	n.d.	<3.73	<4.58	<4.21	<3.56	n.d.
As	n.d.	n.d.	<0.393	4.890	n.d.	n.d.	n.d.	n.d.	<0.445	6.430	1.630	1.790	n.d.
Au	n.d.	n.d.	<0.0033	0.0083	n.d.	n.d.	n.d.	n.d.	0.0140	0.0044	0.0040	0.0034	n.d.
Ba	n.d.	n.d.	102	248	n.d.	n.d.	n.d.	n.d.	69.5	205	304	152	n.d.
Bi	n.d.	n.d.	n.d.	n.d.	n.d.	n.d.	n.d.	n.d.	n.d.	n.d.	n.d.	n.d.	n.d.
Br	n.d.	n.d.	<0.311	<0.340	n.d.	n.d.	n.d.	n.d.	1.140	<0.391	0.367	0.767	n.d.
Cl	n.d.	n.d.	n.d.	n.d.	n.d.	n.d.	n.d.	n.d.	n.d.	n.d.	n.d.	n.d.	n.d.
Co	n.d.	n.d.	38.3	39.1	n.d.	n.d.	n.d.	n.d.	39.9	61.1	48.5	38.8	n.d.
Cr	n.d.	n.d.	316	255	254	n.d.	n.d.	n.d.	334	297	191	207	n.d.
Cs	n.d.	n.d.	<0.405	1.560	n.d.	n.d.	n.d.	n.d.	<0.440	<0.528	<0.480	1.570	n.d.
Cu	n.d.	n.d.	n.d.	n.d.	60	n.d.	n.d.	n.d.	n.d.	n.d.	n.d.	n.d.	n.d.
Mo	n.d.	n.d.	<0.967	<1.240	n.d.	n.d.	n.d.	n.d.	<1.020	<1.450	<1.170	<1.030	n.d.
Nb	n.d.	n.d.	n.d.	n.d.	n.d.	n.d.	n.d.	n.d.	n.d.	n.d.	n.d.	n.d.	n.d.
Ni	n.d.	n.d.	106	83	52	n.d.	n.d.	n.d.	65	200	<31	80	n.d.
Pb	n.d.	n.d.	n.d.	n.d.	2	n.d.	n.d.	n.d.	n.d.	n.d.	n.d.	n.d.	n.d.
Pt	n.d.	n.d.	n.d.	n.d.	n.d.	n.d.	n.d.	n.d.	n.d.	n.d.	n.d.	n.d.	n.d.
Rb	n.d.	n.d.	<7.69	31.20	n.d.	n.d.	n.d.	n.d.	<7.88	<9.93	12.90	29.80	n.d.
S	n.d.	n.d.	n.d.	n.d.	1091	n.d.	n.d.	n.d.	n.d.	n.d.	n.d.	n.d.	n.d.
Sb	n.d.	n.d.	<0.049	<0.055	n.d.	n.d.	n.d.	n.d.	0.755	0.095	0.058	0.116	n.d.
Sc	n.d.	n.d.	43.50	35.20	n.d.	n.d.	n.d.	n.d.	48.00	42.40	45.60	38.70	n.d.
Sn	n.d.	n.d.	<70.6	<78.1	n.d.	n.d.	n.d.	n.d.	<77.2	<90.8	<83.2	<71.7	n.d.
Sr	n.d.	n.d.	n.d.	n.d.	355	n.d.	n.d.	n.d.	n.d.	n.d.	n.d.	n.d.	n.d.
Ta	n.d.	n.d.	0.4120	1.1400	n.d.	n.d.	n.d.	n.d.	0.1290	0.4700	1.0100	0.4990	n.d.
Th	n.d.	n.d.	<0.219	1.350	n.d.	n.d.	n.d.	n.d.	<0.242	0.519	<0.266	4.160	n.d.
U	n.d.	n.d.	<0.148	0.986	n.d.	n.d.	n.d.	n.d.	<0.163	<0.203	0.601	0.933	n.d.
V	n.d.	n.d.	n.d.	n.d.	n.d.	n.d.	n.d.	n.d.	n.d.	n.d.	n.d.	n.d.	n.d.
W	n.d.	n.d.	<0.892	<0.937	n.d.	n.d.	n.d.	n.d.	<0.977	<1.1	<1.05	<0.884	n.d.
Zn	n.d.	n.d.	49	115	74	n.d.	n.d.	n.d.	<54	<69	113	40	n.d.
Zr	n.d.	n.d.	n.d.	n.d.	192	n.d.	n.d.	n.d.	n.d.	n.d.	n.d.	n.d.	n.d.
Y	n.d.	n.d.	n.d.	n.d.	n.d.	n.d.	n.d.	n.d.	n.d.	n.d.	n.d.	n.d.	n.d.
La	n.d.	n.d.	9.500	41.800	n.d.	n.d.	n.d.	n.d.	3.990	29.200	21.000	15.800	n.d.
Ce	n.d.	n.d.	17.9	n.d.	n.d.	n.d.	n.d.	n.d.	n.d.	n.d.	39	n.d.	n.d.
Nd	n.d.	n.d.	13.8	n.d.	n.d.	n.d.	n.d.	n.d.	n.d.	n.d.	26	n.d.	n.d.
Sm	n.d.	n.d.	3.800	4.170	n.d.	n.d.	n.d.	n.d.	2.800	3.140	7.000	4.100	n.d.
Eu	n.d.	n.d.	2.1	n.d.	n.d.	n.d.	n.d.	n.d.	n.d.	n.d.	2.89	n.d.	n.d.
Gd	n.d.	n.d.	n.d.	n.d.	n.d.	n.d.	n.d.	n.d.	n.d.	n.d.	n.d.	n.d.	n.d.
Tb	n.d.	n.d.	0.6	n.d.	n.d.	n.d.	n.d.	n.d.	n.d.	n.d.	1.04	n.d.	n.d.
Tm	n.d.	n.d.	n.d.	n.d.	n.d.	n.d.	n.d.	n.d.	n.d.	n.d.	n.d.	n.d.	n.d.
Yb	n.d.	n.d.	2.1	n.d.	n.d.	n.d.	n.d.	n.d.	n.d.	n.d.	3.1	n.d.	n.d.
Lu	n.d.	n.d.	0.290	<0.110	n.d.	n.d.	n.d.	n.d.	0.554	<0.455	0.420	0.639	n.d.
Comments	1	1	3	1	2	1	1	1	1	1	3	1	1

Appendix 12. cont.

	Ridnitsohkka area										Halti
Sample	106	120	121	122	123	129	136	144A	80D	92B	194A
Lith.	SIL	SIL	SIL	SIL	SIL	SIL	SIL	SIL	GR	GR	GR
SiO2	52.10	49.70	51.20	45.96	50.20	48.70	53.30	53.59	76.00	75.80	73.20
TiO2	1.54	2.03	1.44	1.3	3.42	1.31	1.48	1.47	0.14	0.32	0.22
Al2O3	17.70	17.63	18.35	16.96	17.38	18.64	19.73	19.71	14.25	12.88	13.54
FeO*	7.47	8.55	7.47	7.48	11.39	6.99	8.82	7.70	0.82	2.37	1.09
MnO	0.21	0.18	0.16	0.16	0.25	0.14	0.21	0.13	–	–	–
MgO	6.35	5.97	7.84	7.85	4.43	8.29	5.52	6.58	0.14	0.11	0.17
CaO	8.43	8.73	9.29	9.49	5.66	8.80	6.71	8.66	1.37	0.65	0.75
Na2O	3.81	4.15	1.81	3.89	3.88	3.88	3.88	3.36	4.13	2.77	2.93
K2O	1.01	0.66	0.20	0.53	1.50	0.57	0.55	0.85	3.63	5.00	6.39
LOI	0.44	0.55	0.20	n.d.	0.06	0.38	0.07	–	0.68	1.51	0.87
P2O5	n.d.	n.d.	n.d.	n.d.	n.d.	n.d.	n.d.	n.d.	n.d.	n.d.	n.d.
Total	99.06	98.15	97.96	93.62	98.17	97.70	100.27	102.05	101.20	101.42	99.15
Ag	<4.31	n.d.	n.d.	n.d.	<5.29	<3.46	<3.34	n.d.	n.d.	n.d.	n.d.
As	0.468	n.d.	n.d.	n.d.	0.596	3.060	0.379	n.d.	n.d.	n.d.	n.d.
Au	0.0041	n.d.	n.d.	n.d.	0.0142	0.0147	0.0031	n.d.	n.d.	n.d.	n.d.
Ba	294	n.d.	n.d.	n.d.	568	123	310	n.d.	n.d.	n.d.	n.d.
Bi	n.d.	n.d.	n.d.	n.d.	n.d.	n.d.	n.d.	n.d.	n.d.	n.d.	n.d.
Br	<0.382	n.d.	n.d.	n.d.	<0.468	1.360	<0.293	n.d.	n.d.	n.d.	n.d.
Cl	n.d.	n.d.	n.d.	n.d.	n.d.	n.d.	n.d.	n.d.	n.d.	n.d.	n.d.
Co	29.2	n.d.	n.d.	n.d.	31.5	37.7	28.6	n.d.	n.d.	n.d.	n.d.
Cr	256	n.d.	n.d.	n.d.	81	253	186	n.d.	n.d.	n.d.	n.d.
Cs	1.120	n.d.	n.d.	n.d.	1.820	1.780	0.370	n.d.	n.d.	n.d.	n.d.
Cu	n.d.	n.d.	n.d.	n.d.	n.d.	n.d.	n.d.	n.d.	n.d.	n.d.	n.d.
Mo	<1.190	n.d.	n.d.	n.d.	<1.570	<0.983	<0.944	n.d.	n.d.	n.d.	n.d.
Nb	n.d.	n.d.	n.d.	n.d.	n.d.	n.d.	n.d.	n.d.	n.d.	n.d.	n.d.
Ni	<32	n.d.	n.d.	n.d.	<37	45	25	n.d.	n.d.	n.d.	n.d.
Pb	n.d.	n.d.	n.d.	n.d.	n.d.	n.d.	n.d.	n.d.	n.d.	n.d.	n.d.
Pt	n.d.	n.d.	n.d.	n.d.	n.d.	n.d.	n.d.	n.d.	n.d.	n.d.	n.d.
Rb	59.70	n.d.	n.d.	n.d.	91.40	29.30	15.10	n.d.	n.d.	n.d.	n.d.
S	n.d.	n.d.	n.d.	n.d.	n.d.	n.d.	n.d.	n.d.	n.d.	n.d.	n.d.
Sb	<0.059	n.d.	n.d.	n.d.	<0.074	0.265	0.066	n.d.	n.d.	n.d.	n.d.
Sc	41.00	n.d.	n.d.	n.d.	50.80	36.40	36.20	n.d.	n.d.	n.d.	n.d.
Sn	<85.6	n.d.	n.d.	n.d.	<106.0	<69.9	<67.0	n.d.	n.d.	n.d.	n.d.
Sr	n.d.	n.d.	n.d.	n.d.	n.d.	n.d.	n.d.	n.d.	n.d.	n.d.	n.d.
Ta	0.6160	n.d.	n.d.	n.d.	1.7800	0.5120	1.2000	n.d.	n.d.	n.d.	n.d.
Th	0.411	n.d.	n.d.	n.d.	2.060	2.960	0.851	n.d.	n.d.	n.d.	n.d.
U	<0.190	n.d.	n.d.	n.d.	1.780	1.110	0.750	n.d.	n.d.	n.d.	n.d.
V	n.d.	n.d.	n.d.	n.d.	n.d.	n.d.	n.d.	n.d.	n.d.	n.d.	n.d.
W	<1.04	n.d.	n.d.	n.d.	<1.29	<0.859	<0.836	n.d.	n.d.	n.d.	n.d.
Zn	76	n.d.	n.d.	n.d.	<80	68	116	n.d.	n.d.	n.d.	n.d.
Zr	n.d.	n.d.	n.d.	n.d.	n.d.	n.d.	n.d.	n.d.	n.d.	n.d.	n.d.
Y	n.d.	n.d.	n.d.	n.d.	n.d.	n.d.	n.d.	n.d.	n.d.	n.d.	n.d.
La	14.000	n.d.	n.d.	n.d.	35.500	11.800	26.700	n.d.	n.d.	n.d.	n.d.
Ce	n.d.	n.d.	n.d.	n.d.	n.d.	n.d.	n.d.	n.d.	n.d.	n.d.	n.d.
Nd	n.d.	n.d.	n.d.	n.d.	n.d.	n.d.	n.d.	n.d.	n.d.	n.d.	n.d.
Sm	5.330	n.d.	n.d.	n.d.	10.200	4.330	8.530	n.d.	n.d.	n.d.	n.d.
Eu	n.d.	n.d.	n.d.	n.d.	n.d.	n.d.	n.d.	n.d.	n.d.	n.d.	n.d.
Gd	n.d.	n.d.	n.d.	n.d.	n.d.	n.d.	n.d.	n.d.	n.d.	n.d.	n.d.
Tb	n.d.	n.d.	n.d.	n.d.	n.d.	n.d.	n.d.	n.d.	n.d.	n.d.	n.d.
Tm	n.d.	n.d.	n.d.	n.d.	n.d.	n.d.	n.d.	n.d.	n.d.	n.d.	n.d.
Yb	n.d.	n.d.	n.d.	n.d.	n.d.	n.d.	n.d.	n.d.	n.d.	n.d.	n.d.
Lu	0.631	n.d.	n.d.	n.d.	0.582	0.265	0.391	n.d.	n.d.	n.d.	n.d.
Comments	1	1	1	1	1	1	1	1	1	1	1

Appendix 13. Sampling sites in the Halti-Ridnitsohkka area.

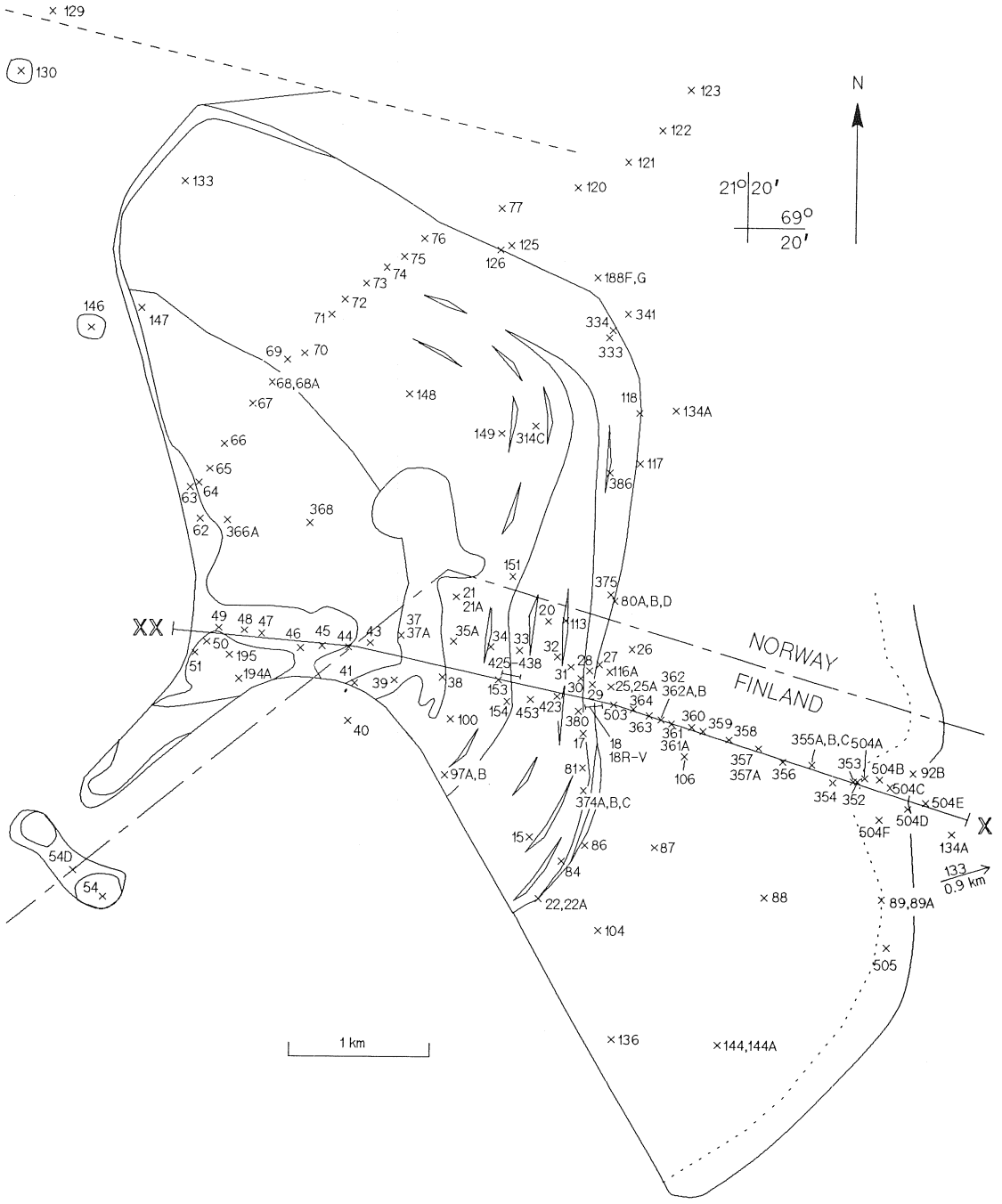

Tätä julkaisua myy

GEOLOGIAN
TUTKIMUSKESKUS (GTK)
Julkaisumyynti
02150 Espoo
☏ 90-46931
Teleksi: 123 185 geolo sf
Telekopio: 90-462 205

GTK, Väli-Suomen
aluetoimisto
Kirjasto
PL 1237
70701 Kuopio
☏ 971-205 111
Telekopio: 971-205 215

GTK, Pohjois-Suomen
aluetoimisto
Kirjasto
PL 77
96101 Rovaniemi
☏ 960-297 219
Teleksi: 37 295 geolo sf
Telekopio: 960-297 289

Denna publikation säljes av

GEOLOGISKA
FORSKNINGSCENTRALEN (GFC)
Publikationsförsäljning
02150 Esbo
☏ 90-46931
Telex: 123 185 geolo sf
Telefax: 90-462 205

GFC, Mellersta Finlands
distriktsbyrå
Biblioteket
PB 1237
70701 Kuopio
☏ 971-205 111
Telefax: 971-205 215

GFC, Norra Finlands
distriktsbyrå
Biblioteket
PB 77
96101 Rovaniemi
☏ 960-297 219
Telex: 37 295 geolo sf
Telefax: 960-297 289

This publication can be obtained
from

GEOLOGICAL SURVEY
OF FINLAND (GSF)
Publication sales
SF-02150 Espoo, Finland
☏ 90-46931
Telex: 123 185 geolo sf
Telefax: 90-462 205

GSF, Regional office of
Mid-Finland
Library
P.O. Box 1237
SF-70701 Kuopio, Finland
☏ 971-205 111
Telefax: 971-205 215

GSF, Regional office of
Northern Finland
Library
P.O. Box 77
SF-96101 Rovaniemi, Finland
☏ 960-297 219
Telex: 37 295 geolo sf
Telefax: 960-297 289

ISBN 951-690-459-9
ISSN 0367-522X